Universitat Autònoma de Barcelona

TARGETING MITOSIS IN OVARIAN CANCER: THE STUDY OF BORA AS A FUTURE THERAPEUTIC AVENUE

Alfonso Parrilla Ocón

ADVERTIMENT. L'accés als continguts d'aquesta tesi queda condicionat a l'acceptació de les condicions d'ús establertes per la següent llicència Creative Commons: http://cat.creativecommons.org/?page_id=184

ADVERTENCIA. El acceso a los contenidos de esta tesis queda condicionado a la aceptación de las condiciones de uso establecidas por la siguiente licencia Creative Commons: http://es.creativecommons.org/blog/licencias/

WARNING. The access to the contents of this doctoral thesis it is limited to the acceptance of the use conditions set by the following Creative Commons license: https://creativecommons.org/licenses/?lang=en

TARGETING MITOSIS IN OVARIAN CANCER:

THE STUDY OF BORA AS A FUTURE THERAPEUTIC AVENUE

PhD thesis presented by

Alfonso Parrilla Ocón

To obtain the degree of

PhD for the Universitat Autònoma de Barcelona (UAB)

PhD thesis carried out at the Cell Cycle and Cancer Laboratory within the Biomedical Research Group in Gynecology, at Vall d'Hebron Research Institute (VHIR)

Thesis affiliated to the Department of Biochemistry and Molecular Biology from the UAB, in the PhD program of Biochemistry, Molecular Biology and Biomedicine

Universitat Autònoma de Barcelona, September 12th 2019

Doctorate	Director	Tutor
Alfonso Parrilla Ocón	Dr. Anna Santamaria Margalef	Dr. Ana Meseguer Navarro

Universitat Autònoma de Barcelona

Vall d'Hebron Barcelona Campus Hospitalari

Vall d'Hebron Institut de Recerca VHIR

TARGETING MITOSIS IN OVARIAN CANCER

The study of BORA as a future therapeutic avenue

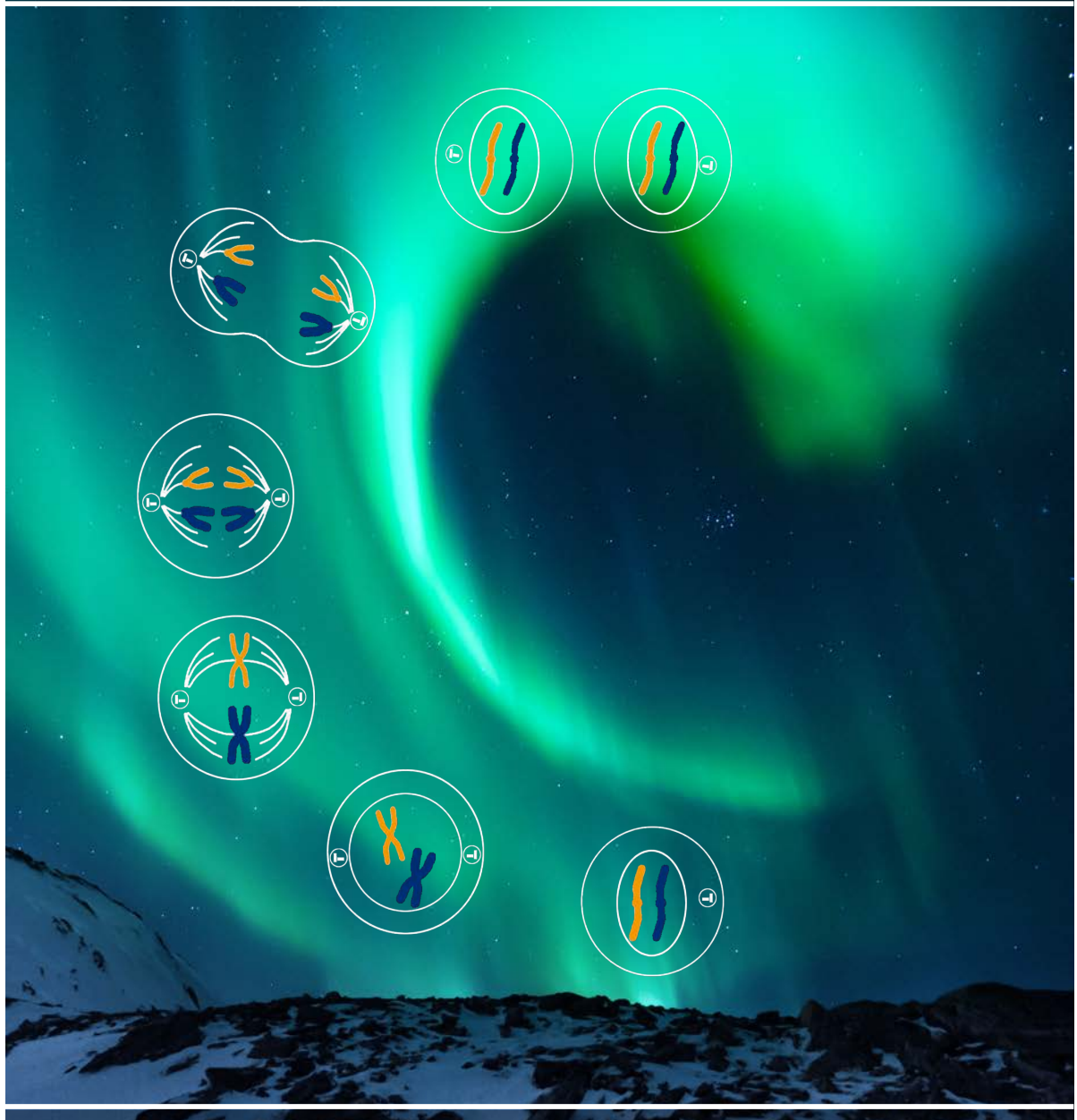

Alfonso Parrilla

PhD Thesis 2019

CLINICAL RELEVANCE OF THIS THESIS

Clinical management of ovarian cancer remains a challenge due to the failure to obtain long-lasting benefits and the development of resistance to current standard therapies. Since the mitotic spindle is a validated target against cancer, using an integrative global transcriptional profiling we searched for novel actionable mitotic candidates, focusing our attention on BORA. This thesis provides the first evidence of unanticipated oncogenic functions of BORA in addition to its previously described role in mitosis. Our data pinpoints BORA as prognostic biomarker and as essential mediator of tumor cell survival. BORA overexpression enhanced tumorigenicity *in vivo* whereas its ablation attenuated tumor growth *in vivo* and compromised the viability of patient-derived tumor cells *ex vivo*, rendering a potential therapeutic target. Furthermore, exploring the BORA silencing landscape led us to identify downstream effectors that can be currently used as targeted therapies for ovarian cancer management.

UAB Universitat Autònoma de Barcelona

Vall d'Hebron Institut de Recerca

A mi familia, en especial a mi padre

ABSTRACT

Ovarian cancer is the most lethal gynecology malignancy, frequently diagnosed at advanced stages with disseminated disease. The genomic and genetic heterogeneity described in ovarian cancer contributes to the development of tumor resistance, hampers effective treatments and ultimately causes disease recurrence. However, it also offers novel potential vulnerabilities that can enhance the effectiveness of existing therapies. In this regard, as the mitotic spindle is a classical target for treating cancer, **chromosomal instability**-exploiting therapies are emerging in the landscape of anti-cancer therapeutic tools yielding better clinical outcomes. In the present thesis we have identified a number of mitotic-enriched genes overexpressed in ovarian cancer associated with poor overall survival. We further characterized the role of ***Aurora Borealis*** **(BORA)**, previously described as a mitotic protein essential in spindle assembly and key activating the master kinase, PLK1. Gain and loss of function assays in mouse models and *ex vivo* patient-derived ascites cultures grown in 3D, together with a whole genome transcriptome analysis in clinically representative cells lines, revealed an **oncogenic role** of BORA in tumor development modulating survival, dissemination and inflammatory related-pathways. Importantly, combinatory treatments of FDA-approved inhibitors against oncogenic downstream effectors of BORA, such BCL-2 and CDK6, offered promising results in ovarian cancer models. Collectively, the data shown in this thesis depict novel evidence regarding the role of BORA in tumorigenesis and provide **novel potential therapeutic opportunities** for ovarian cancer management.

Key words: Aurora Borealis, ovarian cancer, mitosis, prognosis, pro-oncogene, targeted therapy, PLK1

RESUMEN DE LA TESIS

El **cáncer de ovario** es la neoplasia maligna ginecológica más letal, frecuentemente diagnosticada en estadios avanzados cuando la enfermedad se encuentra diseminada. La heterogeneidad, tanto genómica como genética, descrita en cáncer de ovario contribuye al desarrollo de resistencia tumoral, dificulta tratamientos efectivos y finalmente causa la recurrencia de la enfermedad. Sin embargo, también ofrece nuevas vulnerabilidades específicas de las células cancerosas que pueden mejorar la efectividad de las terapias existentes. En este sentido, como el huso mitótico es una diana clásica en el desarrollo de terapias contra el cáncer, el uso de agentes que incrementan la **inestabilidad cromosómica** está emergiendo como nueva herramienta terapéutica aumentando el beneficio clínico de los pacientes. En la presente tesis hemos identificado una serie de genes mitóticos que se encuentran sobre-expresados en cáncer de ovario asociados a una peor supervivencia. En concreto, se ha caracterizado el papel de ***Aurora Borealis*** **(BORA)**, previamente descrita como una proteína mitótica esencial en el ensamblaje del huso mitótico y clave en la activación de la quinasa, PLK1. Los ensayos de ganancia y pérdida de función de BORA en modelos de ratón y en cultivos de células de ascitis provenientes de pacientes en 3D, junto con un análisis transcriptómico en líneas celulares clínicamente representativas de cáncer de ovario, revelaron un **papel oncogénico de BORA** en el desarrollo del tumor que modula la supervivencia celular, la diseminación y las vías inflamatorias. Tratamientos combinados usando inhibidores aprobados en la clínica contra los efectores oncogénicos de BORA, como BCL-2 y CDK6, ofrecieron resultados prometedores en nuestros modelos de cáncer de ovario. En resumen, los datos que se muestran en esta tesis muestran nuevas evidencias sobre el papel de BORA en la tumorigénesis y proporcionan **nuevas herramientas terapéuticas** para el tratamiento del cáncer de ovario.

Palabras clave: Aurora Borealis, cáncer de ovario, mitosis, pronóstico, pro-oncogen, therapia dirigida, PLK1

TABLE OF CONTENTS

LIST OF FIGURES

LIST OF TABLES

LIST OF ABBREVIATIONS & ACRONYMS

A	aa	Aminoacid
	ANOVA	Analysis of Variance
	AML	Acute Myeloid Leukemia
	APC/C	Anaphase-Promoting Complex
	ATCC	American Type Culture Collection
	ATM	Ataxia Telangiectasia Mutated
	ATP	Adenosine Triphosphate
	ATR	Ataxia Telangiectasia and Rad3 Kinase
	A.U.	Arbitrary Units
	AURORA-A	Aurora kinase A
B	B	Benign
	BCL-2	B-Cell CLL/Lymphoma 2
	BCL-2i	BCL-2 inhibitors
	BORA	Aurora Borealis
	BRCA1	Breast Cancer 1
	BRCA2	Breast Cancer 2
	BSA	Bovine Serum Albumin
C	CA-125	Cancer Antigen 125
	CCNE1	Cyclin E1 gene
	CDE	Cell cycle-Dependent Element
	CDH	Cell cycle Homology Region
	CDS	Coding Sequence
	CDKs	Cyclin Dependent Kinases
	CDK1	Cyclin Dependent Kinase 1
	CDK4/6	Cyclin Dependent Kinase 4/6
	CDK6	Cyclin Dependent Kinase 6
	CDK6i	CDK6 inhibitors
	cDNA	Complementary DNA
	CEEA	Comité Ético de Experimentación Animal
	ChIp-Seq	Chromatin Immunoprecipitation Sequencing
	CIN	Chromosomal Instability
	CI	Combination Index
	CT	Computed Tomography
	CTLA-4	Cytotoxic T-Lymphocyte Antigen 4
	Cyst	Cystoadenoma
D	DDR	DNA Damage Response
	DMSO	Dimethyl Sulfoxide
	DNA	Deoxyribonucleic Acid
	dNTPs	Deoxynucleotide Triphosphates
	DSB	Double Strand Break

E	ECACC	European Collection of Authenticated Cell Cultures
	ECL	Enhanced Chemiluminescence
	EDTA	Ethylenediaminetetraacetic Acid
	EMA	European Medicines Agency
	EMT	Epithelial-Mesenchymal Transition
	EOC	Epithelial Ovarian Cancer
	ES	Enrichment Score
	EV	Empty Vector
F	FA	Fraction Affected
	FBS	Fetal Bovine Serum
	FDA	Food and Drug Administration
	FDR	False Discovery Rate
	FFPE	Formalin-Fixed Paraffin Embedded
	FGF	Fibroblast Growth Factor
	FIGO	Federation International of Gynecology and Obstetrics
	FOXM1	Forkhead Box M1
	FTE	Fallopian Tube Epithelium
G	g	Relative centrifugal force
	GO	Gene Ontology
	GSE	GEO Series
	GSEA	Gene Set Enrichment Analysis
	GST	Glutation S-transferase
	G418	Geneticin
H	h	hours
	HE4	Human Epididymis Protein 4
	HGSC	High Grade Serous Carcinoma
	HR	Homologous Recombination
	HUHV	Hospital UniversitariO Vall d' Hebron
	H&E	Hematoxylin and Eosin
	IHQ	Immunohistochemistry
	IOSE	Immortalized Ovarian Surface Epithelium
	IRB	Institutional Review Board
K	KT	Kinetochore
	kDa	Kilodalton
L	LGSC	Low Grade Serous Carcinoma
	lncRNA	long-non coding RNA

	MAPK	Mitogen-Activated Protein Kinases
	MEK	MAPK/ERK pathway
	mg	Miligrams
	mL	Mililitres
	mM	Milimolar
	mm	Milimetres
	min	Minutes
M	miRNA	microRNA
	MRI	Magnetic Resonance Imaging
	mRNA	Messenger mRNA
	MSigDB	Molecular Signatures Database v6.0
	MT	Microtubule
	MTAs	Microtubule Agents
	MTS	Viability Assay
	M-phase	Mitotic phase
	NA	Not Applicable / Not Available
	NACT	Neoadjuvant Chemotherapy
	NES	Normalized Enrichment Score
N	NF-kB	Nuclear Factor kappa-light-chain-enhancer of activated B cells
	ng	Nanograms
	ns	Not statistically significant
	NT	Nucleotide
	OC	Ovarian Cancer
O	OS	Overall Survival
	OSE	Ovarian Surface Epithelium
	P	*P*-value
	PAGE	PolyAcrylamide Gel Electrophoresis
	PARP	Poly ADP Ribose Polymerase
	PARPi	PARP inhibitors
	PARP – FL	Poly ADP Ribose Polymerase - Full Lenght
	PBD	Polo-Box Domain
	PBS	Phosphate-Buffered Saline
	PCR	Polymerase Chain Reaction
	PDX	Patient-Derived Xenograft
P	PD-1	Programmed Cell Death 1
	PD-L1	Programmed Cell Death-Ligand 1
	PFI	Platinum Free Interval
	PFS	Progression Free Survival
	PI	Propidium Iodide
	pIND_Bora	pINDUCER Bora Sequence
	pIND_EV	pINDUCER Empty Vector
	PLKs	Polo Like Kinases
	PLK1	Polo-Like Kinase 1
	PVDF	Polyvinylidine Diflouride
	p65	Transcription factor p65

R	RB	Retinoblastome
	RIPA	Radioimmunoprecipitation assay buffer
	RNA	Ribonucleic Acid
	ROCA	Risk of Ovarian Cancer Algorithm
	rpm	Revolutions per minute
	RT	Room Temperature
	RT-qPCR	Real-Time quantitative PCR
S	SAC	Spindle Assembly Checkpoint
	SCCOHT	Small Cell Carcinoma of the Ovary, Hypercalcaemic Type
	shCTL	Short hairpin RNA - Control
	SEGO	Sociedad Española de Ginecología y Obstetricia
	SEM	Standard Error of the Mean
	shBORA	Short hairpin RNA - targeting Bora
	shRNA	Short hairpin RNA
	siRNA	Small interference RNA
	STIC	Serous Tubal Intraepithelial Carcinoma
T	T	Tumor
	TCGA	The Cancer Genome Atlas
	TF	Transcription factor
	TGF	Transforming Growth Factor
	TILs	Tumor Infiltrating Lymphocytes
	TMA	Tissue Microarray
	TP53	Tumor protein p53
	tRFP	Turbo Red Fluorescent Protein
U	UAB	Universitat Autònoma de Barcelona
	UAT	Servei d'Alta Tecnologia (VHIR)
	UEB	Bioinformatic and Statistical Unit (VHIR)
	µg	Micrograms
	UKTOCS	United Kingdom Trial Ovarian Cancer Screening
	µL	Microliters
	US	Ultrasound
	UTR	Untranslated Region
V	VEGF	Vascular Endothelial Growth Factor
	VHIR	Vall d'Hebron Research Institute
	vs	Versus
W	WHO	World Health Organization

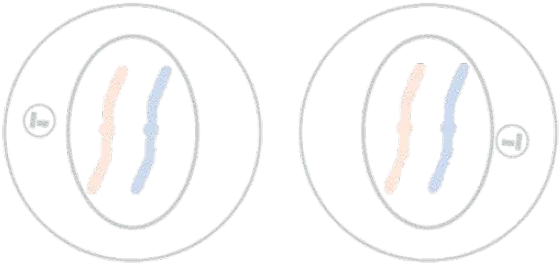

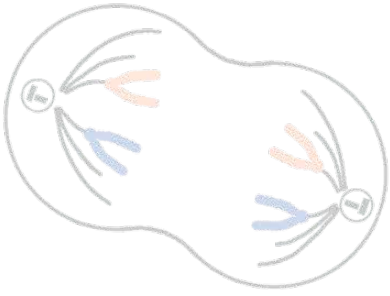

1. INTRODUCTION

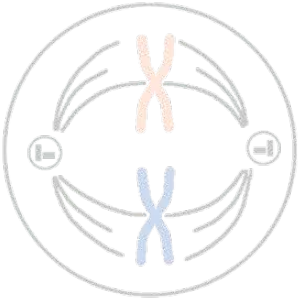

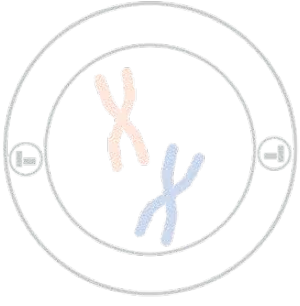

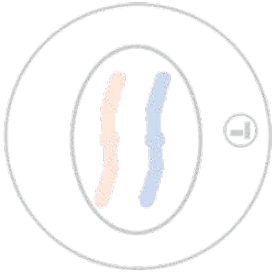

1.1 Cancer: an increasing disease worldwide

The oldest description and surgical treatment of cancer dates back to 3000 *bc* in an Egyptian surgery book, when eight cases of breast tumors were surgically removed and reflected on a papyrus. The writing was accompanied by the sentence: "there is no treatment"[1]. Today the landscape is substantially different. Although cancer is one of the leading causes of death worldwide, in the last years emerging therapeutic approaches have improved considerably the clinical outcomes being closer to turn cancer into a chronic condition. Being still the most important barrier to increase life expectancy, about one-in-five men and one-in-six women worldwide will develop cancer during their lifetime, and ultimately, one-in-eight men and one-in-eleven women will die from cancer[2]. The Globocan 2018, a database with sources of cancer incidence and mortality from countries worldwide, estimates for this year 18,1 million of new cancer cases and 9,6 million of deaths derived from cancer (Figure 1A). The most diagnosed tumors are lung, breast, colorectal, prostate and stomach and the three top cancers can explain one-third of incidence and mortality burden cases. The distribution worldwide varies depending on the societal economic and lifestyle, with more global cancer cases rates in developed countries[2] (Figure 1B).

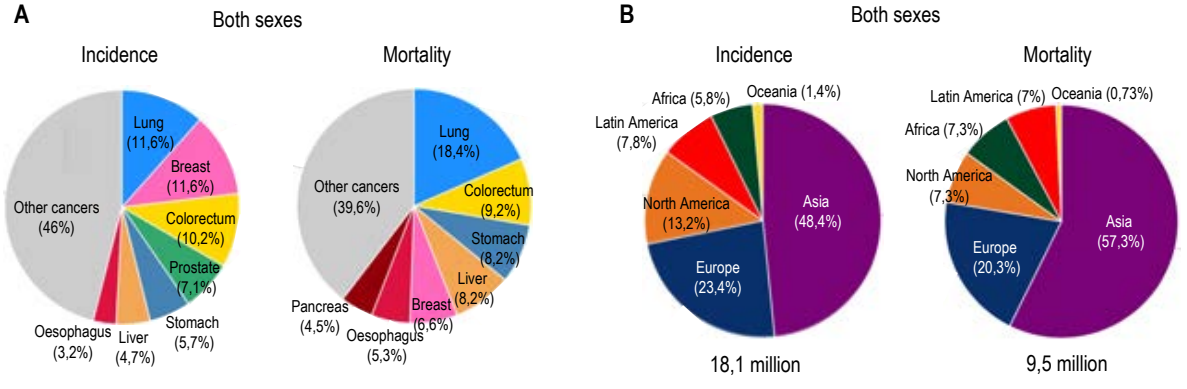

Figure 1. Epidemiology of cancer incidence and mortality worldwide comparing **(A)** cancer types and **(B)** geographical distribution, depicted in a pie chart. As observed in the both charts, the greater the incidence, the greater the mortality. Data source from Globocan 2018[2].

In 2030, 22 million new diagnoses are expected per year[3]. In this scenario, the World Health Organization (WHO) has estimated more cancer-related deaths than those caused by stroke or coronary heart diseases[4]. Thus, this public health problem claims for a better understanding of the disease. The identification of new strategies to allow an earlier detection and a better stratification of the tumors, together with the design of more accurate and less toxic therapies. However, cancer is an extremely complex and continuously evolving with distinct cellular origin and morphology, histological types, mutational profiles and therapeutic responses. These features make cancer not a singular and unique disease, but a collection of hundreds of diseases that represent a clear challenge.

Current therapies do not result in long-lasting benefits mainly due to the spread of the disease and inherited and/or acquired resistance, both key clinical-cancer features that researchers and clinicians face today. Surgery and radiotherapy dominated the field of cancer therapy into the1960s with taxanes and platinum agents used only in determined types of cancer, until investigators noticed radical local treatments had plateaued due to the presence of metastases and the disease relapse. 1970s was the age of adjuvant chemotherapy[5]. Clinicians began to use a combination chemotherapy with vinblastine, methotrexate or 5-flurouracil to cure advanced cancers; some of them currently use in first and second line of treatment in some types of cancer. At that period of time cancer was considered a limited-homogeneous mass of proliferating chaotic cells that had lost its fate and treatments were given to disrupt the proliferative and the DNA replicative activity of the tumor cells[6]. It wasn't until the year 2000, when Hahanan and Weinberg published the hallmarks of cancer[7]. Authors described for the first time the complexity of cancer beyond its proliferative capacity by six biological capabilities or underlying principles, considering these hallmarks as the common features that lead the transformation of normal cells to the tumoral ones. They included sustaining proliferative signaling, evading growth suppressors, resisting cell death, enabling replicative immortality, inducing angiogenesis and activating invasion and metastasis[7]. Chemotherapy transitioned to the age of “targeted therapy.” Antiangiogenic agents and growth signal inhibitors together with therapeutic monoclonal antibodies (e.g. trastuzumab) were implemented into the clinical treatments followed by surgery with successful results in some cancers types[8].

During the last decade cancer research is advancing in many fronts. Further understanding of the molecular cancer biology and its environment have described more key features of these particular cells. We know that cancer is a tightly regulated complex disease, unstable genomically and heterogeneously composed of multiple distinct cell types that interact with other cell types in the microenvironment. This description has led to an extension of the first hallmarks[9]. The emerging hallmarks englobe the potential of genomic instability, inflammation, reprogramming of energy metabolism and evading immune system (Figure 2).

The description of the cancer hallmark principles has promoted the rapidly growing armamentarium of approaches (as illustrated in red in Figure 2) increasingly the therapeutic avenues available, fostering the personalized medicine.

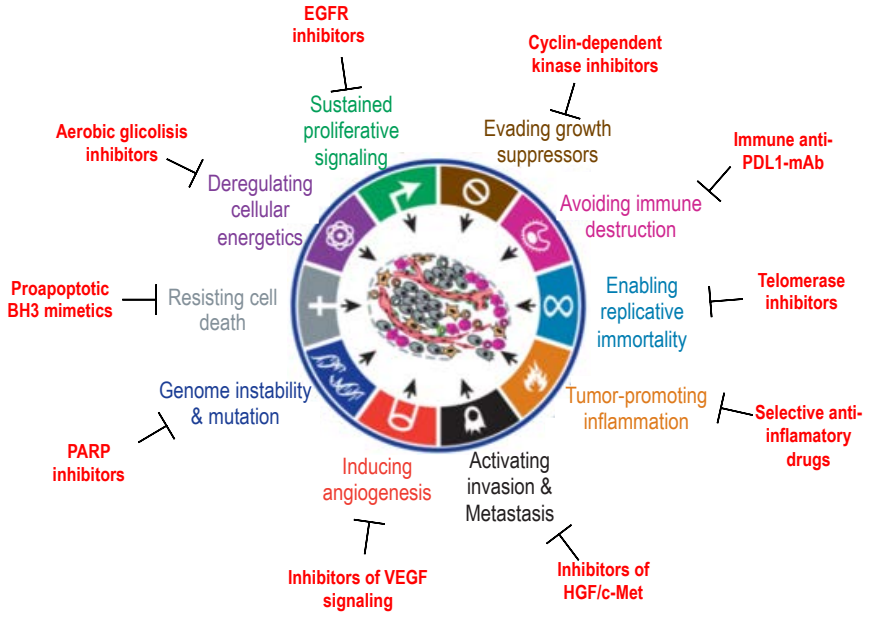

Figure 2. Hallmarks of cancer. Acquired tumor cells capabilities necessary for growth and progression. There is a vast pipeline of candidate drugs with different molecular targets and modes of action in development for most of these hallmarks (depicted in red) or in some cases already approved for clinical use in treating certain forms of human cancer. Adapted from Hanahan and Weinberg[9].

Molecular targeted therapies and immunotherapy are the major breakthroughs in cancer treatment for the last decades. PARP inhibitors have impacted in the ovarian cancer landscape, particularly for those patients with *BRCA*-mutated tumors and recurrent disease with three agents recently approved by the Food and Drug Administration (FDA)[10]. Lately, immunotherapy has produced a paradigm shift in clinical oncology. The objective is to trigger the natural immune response to drive a better response to fight cancer. An explosion of new therapies that involve the immune system have started with the development of anti-PDL-1 checkpoint inhibitors followed by anti-CTLA-4 agents. For example, *Nivolumab*, one of the first immune-agents FDA approved to metastatic melanoma and lung cancer has considerably increased the patient survival while no other options were available for these patients[11]. The latest treatment-success occurred in 2018, when a relapsed metastatic-breast cancer patient treated with *ex vivo* modified autologous tumor infiltrating lymphocytes (TILs) mediated a complete and durable regression highlighting the beneficial use of immunotherapy use for these patients[12]. These results are promising, but its efficacy in other tumor types remains to be demonstrated together with the feasibility and cost-effective outcomes of these methods to all cancer patients.

The next objectives in cancer treatment are to search novel targets exploiting its vulnerabilities to increase the means of cancer treatment thereby maximizing patient outcome and ultimately turning cancer into a chronic disease.

1.2 Ovarian Cancer

1.2.1 Epidemiology and survival

Ovarian cancer (OC) comprises a heterogeneous group of malignant tumors that originates from the ovaries, fallopian tubes or peritoneum[13]. These closely localized tissues share molecular and histology similarities and are managed in the same manner[14]. Altogether, OC ranks as the eighth most common cause of cancer death among women worldwide[2] and it is considered the most lethal gynecological malignancy[15]. Based on the last Globocan data, the worldwide number of estimated new cases in 2018 rises up to 295.414 and the mortality is situated in 184.799 cases[2]. The incidence of OC exhibits a wide distribution with highest age-adjusted incidence rates observed in the developed parts of the world (North America and Central and Eastern Europe with 8,4% and 9,5% respectively), intermediates in Asia (6,4%) and lowest in South America and Africa (6,1% and 5,1%). In Spain, 3.412 new cases were diagnosed in 2017 with a mortality frequency of 1.960 cases[16]. The OvarCost Study reports a disease burden that ranges between 52.061 to 67.684 euros per OC patient reflecting a significant cost to the national health system and to the society as a whole[17].

Woman's lifetime probability of developing OC is 1 in 75, whereas the risk of dying is 1 in 100[18]. The five-year survival rate is below 60% but this rate varies depending on the stage at the time of diagnosis. When OC is localized within the ovary (stage I), the 5-year survival rate raises up to 92%[18], but only a few cases (15%) are diagnosed at this stage, since there are no effective OC screening tools. Instead, OC is frequently presented at late stage (stage III or IV) when the 5-year relative survival rate is only 35%[19].

1.2.2 Risk factors: the importance of the genetics

Established risk factors for OC include lifestyle, age, postmenopausal hormonal therapy and oral contraceptives use, infertility, endometriosis and the most contributing, genetics[20]. It is well-known that women with a family history of OC are themselves at higher risk to suffer OC. The risk for women with one affected first-degree relative is potentially three times greater that for women with no affected relatives[21]. A high proportion of hereditary cancers are due to alterations in genes involved in the homologous-recombination (HR) DNA repair pathway, although such alterations are also common among women with not family history of OC or breast cancer[22]. Prominently, germline mutations in *BRCA1* and *BRCA2* genes are implicated in approximately 24% of OC cases[23,24] most commonly in the high grade serous ovarian cancer (HGSC), a subtype of OC[25]. Both the location of the *BRCA* mutations within the gene and the type of mutation might influence the risk of developing ovarian cancer[26].

Germline mutations in *BRCA1* are associated with the highest rate of OC risk (39%) and 11% of risk for those harboring *BRCA2* mutations[27]. Besides *BRCA* genes, there are alterations in other genes involved in the DNA repair homologous recombination complex that potentiate the risk of suffering OC[28]. This includes mutations in genes such *CHEK2*, *MRE11A*, *RAD50*, *ATM* and *TP53*[29,30] and those that are part of the Fanconi anaemia–BRCA pathway, such as *RAD51C*, *RAD51D*, *BRIP1*, *BARD1* and *PALB2*[25,31,32]. Additionally, the Lynch syndrome can also increase the risk of OC for 4-11%, most commonly in endometrioid and clear-cell carcinomas, two OC subtypes[33]. Lynch syndrome is characrerized by the inheritance of germline mutations in genes involved in the DNA mismatch repair system — namely, *MLH1*, *PMS2*, *MSH2* or *MSH6* (e.g. *MSH2* mutation predispose 24% of OC risk)[34]. Curiosly, near 70% of Lynch-associated OC are diagnosed at earlier stage with an overall survival of 80%; compared to 65% of *BRCA*-driven cancers that are diagnosed in advanced stages with overall survival of 35%[35]. Factors related to lifestyle (depression, smoking or obesity) might affect also the risk of OC[18]. Interestingly, a recent study correlated the consumption of fried food with a 2-fold increase to suffer OC[36] and another study reports that parity and tube ligation are features also associated with an increase in the OC risk[37].

1.2.3 Histology of OC: a heterogeneous disease

OC can be subdivided into different histological subtypes that have different cells of origin, molecular compositions, clinical behavior and treatments[38,39]. These histological subtypes include epithelial cancers (EOC) that account for ~90% of OC and include HGSC (70% of the cases), endometrioid (10%), clear-cell (10%) mucinous carcinomas (5%) and low-grade serous carcinoma (5%) Features of these tumors are described in 1 (page 11). The 10% left accounts for non-EOC including tumors from germ cell, sex cord stromal origin and hypercalcaemia-associated small-cell carcinomas (SCCOTHs)[38].

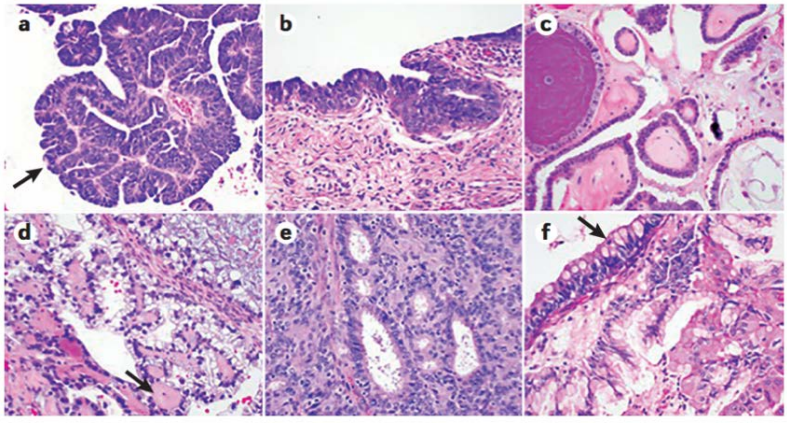

Figure 3. Histological subtypes of EOC. (A) HGSC is characterized by severe nuclear atypia, high nuclear-to-cytoplasmic ratio and abundant mitoses. Papillary architecture (arrow) is also present. **(B)** STIC lesions share the same morphological features as HGSC, with severe atypia, mitoses and lack of polarity. **(C)** Low-grade serous carcinoma shows papillary architecture, but only mild nuclear atypia and a lower nuclear-to-cytoplasmic ratio. **(D)** Clear-cell carcinoma is characterized by large atypical tumor cells with frequent clearing of the cytoplasm and stromal hyalinization (arrow). **(E)** Endometrioid adenocarcinoma is characterized by gland formation that

recapitulates endometrial glands and is graded based on cellular architecture and nuclear atypia. **(F)** Mucinous adenocarcinoma shows mucin-filled tumor cells, with frequent goblet cell forms present (arrow). Adapted from Matulonis *et al.,*[38].

Epithelial tumors can also be classified by histologic grading, which represents the grade of differentiation regarding the architecture of OC cells. This histological grade correlates also with prognosis. Grade 1: well differentiated. Cancer cells resemble normal cells and less aggressive cells. Grade 2: moderately differentiated and grade 3: poorly differentiated cancer cells, linked to the most aggressive cells.

1.2.4 Molecular biology of OC: a disease with genomic complexity

Molecular analyses performed on OC tissues, primarily based on next-generation sequencing, have uncovered a massive genetical and genomic variability and diversity within each specific OC histological type and even inside the individual tumor[40]. The molecular histology diversity allows further refinement of OC classification providing a more simplified molecular-scheme of OC classified as type I or type II tumors[41] (1; page 11). **Type I tumors** englobes low–grade serous carcinoma, endometrioid, mucinous and clear-cell carcinomas. Basically, these tumors are generally characterized by genomic alterations in *CDKN2A*, *PIK3CA*, *PTEN* genes, regulators of the mitogen-activated protein kinase pathway (MAPK) (e.g. activating mutations in *BRAF* or *KRAS*) and alterations in genes encoding β-catenin signaling pathway (e.g. *CTNNB1*)[42–44]. Mutations in *TP53* are rarely seen in these tumors, with the exception of mucinous carcinoma in which *TP53* mutations occur quite frequently (50%)[45]. Clear-cell carcinomas have inactivating mutations in *ARID1A*[46] (a tumor suppressor gene involved in chromatin remodeling) and amplification of *ERBB2* (gene encoding for HER2) in 14% of the cases and in 19% of the cases in mucinous tumors[47].

On the other hand, genomic characterization of the most clinically aggressive **type II tumors** (HGSC) have revealed a high degree of genomic/chromosomal instability. HGSC are mainly characterized by mutations in the tumor suppressor gene, *TP53* (more than 96% of the cases, according to the TCGA)[48,49]. Additionally, high rates of somatic and germline genomic defects in *BRCA1*/2 genes (more than 20%) as well as in other HR related genes (e.g. *RAD51D* or *CHEK2*) have been reported in HGSC patients (1). Hypermethylation of the *BRCA1* promoter has also been shown in a substantial subset of HGSCs[48]. Moreover, other recurrent alterations that can be found in this type II tumor englobes malfunctioning of FoxM1, Notch, phosphoinositide 3-kinase (PI3K) or RAS–MEK signaling pathways as well as high percentage of gene copy number variations in genes encoding proteins in these pathways. Other altered genes frequently found and that could also serve as potential therapeutic targets for OC include *MYC*, *AURKA*, *ERBB3*, *CDK2*, *mTOR* and *BRD4*[38,48]. The number of alterations in multiple

signaling pathways and in different OC types illustrates the genomic complexity of OC. Indeed, next high-throughput technologies will continue delivering a more accurate basis for tumor biology, leading to more detailed signaling pathways alterations and models of OC complexity.

1.2.5 Etiology

Historically, one of the main reasons why the biology and evolution of OC have been so difficult to understand is because most tumor cells do not phenotypically resemble any normal cells in the ovary[50]. Recent molecular discoveries support the different origins of OC subtypes. Most of the OC types (serous, clear cell carcinoma, mucinous and endometrioid tumor), primarily arise from cells that are not normally located in the ovary, while germ cell and sex cord stromal tumors have a clearly anatomical evidence of origin within the ovary[51,52]. The latter ones are confined into the ovary and show histological, immunophenotypic and endocrinological similarities to normal granulosa cells[53]. Mutations in the gene *FOXL2*, that regulates the physiological activity of granulosa cells, through the TGFβ signaling pathway seems to induces granulosa cell tumors[54,55]. Table 1 summarizes all types of OC and its possible origin. On the other hand, the most common ovarian carcinomas are thought to arise from cells that are not normally present in the ovary, however, these cells are linked with ovary development. Most of the HGSC cases start in the fallopian tube epithelium (FTE) through the development of precursors lesions, named as serous tubal intraepithelial carcinomas (STICs). STICs are characterized by DNA damage, mutations in *TP53* and increased proliferative Ki67 expressing cells with reduced number of p21 and p27 positive cells[56]. Evolutionary analyses identified a window of seven years between development of a STIC and the initiation of OC, with metastasis following rapidly thereafter[57,58]. A recent study revealed that the DNA methylomes between HGSC and FTE are significantly and consistently more highly conserved than the methylome between HGSC and ovarian surface epithelial (OSE) cells supporting the hypothesis that HGSC arise from the fallopian tube[59]. STICs can be identified in 60%-80% of HGSC cases[56], so STICs are not found in all patients with HGSCs and alternative pathways for the pathogenesis of HGSC coexists[60]. Other authors have proved that not all HGSC arise from STICs, instead, there are some HGSC that might arise from OSE. A report from Coscia *et al.,* identified a 67-protein signature that separated HGSC into a two predominantly epithelial and mesenchymal tumor clusters, resembling and clustering with FTE and OSE cells ººrespectively, suggesting that a likely origin of HGSC either from the FTE or from the OSE is possible[61].

For mucinous carcinomas, it is thought they are more likely to be metastasis to the ovary, mainly from gastrointestinal tract cancers, pancreas and cervix/endometrium than from the ovary itself[62,63]. For endometrioid and clear cell carcinomas, many studies support that precursor lesions of these diseases

are retrograde endometriosis, since it was found that benign and malignant lesions coexisting in the ovarian tumors, but it is still not known how the precursors develop[50].

Finally, the SCCOHT subtype is the ovarian tumor with still unknown origin, because neither the tumor cell histology nor the phenotype resembles any normal cell in the ovary nor the rest of the peritoneal cavity. Recently, recurrent inactivated somatic or germline mutations in *SMARCA4* (a gene involved in the SWI/SNF chromatin remodeling complex) were identified in this type of OC. SCCOHT tumors show histological and genetic similarities to malignant rhabdoid tumors of the brain and other organs, which are caused by somatic or germline mutations in *SMARCB1,* other component of the SWI/SNF complex[64]. These observations have led to a proposal that SCCOHT is essentially a rhabdoid tumor of the ovary[50]

Table 1. Origin, clinical presentation and molecular features of the different subtypes of OC.

Histology	Type	Histology subtype	Possible origin cells	Precursor lesions	Familiy risk	Grade	Incidence	Age (years)	FIGO Stage	Clinical findings	Response to therapy	Frequency of mutations	Copy number alteration
Epithelial (90%)	I	**Endometrioid**	Endometrial epithelial cell	Endometrioid borderline tumour	Lynch syndrome (MLH1, PMS2, MSH2 and MSH6)	G1-2	<5%	40-50	I-II	Can be associated with endometriosis	Initially sensitive to the standard platinum-based therapy, but reccur	*BRAF* (24%) *PIK3CA* (12%) *PTEN* (14-31%) *ARID1A* (30%) *CTNNB1* (24%)	-
						G3	>5%	40-50	III-IV		Resistant to platinum-based chemotherapy		
		Clear cell	Endometrial epithelial cell	Endometrioid borderline tumour	Lynch syndrome (MLH1, PMS2, MSH2 and MSH6)	G3	10%	55	III	Can present with parenchymal metastases (in the liver and the lungs)	Resistant to platinum-based chemotherapy	*KRAS* (1-7%) *PIK3CA* (25-33%) *PTEN* (5%) *ARIAD1A* (46-57%)	*ERBB2* (14%)
		Mucinous	Unknown; normal ovarian cell, somatic cell within a teratoma or endometriosis	Mucinous borderline tumour, Brenner tumour or teratoma	NA	G1-G2	>5%	45-50	I-II	Presents in younger patients and is typically disseminated	Resistant to platinum-based chemotherapy	*BRAF* (5-23%) *KRAS* (50-68%) *PIK3CA* (14%) *PTEN* (3%) *ARID1A* (9%) *CDKN2A* (19%) *TP53* (52-57%)	*ERBB2* (12-19%)
		Low-grade serous (LGSC)	Fallopian tube secretory epithelial cell or progenitor cell	Serous borderline tumour	NA	G1-G2	<5%	40-55	I-IV	Presenter in younger patients Can be early or late stage at presentation	Responde better to standard treatments	*BRAF* (16-38%) *KRAS* (19-35%) *PIK3CA* (11%) *PTEN* (20%)	-
	II	**Serous**											
		High grade serous (HGSC)	Fallopian tube secretory epithelial cell or progenitor cell	STIC	BRCA1, BRCA2, BRIP1, PALB2, RAD51C and RAD51D - Anemia Fanconi	G3	70%	60-70	III-IV	Can present with peritoneal carcinomatosis, ascites and/or pelvic mass . Typically advanced stage at presentation. Most aggresive	Initially sensitive to the standard platinium-based therapy, but the majority recur	*TP53* (96%) *BRCA1* (12%) *BRCA2* (11%) *RB1* (2%) *NF1* (4%)	*MYC* (31%) *MECOM* (22%) *CCNE1* (20%) *EIF5A2* (18%) *PIK3CA* (17%) *AKT2* (6%) *AURKA* (3%) *RB1* (7%)
Non-epithelial (10%)		**Sex-cord stromal**	Granulosa cell	None	NA	G1	<5%	40-50	I-II	Confined to the ovary	Surgery	*FOXL2*	-
		Germ cells	Granulosa cell or other stromal cell	None	DICER1 Syndrome	G1	<5%	40-50	I-II	Confined to the ovary	Surgery	*DICER1*	-
		SCOOHT	Unknown; normal ovarian cell or somatic cell within immature teratoma	None	RTPS2 (*SMARCA4*)	G1-G3	<1%	20-30	I	Confined to the ovary	Resistant to platinum-based chemotherapy	*SMARCA4* (100%)	-

1.2.6 Diagnosis, screening and staging

Clinical presentation

OC lacks specific warning symptoms. Early signs are vague, non-specific and initially missed or attributed to gastrointestinal disturbances or aging (e.g. early satiety, diarrhea, fatigue or gastrointestinal reflux)[65]. Consequently, the diagnosis is delayed and most patients (70%) are detected in late stage (either stage III or IV) when the cancer has spread to the abdominal cavity and symptoms become apparent, severe and require intervention to palliate them[66]. Late signs include accumulation of ascites, gastrointestinal dysfunction, abdominal bloating, pelvic pain and shortness of breath[66]. These symptoms, and the late presentation largely applied to HGSC patients. By contrast, due to its biology presentation clear and small-cell carcinomas become symptomatic at an earlier stage (30%), usually caused by the pressure and pain of the ovarian masses into the bowel and/or urinary track system. The median age of diagnose is 63 years[19].

Current diagnostic pipeline

Patients with the abovementioned symptoms follow a diagnostic workflow that includes physical examination and radiographic imaging combined with the CA-125 blood test and ultimately laparoscopy surgery. **Physical examination** includes the bimanual pelvic and rectovaginal palpation. These physical tests are limited to irregular ovarian masses (benign or malignant) or nodules that can be found in the uterus. A physical palpation of the abdomen may reveal the presence of ascites. These methods are a first filter to the gynecologist but lack accuracy as screening tests and as a way to distinguish benign from malignant lesions[67]. **Imaging methods** include ultrasonography to assess the presence of ovarian masses and ascites, combined with magnetic resonance imaging (MR) or computed tomography (CT)[68]. MR or CT provide information about the size, location and level of complexity of ovarian masses helping clinicians to determine the level of suspicion for cancer[38]. **CA-125** is a blood biomarker currently into the clinical practice to monitor OC. Although more than 85% of advanced diseases have elevated CA-125 levels (>35 U/mL), the test is not sensitive enough to diagnose early disease (only 40% of stage I patients have elevated CA-125 levels) and 6% of women without cancer have levels superior than 35 U/mL. In addition, CA-125 might be elevated in other disease related to the peritoneum[69]. To confirm the suspicious of OC, **laparoscopy surgery** must be performed to take a biopsy from the ovarian tumor (if feasible; in some cases it is not allowed to avoid disease extension) or a peritoneal implant[70]. Histopathological analysis confirms the malignancy and also gives further information on the tumor histology. Therefore, the **final diagnosis** is not determined until the surgery is performed.

Staging

Based on the findings reported during the exploratory surgery by the gynaecological oncologist, and the histological tumor analysis carried out by the pathologist, each tumor is formally given a **stage.** The stage of the disease is given by the size and localization of the tumor cells into the nearby organs and the peritoneal cavity. The International Federation of Gynecology and Obstetrics (FIGO) system is used to determine the stage of the disease. FIGO system was first published in 1973, but advances in the origin, histology and subtypes urged to revised and actualized the system in 1988 and 2014[71] (Table 2). Staging is the **gold standard** used by the clinicians to determinate the severity of the patient, predict long-term outcome and to plan the appropriate treatment regimen.

Table 2. FIGO Staging of OC. TNM classification of malignant tumors. (N) Regional nodes: (Nx) Regional lymph nodes cannot be assessed; (N0) No regional lymph node metastasis; (N1) Regional lymph node metastasis. (M) Distant metastasis. Adapted from Mutch and Prat[71].

FIGO staging classification for cancer of the ovary, fallopian tube and peritoneum	Corresponding TNM stage
Stage I: Tumor confined to ovaries or fallopian tube	**T1-N0-M0**
IA: Tumour limited to one ovary (with ovarian capsule intact) or fallopian tube; no tumour on ovarian or fallopian tube surface; no malignant cells in the ascites or peritoneal washings	T1a-N0-M0
IB: Tumour limited to both ovaries (with ovarian capsules intact) or fallopian tubes; no tumour on ovarian or fallopian tube surface; no malignant cells in the ascites or peritoneal washings	T1b-N0-M0
IC: Tumour limited to one or both ovaries or fallopian tubes, with any of the following C substages: • IC1: surgical spill intraoperatively • IC2: capsule ruptured before surgery or tumour on ovarian or fallopian tube surface • IC3: malignant cells in the ascites or peritoneal washings	T1c-N0-M0
Stage II: Tumour involves one or both ovaries, or the fallopian tubes with pelvic extension below the pelvic brim or primary peritoneal cancer	**T2**
IIA: Extension and/or implants of tumour on uterus and/or fallopian tubes and/or ovaries	T2a
IIB: Extension of tumour to other pelvic intraperitoneal tissues	T2b
Stage III: Tumour involves one or both ovaries, or the fallopian tubes, or primary peritoneal cancer with cytologically or histologically confirmed spread to the peritoneum outside the pelvis and/or metastasis to the retroperitoneal lymph nodes	**T3**
IIIA: Metastasis to the retroperitoneal lymph nodes with or without microscopic peritoneal involvement beyond the pelvis	T1, T2, T3 a N1
IIIA1: positive retroperitoneal lymph nodes only (pathologically proven)	T3a/T3aN1
• **IIIA1(i):** metastasis up to 10 mm in greatest dimension	
• **IIIA1(ii):** metastasis >10 mm in greatest dimension	
IIIA2: microscopic extrapelvic (above the pelvic brim) peritoneal involvement with or without positive retroperitoneal lymph nodes	T3a2/T3aN1
IIIB: Macroscopic peritoneal metastasis beyond the pelvis up to 2 cm in greatest dimension, with or without metastasis to the retroperitoneal lymph nodes	T3b/T3bN1
IIIC: Macroscopic peritoneal metastasis beyond the pelvis >2 cm in greatest dimension, with or without metastasis to the retroperitoneal lymph nodes (includes extension of tumour to capsule of liver and spleen without parenchymal involvement of either organ)	T3c/T3cN1
Stage IV: Distant metastasis excluding peritoneal metastases	**Any T, any N or M1**
IVA: pleural effusion with positive cytology	
IVB: parenchymal metastases and metastases to extra-abdominal organs (including inguinal lymph nodes and lymph nodes outside of the abdominal cavity)	

Screening and biomarkers

Despite many efforts to identify an effective approach for OC screening, to date no screening test has proven to be effective in reducing OC mortality. Due to the lack of sensitivity and specificity, CA-125 is not recommended for screening asymptomatic patients. Experts agree that biomarkers for early cancer detection should be proven in samples taken before the diagnosis, the stage at which the test would be used in the clinic. At this step any biomarker has rendered good success in OC, as discussed in the review *Missing the Mark*[72]. Most of the biomarkers evaluated were only able to distinguish between healthy controls and subjects with already diagnosed cancer, but most of them were intended to detect the disease when cancer is budding and confined to the ovary, before the symptoms develop[72]. One of the major screening studies carried out was the UKTOCS program (United Kingdom Trial of Ovarian Cancer Screening)[73]. This phase I trial evaluated prospectively the levels of CA-125 in an algorithm termed 'risk of ovarian cancer algorithm' (ROCA). More than 200.000 women were randomly assigned into one of three groups of studies (ROCA (CA-125 levels), ultrasonography or no screening) with a follow-up of 11 years. The proportion of women diagnosed with OC was similar between the three groups but a higher proportion of women diagnosed at lower stages (stage I–IIIA) was observed in the ROCA-screened group. Nevertheless, there was no difference in mortality rate between patients in the ROCA group and those who received transvaginal ultrasonography. Therefore, ROCA test cannot currently be recommended as a screening strategy for OC[38]. The newest serum biomarker is the **Human Epididymis Protein 4** (HE4) that was cleared by the FDA to monitoring patients with a known diagnosis of OC, able to detect recurrence 2 to 3 months in advance of CA-125 levels. HE4 was found to be elevated in more than half of the OC patients who did not have elevated CA-125 levels. However, like CA-125, it does not have a pre-diagnostic indication from the FDA, just in the recurrence. Many efforts are being made in direction to find novel biomarkers not only in blood, also in other body fluids such as saliva or uterine lavages, that might help to improve OC diagnosis[74].

1.2.7 Therapeutic options in OC

Currently there is no cure for advanced OC. Due to the lack of effective screening strategies to detect early OC, most of the patients are diagnose at late stage where the disease has already spread to the rest of the peritoneal cavity. Therefore, the primary aim of treatment at the moment is to maximize cancer control and to palliate the advanced disease consequences for as long as possible. The two main therapeutic strategies for most OC patients are surgery and platinum/taxane-based chemotherapy.

Surgery: the gold standard for OC treatment

Debulking surgery aims to remove much of the tumor to a state of no detectable residual disease. Surgical cytoreduction results are frequently referred to as suboptimal (that is, any focus of residual tumor larger than ≥1 cm in size (R2 resection)), optimal (that is, <1 cm residual cancer (R1 resection)) or no evidence of residual macroscopic disease (R0 resection). Importantly, many studies have demonstrated that patients whose tumors have optimally debulked (R0) have significant improvements in outcomes, both in OS and PFS compared to patients with remaining post-surgery visible tumors (R1 or R2)[75–77]. Thus, a good outcome on surgical cytoreduction is a prognosis factor for improved disease-free and OS in OC. Different surgical strategies are followed depending on the spread of the tumor and its potential cytoreduction. When tumors are confined to the ovaries (Stage I-II) the ovaries are removed in a hysterectomy with bilateral salpingo-oophorectomy. Then, the histopathological examination of the tumor (grade) and possible tumor focus in adjacent tissues will determine the administration of adjuvant chemotherapy or not (Figure 4). In the cases of advanced OC (Stages III-IV), according to the potential resectability capacity, two lines of treatment can be applied:

(1) Primary debulking surgery followed by adjuvant chemotherapy (in those cases that is feasible to reduce the metastasis disease by laparoscopic surgery and then give the chemotherapeutic agents[78]).

(2) Initial neoadjuvant chemotherapy (NACT) followed by the debulking surgery and ultimately another round of chemotherapy as illustrated in Figure 4. The use of NACT is especially indicated for patients with extensive tumor burden to allow macroscopic complete resection and reduce the tumor burden[38].

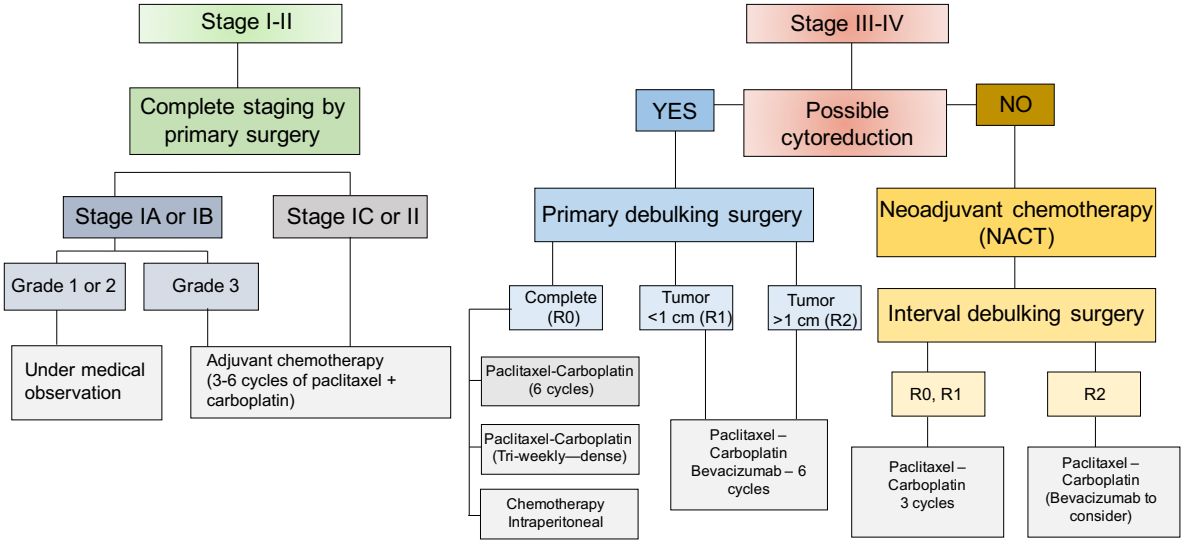

Figure 4. Scheme treatment for early and late OC stage. Adapted from SEGO Oncology Guide[78].

The primary debulking surgery and NACT represent the two-major clinical treatment subgroups of advanced OC. Recently, two randomized trials have reported no difference in the OS nor in the PFS when comparing primary debulking surgery and NACT approaches[79,80]. However, NACT treatment was associated with less morbidity, higher rate of optimal cytoreduction, less blood and ascites loss, as well as less invasiveness and adverse effects due to the surgery[81,82].

Standard Chemotherapy

The accepted standard chemotherapy is six cycles of platinum derivates (*carboplatin* or *cisplatin*) combined with taxanes agents (*paclitaxel* or *docetaxel*)[38]. The administration of chemotherapy depends on the cancer stage, grade and histology. Many patients with grade I do not receive chemotherapy (the surgery eliminates all tumor burden), but those in stage IC-III undergo adjuvant systemic platinum-based chemotherapy that led to an improvement in OS[83]. Advanced OC patients undergo NACT chemotherapy that consists in carboplatin and paclitaxel for three cycles, followed by interval (that is, surgical reduction) and then additional round of chemotherapy post-surgery with a total of six cycles of chemotherapy.

For these patients, the standard is the **combination chemotherapy** with either intravenous carboplatin (starting dose AUC 5–6) and paclitaxel (175mg/m^2) or intraperitoneal cisplatin (100 mg/m^2) and paclitaxel (60mg/m^2), with evidence to support the addition of bevacizumab (7,5-15 mg/kg) every three weeks in selected patients[84]. Although intraperitoneal chemotherapy has been shown to be associated with better PFS and OS (GOG 172 trial reported an increase of 5,5 months in PFS and 5,9 months in OS compared to intravenous chemotherapy) it is not widely used because the increase toxicity and the catheter-related problems prevent the whole schedule-treatment administration in a lot of patients[85,86]. In the GOG 172 trial only 20% of patients in the intraperitoneal group completed 6 cycles of the assigned therapy due to toxicity.

Several efforts have been made to prolong the survival and preserve the quality of patients' life with **maintenance therapy**[87,88]. The widely and currently agent used is *Bevacizumab*, approved as maintenance therapy followed by initial platinum and taxane chemotherapy based on the results from the trials GOG 218 and ICON7 (as explained in section of 1.2.9 Targeted Therapies). Nowadays, the most-promising maintenance-therapy is *Olaparib*, a PARP inhibitor, FDA approved for those *BRCAmut* HGSC patients with recurrent platinum sensitive OC. 60% of patients receiving this compound remained progression-free at three years compared to 27% on placebo group following platinum-based chemotherapy[89].

Recurrence

Although initially more than 80% of the patients response to the first line chemotherapy[87], within the 15 months of the initial treatment, 85% of these patients will develop recurrent disease, which is generally incurable[38,90]. Recurrent OC patients are classified as platinum-sensitive or platinum-resistant. The basis of platinum free interval (PFI) is defined as the period of time "free of recurrence" elapsed between the last cycle of chemotherapy and the first evidence of disease progression. Those patients that relapse in <6 months after initial treatment are considered as **platinum-resistant and platinum-sensitive** for those patients with relapse >6 months. This classification has served as the basis for inclusion criteria in clinical trials or drugs approvals[91]. In fact, treatment options for recurrent OC depends on the PFI. The standard of care for platinum sensitive patients is repetition with platinum/taxane based regimens with response rates of round 50%[92] and more recently with the inclusion of the targeted therapies such PARP inhibitors. Unfortunately, the disease-free period last only few months after some lines of therapy until patients are declared platinum resistant. For those platinum refractory patients, the standard drugs used are anthracyclines (e.g. *Doxorubicin* or *Liposomal Doxorubicin*), topoisomerase inhibitors (e.g. *Etoposide*), nucleoside analogues (e.g. *Gemcitabine*) or Alkylating agents (e.g. *Hexamethylamine*)[87]. Nonetheless, the response rate with these agents in platinum-resistant tumors is only 10–25%[93]. This diminishing response rate is in part due to the development of drug resistance. Despite the fact that most tumors are chemosensitive at first, most tumors acquire resistance thereafter. Considerable progress has been made in understanding molecularly drug resistance, and this has served the basis for the development of novel therapeutic strategies in OC[87].

1.2.8 Molecular chemo-sensitive and resistance landscape

Molecular analyses, primarily based on high-throughput sequencing results, are providing insights about the sensitivity to chemotherapy in certain genetic contexts, but also about the clonal selection and tumor evolution that may be associated with development of chemoresistance. Patients harboring mutations in ***BRCA1* or *BRCA2*** genes and treated with platinum-based adjuvant chemotherapy undergo a more favorable treatment response with longer PFS and OS[94–96]. *BRCA1*/2 genes play multiple and unique roles in HR repair. *BRCA1* is part of a larger molecular complex that helps to survey the DNA for double strand break (DSB) damage[97]; and *BRCA2* has a direct role in repair by assisting the *RAD51* complex in attaching to the repair site[98]. As platinum drugs crosslink the DNA causing DSB that is lethal to the cells[99]; dysfunction of these two proteins makes these *BRCA*-mutant patients more sensitive to DNA-damaging chemotherapy. However, in acquired resistance tissues, the presence of multiple independent reversion mutations of *BRCA1*/2 restores the wild-type *BRCA* reading frame, resulting in a functional BRCA protein, increasing the platinum resistance[100].

Patch and colleagues performed a whole-genome sequencing of 92 HGSC patients involving sensitive and matched resistant tissues[101] with the goal to understand the molecular complexity that underlies the resistance. They reported that acquired resistance was in part due to inactivation of tumor suppressors genes including *RB1*, *NF1*, *RAD51B* and *PTEN*, which contribute to increasing the platinum chemotherapy resistance[101]. Besides, they observed amplification in the chromosome 19q12 locus, which includes *CCNE1* (Cyclin E) also linked to platinum resistance[102]. An abundance on this cell cycle regulator leads the activation of *BRCA1/2* transcription, increasing BRCA protein levels, conferring platinum resistance[48]. Other mechanism that could explain the platinum resistance is the up-regulation of the *ABCB1* gene, that leads the overexpression of the drug efflux pump multidrug resistance protein 1 (MDR1)[101]. This molecular description of chemo-resistance facilitates the comprehension of OC and facilitates individualized treatment selection.

1.2.9 Targeted therapies in OC

Despite changes in the schedule administration of platinum-based chemotherapy and improvements in the surgery approaches, a therapeutic plateau has been reached with these methods. The identification of distinct molecular pathways alterations of individual subtypes has triggered interest for the development of targeted therapies for the management of OC[103,104]. Multiple targeted therapies against specific molecular alterations or pathways (as illustrated in Figure 5) are currently being trialed in OC.

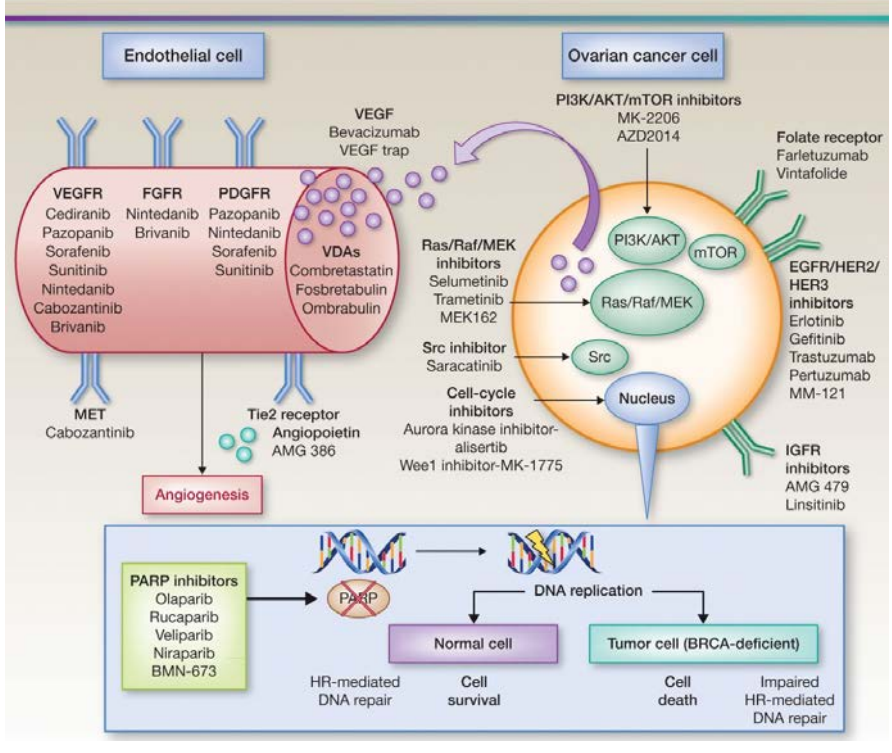

Figure 5. Targeted therapies in OC currently being evaluated. The figure represents the diversity of potential targeted therapeutic approaches that involve different altered molecular pathways. Adapted from Banerjee *et al.,*[103].

Angiogenesis inhibitors

Angiogenesis is necessary for tumor cell survival, growth, and metastasis. Inhibition of this process with existing therapies works synergistically and add therapeutic benefit, in particular, with *Bevacizumab*, an anti-vascular endothelial growth factor (VEGF) antibody[105]. The combination with platinum based-chemotherapy is given as first line treatment and as maintenance therapy in advanced OC patients. Clinical trials (GOG218[106] and ICON7[107]) reported an increase in the PFS when it is added compared to chemotherapy alone. However, the introduction of *Bevacizumab* does not clearly improve the OS, and despite being available in Europe by the EMA, it is not approved by the FDA. Besides, the reported high toxicities and side-effects of *Bevacizumab* are encouraging the study of inhibition other proangiogenic molecules. Interestingly, a recent phase II study have demonstrated that *Cediranib* (other inhibitor of VEGF) in combination with *Olaparib* increases the PFS and the OS in patients with recurrent platinum sensitive OC compared with *Olaparib* alone (16,5 months *vs* 8,8 months and 44,2 *vs* 33,3 months; respectively), suggesting that the two agents may act synergistically[108].

PARP inhibitors

A new successful generation of drugs have emerged targeting PARP enzymes. PARP-1, PARP-2 and PARP-3 are the most abundant of the 17-member superfamily nuclear enzymes that are activated upon DNA damage and have major role in repair the DNA breaks[109]. PARP inhibitors (PARPi) are based on the concept of "synthetic lethality" -targeting one of the genes in a synthetic lethal pair in which the other is defective (e.g. *BRCA* mutation) to selectively kill tumor cells and not normal cells, potentially creating a substantial therapeutic window[103,110]. PARPi results in the accumulation of double-strand DNA breaks that are repaired by the HR pathway, in which BRCA1 and BRCA2 are key proteins[109]. Mutations in *BRCA1/2* compromise DNA damage repair machinery, so that patients with such mutations are more likely to respond to PARP inhibition[111]. Several clinical trials have shown antitumor activity and longer PFS with PARPi compared to placebo among patients with *BRCA* mutation[112–114]. The impact of PARPi may differ according to the *BRCA* mutation status and several analysis suggest that the benefit of PARPi in maintenance therapy, at least in terms of PFS, was larger in germline *BRCA*-mutation carriers[103]. *BRCAness* gene-expression profile or HR deficient tumors are also correlated with longer responsiveness to PARPi[115] and curiously, recent studies also reports beneficial effects of the PARPi *Niraparib*, in non-defective HR tumors compared to placebo[116,117].

Currently there are three PARPi that have been FDA-approved for maintenance therapy in platinum-sensitive recurrent OC: *Olaparib*, *Rucaparib*, and *Niraparib*.

Table 3. PARPi Trials in OC. Review of the PARPi under clinical scrutiny for OC treatment. Table includes the clinical trial reference, the patients' features and the line of treatment.

Agent	Trial	Population	Line of treatment	FDA/EMA APPROVED
Olaparib	**SOLO-1:** Phase III maintenance (Olaparib *vs* placebo) - NCT01844986	BRCAmut; AOC	First line	YES
	SOLO-2: Phase III maintenance (Olaparib *vs* placebo) - NTC01874353	BRCAmut, PSROC	After >2 lines platinum QT	
	SOLO-3: Phase III Olaparib *vs* physician choice QT (standard of care non-platinum based) - NTC02282020	BRCAmut, PSROC	After >2 lines platinum QT	
Rucaparib	**ARIEL 2:** Single arm study -NCT01891344	HGROC	Received >2 prior lines of QT	YES
	ARIEL 3: Phase III maintenace (Rucaparib *vs* placebo) - NTC01968213	HGROC	After >2 lines platinum QT	
	ARIEL 4: Phase III Rucaparib *vs* QT - NTC02855944	BRCAmut; ROC	Received >2 prior lines of QT	
Niraparib	**AQUDRA study:** Single arm phase II study - NTC02354586	HGROC	Must have had 3/4 prior lines of QT	YES
	PRIMA Study: Phase III maintenace (Niraparib *vs* placebo) - NTC 02655016	HRD+VE; AOC	First line	
	NOVA Study: Phase I/II Niparib + Bevacizumab - NTC02354131	HRD+VE; PSROC	No limits on number previous line of QT	
Veliparib	Phase III combination QT followed by maintenance - NTC02470585	BRCAmut; AOC	First line	-
Talazoparib	Phase I/II study - NTC01989546	BRCAmut solid tumors	After > 1 standard QT or no standard Rx	-
	Phase II study - NTC02326844	gBRCA mut, ROC	Progression following a PARPi	

QT - chemotherapy; BRCAmut - mutation in BRCA; gBRCAmut -germline BRCA mutation; PSROC - 'platinum-sensitive' recurrent ovarian cancer; HGROC - high-grade recurrent ovarian cancer; HRD - homologous recombination deficient; AOC - advanced ovarian cancer; Rx - treatment.

Olaparib was the first PARPi FDA approved as maintenance therapy (December, 2014) for *BRCA*-mutated women with recurrent platinum-sensitive OC accordingly to the results obtained from the SOLO-2 trial[118] (Table 3). ***Rucaparib*** is another PARPi approved together with the CDxBRCA test, the first FDA-approved next-generation sequencing-based diagnostic tool to predict *Rucaparib* sensitivity (December 2016)[119]. *Rucaparib* is given in third-line treatment to patients with platinum-sensitive *BRCA*-mutated (germline and/or somatic) advanced OC. ***Niraparib*** is the last PARPi approved for maintenance therapy in all women with recurrent OC who have previously responded to platinum-based chemotherapy (March, 2017)[120]. Importantly, it is the first PARPi for all recurrent OC regardless of the presence of a germline or a somatic *BRCA* mutation. Consequently, and due to the results from the second phase of the SOLO-2 trial, on August 2017, the FDA granted an expanded approval of *Olaparib* for maintenance therapy in recurrent OC patients who have achieved either a complete or partial response to platinum-based chemotherapy irrespective of *BRCA* status. The recent results reported by the second phase of the SOLO-1 trial in which there is a clear benefit giving *Olaparib* in first line treatment for *BRCAmut* patients encourage the approval of *Olaparib* as maintenance therapy[89], but still the FDA has not pronounced about it.

It is importantly pointing out that the combination between PARPi with first-line platinum OC chemotherapy have been tested (e.g. SOLO-2 or ARIEL4 study) but this combinatorial strategy has been

limited due to overlapping myelosuppressive toxicities and further safety studies are required. Additionally, there are multiple clinical trials ongoing for PARPi in combination with other therapies against PI3K/AKT, VEGF, CDKs and KRAS molecular alterations, among others[121].

PI3K/AKT/mTOR Pathway

Alterations associated with genes encoding for components of the PI3K/AKT/mTOR survival network (e.g. *PIK3CA*, *AKT* or *PTEN*) have been identified in type I tumors (see 1). Therapies directed against specific components within this pathway have the potential to interrupt its constitutive signaling[122] but clinically they have shown only a modest activity in OC patients[123,124]. For that, a number of combination therapy approaches involving this class of agents are administered together with chemotherapy or other targeted agents to increase its potential[125]. A phase-II trial is currently investigating the efficacy of *Temsirolimus* (PI3K inhibitor) combined with carboplatin and paclitaxel as first-line therapy in patients with newly diagnosed stage III–IV clear cell carcinomas[126] or the phase I trial that is ongoing evaluating a mTOR1/2 inhibitor in combination with *Olaparib* in recurrent OC[127]. In this line, results from a phase I study show a synergism effect in the combination of an AKT inhibitor, *AZD5363*, plus *Olaparib* in recurrent clear cell OC[128].

RAS/RAF/MEK/ERK Pathway

Clinical trials targeting components of RAS/RAF/MEK/ERK pathway have been carried out in type I tumors given the high frequency of *KRAS* and *BRAF* mutations (see 1). *Selumetinib* a MEK inhibitor was trialed in a phase II study for patients with recurrent low-grade ovarian serous carcinoma with 15% of response rate[129]. Another MEK inhibitor, *Trametinib*, is currently being evaluated in a phase II/III in patients with recurrent or progress low-grade serous OC[130] without results yet. Recently, the efficacy of targeting *KRAS*-mutant in OC was assessed in combination with a CDK4/6 inhibitor, *Palbociclib* (see later), where one-third patients got long-term clinical benefit from the combination[131].

HER-2 therapy

The high frequency of amplification in *ERBB2* gene reported in clear cell and mucinous carcinomas suggested that anti-HER2 directed therapy could be more beneficial in these subgroups. However, rates of response in clinical trials of single agent, *Pertuzumab* or *Lapatinib* have been modest, and no significant change in PFS was observed with the addition of *Pertuzumab* to carboplatin/paclitaxel in a phase II trial of patients with relapsed platinum-sensitive OC[132,133]. However, data from a phase II trial suggest that the combination of *Pertuzumab* with *Gemcitabine* is active in patients with platinum-resistant disease, with a response rate of 13,8% compared to 4,6% in patients receiving *Gemcitabine* with placebo[134].

Immunotherapy in OC

The recent success of immune checkpoint inhibition in melanoma and lung cancer[135,136] has inspired further investigation of these agents in other tumors, including OC. *Pembrolizumab*, *Nivolumab and Avelumab* are checkpoint inhibitors (anti PD-L1 agents) being trialed. However, the results are being disappointing for OC since modest overall responses are reported. For example, the response to *Pembrolizumab* was only 11,5% in recurrent OC and only in those patients with high PD-L1 expressing cells[137]. Additionally, data from a phase II trial that examined the safety and efficacy of *Nivolumab* in patients with platinum-resistant OC showed an overall response of 15% with no significant improved neither in the PFS nor in the OS compared to the placebo group. Surprisingly in this study, PD-L1 expression levels did not respond to *Nivolumab*, indicating that the response is irrespective of PD-L1 status[138]. Similar results are reported for *Avelumab*; where a multicenter phase III trial with the recruitment of 998 women, the agent exhibited only a response rate of 9,5% without any increase in the PFS[139,140].

It is worth nothing the phase I/II TOPACIO/KEYNOTE-162 trial where the combination of *Pembrolizumab* plus *Niraparib* is being evaluated in patients with recurrent OC[141]. The goal is to know whether combining both drugs will give better efficacy in recurrent OC. Preliminary findings from this study showed that the overall response rate was 25% and the PFS was 9,3 months higher than a platinum-based chemotherapy. Interestingly, in the 12 patients with *BRCA*-mutated tumors, the overall response was up to 42%, highlighting the synthetic lethally produced by the PARPi and the triggered immune stimulation[142].

CDK4/6 inhibitors

CDK4/6 inhibition is an emerging cell-cycle therapy currently used in the clinics for breast cancer with two FDA-approved agents, *Palbociclib* and *Ribociclib*[143]. In OC, CDK4/6 inhibitors have shown promise *in vitro*, with better response linked to the mutational status of *CDKN2A* and *RB* genes[144]. However clinical data regarding CDK4/6 inhibition is still being evaluated. On the one hand, the CDK4/6 inhibitor *Abemaciclib* given in monotherapy produce stable disease[145] and two clinical trials of CDK4/6 inhibition in combination with platinum and taxanes based-chemotherapy have been recently opened[146,147]. This year, Xue *et al.,* reported in SCCOHT tumors the efficacy of CDK4/6 inhibitors both *in vitro* and *in vivo* with mice models. The *SMARCA4* lost causes a profound downregulation of Cyclin D1, which limits CDK4/6 kinase activity in SCCOHT cells and leads to susceptibility to CDK4/6 inhibitors[148], encouraging the potential evaluation of *Palbociclib* in clinical trials with this type of OC. These results emphasize the emerging successful application of newly developed cell cycle targeted therapies as treatment in OC.

1.3 Targeting cell cycle in cancer

1.3.1 Cell cycle: a special focus on mitosis

Cell cycle is an evolutionarily conserved process that allows the growth and development of mammalian cells. The entire process is driven by an orchestration of sequential series of events that leads the faithful transmission of the genetic information into two daughter cells[149]. Cell cycle is classically divided into four phases G1, S (DNA synthesis), G2, and M (mitosis). Some cells might enter into a G0 stage, where cells are quiescent, in a resting state. Proliferative stimuli, like growth factors and nutrients, stimulate cells to enter G1 where the cell is prepared for DNA synthesis. In S phase, DNA is replicated and in G2 cell prepares to undergo mitosis. In M phase, the genetic material is equally distributed to the forthcoming daughter cells followed by the separation of the cytoplasm, defining the completion of one cell cycle (Figure 6). The rhythm of cell cycle progression is marked by the activity of the **cyclin dependent kinases** family (CDKs), a set of serine/threonine kinases that represent the major cell cycle regulators. CDK activity is subjected to a tight spatial and temporal regulation[150] by sequential waves of synthesis and degradation of cyclins that are translated into activation and inactivation of the CDK kinases[151–153]. In this way, specific CDK/cyclin complexes characterize every cell cycle phase (Figure 6).

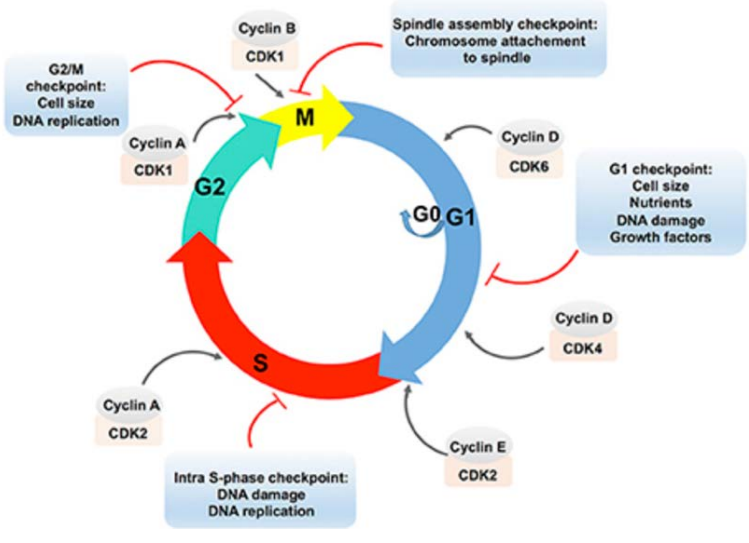

Figure 6. Cell cycle phases and its regulation. The eukaryotic cell cycle consists of two gap phases, the G1 and the G2 phase, the S-phase, and the M phase. Cells might enter a quiescent state, the G0 phase. Cell cycle phases are indicated by colored arrows. The cell cycle is regulated by complexes that are composed of Cyclins, which are bound to CDKs. CDK-Cyclin complexes are positioned in the front of the arrow that designates the corresponding cell cycle phase. CDK-Cyclin complexes are controlled via checkpoint pathways whose role is to prevent the cell from progressing to the next stage until the previous one is not faithfully completed. Multiple stimuli that exert the checkpoint control are indicated in an appropriate text insert. Adapted from Filho *et al.,*[154].

The **M phase** is triggered by the complex CDK1-Cyclin B1 that orchestrates phosphorylation of mitotic proteins and regulates their activity to allow entry into mitosis[155]. Mitosis proceeds in five phases: prophase, prometaphase, metaphase, anaphase, and telophase. In prophase, the chromatin starts to condense and the two centrosomes start to assemble highly dynamic microtubules (MTs). Nuclear-envelope breakdown marks the beginning of prometaphase, triggering initiation of spindle assembly. Metaphase is reached when all the chromosomes are attached to both spindle poles, aligned on the metaphase plate and attached to the MT fibers. Chromosome segregation towards opposite poles of the spindle is the main event that characterizes anaphase. In telophase, chromosomes descondense and a nuclear envelope reforms around the two masses of chromatin. In cytokinesis, the cleavage furrow causes the cytoplasm division of the two daughter cells[156].

This highly dynamic morphological reorganization of the cell is tightly regulated, not only by the CDK family, also by other relevant mitotic kinases, such as Polo-like kinases (PLKs), members of the Never In Mitosis (NIMA) kinase family as well as the Aurora kinase family[157–159]. In addition, microtubule motor proteins, known as kinesins (45 different kinesins are described in human cells) regulate the spindle formation[160] and core components of mitotic chromosomes, namely, histones, topoisomerase IIα and condensins allow chromosome condensation and segregation[161].

The precise regulation of all this spectrum of proteins is necessary for mitosis to properly take place. A key mechanism governing mitosis is the specific timing of more than 32,000 phosphorylation and dephosphorylation events carried out by the network of mitotic kinases and the counterbalancing phosphatases that regulate the specific localizations and activities in the spindle[162,163]. Additionally ubiquitination plays a key role for timely degradation of substrates to regulate their functions[164]. The activity of E3 ubiquitin ligase APC/C^{CDC20} destructs many mitotic proteins, including Cyclin B1[165].

However, under determined circumstances (e.g. upon some stressors) there is a cell cycle dysregulation that negatively impacts on the fidelity of the cell division. To ensure that cell division takes place correctly different **checkpoints** along the entire cell cycle phases have evolved to induce cell-cycle arrest in response to the detection of defects that may have arisen during DNA replication or in the spindle reorganization[166]. When a checkpoint is activated, the cell cycle is arrested and allows repair the defected genomes or spindles so that only intact genomes can be divided. Cell-cycle checkpoints are effectively triggering processes (e.g. apoptosis, mitotic catastrophe and senescence) that prevent the propagation of severely damaged or high-risk cells[167]. Failure of this precise network of cell surveillance leads to chaotic cell division[168].

1.3.2 Clinical therapeutics targeting the cell cycle

Loss of normal cell division is a hallmark of cancer disease, resulting in unscheduled cellular proliferation and genomic instability. Therefore, therapies targeting key pathways that drive and execute cell division have been a major research goal. The somatic cell division cycle culminates in mitosis, when the MT-based mitotic spindle captures, aligns and then equally distributes chromosomes into daughter cells (Figure 7). Inhibiting the essential spindle MT dynamics is an effective way to delay or stop exit from mitosis[169–171]. The two-conventional microtubule-targeting agents (MTAs); **the vinca alkaloids and the taxanes**, have been shown to be effective in the treatment of different types of cancer. Taxanes (including *paclitaxel*, *docetaxel* and *ixabepilone*) disrupt the MT dynamics through stabilization inducing prolonged mitotic arrest and eventually cell death[172]. In contrast agents such vinca alkaloids (that include *vinblastine*, *vincristine*, *vinorelbine*, and *estramustine*) destabilize MTs[169,173]. Both types are currently into clinics to treat lung, breast, ovarian, prostate cancer, lymphomas and myelomas[174]. While efficacious, these drugs have certain limitations. The dose-limiting toxicities of these drugs induces cumulative neurotoxicity and peripheral neuropathy since MTAs also affect organelle and neuronal transport processes in non-tumoral cells[172]. Additionally, the acquisition of resistance is very common in patients treated with these compounds[175]. This fact underlies the importance of understanding the molecular mechanisms for regulating their function and identify new target proteins to refine and improve anti-mitotic strategies.

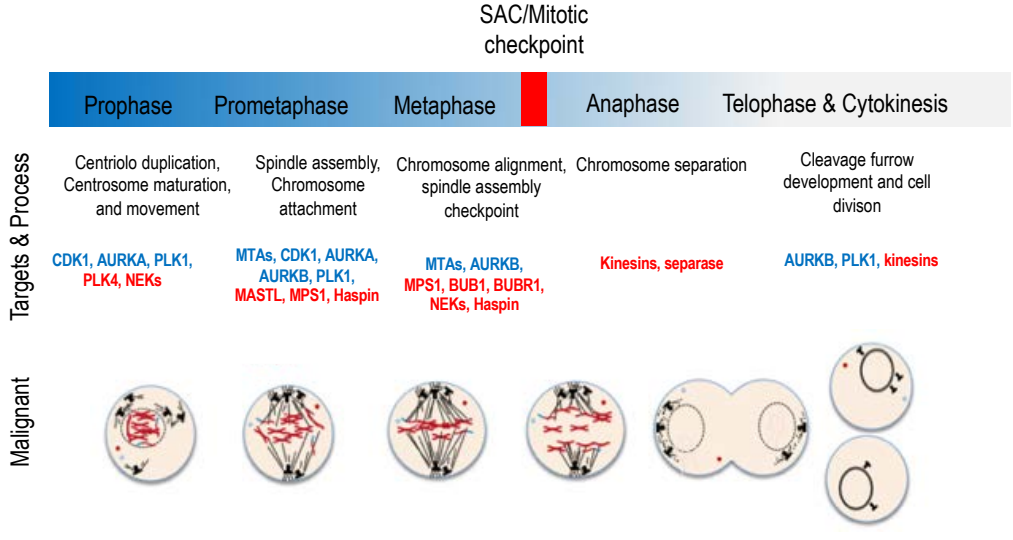

Figure 7. Summary of mitotic components targeted for cancer therapy. Numerous compounds designed to target various steps of mitosis have been developed, including spindle microtubules, mitotic CDKs, non-CDK kinases, motor proteins, and multi-protein complexes such as the spindle assembly checkpoint (SAC). Anti-mitotic therapeutic targets currently being evaluated are printed in red and blue. Adapted from Dominguez-Brauer *et al.,*[176].

1.3.3 Understanding mitotic death

The exposure of cancer cells to antimitotic compounds actives the spindle assembly checkpoint (SAC) leading to a mitotic arrest[177], but what happens next? Gascoigne and Taylor reported an elegant work using a single-cell-based approach combined with time-lapse microscopy to describe how different types of tumor cells respond to different anti-mitotic drugs[178], in other words, they monitored cell fate upon different anti-mitotics treatment. Following a prolonged mitotic arrest, most of the cancer cells die in a caspase-dependent process (85%)[178–180], whereas other cells exit mitosis without dividing, a process known as mitotic slippage[181] and return to interphase (15%). Once in G1, some cells undergo cell-cycle arrest, dying and others re-replicate their genomes (endocycle)[178]. The cell fate (to die into mitosis or exit mitosis) is determined by two competing and independent networks; one that involves the activation of cell death pathways (caspase-dependent), and another that controls the degradation of Cyclin B1 and thus exit from mitosis[182] (Figure 8). During a prolonged arrest, these networks work in opposite directions: while cell death signals become stronger, Cyclin B1 levels slowly fall due to incomplete penetrance of SAC-mediated APC/C inhibition. Both networks have thresholds and the fate of the cell is dictated by which threshold is breached first. Thus, if Cyclin B1 levels fall below the mitotic-exit threshold first, slippage occurs (Figure 8A). If the death threshold is breached first, the cell dies in mitosis as illustrated in Figure 8B.

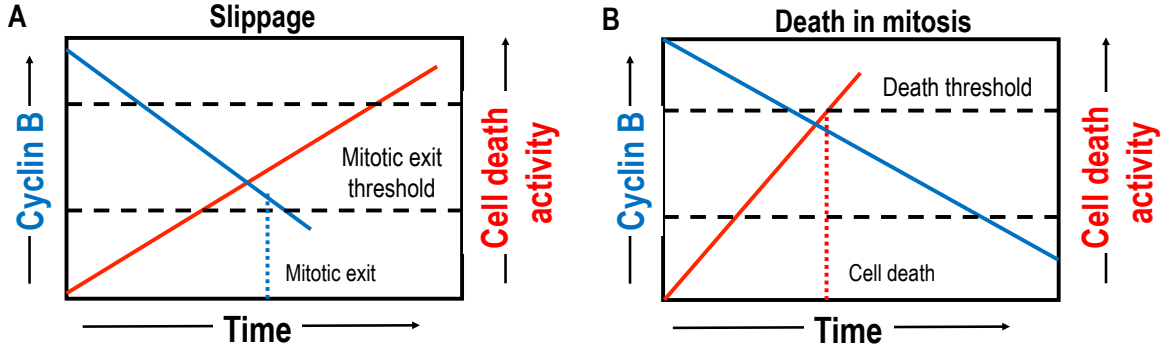

Figure 8. The competing-networks model. The decision to die in mitosis or to exit and return to interphase (slippage) is dictated by two competing networks, one that involves the activation of cell death pathways and the other that protects Cyclin B1 from degradation. Adapted from Topham and Taylor[183].

The death of mitotically arrested cells is principally mediated by the **caspase-dependent apoptotic pathway** controlled by the BCL-2 protein family[184,185]. This family comprises the set of anti-apoptotic molecules including BCL-2, BCL-xL and MCL1; and their antagonists, the BH3 pro-apoptotic proteins; NOXA and BAX. In a prolonged mitotic arrest, CDK1-Cyclin B1 mediates BCL-2 and BCL-xL phosphorylation preventing association with BAX/BAK complex and thus promoting cell death[186–188].

Indeed, overexpression of BCL-2 can partially prevent death and increase mitotic slippage in response to paclitaxel[189,190]. Concurrently, MCL1 degradation by the ubiquitin-proteasome system is also substantially critical for the induction of apoptosis. The pro-apoptotic protein NOXA contributes to MCL1 degradation by directly binding to it and acting as a scaffold for a common E3 ubiquitin ligase in M-arrest[190] (multiples E3 ligases have been shown to ubiquitinate MCL1 including MULE, APC/C-Cdc20 and/or SCF/FBW7[191,192]). Therefore, MCL1 stability is another key factor governing mitotic cell survival. One recent report shows that cells with low levels of BCL-2/BCL-xL, degradation of MCL1 during a mitotic arrest is sufficient to cause death, whereas in cells with higher levels of these two proteins, MCL1 degradation alone is insufficient[193]. Furthermore, pharmacological inhibition of BCL-2/BCL-xL with *Navitoclax* (BCL family inhibitor) accelerates mitotic death in human tumor cell lines treated with a KIF11 inhibitor[193]. In this sense is reported that *Navitoclax* sensitizes non-small cell lung cancer lines to paclitaxel[194]. These observations support the notion that functional redundancy exists between MCL1 and BCL-2/BCL-xL when neutralizing pro-apoptotic signals during mitosis, and highlight that it is possible to sensitize cancer cells to antimitotics[183]. The role of CDK1-Cyclin B1 and E3 ligases, indicates the present crosstalk between the mitotic and apoptotic networks also emphasized by CDK1-Cyclin B1-mediated phosphorylation of other apoptotic proteins, such caspase 9[183,195]. Additionally, other proteins can play roles promoting death into mitosis. Topham *et al.,* recently described that MYC and EGR1 promote the repression of BCL-xL and also increase the levels of certain BH3 proteins (BIM, BID, and NOXA) after a prolonged exposure to taxol[196]. Besides, MYC promotes the caspase dependent apoptosis following a mitotic slippage via the ARF-MDM2-p53 pathway[197,198]. The emerging picture about cell death into mitosis is complex, with multiple different classes of protein families and ubiquitin E3 ligases implicated.

1.3.4 Emerging mitotic strategies: CIN-exploiting therapies in cancer

Since the mitotic spindle is a validated target as chemotherapy drug in cancer, novel anti-mitotic therapies are focus to keep targeting unexplored mitotic cell-cycle features that are distinctive to tumor cells, to specifically kill them and to avoid dose-limiting toxicities[176]. Other strategies aim to increase the effectiveness of existing mitotic kinase inhibitors targeting new protein domains distinct to the kinase pocket to overcome acquired resistances. Either one strategy or the other, what most new cell cycle inhibitors have in common is that they are based on the concept of exploiting the genome instability to maximize therapeutic benefits and get better outcomes in patients.

Chromosome instability (CIN) is the most common form of genome instability. CIN is defined as an increase in the rate at which whole chromosomes (numerical CIN) or chromosomal fragments (structural CIN) are gained or lost, typically resulting in aneuploidy or abnormal DNA content[199,200]. The numerical

and/or structural chromosome alterations occur as a result of defects in numerous cellular pathways, including centrosome dynamics, mitotic spindle assembly, kinetochore-microtubule attachment, sister chromatid cohesion, chromosome segregation, cytokinesis and/or DNA damage repair[201–203]. Consequently, CIN is frequently reported in a wide range of cancers types[204], but is best understood in colorectal cancer, where it is observed in up to 85% of all cases[205].

There are two types of CIN-exploited therapies, commonly referred to as either CIN-reducing or CIN-inducing approaches[201,206] (Figure 9). The first one aims to slow down the rate of CIN by preventing the acquisition of further chromosomal alterations to limit cancer progression and drug resistance. *In vitro* studies have identified promising targets as RB or CHK2, but with unsuccessful results regarding the translation to the clinics[207–209].

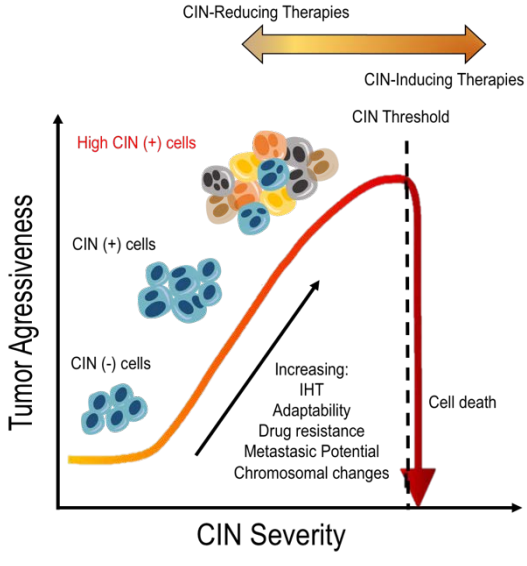

Figure 9. Therapeutic strategies to exploit chromosome instability (CIN) in cancer. Scheme presenting the relationship between increasing CIN and key tumor features (e.g. adaptability, intratumoral heterogeneity (ITH), drug resistance, metastatic potential and chromosomal changes). Two alternative therapeutic strategies that exploit CIN are presented (arrow, top). (1) CIN-reducing treatment strategies suppress CIN in CIN- tumors to slow and/or prevent acquisition of additional chromosomal alterations. Ideally, this will hinder tumor adaptability, cancer cell evolution, and the acquisition of drug resistance, thereby reducing tumor aggressiveness. (2) Alternatively, CIN-inducing strategies seek to generate extensive levels of numerical and/or structural CIN beyond a critical threshold (black dotted line) to induce cell death. +: positive; −: negative. Adapted from Thompson *et al.,*[206].

On the other hand, the paradoxical relationship reported between widespread CIN and improved patient outcome in various cancers[210,211] encourages the development and utilization of **CIN-exploiting therapies**. In particular, these therapies aim to aggravate CIN by increasing the levels of chromosome missegregation and DNA damage in cancer cells. The idea is to exceed a CIN threshold that induces cell cytotoxicity and cell death[201,212]. Many inducing therapies target processes related to mitosis and chromosome dynamics that are specifically altered in cancer cells and not in normal cells[212]. In this sense new targets are emerging with some of them already are under clinical scrutiny trying to maximize the patient outcome. Here we review some CIN-inducing therapies related to the mitotic spindle.

1.3.5 Targeting cyclin dependent kinase 1 (CDK1)

CDK1 in complex with Cyclin B1 is the central driver of mitosis. Aberrant expression of CDK1 has been linked to increase proliferation and paclitaxel resistance in OC[213,214] whereas its depletion blocks mitotic

progression and interferes with DNA replication[215]. More recently, CDK1 was also reported as a novel mediator of apoptosis resistance in *BRAF*^{V600E} mutant colorectal cancer whose dual targeting with a MEK inhibitor is therapeutically effective[216]. Nonetheless, CDK1 inhibitors also target normal cells with considerable side effects in patients. New evidences suggest that to proliferate, tumor cells rely on interphase CDKs such as CDKs 2, 4, and 6, unlike normal cells[217]. Anti-CDK4/6 agents in breast cancer have demonstrated promising efficacy with manageable side effects[218] and *Palbociclib* (the most promising CDK4/6 inhibitor) was recently approved by FDA for the treatment of advanced ER+, HER2- breast cancer[219].

1.3.6 Targeting kinesins: KIF11 and CENP-E

Kinesins are a family of motor proteins that use ATP energy to travel unidirectionally along microtubule tracks to fulfil their many roles in intracellular transport or cell division[160]. To date, 16 kinesins have been shown to have crucial mitotic functions in spindle assembly, chromosome alignment and segregation, and cytokinesis[220,221]. Therefore, many of them are emerging as a target for chemotherapeutic intervention[221], specially two mitotic kinesins: Eg5 (also known as KIF11) and centromere-associated protein E (CENP-E). **KIF11** is responsible for the bipolar spindle formation regulating the centrosome separation and, consequently, its inhibition results in a monopolarity and mitotic arrest[222]. In preclinical studies, agents targeting KIF11 show high efficacy, including total regression of tumors in mouse xenografts[223]. Attractive results have been reported in more than 38 Phase I or Phase II clinical trials involving KIF11-targeting agents that are ongoing or have been completed[221]. **CENP-E** mediates chromosome alignment on the metaphase plate. Its inhibition causes defects in chromosome segregation and SAC signaling that leads to aneuploidy and cell death[224–226]. Highly selective inhibitors developed against this target showed robust cytotoxic activity *in vitro* and in several human tumor xenografts *in vivo*[227] and some of them are currently into several clinical trials with successful results in refractory solid tumors[228]. Multiple mitotic kinesins are now being evaluated preclinically such as **KIF15**[229] (with the inhibitor *Quinazolinedione*) or with *Paprotrain*, the inhibitor of **MKLP2** protein[230], due to its involvement in tumorigenesis, with promising results[221].

1.3.7 Targeting the spindle assembly checkpoint

The spindle assembly checkpoint, also referred as the mitotic checkpoint, is a signaling cascade that prevents chromosome missegregation by arresting the cell cycle in mitosis until all chromosomes are properly attached to the spindle[231]. SAC inhibitors aim to force cells an abnormal mitosis, inducing massive chromosome/genetic imbalance and subsequently undergo cell death or senescence[232,233]. **MPS1 or TTK** is a serine/threonine kinase required for chromosome alignment and error correction,

being critical for the recruitment of SAC proteins to unattached kinetochores, the mitotic checkpoint complex formation and the APC/C inhibition[234,235]. To date, a number of MPS1 inhibitors have reported severe chromosome missegregation, aneuploidy and eventually loss of cell viability *in vitro* and anti-tumorigenic efficacy in xenograft models[236], particularly with the *NMS-P715* inhibitor that has only minor effects on the growth of normal cells, and its antitumorigenic doses are well tolerated in mice[237]. **BUB kinases** include the paralogous serine/threonine kinases **BUBR1 and BUB1**. While BUBR1 contributes to stabilizing kinetochore-MT attachments and aligning chromosomes, BUB1 is required for chromosome segregation, localization of SAC proteins to kinetochores and establishing efficient bipolar chromosome attachments to spindle[176]. Preclinically, inhibition of these kinases efficiently kills tumor cells and reduce tumor growth in mice. BUB1 inhibitor, *BAY-1816032*, in combination with taxanes and PARPi enhance its efficacy and potentially overcomes resistance to platinum[238]. Currently there is no clinical trial ongoing with inhibitors of these two kinases.

1.3.8 Inducing tetraploid: AURORA B and MASTL

Inhibition of cytokinesis process leads to the formation of a tetraploid daughter cell containing twice DNA information, a process called mitotic slippage. A particularly important kinase that acts during cytokinesis is **AURORA B**[239] whose inhibition results in efficient tumor cell killing in a variety of tumor types *in vitro* and *in vivo*[240], and does not seems to have a prominent effect on non-dividing cells[241,242]. AURORA B inhibition is more prominent in p53-deficient cells, offering therapeutic advantage in p53-mutated tumors[243,244]. The most promising inhibitor is *BI-811283* currently being evaluated in leukemia and patients with advanced solid tumors[245,246]. On the other site, the protein **MASTL** acts as a regulator of mitotic progression by promoting the inactivation of the tumor suppressor protein phosphatase 2A (PP2A) associated with the B55d regulatory subunit[247]. MASTL depletion results in abnormal spindle assembly, chromosome missegregation and genomic instability lethal to cancer cells both *in vitro* and *in vivo*[248–250]. The development of pharmaceutical compounds targeting MASTL is currently on going[251,252].

1.3.9 Targeting G2/M checkpoint

When cells encounter DNA damage in G2 phase, the G2/M checkpoint ensure that the damaged DNA is detected and actives the DNA damage response (DDR) to repair the corrupted DNA and prevent the division before the damage is repair[253]. The DDR leads a complex series of events involving different post-translation modifications such phosphorylation and poly(ADP)ribosylation to orchestrate a controlled recruitment and activation of repair proteins with inactivation of the cell cycle machinery[254]. The phosphatidylinositol-3-kinase-like family members, **ATM and ATR kinases**, are the principal sensors of DNA damage[255]. Once active, ATM and ATR phosphorylate and activate the **effector**

kinases CHK1 and CHK2, which propagate the signal to downstream targets as well as mediate proteins to DNA break, such as BRCA1 or 53BP1[256]. Thus, mitosis is inhibited to prevent the propagation of errors until DNA is repair. The effector kinases mediate the inactivation of **Polo like kinase-1** (PLK1), AURORA A and the CDC25 phosphatases, while activating MYT1 and WEE1, thus promoting the inactivation of CDK1/Cyclin B1. In fact, ATR phosphorylates also BORA at T-501 to degradation and thus keep PLK1 inactive and cell cycle arrested. When DNA is repair, cells needs to shut down the DDR and re-activate cell division. PLK1 plays a crucial role in this process by targeting several components of DDR and reactivates the CDK1/Cyclin B1 complex. PLK1 targets WEE1 and Claspin for degradation, inactivates MYT1 and CHK2 and release 53BP1 form the site of damage. In contrast CDC25 is reduced and CDC25B re-activates CDK1/Cyclin B1 to ensure mitotic entry. Recent data describe the discovery and development of DDR kinase inhibitors (e.g. Inhibitors of ATM, ATR, WEE1 and PLK1 are being investigated in clinical trials with successful results). A phase I clinical trial of an ATM inhibitor, *AZD0156* used either as a single agent or in combination with the PARPi *Olaparib* is currently ongoing[257]. In the same manner, the ATR inhibitor *AZD6738* alone and in combination with palliative therapy is being evaluated in solid tumors[258]. On the other hand, results from WEE1 inhibitors have been promising. For example, the combination of the WEE1 inhibitor *AZD1775* in combination with neoadjuvant chemotherapy has shown promising results in solid tumors[259], especially in OC, where in a phase II trial, *AZD1775* enhances carboplatin efficacy in TP53-mutated tumors with an overall response rate of 42%[260]. Attractive results are obtained from PLK1 inhibitors, another pivotal G2/M checkpoint protein. *Volasertib*, the most promising PLK1 inhibitor, received the category of breakthrough therapy by the FDA in 2017 owing to its substantial therapeutic value in acute myeloid leukemia[261], as discussed in the next section.

In the future, personalized medicine strategies that exploit CIN might become effective treatment options for both primary and metastatic tumors. In this sense, treatment with inhibitors targeting the protein components of the G2/M checkpoint could potentially make tumors more immunogenic by increasing their mutational load and the genome instability exceeding the damage threshold to ultimately lead cell death and/or enhance the effect of other therapies such immune inhibitors. However, before this can be achieved, a more comprehensive understanding and identification of the aberrant proteins and mechanisms giving rise to CIN is required.

1.4 Polo-like kinases

Polo-like kinases (PLKs) constitute a family of serine/threonine kinases that are critical regulators of multiple intracellular processes including cell cycle progression, DNA replication and stress response. The *polo* gene was first cloned from *Drosophila melanogaster* in 1988, and it was observed that mutations in *polo* displayed abnormal spindle poles during mitosis[262]. It is a well conserved gene throughout various species as diverse as yeast or humans[263,264]. In mammals, five homologous for *polo* have been identified: PLK1, PLK2, PLK3, PLK4 and PLK5; characterized by different chromosomal location, expression and biological function but with similar protein structure[265]. From PLK1 to PLK4, the structure comprises a kinase domain located in the amino terminal part and a regulatory domain consisting of one (as in PLK4) or two (as in PLK1 to PLK3) polo-box domains (PBDs) located in the carboxyl terminal part. Distinct from the other PLK family members, PLK5 is a PBD-containing protein without the kinase domain[266]. Functionally, all PLKs member are implicated in the regulation of cell cycle progression (reviewed in Zitouni *et al.*,[267]).

1.4.1 PLK1: controlling mitotic orchestra and beyond

PLK1 is the most characterized PLK member considered as a master regulator of eukaryotic cell division. By phosphorylating different substrates, PLK1 plays pleiotropic roles during mitosis including centrosome maturation, kinetochore-microtubule attachment, bipolar spindle formation and cytokinesis[268,269]. In mouse models, homozygous loss of PLK1 (*PLK1*$^{-/-}$) resulted in early embryonic lethality, with embryos displaying developmental delays and a lack of mitotic spindle assembly at 4-8 cell stage, preventing the primary cycling of the mammalian cells. In contrast, while mice heterozygous for PLK1 (*PLK1*$^{+/-}$) are healthy at birth with no obvious defects from the loss of one PLK1 allele, old *PLK1*$^{+/-}$ mice developed tumors due to the aneuploidy produced by not having enough PLK1, supporting also a role of PLK1 in genomic stability[270].

Preclinical studies in human cell lines have demonstrated that PLK1 activity is essential in numerous stages of mitosis. Primordially, PLK1 is part of the regulatory network controlling CDK1-Cyclin B1 activity at the G2/M transition[271]. PLK1 directly phosphorylates and activates CDC25[272] phosphatases, resulting in subsequent de-phosphorylation of the inactive CDK1/Cyclin B1 complex[271]. Further, PLK1 performs inhibitory phosphorylation of WEE1 and MYT1[273,274], negative regulators of CDK1, activating the CDK1/Cyclin B1 complex and therefore ensuring the mitotic entry (Figure 10). Once cells have entered into mitosis, PLK1 controls the centrosome maturation by the recruitment of the γ-tubulin ring complex (γ-TuRC), which can nucleate new microtubules needed for chromosome segregation, to the centrosomes during prophase stage[275] (Figure 10). PLK1-mediated phosphorylation of Ninein-like

protein (NLP), an important component of the centrosomes, switch these structures from an interphasic state to mitotic state[276]. PLK1 also regulates the localization of AURORA A, which has a key role in the function and maturation of centrosomes[277,278].

In addition, PLK1 is reported to control the kinetochore attachment to chromosomes and its segregation by phosphorylation of the SA2 subunit of cohesin[279] and the subunits of the anaphase-promoting complex/cyclosome (APC/C) allowing the progression beyond prometaphase[280] (Figure 10). The complete chromosome segregation and the exit from mitosis is synchronized by the PLK1 regulation of APC/C, required for degradation of mitotic cyclins and facilitation of sister chromatid segregation[280,281]. In late-stage mitosis, PLK1, self-organized onto the central spindle, phosphorylates HsCYK4 creating a docking site for the RhoGAP/Ect2 complex[282], leading the cleavage furrow formation necessary for the cytokinesis[283].

To carry out all these multiple functions PLK1 has a dynamic subcellular localization, shuttering between cytoplasm and nucleus. During interphase PLK1 is found in the cytoplasm, microtubules and centrosomes; and in mitosis and during cytokinesis, it is predominantly concentrated to the kinetochores and the central spindle (Figure 10). Regarding its expression, PLK1 is tightly regulated during cell cycle progression, with low levels during interphase and high levels in G2 phase to drive the mitotic phase[284].

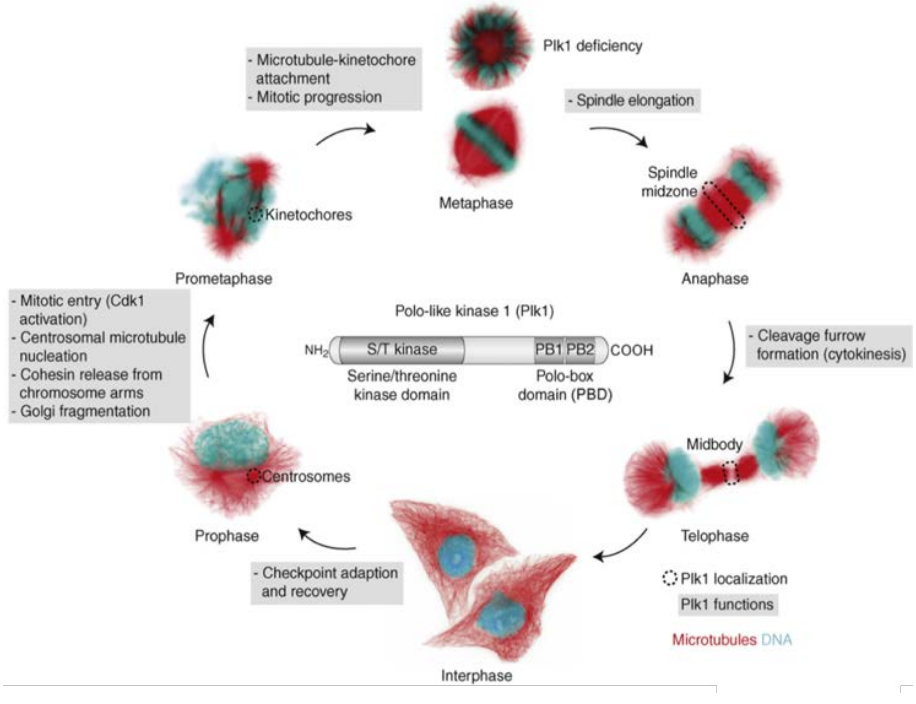

Figure 10. Domains structure, localization and functions of PLK1 throughout mammalian cell division. The domain structure of PLK1 is shown in the center of the figure. The PBD is responsible for the subcellular targeting of PLK1. Functions of PLK1 are listed in gray boxes at the corresponding cell cycle stages, which are illustrated by immunofluorescence images of cultured human cells (microtubules are shown in red, DNA in cyan). Localization of PLK1 to subcellular structures is indicated by dashed objects. PLK1 localization to centrosomes and kinetochores persists throughout most of mitosis. Adapated from Takaky *et al.*,[285].

PLK1 is emerging as a critical player in pathways beyond mitosis, including DNA replication, recovery from G2-DNA damage checkpoint, p53 regulation, interactor with oncogenic and tumor suppressor genes and in the cardiovascular function of smooth muscle cells. In replication, the PLK1-dependent phosphorylation on HBO1 at late mitosis is required for the pre-replicative complex formation allowing DNA synthesis during the S-phase[286,287]. PLK1 thus can phosphorylates Topo IIα increasing its decatenation activity, which is critical for sister-chromatid segregation[220] or phosphorylates TRF1 forming a complex that regulates its telomeric DNA binding ability[288]. One striking interaction is with the tumor suppressor *TP53*. The kinase domain of PLK1 binds to the DNA binding domain of *TP53* inhibiting its activity, decreasing its mediated transcription of *p21*, *MDM2* and *BAX* promoters[289]. Additional experiments showed phosphorylation of Topors by PLK1 inhibits sumoylation of p53, enhancing the ubiquitination of p53, leading to a PLK1-depedent degradation of p53[290,291]. Recently, more studies are coming up revealing a diverse range of functions in which PLK1 activity in involved. For example, PLK1 regulates contraction of smooth muscle cells and is required for vascular homeostasis. Mechanistically, authors found that PLK1 regulates angiotensin II-dependent activation of RhoA and actomyosin dynamics in vascular smooth muscle cells in a mitosis-independent manner[292]. Further, PLK1's activity is directly regulated by checkpoints pathways, involving BRCA1/2, CHK1/2, ATM and ATR proteins[293–296] or in regulatory loops with FoxM1 and STAT3[297,298]. Importantly PLK1 have been identified as interactor with multiple oncogenes including AKT, MYC, CTNNB1 and tumor suppressors proteins such as RB and PTEN[299–302]. Indeed, a recent review of the cancer genome landscape by Vogelstein *et al.,* categorized cancer driver genes in twelve signaling pathways that regulates the three cores: cell fate, survival and genome maintenance and PLK1 has direct interaction with the three core processes and involved in 75% of the signaling pathways[303,304].

1.4.2 Development of PLK1 inhibitors: from the laboratory to the clinics

As PLK1 plays an important role in cell cycle progression in normal proliferating tissues, it is not rare to found PLK1 overexpressed in many cancer types, including melanoma, breast, colorectal, prostate, pancreatic, ovarian as well as non-Hodgkin's lymphomas and acute myeloid leukemia[278,304], in contrast to the very low levels reported in most normal tissues[265]. Further, the overexpression of PLK1 has been linked to poor disease prognosis and a worse overall survival in all these tumor types[305,306].

In this sense, inhibition of cell proliferation and induction of apoptosis are basic principles of anticancer therapy, as commented before. Antimitotic therapy based on conventional microtubule targeting agents is standard for many cancer types, but lack of selectivity is associated with adverse effects, such as neurotoxicity and myelosuppression[278]. Therefore, more specific mitotic agents are on the focus for drug development. Since PLK1 is a master regulator of several essential cell cycle events with high levels in

a wide range of tumors, this kinase has arisen as an intriguing druggable target, prompting the research and development of PLK1 inhibitors as mean for cancer management. Preclinical studies inhibiting PLK1 using small interfering RNA (siRNA) or small molecules compounds have been published with high efficacy killing different cancer cells *in vitro*[307,308] and inducing tumor regression in different xenograft tumor models *in vivo*[309]. Indeed, a vastly number of PLK1 inhibitors have been developed and tested preclinically in almost all types of cancer[269,310]. To date, there are three groups of PLK inhibitors; ATP-competitive inhibitors targeting the ATP-pocket of the N-terminal kinase domain, PBD inhibitors targeting the C-terminal polo box domain and RNAi-based therapies targeting the mRNA of PLK1, resulting in PLK1 protein depletion. All PLK1 inhibitors that are being clinically investigated so far either as monotherapy or in combinational therapy in clinical trials are outlined in Table 4.

Table 4. PLK1 inhibitors running in clinical trials. The different PLK1 inhibitors that have been tested into clinical trials. Source: *https://clinicaltrials.gov*

Agent	Target	Company	Regimen	Disease	Phase	Clinical trial status	Reference
BI-2536	ATP-binding domain	Boehringer-Ingelheim	Single agent	AML	II	Completed	NCT00701766
			Single agent	Advanced Pancreatic Cancer	II	Completed	NCT00710710
			Single agent	Prostate Cancer	II	Completed	NCT00706498
			Single agent	Recurrent solid tumors	II	Completed	NCT00526149
			Single agent	Small Cell Carcinoma	II	Completed	NCT00412880
BI-6727 *(Volasertib)*	ATP-binding domain	Boehringer-Ingelheim	with Itraconazole	Solid tumor	I	Active	NCT01772563
			Single agent	Solid tumor	I	Active	NCT02273388
			with Cytarabine	AML	II	Active	NCT00804856
			with LDAC	AML	III	Active	NCT 01721876
			with Decitabine	AML	I	Completed	NCT02003573
			with BIBF1120	Solid tumors	I	Completed	NCT01022853
			with Cisplatin or Carboplatin	Advanced or Metastatic Solid Tumor	I	Completed	NCT00969761
			with Oral BIBW 2992 (Afatinib)	Solid tumor	I	Completed	NCT01206816
			with Pemetrexed	Non-Small-Cell Lung	II	Completed	NCT00824408
			Single agent	Urothelial Cancer	II	Completed	NCT01023958
			Single agent	OC	II	Completed	NCT01121406
			with Chemotherapy	AML	II	Completed	NCT02198482
Tak960	ATP-binding domain	Millenium	Single agent	Advanced Nonhematologic Malignancies	I	Terminated	NCT01179399
NMS-P937	ATP-binding domain	Nerviano	Single agent	Advanced/Metastatic Solid Tumors	I	Completed	NCT 01014429
NMS-1286937	ATP-binding domain	Nerviano	Single agent	Advanced/Metastatic Solid Tumors	I	Completed	NCT01014429
ON 01910.Na (*Rigosertib*)	Polo box domain	Onconova	Single agent	Squamous Cell Carcinoma	I/II	Recruiting	NCT03786237
			Single agent	AML	II	Recruiting	NCT02730884
			Single agent	Myelodysplastic Syndrome	III	Recruiting	NCT02562443
			Single agent	AML	II	Active	NCT01926587
			Single agent	Chronic Myelomonocytic Leukemia	III	Active	NCT01241500
			with Platinum-based Chemotherapy	Head and Neck Cancer	I	Completed	NCT02107235
			Single agent	Solid tumor	I	Completed	NCT01168011
			Single agent	Advanced Cancer	I	Completed	NCT01538537
			with Irinotecan or Oxaliplatin	Solid malignancies	I	Completed	NCT00861328
			Single agent	AML	I	Completed	NCT00854646
			Single agent	OC	I	Completed	NCT00856791
			Single agent	AML,ALL	I/II	Completed	NCT01167166
			Single agent	Metastatic Squamous Cell Carcinoma	II	Completed	NCT01807546
			Single agent	Metastatic Pancreatic Cancer	III	Completed	NCT 01360853
			with Gemcitabine	Metastatic Pancreatic Cancer	III	Completed	NCT01360853
Onvansertib	ATP-binding domain	Trovagene	with Cytarabine or Decitabine	AML	I/II	Recruiting	NCT03303339
			with Abiraterone and Prednisone	Castration-Resistant Prostate Cancer	II	Recruiting	NCT03414034
GSK4611364A	ATP-binding domain	GlaxoSmithKline	Single agent	Solid tumor and Non-Hodgkins Lymphoma	I	Ongoing	NCT 00536835
TKM-080301	Lipid nanoparticle of a siRNA against PLK1	Arbutus Biopharma	Single agent	Primary or Secondary Liver Cancer	I	Completed	NCT01437007
			Single agent	Solid tumors or lymphomas	I/II	Completed	NCT01262235
			Single agent	Advanced Hepatocellular	I/II	Completed	NCT02191878

ALL: Acute Lymphoblastic Leukemia; AML: Acute Myeloid Leukemia; OC: Ovarian Cancer

It's worthwhile pointing out that PLK1 inhibition could be particularly effective in cancers with determined genetic background profiles. For example, pharmacological PLK1 inhibition in *KRAS*-mutant cancer cells exhibited a strong efficient to induce apoptosis and cell cycle arrest, being a potential treatment of cancers harboring *RAS* mutations[311,312]. Besides, in some *MYC*-amplified tumors such aggressive B lymphoma and glioma, PLK1 depletion triggers degradation of MYC inducing the apoptosis of the cancer cells[313,314], supporting that the genomic *MYC* alteration might serve as biomarker for PLK1 inhibitor sensitivity[313]. Additionally, *PLK1* is one of the genes responsible for the estrogen-independent transcriptional activity in breast cancer cells, driving the estrogen-independent cellular growth. For those patients that have been resistant to the estrogen deprivation therapy, PLK1 inhibition represents a promising therapy waiting to be trialed[315,316]. Similarly, pharmacological inhibition of PLK1 by *BI-2536* prevented tumor progression and metastasis in tamoxifen-resistant breast cancer cells being a potential drug candidate to those hormonal resistant breast cancer patients[317]. In addition, it is reported PLK1 activity drives DNA replication under stress, resulting in acquired *Gemcitabine* resistance in pancreatic cancer cells[318]. Although *in vitro* inhibition of PLK1 sensitizes pancreatic-derived xenograft tumors to *Gemcitabine*, in a phase III trial of metastatic pancreatic adenocarcinoma, the combination produced a modest partial response in 19% of patients compared to 13% of patients treated with *Gemcitabine* alone without an increase in the OS (6,1 months *vs* 6,3 months respectively). The combination was thus deemed unsuccessful in the clinical trial.

Although the success of PLK1 inhibitors preclinically in unquestionable, only modest antitumor activity in solid tumors has been so far reported for the majority of PLK1 inhibitors in the clinical trials. Given as monotherapy, only partial response is observed in few patients with a minority of them reaching a stable disease. Another example is related to the phase II trial performed with *Volasertib* in recurrent ovarian neoplasms, with patients from Vall Hebron hospital. *In vitro* and in mice xenograft tumors, *Volasertib* efficiently kills OC cells, but in the clinical trial the median PFS for *Volasertib* was 13,1 weeks *vs* 20,6 weeks for standard chemotherapy. Although, 11% of patients treated with *Volasertib*, achieved a PFS for more than 1 year, whereas no patient receiving platinum chemotherapy achieved PFS greater than 1 year[319]. This discrepancy observed between the preclinical and the patient outcome in clinical trials can likely be attributed to the difference in drug exposures between laboratory, mice models and humans, together with the tumor heterogeneity[320]. In fact, there is no PLK1 inhibitor currently approved for any tumor treatment. Optimistically, the most promising PLK1 inhibitor, *Volasertib* (BI-6727), has shown considerable potential benefit in clinical studies, having reached phase III trials. In fact, this agent received in 2017 the FDA Breakthrough Therapy designation for its effect in AML in combination with *Cytarabine*[321]. Notably, leukemic cells are more sensitive to PLK1 inhibition since these cells are more dependent on PLK1 due to higher proliferation rates compared to normal bone marrow cells[322].

Remarkably, *Rigosertib* (ON 01910.Na) is a non-ATP competitive multi-kinase inhibitor with dual targetability affecting both PLK1 and PI3K signaling pathways[323,324]. Although it is not specific to PLK1, attacking two important pathways in cancer increases the action on malignancy tumors. This agent is currently being tested in various phase III trials (Table 4). Importantly the combinatorial treatment of PLK1 inhibitors with conventional chemotherapeutic drugs induces a strong synergism in clinical trials better than monotherapy, with no reported neuropathy and only few hematological adverse effects that were reversible and clinical manageable in AML and head and neck cancer[321,325,326]. A considerable number of trials are running with combinatorial approaches as illustrated in Table 4.

Following these observations, two urgent clinical needs emerge to be addressed. The first one, a better understanding of the mechanisms and proteins involved in PLK1 activation to design additional next generation specific PLK1-based inhibitors to be used in cancer. And on the other hand, strengthen the use of combinational studies to search for synergistic drugs that can increase the therapeutic window

1.5 BORA, a functionally conserved mitotic protein from *Drosophila* to *Homo Sapiens*

BORA was first identified in *Drosophila melanogaster* as a co-activator of AURORA A in a screening for mutants defective in asymmetric cell division. Hutterer and colleagues observed that BORA mutants had defects identical to those observed in AURORA A protein, and the overexpression of BORA could rescue the defects caused by mutations in the AURORA A kinase[327]. Different to *Drosophila*, in *Caenorhabditis Elegans* (*C. elegans*), *Xenopus* and *Homo Sapiens*; BORA or its orthologue Suppressor of PAr-2 defect (SPAT-1) is reported to function as PLK1 activator rather than AURORA A activator. BORA/SPAT-1 binds PLK1, changing its conformational status, enhancing AURORA A-mediated T-loop phosphorylation of PLK1[328–332] which is crucial for the full PLK1 activation. Thus, BORA is a highly-conserved mitotic protein through species as diverse as *Drosophila* or humans, specifically the N-terminal domain of the protein[327].

Indeed, different reports in human cells and worms support that the first 225 amino acids of BORA are enough to support the CDK1-dependent phosphorylation to trigger PLK1 activation *in vitro*[333,334]. Interestingly, a multiple protein sequence alignment of BORA among different species shed light about two Cyclin-binding sites (Cy motives; 192LRRKLFLD199 *human sequence*) and three phosphorylation sites (S41, S112, and S137 *human sequence*) conserved N-terminally. In human cells, experiments mutating these sites abrogate the ability of the N terminus part of BORA, not only to promote PLK1 activation, also to ensure mitotic entry in G2/M checkpoint recovery conditions[333,335]. Similarly, in worms, mutations in the SPAT-1 conserved Cy docking motives and S119, S190, T229 residues (corresponding to S41, S112, and S137 in human cells) severely delayed mitotic entry and displayed a cell-cycle length similar to embryos without expressing the N-terminal part of SPAT-1, highlighting the importance of these phosphosites[329,333,334].

Firstly, it was considered that Cyclin B1 was responsible for the phosphorylation of these Cy docking sites together with CDK1. Indeed, Cyclin B1 is recovered in Bora immunoprecipitates from mitotic cells[333] and the CDK1/Cyclin B1 participates in a feedback loop with PLK1 and BORA during mitosis[336]. Alternatively or additionally, it was thought that CDK1/Cyclin A, which is known to trigger CDK1/Cyclin B1 activation in G2, might phosphorylate BORA in G2 and thereby contribute to PLK1 activation, which occurs prior CDK1/Cyclin B1 activation. Importantly, CDK1/Cyclin A is active at the time point where BORA is maximally phosphorylated[333], suggesting the contribution of Cyclin A should be also considered. Vigneron *et al.,* recently addressed this issue and reported that it is Cyclin A and not Cyclin B1 responsible for the BORA phosphorylation. Experiments combining mathematical models with classic

biochemical assays performed in *Xenopus* extracts showed that the phosphorylation of CDK1/Cyclin A in the S110 BORA-residue (corresponding to the residue S112 in humans) was essential for Plx1 activation and mitotic entry. The conserved S38 and S135 amino acids (corresponded to S41 and S137 in humans respectively) partially restored Plx1 activation and mitotic entry[332], thereby supporting CDK1/Cyclin A as the kinase promoting AURORA A-dependent phosphorylation of PLK1 and triggering mitotic entry through the phosphorylation of BORA on S110. Interestingly, they confirmed BORA was able to promote entry into mitosis in Cyclin B1-depleted interphase extracts, excluding the possibility of Cyclin B1 as the factor to phosphorylate BORA. (Figure 11).

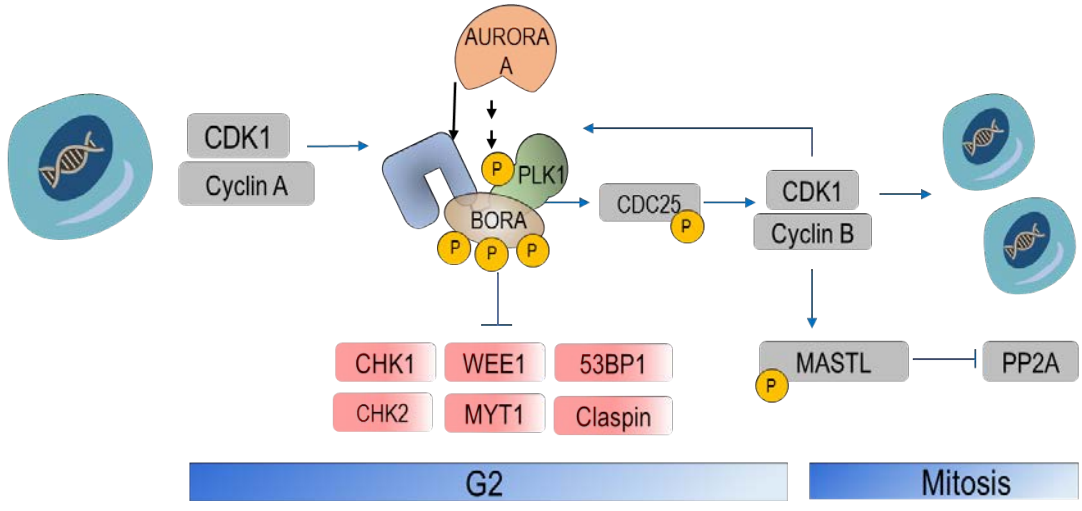

Figure 11. CDK1/Cyclin A -dependent BORA phosphorylation triggers mitotic entry. Active CDK1/Cyclin A phosphorylates BORA to promote PLK1 activation by AURORA A. PLK1 activates CDC25, which removes the inhibitory phosphorylation of CDK1/Cyclin B1. Active CDK1/Cyclin B1 further activates PLK1 and CDC25, forming a feedback loop. CDK1/Cyclin B1 also activates MASTL kinase, which suppresses PP2A to entry mitosis. Collectively, these mechanisms enable switch-like CDK1 activation, substrate phosphorylation and entry into mitosis. Adapted from Zheng *et al.*,[337].

1.5.1 BORA, a multi-phosphorylated protein

BORA is subjected to post-translational phosphorylation modifications by different kinases to timely control its function. CDK1 also phosphorylates BORA on multiple sites along the entire protein, beyond the N-terminal part. Phosphorylation of Serine-252 triggers BORA interaction with the PLK1-PBD, being a PLK1 docking site[338]. When cells enter into mitosis, PLK1 timely phosphorylates BORA on the putative degron sequence (S496-DSGYNT-T501) for the Skp1-Cullin-F box (SCF) β−TrCP E3-Ligase targeting BORA for proteasomal degradation[330,338]. By contrast, phosphorylation of Threonine-52 by CDK1 prevents the full BORA degradation in mitosis[339] which might be required to maintain sufficient BORA residual levels to sustain PLK1 activity during mitosis[336]. So, in addition to control PLK1 activation and mitotic entry, CDK1 thus can control the time and the levels of BORA degradation by phosphorylating different residues on BORA.

Additionally, BORA is exposed to phosphorylation by other protein kinases such GSK3β in the S274 and S287 to trigger the AURORA A dependent phosphorylation on T210 and mitotic entry[340] or by ATR[341]. Upon DNA damage, ATR phosphorylates BORA at T-501 targeting BORA for proteasomal degradation, contributing to maintain PLK1 inactive and to keep the G2/M checkpoint arrested until the damage is repair[341].

1.5.2 BORA, an essential activator of PLK1

Phosphorylation of BORA is crucial for PLK1 activation. But how exactly BORA promotes this phosphorylation and subsequently PLK1 activation by AURORA A is still an open question. The classical conception conceives that BORA promotes a drastic conformational change in PLK1 structure that relieves the auto-inhibition produced by the PBD on the kinase domain thereby separating the N and C-terminal regions and exposing the activation loop (T210) for phosphorylation by AURORA A kinase[330,338] (Figure 12).

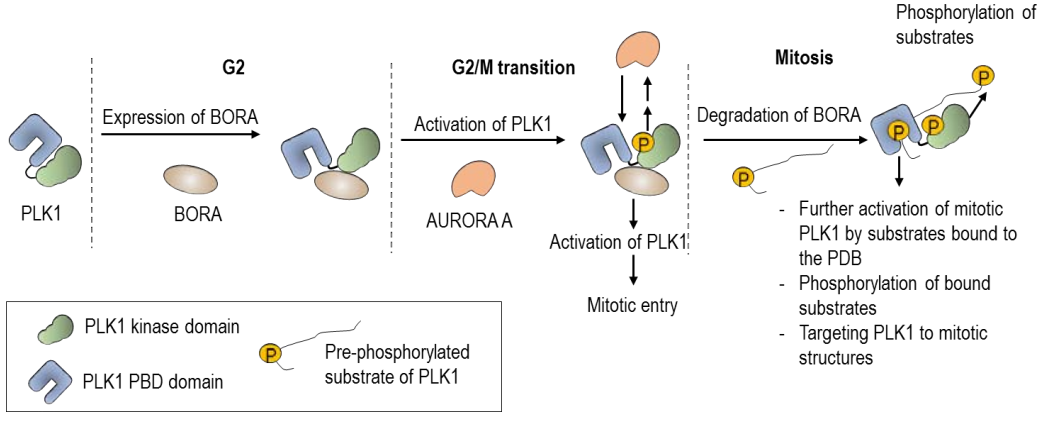

Figure 12. Model of the BORA-mediated phosphorylation of PLK1 at Thr210 by AURORA A. BORA associates first with the inactive form PLK1. This association controls the accessibility of the activation loop of PLK1 to AURORA A in G2/M. Phosphorylation of the conserved threonine residue (Thr210) in the activation loop (T-loop) of the PLK1 domain by AURORA A dramatically elevates the enzymatic activity of PLK1 at the entry into mitosis. This mechanism seems to induce an open conformation of PLK1 and allows activated PLK1 to recruit substrates binding its PBD. PLK1 function is spatially regulated through the targeting activity of the conserved PBD domain. Adapted from Strebhardt *et al.,*[278].

Although this is the most accepted hypothesis, recent cross-linking mass spectrometry-based approaches describe the interplay as a dynamically changing phosphorylation and interaction network[342]. Authors suggest a first step characterized with a stable protein interaction between BORA-AURORA A that directly catalyzed PLK1 activity, leading to a succession of phosphorylation reactions in BORA. This BORA hyper phosphorylation stage leads a conformational change of BORA that promotes a stable PLK1-BORA complex formation. In contrast, BORA-AURORA A complex is continuously present, raising the possibility that this complex acts as the PLK1 activator[342]. Although

these observations strongly suggest that PLK1 does not undergo massive conformational changes separating the N and C-terminal region, they do not exclude the possibility that BORA induces more subtle conformational changes, not detectable by this method. Alternatively, BORA could be required to activate AURORA A, as originally proposed in *Drosophila*. However, it has been reported that human BORA does not modify AURORA A activity *per se* and does not significantly increase AURORA Activity toward substrates other than PLK1[330,331]. The function of BORA during PLK1 activation could be required for the establishment of a transient but stable AURORA A-BORA-PLK1 ternary complex[338].

1.5.3 BORA localization and PLK1 activation: where and how mitotic begins?

Whereas in *Drosophila* BORA is located into the nucleus and shuttles in to the cytoplasm in early prophase[327], in humans and *Xenopus*, BORA appeared to be strictly cytoplasmic[339,343]. Bruisma *et al.,* reported an exhaustive work about BORA localization using an inducible GFP-BORA cell line combined with fractional assays, pointing out BORA is exclusively cytoplasmic in human cells throughout the interphase[343]. Notably, BORA levels are irregular during cell cycle. A gradually increase of BORA is reported when cells approach mitosis phase, with peak levels in G2, and begin to decrease upon Cyclin B1 degradation, just before mitosis[338]. Curiously, PLK1 localizes to kinetochores during G2 and it is first activated in this phase[344]. The fact that BORA is exclusively located in the cytoplasm and its levels intensively peaks in G2 strengthen the fact that initial phosphorylation of PLK1 at T210 by AURORA A and BORA occurs at the centrosomes, where AURORA A predominantly is localized at G2 phase. Once phosphorylated at T210, PLK1 is subsequently translocated to the nucleus to promote mitotic entry, phosphorylating downstream targets. Consequently, BORA is targeted for degradation approximately 2 hours before mitosis in a PLK1- and βTrCP-dependent manner, but a small residual pool of BORA is left during mitosis, sufficient to sustain the AURORA A-dependent phosphorylation and maintain PLK1 active[336]. The AURORA-A–BORA-mediated PLK1 activation acts as a bistable system, like an interlinked feedback loop that render cell cycle transition irreversible as switching on occurs at a high threshold, but once switched on, this system enforce their own activation making it difficult to switch them off[336,345]. This mode of action for the AURORA A–BORA–PLK1 activation loop is an important contribution to the all-or-nothing decision of cells on the mitosis entry[336].

1.5.4 Regulation of the mitotic spindle

Mechanistically, BORA regulates the spindle stability, the polymerization of microtubules and controls the chromosome segregation during mitosis. In a report carried out by Chan *et al.,* BORA knockdown cells displayed bipolar spindles larger and heavier than the normal ones and occasionally with multipolar spindles. Moreover, these cells showed long and wavy spindles and lagging chromosomes[338].

Accordingly, Seki *et al.,* observed that BORA-depleted cells increased the mitotic index, though did not substantially affect the progression through prometaphase stage, significantly prolonged the length of metaphase with unaligned chromosomes outside of the metaphase plate. At that stage, depletion of BORA reduced the interkinetochore tension as a twofold increase in kinetochore BubR1 signals was reported compared to control metaphase cells[346]. Density of spindle microtubules was also increased with k-fibers remained largely intact in BORA-depleted cells[338]. These changes in the spindle dynamics affects the rate of chromosome segregation in the anaphase stage. Indeed, the velocity of anaphase chromosome movement was reduced by 40% in BORA knockdown cells[346]. The exact mechanisms underlying these spindle defects remain to be unraveled, but since Chan *et al.,* observed that BORA and TPX2 compete and do not bind simultaneously to AURORA A, any reduction in BORA levels is expected to favor complex formation between AURORA A and spindle-associated activators, like TPX2, enhancing the activity of downstream effectors in the spindle, leading to a destabilization of centrosome-dependent microtubule assembly in mitosis.

1.5.5 BORA and cancer

In human cells, *BORA* gene is located in the chromosome 13q22.1 and spans 2,8 kb including 12 exons. This locus has been associated with malignant susceptibility in several types of cancer[347] specially in prostate cancer, where the deletion is associated with an aggressive disease[348,349]. *BORA* gene sequence codifies for at least 2 isoforms, the canonical isoform contains 559 amino-acids with 61,23 kDa and the second isoform 449 amino-acids and 53,40 kDa. BORA protein appears to lack a well-structured three-dimensional fold being intrinsically a disordered protein. This kind of proteins join their targets in a process known as "coupled folding and binding"[350]. Phosphorylation of the three conserved residues might promote the folding and binding of BORA to PLK1, nonetheless, further structural analysis of the minimal BORA fragment in complex with PLK1 and AURORA A is required to elucidate more about the BORA structure[335]. Since BORA governs PLK1 activation and subsequently controls cell cycle progression and genome stability, two hallmark features of cancer, it is tempting to speculate that BORA phosphorylation by CDK1/Cyclin A might contribute to PLK1 and AURORA A hyperactivation and tumorigenesis. In this sense, it is not rare to find BORA itself overexpressed in cancer. Recently, BORA protein expression was linked as biomarker for poor prognosis in breast, lung, and gastric adenocarcinomas[351]. Although the role of AURORA A and PLK1 have been exhaustively reported with inhibitors successfully working in different clinical trials in cancer, the study of BORA in cancer scenario is still reduced with no knowledge about its mechanistic role in cancer development or its potential capacity to become a therapeutic target more specific than targeting PLK1 and AURORA A kinases.

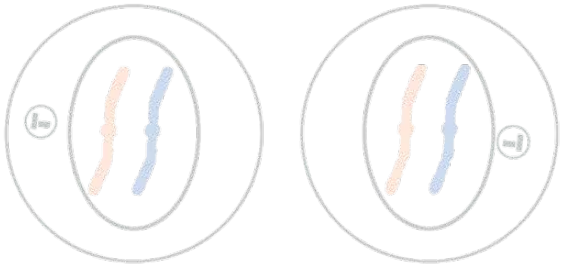

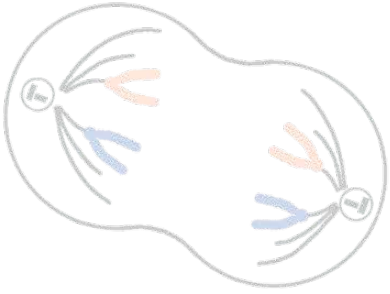

2. HYPOTHESIS & OBJECTIVES

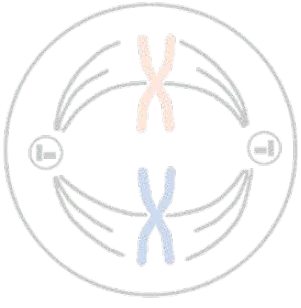

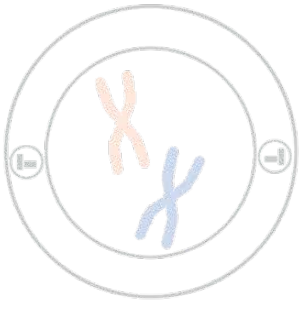

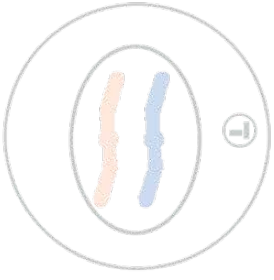

OC is the leading cause of death due to gynecologic malignancy. Despite increasing surgical approaches and platinum chemotherapy-based regimens, survival has remained largely invariable during the las two decades. Molecular targeted therapy has successfully impacted into the OC management with the inclusion of antiangiogenic agents and PARP inhibitors routinely in the clinic. However, these agents only provide efficacy in a subset of patients highlighting the clinical need of searching novel approaches for a larger number of OC patients. Numerous findings expose that cell cycle aberrations are a hallmark of cancer, playing important roles in tumor development and aggressiveness. Therefore, therapies targeting key pathways that drive and execute cell division are a major research goal with some of them currently used in clinics as standard of care for some types of cancer.

Volasertib, the most promising PLK1 kinase inhibitor, received the breakthrough designation therapy by the FDA due to its substantial therapeutic effect in cancer patients. However, its non-specificity might have undesirable adverse side effects in some patients, reconsidering its use as clinical compound. Under this scenario, improved and less toxic therapies should be designed to increase the treatment strategies and maximize patient outcome. Turning on PLK1 kinase activity is responsibility of BORA, a protein also described as regulator of spindle stability and essential for proper chromosome segregation. Even though BORA depletion has reported to have detrimental consequences to the spindle and the mitotic entry our understanding of its relevance and role in human cancer is hitherto unknown.

Hypothesis: Based on the contribution and therapeutic value of mitotic proteins in cancer, and particularly the significance of PLK1 inhibitors, we hypothesize that BORA might contribute to ovarian tumorigenesis and its inhibition might serve as potential therapeutic avenue. We will validate our hypothesis through the following objectives:

Objective 1: Identification of **novel druggable mitotic candidates** to be therapeutically exploited in OC.

Objective 2: Analyze the expression levels of BORA in **human OC samples** to correlate its expression with clinical and molecular variables such as histological grade, disease stage and/or survival.

Objective 3: Provide new insights into the mechanistic role of BORA in OC *in vitro*, *in vivo* and *ex vivo* by (3.a) **gain of function assays** ectopically overexpressing BORA and characterizing its possible implication as pro-oncogenic protein.

(3.b) **loss of function** experiments silencing BORA and exploring whether it could represent a promising novel therapeutic approach.

Objective 4: Characterize the mechanisms of action of BORA and anticipate new BORA targeted therapy to **manage OC treatment**.

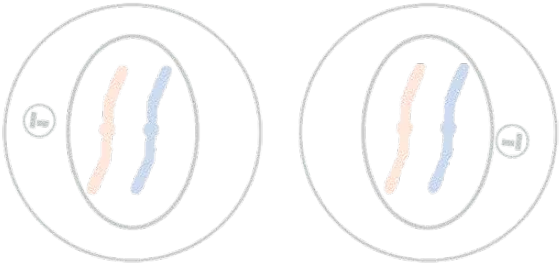

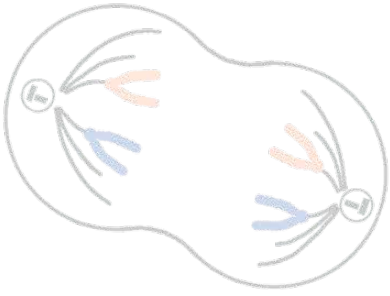

3. MATERIALS & METHODS

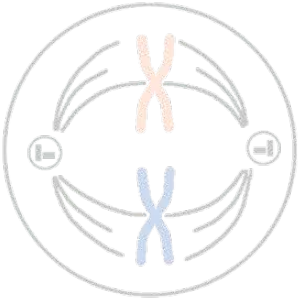

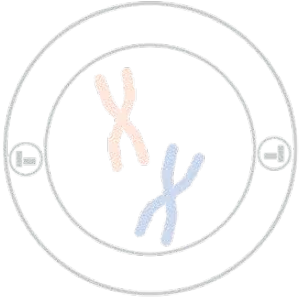

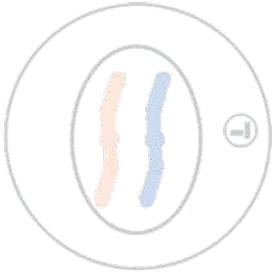

3.1 Analysis of OC gene expression datasets

An integrative bioinformatic screening approach was planned to evaluate potential therapeutic targets in advanced OC. This analysis encompassed the use of transcriptome data sets combined with survival data. First, we used the public transcriptome data set GSE14407 to identify genes associated with the initiation and/or progression in OC. This public data set contains the comprehensive genomic information of normal ovarian surface epithelial cells collected from 12 healthy ovaries and primary OC cells from 12 serous patients. Raw data (CEL files) were downloaded from Gene Expression Omnibus (GEO) and analyzed with the Transcriptome Analysis Console (TAC) software, developed by Affymetrix. Differentially expressed genes were filtered at 1% false discovery rate (FDR) and fold change >± 2,5. Functional annotation was performed with DAVID Bioinformatics Resources 6.8[352] and adjusted *p*-value<0,05 was determined to select the enriched gene sets terms.

Those genes included in mitotic term were chosen for further analysis. For the association of gene expression with clinical outcome in OC patients, we mined through the Kaplan-Meier Plotter online platform[353] using overall survival and default cutoff options. The correlation between *BORA* expression (Affymetrix ID: 219544_at) with OS curves in other tumor types was also obtained from the Kaplan-Meier Plotter tool. The number of patients included for each tumor analysis are detailed in Table 5.

Different clinically representative ovarian data sets comparing benign samples *vs* tumoral specimens were used to confirm BORA up-regulation. Four data sets were selected: GSE26712 (n=10 benign, n=185 tumors); GSE27651 (n=6 benign, n=35 tumors); GSE28666 (n=12 benign, n=18 tumors) and GSE54388 (n=6 benign, n=16 tumors). *BORA* mRNA levels were retrieved from these data sets using the GEO2R tool.

BORA expression was also explored among different tumor types from the TCGA database collection. The expression data for all available tumor types and the annotated number of genomic alterations for each type were retrieved using the R2 Genomics Analysis and Visualization Platform and cBioPortal websites (Table 5). Gene expression data from the ovarian TCGA cohort was used to correlate BORA expression with clinic-pathological and molecular variables. Correlation of BORA expression with different parameters such as disease stage, histological grade, the proliferative marker Ki67, *CIN25* score and *MUC16* expression levels was conducted. Graphs were plotted on GraphPad Prism Software for visual representation and statistical calculation.

Table 5. Data sets and bioinformatic tools used in this study.

Dataset	Number of samples	Cancer Type	Status	References	Tool
GSE14407	24	OC	Public	-	GEO2R
GSE26712	195	OC	Public	-	GEO2R
GSE27651	41	OC	Public	-	GEO2R
GSE38666	30	OC	Public	-	GEO2R
GSE54388	22	OC	Public	-	GEO2R
Kaplan-Meier Plotter	1656	OC	Public	Gyorffy B *et al.,* (2012)	http://kmplot.com
Kaplan-Meier Plotter	1402	Breast	Public	Gyorffy B *et al.,* (2010)	http://kmplot.com
Kaplan-Meier Plotter	1926	Lung	Public	Gyorffy B *et al.,* (2013)	http://kmplot.com
Kaplan-Meier Plotter	364	Liver	Public	Menyhart O *et al.,* (2018)	http://kmplot.com
cBioPortal	-	23 types	Public	Gao *et al.,* (2013)	http://www.cbioportal.org/
DAVID	-	-	Public	Huang W *et al.,* (2007)	http://david.abcc.ncifcrf.gov
GSEA	-	-	Public	Subramanian *et al.,* (2005)	http://www.broad.mit.edu/gsea/
Venny Diagram	-	-	Public	Oliveros, J.C. (2007-2015)	http://bioinfogp.cnb.csic.es/tools/venny
R2 genomics	-	-	Public	-	http://r2.amc.nl

3.2 Human samples

3.2.1 Fresh tissues

A total of 60 fresh primary tissues, including 20 benign ovaries and 40 ovarian tumors, were obtained from patients enrolled at the Vall d'Hebron Hospital Campus (Barcelona, Spain) to analyze *BORA* mRNA expression levels (Table 6). For immunoblot analysis, BORA protein levels were assessed in a total of 6 benign ovaries and 8 HGSC specimens (Table 7). All tissue-samples were examined by the pathologist to confirm the diagnosis. All patients gave their written informed consent and tissues were collected under the ethical committee approval from patients of the Gynecology department. Institutional Review Board (IRB) number: PRAMI3082015. Tissues were collected the day of the surgery and stored at -80ºC until processing.

Table 6. Fresh-frozen tissue samples of the ovary for mRNA analysis.

N	Group	Type	FIGO stage	Grade
1	B	Folicular cyst	-	-
2	B	Folicular cyst	-	-
3	B	Folicular cyst	-	-
4	B	Folicular cyst	-	-
5	B	Folicular cyst	-	-
6	B	Simple mucinous cyst.	-	-
7	B	Simple mucinous cyst.	-	-
8	B	Simple mucinous cyst.	-	-
9	B	Simple mucinous cyst.	-	-
10	B	Simple mucinous cyst.	-	-
11	B	Simple serous cyst.	-	-
12	B	Simple serous cyst.	-	-
13	B	Simple serous cyst.	-	-
14	B	Simple serous cyst.	-	-
15	B	Simple serous cyst.	-	-
16	B	Simple serous cyst.	-	-
17	B	Simple serous cyst.	-	-
18	B	Fibroma	-	-
19	B	Fibroma	-	-
20	B	Fibroma	-	-
21	Early	Mucinous	IC	2
22	Early	Mucinous	IIB	2
23	Early	Mucinous	IA	2
24	Early	Mucinous	IC	2
25	Early	Endometrioid	IA	3
26	Early	Endometrioid	IC	2
27	Early	Endometrioid	IC	2
28	Early	Endometrioid	IC	1
29	Early	Endometrioid	IC2	1
30	Early	Endometrioid	IA	3
31	Early	Clear cell	IIB	3
32	Early	Clear cell	IC	3
33	Early	Clear cell	IIB	3
34	Early	Papillary serous	IC	3
35	Early	Papillary serous	IIA	3
36	Early	Papillary serous	IIb	1
37	Early	Papillary serous	IA	3
38	Early	Papillary serous	IC1	3
39	Late	Clear cell	IIIC	3
40	Late	Clear cell	IIIC	3
41	Late	Not typified	IIIC	2
42	Late	Mucinous	IA	-
43	Late	Papillary serous	IIC	3
44	Late	Papillary serous	IIIC	3
45	Late	Papillary serous	IV	3
46	Late	Papillary serous	IV	3
47	Late	Papillary serous	IIIA	3
48	Late	Papillary serous	IIIC	3
49	Late	Papillary serous	-	3
50	Late	Papillary serous	IIIC	3
51	Late	Papillary serous	IIIC	3
52	Late	Papillary serous	IIIC	3
53	Late	Papillary serous	IIIC	3
54	Late	Papillary serous	IIIC	3
55	Late	Papillary serous	IV	3
56	Late	Papillary serous	IIIC	3
57	Late	Papillary serous	IIIC	3
58	Late	Papillary serous	-	3
59	Late	Papillary serous	IIIC	3
60	Late	Papillary serous	IIIC	3

"B" benign ovary; Early and Late: stage of the primary tumors; "cyst." means cystadenoma, a type of benign cyst of the ovary; "Grade" means grade of cell differentiation.

Table 7. Fresh-frozen tissue samples of the ovary for protein analysis.

N	Group	Type	FIGO stage	Grade
1	B	Simple serous cyst.	-	-
2	B	Simple serous cyst.	-	-
3	B	Simple serous cyst.	-	-
4	B	Fibroma	-	-
5	B	Simple serous cyst.	-	-
6	B	Fibroma		
7	T	Papillary serous	IV	3
8	T	Papillary serous	IV	3
9	T	Papillary serous	IIIC	3
10	T	Papillary serous	IVB	3
11	T	Papillary serous	IIIC	3
12	T	Papillary serous	IIIA1	3
13	T	Papillary serous	IIIB	3
14	T	Papillary serous	IIIB	3

"B" benign ovary; "T" Primary tumor; "cyst." means cystadenoma, a type of benign cyst of the ovary; "Grade" means grade of cell differentiation.

3.2.2 Formalin-fixed embedded tissues

Twenty-six formalin-fixed paraffin embedded (FFPE) primary and metastatic paired tissues from 13 HGSC patients were obtained from the repository of the Pathology Department of Vall d'Hebron Hospital

Campus (Barcelona, Spain) under the protocol approved by the IRB. Clinical data were obtained from patients' medical records (Table 8).

Table 8. FFPE paired primary tumor and metastases specimens.

Patient	Type	FIGO stage	Grade	Tumor (Yes/No)	Metastasis (Yes/No)
1	Papillary serous	IIIC	3	Yes	Yes
2	Papillary serous	IIC	3	Yes	Yes
3	Papillary serous	IIIC	3	Yes	Yes
4	Papillary serous	IIIC	3	Yes	Yes
5	Papillary serous	IIIC	3	Yes	Yes
6	Papillary serous	IIIC	3	Yes	Yes
7	Papillary serous	IIIC	3	Yes	Yes
8	Papillary serous	IIIC	3	Yes	Yes
9	Papillary serous	IIIC	3	Yes	Yes
10	Papillary serous	NA	NA	Yes	Yes
11	Papillary serous	IIIC	3	Yes	Yes
12	Papillary serous	IIIC	3	Yes	Yes
13	Papillary serous	IV	3	Yes	Yes

NA: Not Available

3.3 Gene expression analysis by RT-qPCR

3.3.1 RNA extraction

RNA from tissue samples was obtained using the miRNeasy Mini Kit (Qiagen). Briefly, ~ 2-3 cm^2 of tissue was cut in dried ice in small pieces and homogenized using FastPrep 24 Lysing Matrix Tubes (MP Biomedicals) with 700 µL of Quiazol Lysis Reagent (Qiagen) in the Fast-Prep-24 instrument for 30 sec at 6.5 r/p for 3 times. Then, homogenates were centrifuged for 5 min at 800 g at 4ºC to eliminate cell debris. Supernatant fraction was then transferred into a 1,5 mL Eppendorf and 140 µL of chloroform was added to continue with the extraction following the kit instructions. **RNA from FFPE tissues** was extracted using the RNeasy FFPE Kit (Qiagen) following the manufacturer conditions. **Total RNA from cell lines** was extracted from cell lysates using miRNeasy Mini Kit (Qiagen) following manufacturer instructions. Briefly, cells were pelleted at 800 g and washed once with 1X phosphate-buffered saline (PBS). Then, 700 µL of Quiazol Lysis Reagent was added to each pelleted sample and manufacturer instructions were followed. All RNA samples were subjected to DNase treatment and diluted in 30-35 µL of RNA-se water (pre-heater 10 min at 50ºC). Quantity and quality of RNA was measured by Nanodrop 2000 and the samples with a ratio A260:A280 between 1.8 and 2.0 were accepted for subsequent analyses.

3.3.2 cDNA retrotranscription

One µg of total RNA was retrotranscribed into cDNA using SuperScript III reverse transcriptase following manufacturer protocol (Invitrogen). The retrotranscription was carried out in a thermal cycler under the

following protocol: 25ºC during 10 min and 42ºC during 60 min to retro- transcribe RNA; 95ºC during 5 min to stop the reaction and then 4ºC to maintain samples in optimal conditions. The resulting cDNA was stored at -20ºC until further use.

3.3.3 Quantitative real time PCR

RT-qPCR of *BORA* and *GAPDH* genes were performed using Taqman probes (Hs00227229_m1 for BORA and Hs02786624_g1 for *GAPDH*). For *BCL2*, *CDK6*, *RERG, CLASP2*, *MARK2*, *SFRP1, SLC25A10*, *MMP7*, *IL1B*, *TPM1*, *MAD2L1*, *SHROOM2*, *GAPDH* and *RHOB* genes, RT-qPCR was performed using SYBR green fluorescence technology (Applied Biosystems) at the Genomics facility in VHIR. Primers were designed using the ProbeFinder Assay Design Software from Roche website and synthetized through Sigma-Aldrich. All primer sequences are listed in Table 9. Designed primers were firstly tested in a conventional PCR and then used at 0,1 µM final reaction concentration. *GAPDH* was used as an internal standard. Relative quantification of gene expression was performed with the $2^{\wedge(-\Delta\Delta Ct)}$ method[354].

Table 9. Primer sequences for genes detected by Sybr-Green RTqPCR technology.

Gene Name	NM_number (GeneCards)	Catalog #	Primer sequence (5'-3')	Amplicon length
TPM1	NM_001018004	4689011001	ctctgaggctctcaaagatgc cagctggatgcgtctgttc	104 nt
SHROOM2	NM_001649.3	4685016001	gaggtcccggtcttcacc ctgccttcgcagttcgac	67 nt
MMP7	NM_002423.4	4685032001	cggatggtagcagtctaggg aggttggatacatcactgcattag	111 nt
CDK6	NM_001145306.1	4684982001	tgatcaactaggaaaaatcttggac ggcaacatctctaggccagt	70 nt
BCL2	NM_000633.2	4688988001	agtacctgaaccggcacct gccgtacagttccacaaagg	74 nt
MAD2L1	NM_002358.3	4687655001	cgcgtgctttgtttgtgt gctgttgatgccgaatgag	117 nt
SFRP1	NM_003012.4	4687990001	gctggagcacgagaccat tggcagttcttgttgagca	75 nt
CLASP2	NM_001207044.1	4689089001	cgaccaagtgtgagtcaagg gatctggaatggtgtctggag	110 nt
MARK2	NM_017490.3	4685008001	tggaagtcgctggtagtcct ccccgaatcatgttggac	95 nt
SLC25A10	NM_001270888.1	4688031001	cccgcagacttggtcaac tacgcggtacaggccatc	99 nt
IL1B	NM_000576.2	4689011001	tacctgtcctgcgtgttgaa tctttgggtaatttttgggatct	76 nt
RHOB	NM_004040.3	4688589001	gcatgaacaggacttgacca ctgtgtcctccccaagtcag	71 nt
RERG	NM_032918.2	4689038001	aacttgcagaggaccgtagc ttggaagagtccacaatcctg	64 nt
GAPDH	NM_002046	04689003001	caacgaccactttgtcaagc ggtggtccaggggtcttact	115 nt

"nt" means nucleotides

3.4 Protein analysis detection

3.4.1 Protein extraction

Protein extracts were obtained in 1X RIPA buffer (Tris HCl 1,5 M pH=8,8, NaCl 5 M, Triton X-100, EDTA 500 mM) supplemented with 1X EDTA-free complete protease inhibitor (Roche) and phosphatase cocktail inhibitors (P5726, P0044, Sigma). **For human ovarian samples and tumor xenografts from mice**, tissues were chopped with a lancet and then homogenized for 10 seconds three times per sample. Then, samples were sonicated at amplitude 60A for 5 seconds. Protein fraction was then obtained after a centrifugation at 22.000 g for 15 min at 4ºC. Protein lysates were store at -20ºC. In the case of **cell lines and spheroids**, cells were centrifuged at 3.000 rpm to collect all cells, including the death ones, and washed once with 1X PBS. Pelleted cells were lysed with 1X RIPA Buffer on ice for 1h incubation with 1-minute vortex every 15 minutes. Protein fraction was then obtained after a centrifugation at 22.000 g for 15 min at 4ºC.

3.4.2 Immunoblot

Proteins (50-100 µg) were resolved in NuPAGE 4-12% Bis-Tris gels at 200V, transferred onto PVDF membranes blocked for 1h with 5% non-fat milk (Panreac) or 5% bovine serum albumin (BSA) (Sigma) and probed overnight at 4ºC with the indicated antibodies (Table 10). After 1h of incubation with horseradish peroxidase-conjugated secondary antibodies (Sigma) signal was acquired with Immobilon Western (Millipore) or ECL substrate (GE Healthcare).

3.4.3 Antibodies

The list of antibodies used in this thesis are detailed in the following table.

Table 10. List of antibodies used in this thesis.

Antibody	Cataog number	Source	Application	Conditions
AURORA A	610938	BD Biosciencies	IB	1:1000 dilution, 5% nonfat milk
BCL-2	M0887	DAKO	IB	1:1000 dilution, 5% nonfat milk
BORA	#12109	Cell Signaling	IB	1:1000 dilution, 5% nonfat milk
Caspase 3	#9665	Cell Signaling	IB	1:1000 dilution, 5% BSA
Caspase 3 Cleaved	#9661	Cell Signaling	IB	1:750 dilution, 5% BSA
CDK6	#13331	Cell Signaling	IB	1:1000 dilution, 5% nonfat milk
Cyclin B1	#05-373	Merk Millipore	IB	1:1000 dilution, 5% nonfat milk
JNK1	#3708	Cell Signaling	IB	1:1000 dilution, 5% nonfat milk
Ki67	790-4286	Roche (Ventana Med.Syst.)	IHQ	-
mCherry	96752FR	Novus Biologicals	IB	1:1000 dilution, 5% nonfat milk
PARP1	#9542	Cell Signaling	IB	1:3000 dilution, 5% BSA
PLK1	#4535	Cell Signaling	IB	1:1000 dilution, 5% nonfat milk
pTCTP (Ser46)	#5251	Cell Signaling	IB	1:3000 dilution, 5% BSA
p27 Kip1 (D69C12)	#3686	Cell Signaling	IB	1:1000 dilution, 5% nonfat milk
p53	sc-126	Santa Cruz Biotechnology	IB	1:1000 dilution, 5% nonfat milk
p65	#8242	Cell Signaling	IB	1:1000 dilution, 5% nonfat milk
α-Tubulin	T9026	Sigma Aldrich	IB	1:5000 dilution, 5% nonfat milk
β-Actin	sc-47778	Santa Cruz Biotechnology	IB	1:10.000 dilution, 5% nonfat milk
anti-Rabbit IgG	A0545	Sigma Aldrich	IB	1:5000 dilution, 5% nonfat milk
anti-Mouse IgG	A9044	Sigma Aldrich	IB	1:5000 dilution, 5% nonfat milk; 1:10.000 for α-Tubulin

"IB" means Immunoblot; "IHQ" means Immunohistochemistry

3.5 Cell Culture

3.5.1 Commercial cell lines

Commercial cell lines OAW42, 59M, OAW28, OVCAR4 and TOV112D were acquired from European Collection of Authenticated Cell Cultures (ECACC) whereas SK-OV-3, UWB1.289 and UWB1.289+BRCA1 were acquired from American Type Culture Collection (ATCC). A2780p and A2780cis were a generous gift from Dr. Francesc Viñals (IDIBELL, Spain). BIN-67 were also kindly provided from Dr. Barbara Vanderhyden (Ottawa Hospital Research Institute, Canada) and IGROV-1 from Dr. Antonio Rosato (Istituto Oncologico Veneto, Italy). IOSE-503 and IOSE-385 immortalized ovarian surface epithelium cell lines were obtained from the Ovarian Cancer Research Team OvCaRe (Vancouver, Canada). HEK-293T and Hela S3 were acquired from Dr. Erich A. Nigg lab´s. (Universität Basel, Switzerland). SK-N-B2 cell line was obtained from Dr. Miquel Segura (VHIR, Barcelona, Spain). MDA-MB-231 from Dr. Stephan Hummer (VHIR, Barcelona, Spain). LNCAP from Dr. Rosanna Pacucci (VHIR, Barcelona, Spain). Table 11 summarizes all ovarian cell lines including information about

histological subtype, origin, culture conditions and *in vitro* handling. All culture mediums were supplemented with 10% of heat-inactivated fetal bovine serum (FBS) except for BIN-67 cells that 20% of FBS was used. All media were supplemented with 2 mM L-glutamine, 100 U/mL penicillin and 100 µg/mL streptomycin. All cultures were maintained at 37ºC in a satured atmosphere and 5% of CO_2. Ovarian cancer cell lines were authenticated in 2015 by short tandem repeat profiling, using the GenePrint 10 System (UAT, VHIR). Cells were regularly tested for mycoplasma contamination. All cell lines were expanded and stored in liquid nitrogen.

Table 11. General characteristics of the human ovarian cell lines used.

Ovarian Cancer Cell Line	Tumor Type	Source	Growth properties	Medium	Passages	*In vitro* Handling
TOV112	High-grade Endometrioid Adenocarcinoma	Primary tumor	Monolayer. Morphology: epithelial	Mixt medium: mixture (1:1) of MCDB-105 and M-199 mediums (Biological Industries)	2-3 days	++
SKOV3	Epithelial Ovarian Adenocarcinoma	Ascites	Monolayer. Morphology: mesemchymal	McCoy's 5A (Biowest)	2-3 days	+++
OAW42	Epithelial Ovarian Adenocarcinoma	Ascites	Monolayer. Morphology: mesemchymal	DMEM High glucose (Biowest)	3-4 days	++
OAW28	High Grade Serous Carcinoma	Ascites	Monolayer. Morphology: epithelial	DMEM High glucose (Biowest)	3-4 days	++
59M	Endometrioid carcinoma of ovary (with clear cell components)	Ascites	Monolayer. Morphology: mesemchymal	DMEM High glucose (Biowest)	4-5 days	+
OVCAR4	High Grade Serous Carcinoma	Primary tumor	Monolayer. Morphology: epithelial	Mixt medium: mixture (1:1) of MCDB-105 and M-199 mediums (Biological Industries)	4 days	+
A2780p	High-grade Endometrioid Adenocarcinoma	Primary tumor	Monolayer. Morphology: epithelial	RPMI (Biowest)	2-3 days	+++
A2780cis*	High-grade Endometrioid Adenocarcinoma	Primary tumor	Monolayer. Morphology: epithelial	RPMI (Biowest)	2-3 days	+++
BIN-67	Small cell carcinoma of the ovary hypercalcemic type (SCCOHT)	Primary tumor	Monolayer. Morphology: epithelial	100 mL de DMEM F12 (Biowest) + 100 mL DMEM High Glucose (Biowest) + 50 mL de FBS	3-4 days	++
IGROV-1	High-grade Endometrioid Adenocarcinoma	Primary tumor	Monolayer. Morphology: epithelial	RPMI (Biowest)	1-2 days	+++
IOSE 503	Immortalized Ovarian Surface Epithelium	Ovarian surface tissue	Monolayer. Morphology: epithelial	Mixt medium: mixture (1:1) of MCDB-105 and M-199 mediums (Biological Industries)	1-2 days	+++
IOSE 385	Immortalized Ovarian Surface Epithelium	Ovarian surface tissue	Monolayer. Morphology: epithelial	Mixt medium: mixture (1:1) of MCDB-105 and M-199 mediums (Biological Industries)	1-2 days	+
UWB1.289	High Grade Serous Carcinoma	Primary tumor	Monolayer. Morphology: mesenchymal	1:1 mixture of medium RPMI (Biowest)+ MEGM (FBS 3%)	3-4 days	+
UWB1.289 + BRCA1	High Grade Serous Carcinoma	Primary tumor	Monolayer. Morphology: mesenchymal	1:1 mixture of medium RPMI (Biowest) + MEGM (FBS 3%) + G418	2-3 days	++

Footnote: *Resistant OC cell line to cisplatin, derived from the parental A2780p. "+" means *in vitro* ease of handling

3.5.2 Patient-derived ascites primary cultures

Primary cultures were established using freshly ascitic fluid collected the day of surgery from advanced OC patients (Table 12). Isolation of patient-derived tumoral cells was performed following the previous described protocol[355]. Basically, after surgery, ascitic fluid containing the tumor cells was mixed (1:1) with Mixt medium (50% MCDB109, 50% M-199; Biological Industries), 15% FBS, 2 mM L-glutamine, 100 U/mL penicillin and 100 µg/mL streptomycin, and seeded in standard culture flask. The flask was not manipulated for a week to allow the tumor/spheroids cells to disaggregate and adhere to the surface of the flask. Then, culture media was washed to remove blood, fat particles and other non-tumoral cells. Primary cultures were maintained at 37ºC and 5% of CO_2. Adherent cells were grown with the medium until 80% of confluence. At this point, cells are able to split. Cells were used from 2 to 6 passages.

Table 12 Patient-derived ascites from advanced stage OC used in this thesis.

# Patient	Type	FIGO stage	Grade	Culture conditions
VH-01	Clear cell	IIIC	3	Mixt medium: mixture (1:1) of MCDB-105 and M-199 mediums (Biological Industries), with 15% FBS, 2 mM L-glutamine, 100 U/mL penicillin and 100 µg/mL streptomycin
VH-02	Papillary serous	IIIC	3	
VH-03	Papillary serous	IIIA1	3	
VH-04	Papillary serous	IIIC	3	
VH-05	Papillary serous	IIIC	3	
VH-06	Papillary serous	IIIC	3	

*VH means Vall Hebron Hospital

3.6 Plasmids and cloning

Gene silencing via lentiviral transduction of constitutive shRNA particles

For stable depletion of BORA, short hairpin RNAs targeting the coding sequence 5'-CCGGTTGATAATGGCAGTTTA-3' for shBORA#1 and 5'-TAACTAGTCCTTCGCCTATTT-3' for shBORA#2 were designed and cloned into a pLKO.1-puro plasmid (Addgene Plasmid #10878). These two sequences were selected based on the successful depletion observed by siRNAs in Chan *et al.,*[338]. Primers for the two target sequences were designed, annealed and cloned into the pLKO.1 TRC Cloning Vector (Addgene #plasmid10878) following an adapted protocol[356]. Plasmids that were successfully ligated were sequenced using a primer against the human U6 promoter (sequence: 5'-GACTATCATATGCTTACCGT-3'). Both designed shRNAs particles efficiently knock-downed BORA protein expression, as confirmed by immunoblot. Control included non-targeting shRNA (shCTL) was a generous gift from Dr. Miquel Segura (VHIR, Barcelona). Inducible lentiviral shRNAs for BORA depletion were purchased from Open Biosystems (Dharmaon, GE Healthcare) in the pTRIPZ system. (pTRIPZ_BORA-V1: ID# THS_157921; pTRIPZ_BORA-V2: Clone ID# THS_393909). The BORA-

targeted sequences with this inducible system are detailed in Table 13. pTRIPZ empty vector was kindly provided from Dr. Miquel Segura (VHIR, Barcelona).

BORA genetic editing using CRISPR/Cas9 technology

BORA gene targeting in SK-OV-3 cells was carried by CRISPR/Cas 9 system. BORA sgRNA was designed using the CRISPR Design tool (http://crispr.mit.edu) targeting the second exon of all BORA isoforms and with the smallest number of off-targets. The sgRNA sequence selected was 5'-GTGTCATCGTACCCTCTCCT-3'. Gene-specific sgRNA oligos were designed, annealed and subcloned into the CRISPR/Cas9 plasmid pSpCas9(BB)-2A-GFP (pX458) following the protocol described by Ran *et al.,*[357]. pX458 plasmid (#Addgene plasmid 48138) was kindly provided by Dr. Diego Arango (VHIR, Barcelona).

Lentiviral constructs for BORA overexpression

For BORA overexpression system, the human coding sequence (CDS) of BORA cloned into a pENTR/D-TOPO vector was obtained from Dr. Erich Nigg's Lab and previously published in Chan *et al.,*[338] . Gateway LR Clonase II reaction (Life Technologies) was used to transferred the BORA CDS into the pINDUCER20 lentiviral Tet-on System (Addgene plasmid #44012), following the manufacturer's protocol. The obtained vectors were sequenced using pINDUCER20 forward primer (5'-ACCTCCATAGAAGACCC-3') in the UAT at VHIR. BORA overexpression was confirmed by immunoblotting and by RT-qPCR.

Table 13. Plasmids and vectors used in this thesis.

Vector	Function	Supplier	Sequences
pSpCas9(BB)-2A-GFP (PX458)	CRISPR/Cas9 Empty vector	Addgene plasmid #48138 / Dr. Diego Arango (VHIR)	
pSpCas9(BB)-2A-GFP_ Bora	CRISPR/Cas9 Targeting Bora Exon 2	-	5'-GTGTCATCGTACCCTCTCCT-3'
pLKO.1-TRC	Empty vector TRC cloning	Addgene plasmid #10878	
pLKO-shCTL	Constitutive CTL shRNA	Sigma Aldrich / Dr. Miquel Segura (VHIR)	
plLKO.1- shBora#1	Constitutive Bora shRNA	-	5'-CCGGTTGATAATGGCAGTTTA-3'
plLKO.1- shBora#2	Constitutive Bora shRNA	-	5'-TAACTAGTCCTTCGCCTATTT-3'
pTRIPZ - Empty Vector	Tet-inducible lentiviral vector for empty backbone	Dharmaon, GE Healthcare / Dr. Miquel Segura (VHIR)	
pTRIPZ_Bora-V1	Tet-inducible lentiviral vector for Bora shRNA	Dharmaon, GE Healthcare ID Clone V2THS_157921	5'-TTCTTTCTCAGAAGCACTG-3'
pTRIPZ_Bora-V2	Tet-inducible lentiviral vector for Bora shRNA	Dharmaon, GE Healthcare ID Clone V3THS_393909	5'-AAACTGCCATTATCAACCG-3'
pDNOR CDS Bora	Coding Sequence of human Bora cloned	Dr. Erich Nigg (Universitat de Basel, Switzerland)	
pINDUCER20	Tet-inducible lentiviral vector for ORF expression	Addgene plasmid #44012	
pIND_EV	Tet-inducible lentiviral empty vector	-	
pIND_Bora	Tet-inducible lentiviral vector for Bora expression	-	
psPAX2	2nd generation lentiviral packaging plasmid	Addgene plasmid #12260	
pMD2.G	2nd generation lentiviral envelope plasmid	Addgene plasmid #12259	
PLK1-FRET	Untargeted Plk1 phosphorylation sensor	Dr. Michael Lampson (University of Pennsylvania)	BRCA2 sequence PPSLSSTVLIVRN

3.7 Förster resonance energy transfer (FRET)

A Hela S3 cell line stably expressing an untargeted PLK1 phosphorylation sensor[358] (plasmid was a kind gift from Michael Lampson, University of Pennsylvania, Philadelphia, US) was generated. Briefly, cells were transfected using X-tremeGENE 9 regent following the manufacturer recommendations. Cells expressing the sensor were selected by G418 (500µg/mL) for five days and single cells populations were selected. Cells were grown on LabTek II 8-well chamber and were transiently transfected with the indicated mCherry-BORA constructs and depleted of BORA or control siRNA. Live imaging of the PLK1 sensor was performed at the Advanced Light Microscopy Unit at the Centre for Genomic Regulation (CRG, Barcelona), on a Leica TCS SP5 II CW-STED microscopy using a 40 x 1.25 NA objective and a charge-coupled device camera (ORCA-AG; Hamamatsu Photonics). CFP was excited with a CFP excitation filter, and CFP and YFP emissions were acquired sequentially by switching between CFP and YFP emission filters using a filter wheel (Ludl Electronic Products). The CFP/YFP emission ratio in each image was calculated after background subtraction and averaged over multiple cells using an ImageJ script.

3.8 Lentiviral production and transduction

Lentiviral particles were produced in HEK-293T cells using the 2nd generation lentiviral plasmids following an adapted protocol from the one described by Naldini *et al.,*[359]. Briefly, one day before the transfection, $4 \cdot 10^6$ of HEK-293T cells were seeded on a 10 cm culture plate. On the transfection day, Lipofectamine 2000 were mixed in Opti-MEM serum free media with the vector of interest and the packaging psPAX2 (Addgene plasmid #12260) and envelope pMD2.G (Addgene plasmid #12259) lentiviral plasmids; during 20 min to allow complex formation. Then complexes were added to the cellular culture (Opti-MEM supplemented with 5% FBS). Culture media with the complexes was changed after 4-6h of transfection in order to avoid Lipofectamine 2000 toxicity. After 48h, viral supernatant was filtered through a 0,45 µm filter and the indicated cells were transduced with the fresh viruses plus 5-8 µg/mL of polybrene (Milipore) to enhance the transduction of the ovarian cells. After 24h of incubation, the media of the infected cells was replaced with growth medium.

3.9 Generation of stable cell lines

CRISPR/Cas9 stable clones were obtained by single-cell cloning. Briefly, SK-OV-3 cells were firstly transfected using X-tremeGENE 9 DNA transfection reagent (Roche) following manufacturer's protocol. Forty-eight hours later, cells were diluted and plated at 1 cell per well onto 96-well plates. Single cell-

derived clones were isolated and further expanded. BORA protein expression was monitored in those clones that were able to grow by immunoblot analysis to select potential knock-out or knockdowns clones. For selection of stable pTRIPZ lines, SK-OV-3 cells were transduced with lentiviral particles coding the pTRIPZ-EV or the pTRIPZ-BORA-V1 or pTRIPZ-BORA-V2 vectors and 0,75 µg/mL of puromycin was added to the growth medium for 5-7 days. IOSE-503 and SK-OV-3 pINDUCER20 transduced cell lines were selected with 0,5-1 mg/mL of geneticin (G418). To avoid clonal variation, stable cell lines were established from a mixed population of multiple clones. BORA knockdown or overexpression was monitored by immunoblot or RT-qPCR.

3.10 Cellular viability assays

3.10.1 Proliferation assays

For BORA gain of function assays, IOSE and SK-OV-3 pIND_EV and pIND_BORA cells were seeded at $6 \cdot 10^4$ cells into 35 mm-dish with or without doxycycline (0,25 µg/mL). Cells were counted using trypan blue and reseeded at days 3, 6 and 9 (n= 3/condition). For BORA loss of function experiments, cells were seeded at $3 \cdot 10^5$–$1 \cdot 10^6$ cells per p60 plate and infected with shCTL, shBORA#1 or shBORA#2 lentiviruses. Twenty-four hours post-transduction cells were seeded at $2{,}5 \cdot 10^3$–$1 \cdot 10^4$ cells per well onto 96-well plate (n= 6/condition). Between 6 and 8 hours post seeding, the first plate was fixed as time zero. At the indicated times (24h, 48h, 72 and 96h), plates were fixed in formaldehyde 4% solution during 20 minutes and stored in PBS 1X at 4°C. At the end of the experiment, cells were stained with 0.5% crystal violet. Crystals were dissolved with 15% acetic acid and optical density was read at 590 nm using a microplate spectrophotometer. Normalization against time zero gave us the rate of proliferation. pTRIPZ_EV, pTRIPZ-BORA_V1 and pTRIPZ-BORA_V2 stable SK-OV-3 cells were seeded at $6 \cdot 10^4$ cells onto 35 mm-dish with or without doxycycline (1 µg/mL). Cells were counted using trypan blue and reseeded at days 3, 6 and 9 (n= 3/condition). Proliferation assays using the CRISPR/Cas9 BORA knockdown clones were performed by cell counting with trypan blue at days 3, 6 and 9.

3.10.2 Colony formation

Colony formation assays were performed by seeding the ovarian cell lines (IOSE-503, SK-OV-3, OAW42, TOV112D, A2780p, IGROV-1 and SK-OV-3 pTRIPZ derived cells) onto six-well plates in triplicates ($5 \cdot 10^2$ - $1 \cdot 10^3$ cells/well; n=3/condition). Media was refreshed every 3 days and in the indicated cells doxycycline (1 µg/mL) was added. After 9-11 days, cells were stained with 0,5% crystal violet, photographed and scored. Differences in colony formation where assessed by comparing the number of colonies against control.

3.10.3 Apoptosis assay

Cells transduced with either shCTL or shBORA#2 viruses were plated onto 24-well plates ($15 \cdot 10^3$ – $10 \cdot 10^4$ cells/well). 96h post-transduction, cells were stained with 0,05 mg/mL Hoechst for 30 min at RT. Condensed or fragmented nuclei were counted as dead cells as described previously[360]. Five hundred cells were counted for each data point, and the count was repeated three times in independent experiments.

3.10.4 Drugs combination studies

For drug toxicity assays, OC cell lines (SK-OV-3, and A2780p) were seeded at $1\text{-}5 \cdot 10^3$ cells/well onto 96-well plates (n= 6/condition). The day after, cells were treated with doses from 0,01 µM to 25 µM of *Navitoclax*, *Venetoclax*, *Palbociclib* and *Amebaciclib* compounds (Selleckchem). Stock solutions were made for each compound in DMSO at 5000× concentrations used in experiments. Structures for all agents are publicly available in Selleckchem. Five days later, cells were fixed and stained with crystal violet. Cell proliferation was compared *vs* vehicle-treated cells (DMSO). For drug combination experiments, A 4x4 checker-board matrix format was used to assess two-drug combination at five clinically achievable concentrations of *Palbociclib* and *Navitoclax*. After 5 days, cells were fixed and stained with crystal violet. Synergism, additivity or antagonism of the combination was determined by the Chou–Talalay method[361] using the Compusyn Software (ComboSyn Inc.). Drugs were combined at different non-constant ratios at the concentrations indicated (range from 0,01 µM to 7,5 µM).

3.11 Cell cycle analysis

SK-OV-3, A2780p and IOSE-503 cells transduced with shCTL or shBORA viruses for 72h were used to analyzed the cell cycle profile. Flow cytometry analysis of DNA content was performed by cell fixation with 30% 1X PBS and 70% cold ethanol. Ethanol was slowly added while mixing to avoid cell-aggregates at a concentration of $1 \cdot 10^6$ cells/mL. Samples were stained by a treatment solution with sodium citrate (38 mM), propidium iodide (500 µg/mL) and RNase A (10 mg/mL) at 4°C overnight. Data were acquired using a FACS Calibur flow cytometry (FACS Calibur; Becton–Dickinson). Cell aggregates were excluded using pulse processing and a minimun of 10.000 single events were mesuared per sample. Cell cycle phase distribution was analyzed using FlowJo 9.6.4 software (Treestar).

3.12 Boyden chamber migration assay

Transparent PET membrane 8.0 µm pore size inserts for 24-well plates (Falcon) were used to evaluate the migration capacity of OC cell lines. SK-OV-3 transduced cells (shCTL or shBORA) and IOSE-503

(pIND_BORA or pIND_EV) cells were trypsinized, pelleted, washed twice with 1X PBS, and resuspended in medium without 10% FBS. One hundred µL of cell suspension ($1 \cdot 10^6$ cells) were loaded in the upper compartment of the cell culture inserts, while 600 µL of medium with 10% FBS were added in the lower compartment. When appropriate, 0,25 µg/ml doxycycline was added to the medium. Cells were allowed to migrate for 4h at 37ºC in a humidified atmosphere at 5% CO_2. Then, they were fixed with 4% formaldehyde during 30 min at RT. Cells that had attached to the membrane but not migrated were completely removed using a cotton swap. Migrated cells were stained for nuclei with 1 µL/mL Hoechst 33258 during 10 min at RT. Migration was evaluated by counting randomly cell nuclei in 5 fields/well under 20x objective of Eclipse TE2000-S microscope.

3.13 Anchorage independent growth assay (soft agar)

To monitor anchorage independent growth, IOSE-503 and SK-OV-3 transduced cell lines (pIND_EV or pIND_BORA) were suspended in complete Mixt medium containing 0,3% agar with or without 0,25 µg/mL doxycycline and then plated onto six-well plates on top of 0,6% agar in Mixt medium previously polymerized (n =3/condition). Cultures were grown for 21 days until colonies were visible. Macroscopically colonies were photographed (3 fields per well) and scored. Differences in colony formation were assessed by comparing the number of colonies against control (pIND_EV).

3.14 Growth inhibition activity assay

Cell density is a signal for inhibition of cell growth. To monitor whether the overexpression of BORA could bypass this inhibitory signal, IOSE-503 pIND_EV and pIND_BORA cells were seeded onto 6-well plates ($3 \cdot 10^5$ cells/well, i.e. high density) with 3 mL of medium with or without 0,25 µg/mL doxycycline and incubated at 37ºC in a humidified atmosphere at 5% CO_2 during 10-15 days after 100% confluence. Cell medium was renewed every 2-3 days and plates were photographed every 3-4 days.

3.15 OC mouse xenografts experiments

All animal experiments were carried out in the Animal-VHIR facilities (VHIR, Barcelona) under the supervision of the Comité Ètic d'Experimentació Animal (CEEA) approved by the protocol number 04/18.

To assess the role of BORA on tumor engraftment, SK-OV-3 xenotransplant cells were transduced with the constitutive lentiviral particles shCTL or shBORA for 48h before injection. $2 \cdot 10^6$ cells were subcutaneously injected into the flank of 6-week old female NMRI-Nude mice (ENVIGO, n=7/group) in 300 µL of 1X PBS and Matrigel (1:1).

To assess the role of BORA on tumor growth, SK-OV-3 xenotransplant transduced cells with pTRIPZ_BORA-V1 vector were injected in the flank of 6-week-old female NMRI-nude mice ($2 \cdot 10^6$ cells/mouse; ENVIGO) in 300 µL of 1X PBS and matrigel (1:1). When tumors reached approximately 150 mm^3, mice were randomly divided in two experimental groups (n=7/group). The control one was maintained with 2% of sucrose (untreated) and the second group was administered with doxycycline-supplemented water (1 mg/mL) and 2% of sucrose *ad libitum*. Animals were weighted every 2-3 days.

To analyze the transformation capacity of BORA, IOSE-503 stable cells lines expressing either pIND-EV or pIND-BORA were injected into the two flanks of 7-week-old female NMRI-nude mice (ENVIGO, n=4/group) in a total volume of 300 µL of PBS and Matrigel (1:1). Two approaches were carried out: one injecting $5 \cdot 10^5$ cells and the other one injecting $5 \cdot 10^6$ cells per flank. Animals were administered with 1 mg/mL of doxycycline in 2% sucrose once week before the injection. Doxycycline was continually administrated in drinking water throughout the remainder of the study. Tumor engraftment was analyzed twice per week. SK-OV-3 xenotransplant cells transduced with pIND-EV or pIND-BORA were subcutaneously injected into one flank of 7-week old female NMRI nude mice (ENVIGO; $2 \cdot 10^6$ cells; n=7/group) in 300 µL of PBS 1X and Matrigel (1:1). Doxycycline (1 mg/mL) was added to the drinking water with 2% sucrose one-week pre-injection and during the whole experiment.

In all procedures, tumor volume was measured by electronic caliper 2-3 times weekly and estimated by the formula [Volume = $(Width)^2$ x $Length/2$], where *W* is shortest and *L* is the longest radius of the tumor (mm). At the end of the experiments mice were euthanized and tumors were removed and weighted. Each tumor was then longitudinally split in several pieces. One piece was fixed in 10% of formalin paraffin-embedded, and 5 µm sections were performed for hematoxylin and eosin (H&E) and Ki67 staining. The other pieces were snap frozen in liquid nitrogen and stored at –80°C for later protein extraction.

3.16 Immunohistochemistry

Tumor tissues collected from the mouse were fixed in formalin 10% for two days and then stored at 1X PBS until they were processed into paraffin in Anatomy Patology facility at Vall Hebron Hospital. Immunohistochemistry was performed for Ki67 detection on a BenchMark Ultra platform (Ventana Medical Systems) following the recommended protocol, in collaboration with the Pathology Department from VHUH. Antigen retrieval was performed with CC1 buffer for 20 min. A rabbit monoclonal 30-9 antibody was used to detect Ki67 protein (Ventana Medical Systems) and the incubation time was of 32 min. Detection system was Ultraview DAB, used following the recommended protocol. Percentage tumoral cells and Ki67 positive cells was evaluated attending the help of a pathologist, considering the

number of tumor cells in three high power fields, detected morphologically, and counting the number of nuclear stained cells with Ki67 immunohistochemistry using the ImageJ software. H&E staining was performed following conventional procedures at the Pathology Department of HUVH.

3.17 Multicellular tumor spheroids

For tumor sphere formation score, cells were reversely transduced with the lentiviral particles shCTL and shBORA#2 plus 8 µg/mL of polybrene and seeded in a cell density of $15 \cdot 10^3$ cells/well in a non-adherent 24-well plates (coated with 0.5% agarose with non-supplemented Mixt medium). Cells were grown in serum-free Mixt-medium supplemented with 1X B27 (Invitrogen), 2 mM L-glutamine (Invitrogen), 20 ng/mL EGF (ProSpec-Tany Technogene Ltd) and 20 ng/mL FGF (ProSpec-Tany Techno- gene Ltd). To quantify the number and compactaction of spheres, thirty-six hours later, the number of spheres was scored (spheres between 50-100 µm, ≥ 100 µm, ≥ 200 µm if applicable in diameter). The variation between the number of spheroids between the two experimental groups was represented and scored with the applicable diameters depending of each patient.

To **assess the viability** of the tumor spheroids with the depletion of BORA, $3 \cdot 10^5$ cells were seeded and reversely transduced with the lentiviral particles onto non-adherent 6-well plates in serum-free mixt-medium supplemented with the complements above described (n=3/condition). At 96h post-transduction, MTS assay was performed. For viability assays using the FDA-approved inhibitors *Navitoclax* and *Palbociclib*, once spheroids were formed (24h) they were treated during 96h with the indicated drug concentrations (*Navitoclax*: 4 µM; *Palbociclib*: 12 µM). Viability was measured by MTS assay. Briefly, tumor spheroids were collected, pelleted at 3.000 g during 5 min at RT and washed once with 1X PBS. Then spheroids were disaggregated with 0.5 mL of 1X StemPro® Accutase® Cell dissociation Reagent (GibcoTM, ThermoFisher Scientific) prior to the MTS assay. Then PMS and MTS reagents were mixed using a ratio of 1:20 and the mixture was added to each well (96-well plate) containing 100 µL of disaggregated patient-cell (in culture medium) at a ratio of 1:10. MTS was measured between 2-5h of incubation at 490 nm (optical density), depending on each patient.

For **tumor spheroids protein extraction**, $3 \cdot 10^5$ cells were seeded onto 6-well plates coated with 1 mL of 0,5% of agarose non-supplemented medium (n=2/condition). Spheres were collected at 96h post-transduction or 96h post-drug treatment and proceeded to obtain the protein lysates for immunoblot as explained before (section 3.4)

3.18 Microarray gene expression analysis

Transcriptome expression profile of triplicate experimental samples for SK-OV-3 shCTL and shBORA-infected cells was performed using the Affymetrix microarray platform and the Genechip Human Gene 1.0 ST Array. Concentration and quality of extracted RNA were measured by Nanodrop and RNA Nano Chip Bioanalyzer (Agilent Technologies), respectively. The efficiency of BORA depletion was measured by RTqPCR. Human Clariom™ S assay (Affymetrix) was used to analyze gene-level whole-transcriptome expression profiling, which accurately detects more than 20,000 well- annotated genes, with more than 200,000 probes. The VHIR Genomic Facility performed next steps after RNA extraction, including the conversion of mRNA in cDNA, the biotinylation, hybridization, labeling and scanning of the chips. Raw data was obtained and processed using the Expression Console and the Transcriptome Analysis Console (version 3.0) software's, both from Affymetrix. Principal component analysis was generated by Expression Console and for the differential gene expression analysis between shCTL and shBORA data the Transcriptome Expression Console was used, which automatically analyze the fold change and statistical *p*-values based on one-way ANOVA *t*-test. The functional annotation of resulting gene list was performed using the Gene Set Enrichment Analyses databases (GSEA) (Broad Institute, Boston USA). GSEA was performed using javaGSEA Desktop Application (Broad Institute). All collections of publically available gene sets used were extracted from Molecular Signatures Database v6.0 (MSigDB). Nominal *p*-value<0,05 or FDR<0,5 were chosen as the cut-off criteria to identify the significantly enriched gene sets. Heatmaps were generated for pathways enriched in both conditions by normalization to the median and log2 transformation of the array expression values. Heatmaps include genes contained in the enriched gene sets and differentially expressed. The accession number for microarray analysis reported in this work is GSE133635.

3.19 Statistical methodologies

Statistical significance was determined by two-sided unpaired Student's *t*-test, One-way ANOVA test or Two-way ANOVA analysis (GraphPad Prism Software). Correlation analysis was performed using Pearson´s test or, alternatively, Spearman's test for non-normal distributions. Unless otherwise indicated, mean ± SEM values are the average of a minimum of three independent experiments. Data with *p*-value <0,05 were considered statistically significant. *,#,$*P*<0,05; **,##,$$*P*<0,01; ***,###,$$$*P*<0,001; ****,####,$$$$*P*<0,0001. The normal distribution of the data was verified (Shapiro-Wilk and Kolmologrov tests) and accordingly, non-parametric tests (Mann Whitney) were used for comparisons between groups when analyzing human ovarian tissues.

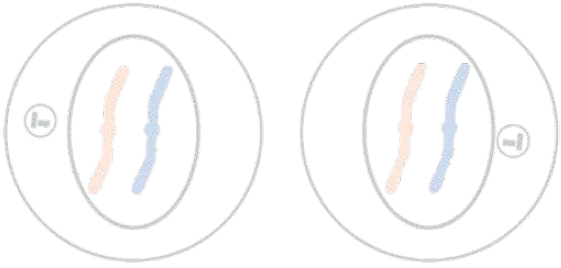

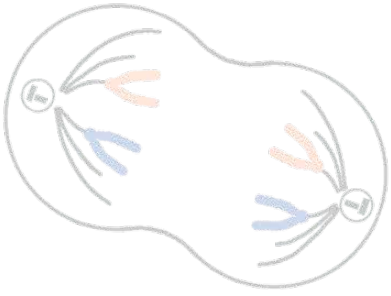

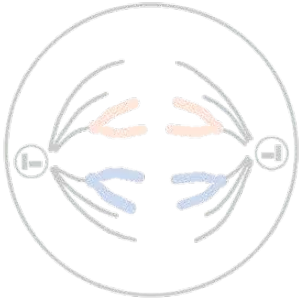

4. RESULTS

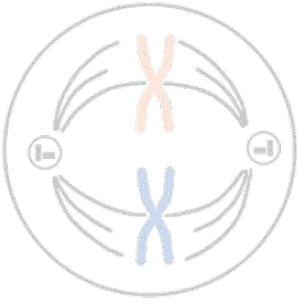

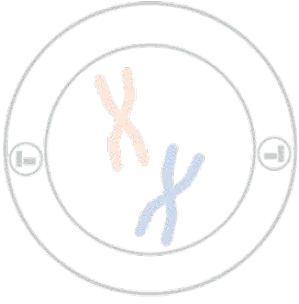

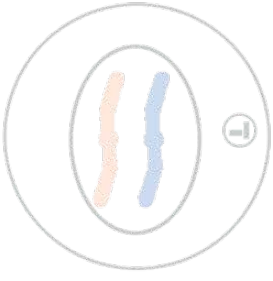

4.1 An integrated -bioinformatics screening identifies mitotic regulators potentially involved in OC

In an attempt to identify therapeutically actionable candidates in OC, we performed an integrative computational analysis of transcriptomics data combined with clinical survival outcome using different cohorts of OC specimens. Firstly, we analyzed the public data set GSE14407, which includes comprehensive genomic information of healthy ovarian surface epithelia samples (n=12) compared to serous OC epithelia tissues (n=12) (

Figure **13**A). A total of 2280 genes were found differentially expressed between the two groups (Fold change >± 2,5 and FDR=0,01). Most genes were linked to relevant cancer related functions; including cell cycle, p53 and PI3K-AKT signaling KEGG pathways (

Figure **13**B).

A

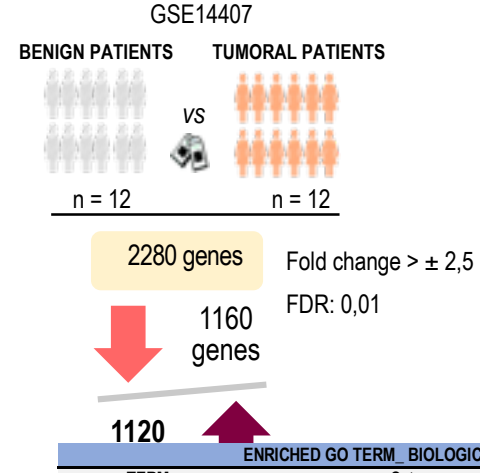

B

ENRICHED KEGG PATHWAYS			
TERM	Category	Genes	*p-value*
KEGG_PATHWAY	Cell cycle	33	2,90E-06
KEGG_PATHWAY	Pathways in cancer	74	3,80E-06
KEGG_PATHWAY	Proteoglycans in cancer	42	5,70E-05
KEGG_PATHWAY	Ras signaling pathway	44	2,30E-04
KEGG_PATHWAY	Oocyte meiosis	26	3,60E-04
KEGG_PATHWAY	Fc gamma R-mediated phagocytosis	21	6,50E-04
KEGG_PATHWAY	p53 signaling pathway	18	7,50E-04
KEGG_PATHWAY	PI3K-Akt signaling pathway	58	1,10E-03
KEGG_PATHWAY	Circadian entrainment	22	1,30E-03
KEGG_PATHWAY	Dopaminergic synapse	27	1,50E-03
KEGG_PATHWAY	Small cell lung cancer	20	2,00E-03
KEGG_PATHWAY	Rap1 signaling pathway	38	2,60E-03
KEGG_PATHWAY	Glutamatergic synapse	24	2,90E-03
KEGG_PATHWAY	HIF-1 signaling pathway	21	3,60E-03
KEGG_PATHWAY	Axon guidance	25	5,80E-03

C

ENRICHED GO TERM_ BIOLOGICAL FUNCTION			
TERM	Category	Genes	*p-value*
GOTERM_BP_DIRECT	Cell division	57	1,90E-14
GOTERM_BP_DIRECT	DNA replication	32	4,50E-11
GOTERM_BP_DIRECT	Mitotic division	39	1,10E-09
GOTERM_BP_DIRECT	Sister chromatid cohesion	23	8,30E-09
GOTERM_BP_DIRECT	G1/S transition of mitotic cell cycle	19	3,60E-06
GOTERM_BP_DIRECT	Mitotic metaphase plate congression	11	1,10E-05
GOTERM_BP_DIRECT	DNA replication initiation	10	2,20E-05
GOTERM_BP_DIRECT	Mitotic sister chromatid segregation	9	2,20E-05
GOTERM_BP_DIRECT	Angiogenesis	28	2,70E-05
GOTERM_BP_DIRECT	Regulation of cyclin-dependent protein kinase	10	1,20E-04

Figure 13. Identification of up-regulated proteins in OC sample patients. (A) Gene expression analysis comparing non-transformed human epithelial ovarian cells to ovarian carcinoma cells using data contained in GSE 14407 and analyzed with the Affymetrix Transcriptome Analysis Console software. **(B)** Functional annotation of differentially expressed genes as reported by DAVID Bioinformatics 6.8. Enriched KEGG pathways using all genes

were plotted. **(C)** For the up-regulated genes, the enriched GO term biological processes with *p*-value <1,2·10^{-4} were plotted.

Focusing on the up-regulated genes, Gene Ontology (GO) functional term enrichment identified 10 GO gene clusters being cell division and mitotic process the top significant enriched categories (

Figure **13**C). Taking into consideration that the mitotic spindle apparatus encompasses a plethora of validated targets currently used as standard-of care in multiple cancers[176,221], we searched for novel actionable candidates within these top-deregulated GO terms. Candidates selected for functional studies were filtered as for:

(i) Genes included in the mitosis (and cell division) GO term.
(ii) The correlation between gene expression in tumor samples and patients' outcome.
(iii) Genes no previously reported in relation to ovarian tumorigenesis.

We checked the correlation between the gene expression and patient survival using the Kaplan Meier-Plotter online platform in a cohort of more than 600 OC patients[353]. We only considered those genes whose high expression was correlated with worse overall survival (*p*-value <0,05) (Table 14; third column), and of these, we explored if their involvement in OC was already described. Those genes already described either as prognosis biomarker or with potential therapeutic capacities in OC cells were not further selected (Table 14; fourth column).

Scoring through these filters a total of eight gene-candidates were found for further analysis: *SPC25*, *BORA*, *CDCA5*, *CCNA*, *FAM64A*, *KIF20B*, *OPI5* and *SPC24* (Table 14B). Taken together, using an integrative computational analysis of transcriptomics data and clinical records from human cancer specimens enabled the identification of unexplored up-regulated mitotic candidates to target in OC.

Matching our previous interest in the laboratory on the activation of PLK1 kinase by BORA[333,335,338], together with our interest in searching potential novel cell cycle blocking therapeutics, we further explored BORA in this study as possible cancer target. We firstly delved into the mechanisms of BORA protein regulation to carry out its function in mitotic entry and after we investigated its role in a cancer context. Nevertheless, we are considering some of the other seven proteins as attractive targets to be explored in the near future.

Table 14. Bioinformatic screening identifies a range of novel upregulated mitotic genes in OC. (A) The "+" and "-" symbols refer to (1) included or not in the mitotic process GO term or (2) if the gene or protein –function in OC has already been reported or not in the literature. High and Low refers to the gene expression correlated with worse survival outcome. References for genes already described in OC are also indicated. **(B)** Venn diagram showing the overlap of genes with the indicated features.

A

Cell Division	Mitotic process	Correlation with Survival: Worse if (*p*-value)	Ovarian cancer related function	
SPC25	+	High (0.0006)	+	
BORA	+	High (0.0216)	+	
CDCA5	+	High (0.0069)	+	
CCNA	+	High (0.0199)	+	
FAM64A	+	High (0.0137)	+	
KIF20B	+	High (0.0007)	+	
OPI5	+	High (0.0337)	+	
SPC24	+	High (1.1e-5)	+	
ARF6	-	Low (0.0259)	-	Broner et al., 2017
BUB1B	+	High (0.0007)	-	Sun et al., 2017
BUB1	+	High (0.0029)	-	Sun et al., 2017
CKS1B	-	High (0.0002)	-	Kawahara et al., 2017
CKS2	-	High (0.0046)	+	
CABLES1	-	High (0.0322)	-	Sakamoto et al., 2008
ERCC6L	-	High (0.2838)	+	
NEK2	+	High (0.0463)	-	Liu et al., 2014
NUF2	+	High (2.9e-5)	-	Sethi et al., 2012
ARHGEF2	+	Low (0.0501)	+	
SAC3D1	+	High (0.2219)	+	
TPX2	+	High (0.0013)	-	Tian et al., 2018
ZWINT	-	High (0.0021)	-	Xu et al., 2016
AURKA	+	High (9.6e-6)	-	Chiba et al., 2017
BIRC5	+	High (0.1289)	-	Wang et al., 2018
CDC20	+	High (0.0745)	-	Gayyed et al., 2016
CDC25A	+	High (0.0117)	-	Brogini et al., 2000
CDC25C	+	High (0.2129)	-	Gao et al., 2018
CDC6	+	High (0.1469)	-	Deng et al., 2016
CDC7	-	High (0.1324)	-	Kulkarn et al., 2009
CDCA3	+	High (4.5e-5)	-	Itzel et al., 2015
CDCA8	-	High (0.2284)	-	Wrzeszczynski et al., 2011
CENPE	-	High (0.0052)	-	Chong et al., 2018
CENPF	+	High (3.5e-5)	-	Xu et al., 2016
CCNB1	-	High (1.1e-9)	-	Ye et al., 2015
CCNB2	+	High (0.0488)	-	Fridley et al., 2018
CCNB3	-	High (0.0193)	+	
CCNE1	-	High (0.001)	-	Ayhan et al., 2017
CCNE2	-	High (0.0005)	-	Xie et al., 2017
CCNY	-	High (0.1277)	-	Liu et al., 2016
CDK1	+	High (0.0006)	-	Yang et al., 2016
FAM83D	+	High (8.1e-6)	-	Ramakrishna et al., 2010
HMGA2	+	High (0.0364)	-	Wu et al., 2011
KIF11	+	High (0.0016)	-	Xu et al., 2016
KIF14	-	High (2.5e-5)	-	Qiu et al., 2017
KIF18B	-	High (0.0132)	-	Itzel et al., 2015
KIF2C	+	High (0.0377)	-	Zhao et al., 2014
KIFC1	-	High (0.0104)	-	Mittal et al., 2016
NCAPG	-	High (0.0022)	+	
HNCAPH	-	High (0.0172)	+	
PTTG1	-	High (0.0498)	-	Nakachi et al., 2016
PSRC1	-	High (0.0221)	+	
RCC2	-	High (1.4e-5)	-	Wu et al., 2018
SETP11	-	High (0.0433)	+	
SPAG5	-	High (0.0009)	+	
SMC1A	-	High (0.0443)	-	Liu et al., 2014
TIMELESS	+	Low (0.0165)	-	Jim et al., 2015
TACC3	-	High (0.0548)	-	Lauffart et al., 2005
UBE2C	-	High (0.0004)	-	Martínez et al., 2018

B

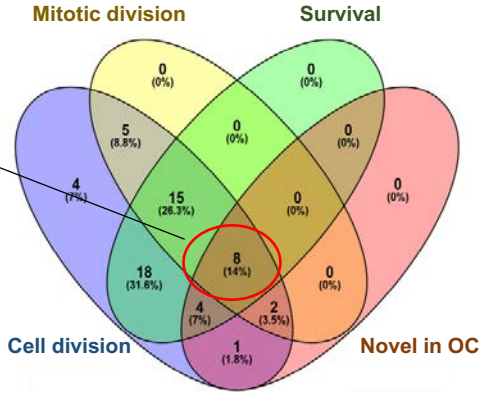

4.2 CDK1-dependent BORA phosphorylation on three conserved residues is essential for PLK1 activation and mitotic entry

Previous experiments from our group and collaborators have demonstrated that the CDK1-dependent N-terminal BORA phosphorylation is essential for PLK1 activation in G2/M checkpoint recovery, where PLK1 is indispensable to re-enter into mitosis[331]. We also know that there are three phosphorylation sites (S/P) conserved in the BORA N-terminal part among different species (S41, S112, and S137 aa in human BORA) that are important to its function as demonstrated in Thomas *et al.*[333]. In this report, we monitored PLK1 activity measuring the phosphorylation on the T-loop of PLK1 by immunoblotting with different BORA constructs (a BORA siRNA-resistant transgene, $BORA^{R}$; and a mutated BORA transgene in the three conserved residues (S41A, S112A, and S137A; $BORA^{R3A}$). The expression of $BORA^{R}$ but not BORA mutated in the three conserved residues, $BORA^{R3A}$, was accompanied by an increase in the phosphorylation of PLK1-T210[333]. Although phosphorylation of T210 is associated with activation of PLK1, it is not a direct readout of PLK1 activity itself and it does not allow monitoring other possible mechanisms of PLK1 activation independent of PLK1-pT210. Moreover, antibodies targeting T210-phosphorylated PLK1 have been shown to recognize off-target epitopes, making analysis based on these signals ambiguous[336].

To address this issue and to be able to obtain results at single cell level, we developed a HeLa cell line stably expressing an untargeted fluorescence resonance energy transfer (FRET) sensor to track PLK1 activity changes in real time. The probe consists of two fluorophores, a donor fluorophore (cyan fluorescent protein, CFP) and an acceptor fluorophore (yellow fluorescent protein, YFP), which are joined in the linker region between donor and acceptor by a consensus PLK1 motif shown to be phosphorylated specifically by PLK1 in mitosis[358]. Phosphorylation of the probe by PLK1 is expected to induce a conformational change within the sensor that leads to a low resonance energy transfer between YFP and CFP (low FRET; high CFP/YFP ratio)[362], whereas dephosphorylation results in high-energy transfer (high FRET; low CFP/YFP ratio). Following the experimental set up shown in Figure 14A, depletion of BORA resulted in decreased CFP/YFP ratio compared to control cells, consistent with a decrease of PLK1 activity (Figure 14B-C). Cells transfected with wild type siRNA-resistant BORA, $BORA^{R}$, displayed similar FRET levels to those seen in control cells (high CFP/YFP ratio; Figure 14B). In contrast, in $BORA^{R3A}$ expressing cells, the sensor was dephosphorylated resulting in higher FRET (low CFP/YFP ratio), indicating that PLK1 activity was reduced (Figure 14B-C). Therefore, we confirmed with a different *in vivo* assay that phosphorylation on the three evolutionary conserved N-terminal sites of BORA is required for PLK1 activity when cells recover from a G2 DNA damage induced arrest.

To assess whether non-phosphorylatable BORA was abrogating PLK1 activity leading to impaired entry into mitosis or it was simply delaying mitotic entry, we monitored the percentage of cells in mitosis by means of phosphorylated Histone 3 (pS10-H3) staining in fixed samples and by counting the percentage of mitotic transfected cells (mCherry positive) in our live FRET set up at 9h and 18h of nocodazole treatment. We observed accumulation of mitotic cells after 18h of nocodazole treatment in control cells and BORA^{R} rescued cells, but no significant increment was seen upon BORA depletion or in cells transfected with the BORA^{R3A} version (Figure 14D), indicating that either there is no residual PLK1 activity when BORA is not phosphorylated in the three abovementioned CDK1 sites or that any residual activity is not sufficient to drive mitotic entry.

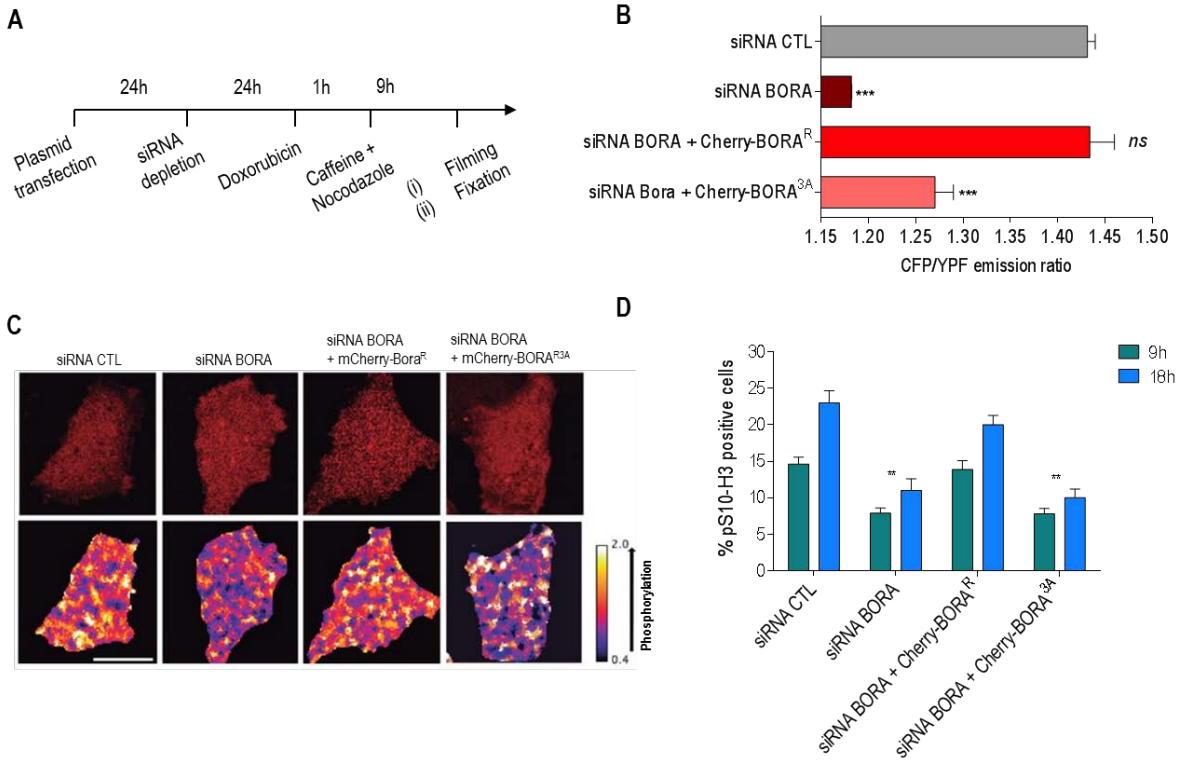

Figure 14. CDK1-dependent BORA phosphorylation on the conserved phosphorylation sites is essential for PLK1 activation and mitotic entry. (A) Scheme of the assay used to test the effect of CDK1-dependent sites on BORA for PLK1 activation in living cells and for pS10-H3 staining assessment in fixed cells. **(B)** Histogram showing CFP/YFP emission ratios averaged over multiple cells (n ≥ 15 per condition) expressing an untargeted PLK1 phosphorylation sensor after G2 checkpoint recovery of control or BORA-depleted cells transfected with mCherry-BORAR and mCherry-BORA^{R3A}constructs. N=4 independent experiments. Mean ± standard deviation is shown. Statistical significance was determined using Student's *t*-test: ns=not significant; ***P<0,001. **(C)** Representative images showing the mCherry channel (top panels) and the false-colored coded CFP/YFP emission ratios (bottom panels). Scale bar: 10 µm. **(D)** Histogram showing the percentage of pS10-H3 positive cells after G2-checkpoint recovery of control or BORA-depleted cells transfected with Cherry-BORA constructs after 9 hours and 18 hours treated with nocodazole as in (A), n=3 independent experiments. Statistical significance was determined using Student's *t*-test: **P<0,01 for BORA-depleted cells or mCherry-BORA^{R3A} –rescued cells and siRNA BORA cells compared to mCherry-BORA^{R}–rescued cells.

4.3 BORA overexpression is associated with worse overall patient survival in OC

The abovementioned findings support a key mechanistic role of BORA in cell division and progression. Together with the fact that BORA has been recently found up-regulated in other tumor types[351] we speculated that BORA could have some implication in OC as well. We first confirmed that BORA levels were consistently up-regulated in tumor patient-derived ovarian samples compared to benign ovaries in four representative public datasets, as depicted in Figure 15.

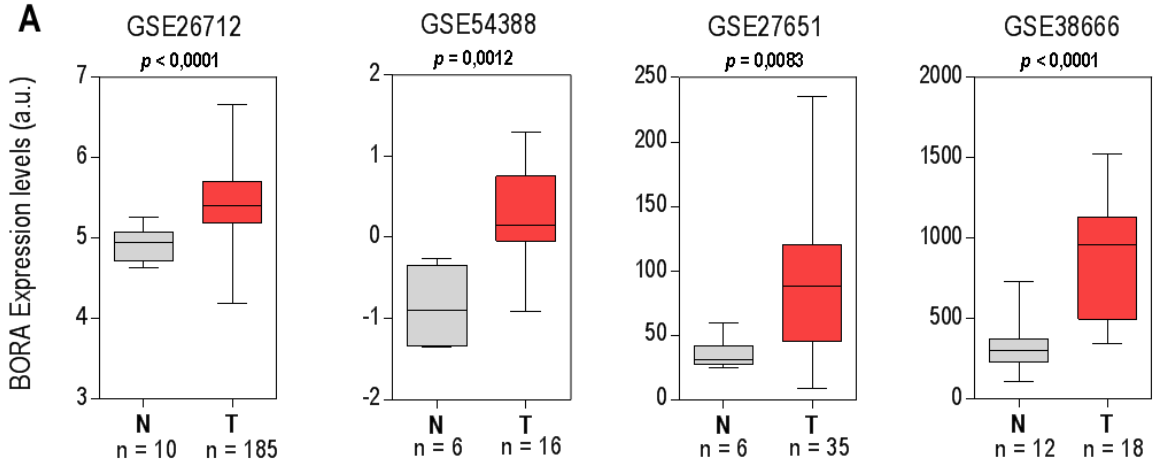

Figure 15. Examination of *BORA* expression in published ovarian transcriptomic profiles. (A) Different data sets were mined to confirm *BORA* overexpression at mRNA levels in ovarian –tumor and benign samples. "N" means Normal ovaries and "T" means Tumor ovaries. Sample size (n) for each group is illustrated under the graphs. *P*-values were calculated using a two-tailed Student's *t*-test. Data was retrieved using the GEO2R platform.

Secondly, we mined throughout The Cancer Genome Atlas data set, which includes the genomic information of 541 patients[363]; to further explore the involvement of *BORA* in OC. In these patients, we observed that *BORA* expression positively correlated with high histological grade, which exemplifies those cancer cells poorly differentiated, hence the most aggressive ones, and with advanced clinical stage; that englobes those patients with the worse survival outcome (Figure 16A-B). In agreement to the already established function of BORA in mitotic division, we analyzed the expression of *BORA* in compared to the *CIN25* score expression, a measure of chromosome instability linked to tumor aggressiveness[204,364], and we found a strong positive correlation in the TCGA ovarian cohort (r=0,58; Figure 16C). In addition, high *BORA* expression was also significantly correlated with increased *MKI67* expression, suggesting that *BORA* might identify highly proliferative tumor cells (Figure 16D). In contrast, no correlation was observed with *MUC16* expression (CA-125 protein antigen), a routinely serum protein biomarker of OC recurrence[365] (Figure 16E).

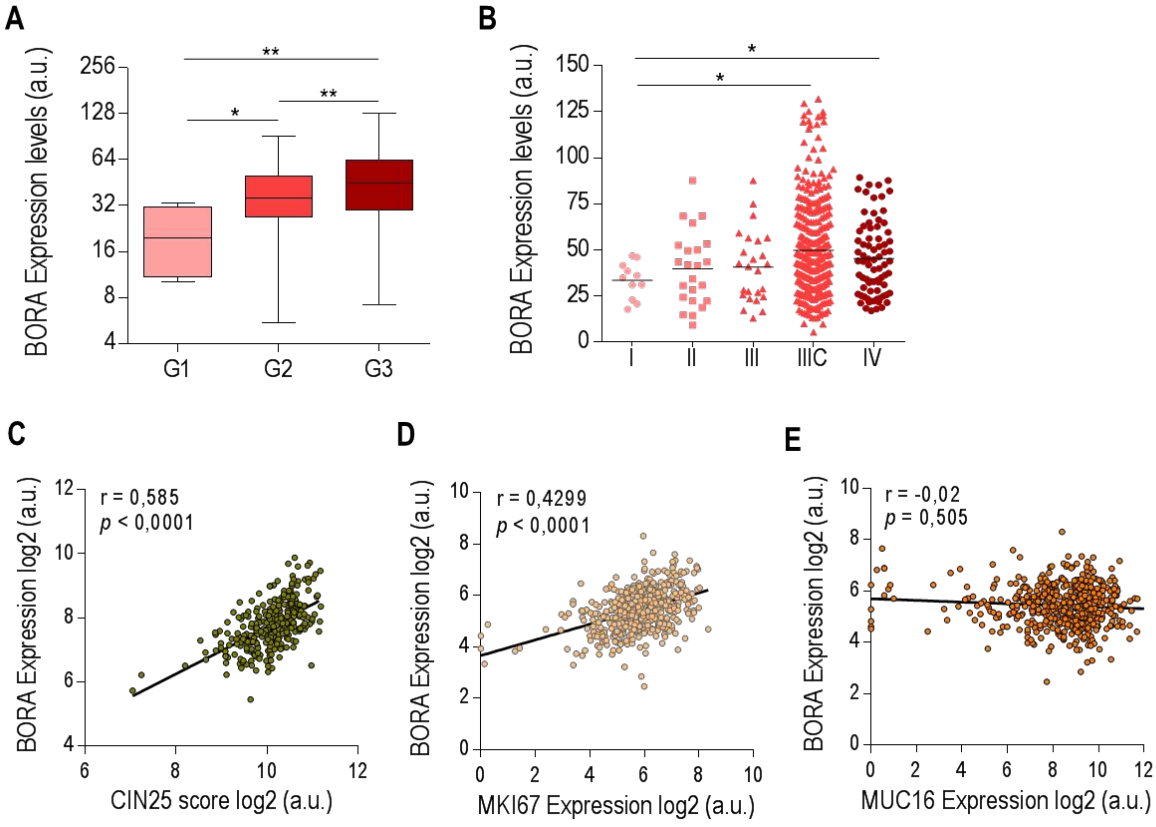

Figure 16. *BORA* is overexpressed in aggressive and advanced OC tumors. (A) *BORA* mRNA expression in TCGA ovarian samples (n=541 specimens) categorized by histological grade and **(B)** clinical disease stage. **(C)** Correlation (Pearson) between *BORA* and *CIN25* expression, a score of 25 genes expression related to chromosomal instability and with **(D)** *MKi67* expression in TCGA ovarian samples. **(E)** Correlation of *BORA* expression with *MUC16* expression (CA-125 antigen protein), the solely current biomarker used into the clinics to detect OC recurrence. *P*-values were calculated using a two-tailed Student's *t*-test. **P*<0,05; ***P*<0,01; ****P*<0,001.

To interrogate whether *BORA* up-regulation also apply to other malignant tumors, we mined throughout the different TCGA publicly available data sets for all major cancer types. Interestingly, *BORA* was found to be higher in a broad number of tumor types, particularly in head and neck, leukemia and colon carcinomas when compared to a data set that comprises the expression levels of normal tissues (GSE3526) (Figure 17A). Interestingly, overexpression of *BORA* also correlated with poor survival in breast, lung and liver cancer patients (Figure 17D), concurred with the results in OC, and indicating BORA might be used as prognostic biomarker in these carcinomas.

Intriguingly, even if pooling mutations, amplifications and deletions, the frequency of genomic alterations per *BORA* was rather low in all types of cancer (Figure 17B). The mutation rates of BORA protein ranged from 0 to 4% across various cancer types (Figure 17B; green bar) and were uniformly spread across the length of the protein without any particular hotspot mutation (Figure 17C). *BORA* amplification was observed in up to 8% of the cases in adrenocortical carcinoma (orange bar; Figure 17B), whereas the deletion is reported in prostate cancer in 10% of the cases (blue bar).

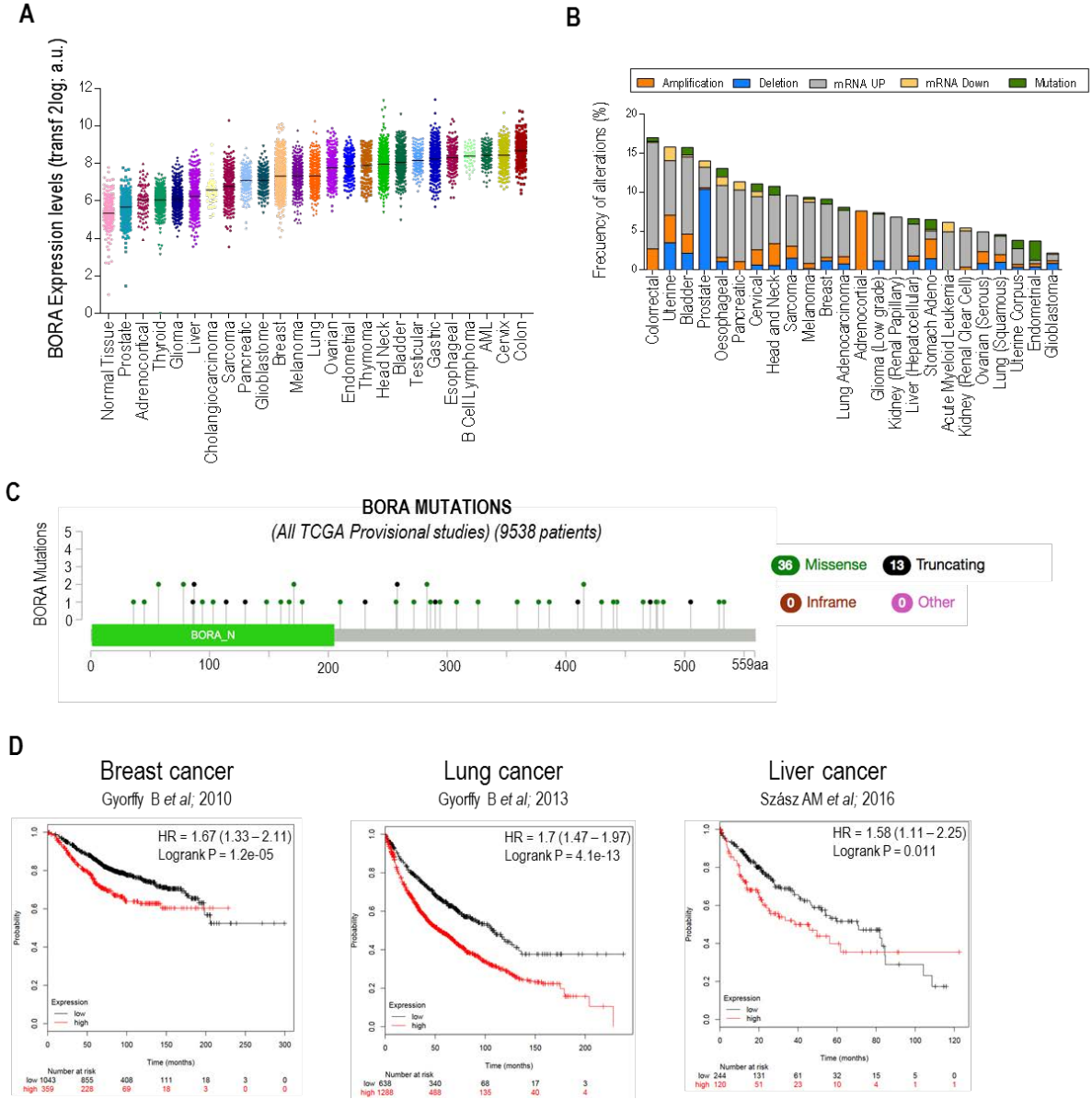

Figure 17. *BORA* expression across different tumor types. (A) *BORA* mRNA levels in different tumor types from the TCGA repository. Data were retrieved from the TCGA database using the R2 Genomic Visualization platform. **(B)** Frequency (%) of *BORA* mutations and/or copy number alterations (deletions or amplifications) across the spectrum of human cancers currently annotated in the TCGA provisional studies. Data were retrieved from the TCGA databases using the cBioPortal website. **(C)** Histogram of BORA protein showing the mutational profile in 23 TCGA tumor types. **(D)** Kaplan–Meier survival analysis based on the expression levels of *BORA* in breast, lung and liver carcinomas. *P*-values were estimated using a log-rank test to determine the difference in outcomes between patients with higher *BORA* expression levels (red) *vs* those with lower/no levels (black).

To validate the results found in the screening and in the *in silico* analysis, we analyzed the expression of *BORA* in an independent cohort of tissues from Vall Hebron Hospital (Barcelona, Spain) including benign (n=20) and tumoral ovaries (n=40). Accordingly, analysis of tumor tissues confirmed increased *BORA* expression levels compared to benign samples (p<0,001; Figure 18A). As depicted in Figure 18B, *BORA* expression increased in patients diagnosed at early stage (p<0,01) but more sharply in late stages

(*p*<0,001). No differences in *BORA* expression were observed among the different histological subtypes of OC (Figure 18C A) and a positive tendency, albeit not significant, was observed with undifferentiated grade tumors (Figure 18D). Additionally, we also checked the mRNA levels of *PLK1* in this cohort of specimens, showing an increase in tumoral tissues compared to benign samples (Figure 18E). Notably, a positive correlation was observed between *BORA* and *PLK1* in the tumoral samples at mRNA level (n=40; Spearman correlation: 0,275; Figure 18F).

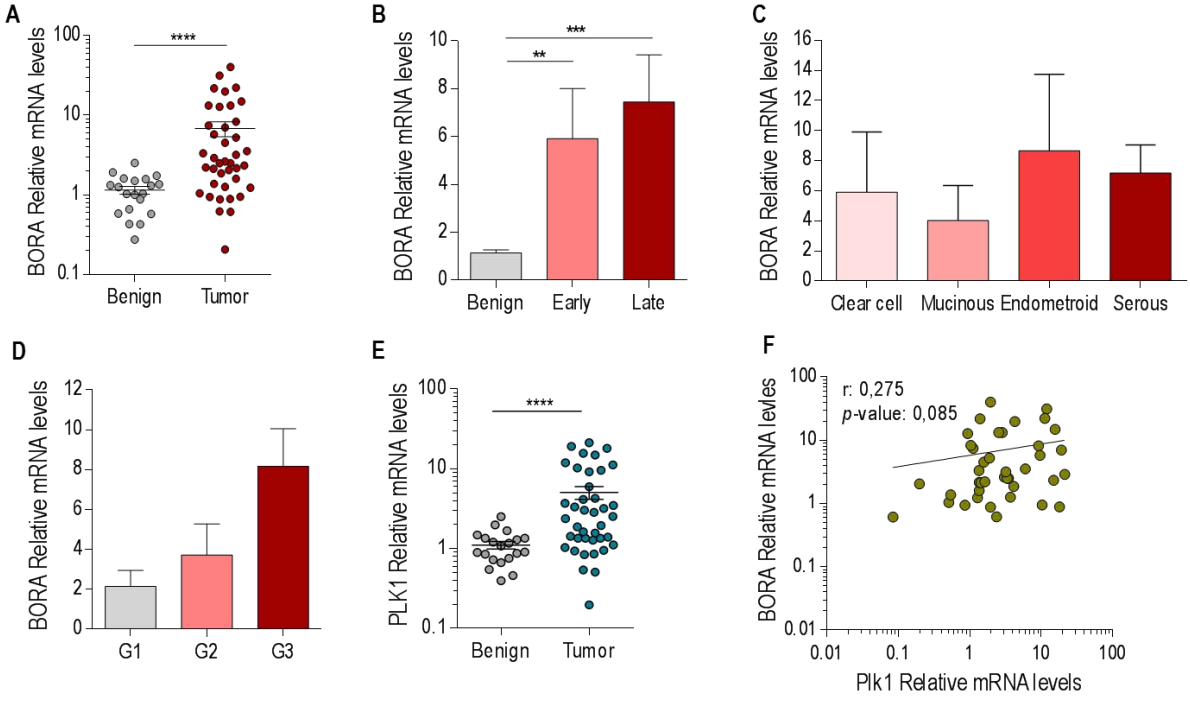

Figure 18. *BORA* mRNA expression levels are higher in tumoral samples and correlate with undifferentiated histological grade and late clinical stage. (A) *BORA* expression is higher in tumoral OC primary samples compared to benign ovaries. All values of mRNA were normalized to *GAPDH*. **(B)** *BORA* expression is associated with late clinical stages. **(C)** *BORA* expression within the different histological subtypes of OC. **(D)** Undifferentiated tumor cells exhibit high *BORA* mRNA levels. **(E)** *PLK1* expression is higher in tumoral OC primary samples compared to benign ovaries. All values of mRNA were normalized to *GAPDH*. **(F)** Spearman correlation between *PLK1* and *BORA* mRNA expression using the tumoral samples (n=40). *P*-values were calculated using a two-tailed Student's *t*-test. ***P*<0,01; ****P*<0,001; *****P*<0,0001.

We then proceed to analyze BORA protein levels in ovarian tissues by immunoblotting. Mild or not detectable BORA levels were found in the majority of benign samples, in contrast to the consistent expression detected in all HGSC tissue specimens tested (Figure 19). PLK1 protein expression and its activity levels through a subrogated marker; the phosphorylation in pTCTP-Ser46^{366}, displayed also an increase in HGSC samples compared to the benign ovaries. Though we observed a correlation between PLK1 expression and pTCTP-Ser46 within each patient sample, we did not discern a clear pattern of correlation with BORA levels.

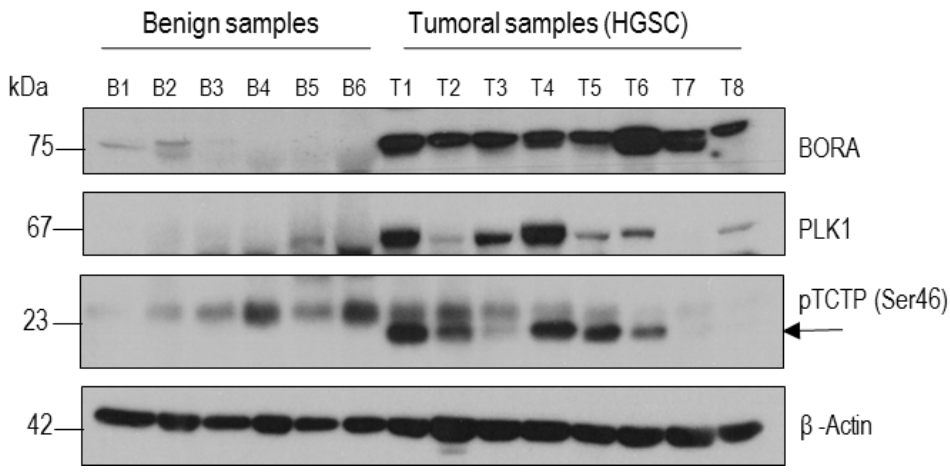

Figure 19. BORA protein is upregulated in HGSC tumors. (A) Immunoblot of BORA, PLK1 and pTCTP (Ser46) in six benign ovaries and eight HGSC tissues. β-Actin was used to control equal protein loading. **"**B" means benign ovaries and "T" means tumoral HGSC ovaries.

Collectively, these results suggest that BORA is abundantly expressed in advanced stages of OC tumors and correlates with increased proliferation, tumor grade, stage and CIN; thereby rendering an indicative prognostic factor for aggressiveness and overall survival in OC.

4.4 BORA is overexpressed in OC cell lines

Next, we analyzed BORA mRNA and protein levels in a panel of 12 OC cell lines with different clinical features; such histology and mutational profile, and also including two non-tumoral immortalized ovarian surface epithelium (IOSE) cell lines (IOSE-503 and IOSE-385). Concomitant with previous results, both mRNA and protein levels confirmed the upregulation of BORA in the tumoral lines compared to the non-tumorigenic immortalized IOSE lines (Figure 20A-B). Regarding tumoral lines, BORA was differentially expressed without an obvious correlation with the p53 or BRCA1 status, two oncogenic features of OC; neither with the basal and activity levels of PLK1 nor with the total AURORA A levels (Figure 20A). We didn't observe any correlation pattern between the protein levels of BORA and the histological subtype of the different OC cell lines, in accordance with previous observations in the clinical tissue samples. A significant positive correlation between BORA at mRNA and protein level was detected in OC cells lines (Pearson's r=0,6 and *p*-value=0,018; Figure 20C). The characterization of BORA levels in a panel of multiple cell lines was important to select those cell line models more adequate to modulate BORA expression in next assays.

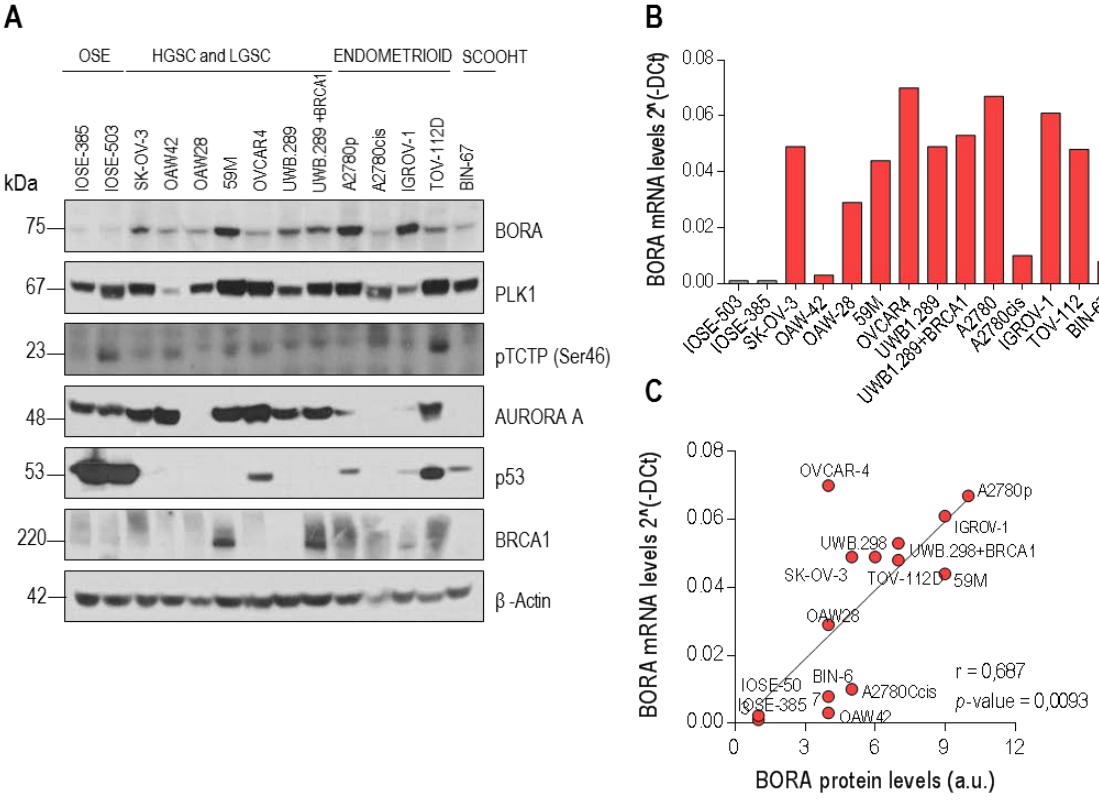

Figure 20. BORA expression levels in a panel of fourteen ovarian cell lines. (A) Immunoblot illustrating BORA levels in a range of two normal ovarian epithelial lines and various OC cell lines with diverse histology and mutational profile. PLK1, pTCTP (Ser46), AURORA A, p53 and BRCA1 protein expression was also detected. β-Actin was used to control equal protein loading. **(B)** Values of *BORA* mRNA expression in the different ovarian cell lines. (TaqMan, RT-qPCR). All values of mRNA were normalized to *GAPDH*. **(C)** Correlation (Pearson) of BORA protein and mRNA from normal and OC cell lines. The different cell lines are indicated in the graph.

4.5 BORA overexpression renders malignant transformation of non-tumoral cells *in vitro*

The fact that BORA is aberrantly up-regulated in OC prompted us to speculate that BORA might be a potential causal factor in promoting ovarian tumorigenesis. To test this, we selected the non-tumorigenic IOSE line, which was derived from the human epithelium ovarian surface (immortalized by SV40 T/t virus) and, importantly, displays very low endogenous protein levels of BORA. Technically, we engineered an IOSE cell line that overexpresses BORA and its counterpart with the empty vector (EV) using the pINDUCER20 lentiviral toolkit[367] to performed gain of functions assays. The coding sequence of BORA was successfully cloned into the pINDUCER20 system as confirmed by immunoblotting and by RT-qPCR (Figure 21A-B). Functionally, we firstly examined the ability of BORA-overexpressing cells (IOSE-pIND_BORA) to grow in anchorage-independent soft agar (semi-solid media), a classical hallmark that correlates with cellular malignant transformation *in vitro*[368,369]. Interestingly, we found that whereas control IOSE cells formed a few colonies, BORA overexpressing cells double at least the

number of colonies formed after 3-4 weeks of growth (Figure 21C). In addition, BORA-overexpressing colonies were larger in shape than those formed with the EV as depicted in Figure 21C-D. Concomitantly, BORA-overexpression accelerated the migration capacities of IOSE cells by twofold compared to pIND_EV cells (Figure 21E). Importantly, ectopic BORA expression also resulted in a significant increase in the speed of the proliferation capacities of IOSE cells, measured by direct cell-count compared to its respective control, thereby regulating epithelial cell motility *in vitro* (Figure 21F). Interestingly, when we let the cells grow in culture to confluence, IOSE-pIND_BORA cells kept growing with cells forming multiple layers (with "spheroid"-like structures), while control cells died after contact inhibition. The result was consistent with a nesh-network in BORA overexpressing cells, promoting the loss of contact inhibition, another property correlated with cellular tumorigenicity (Figure 21G)[370]. Taken together, these results indicate that BORA overexpression renders malignant transformation of IOSE cells *in vitro*.

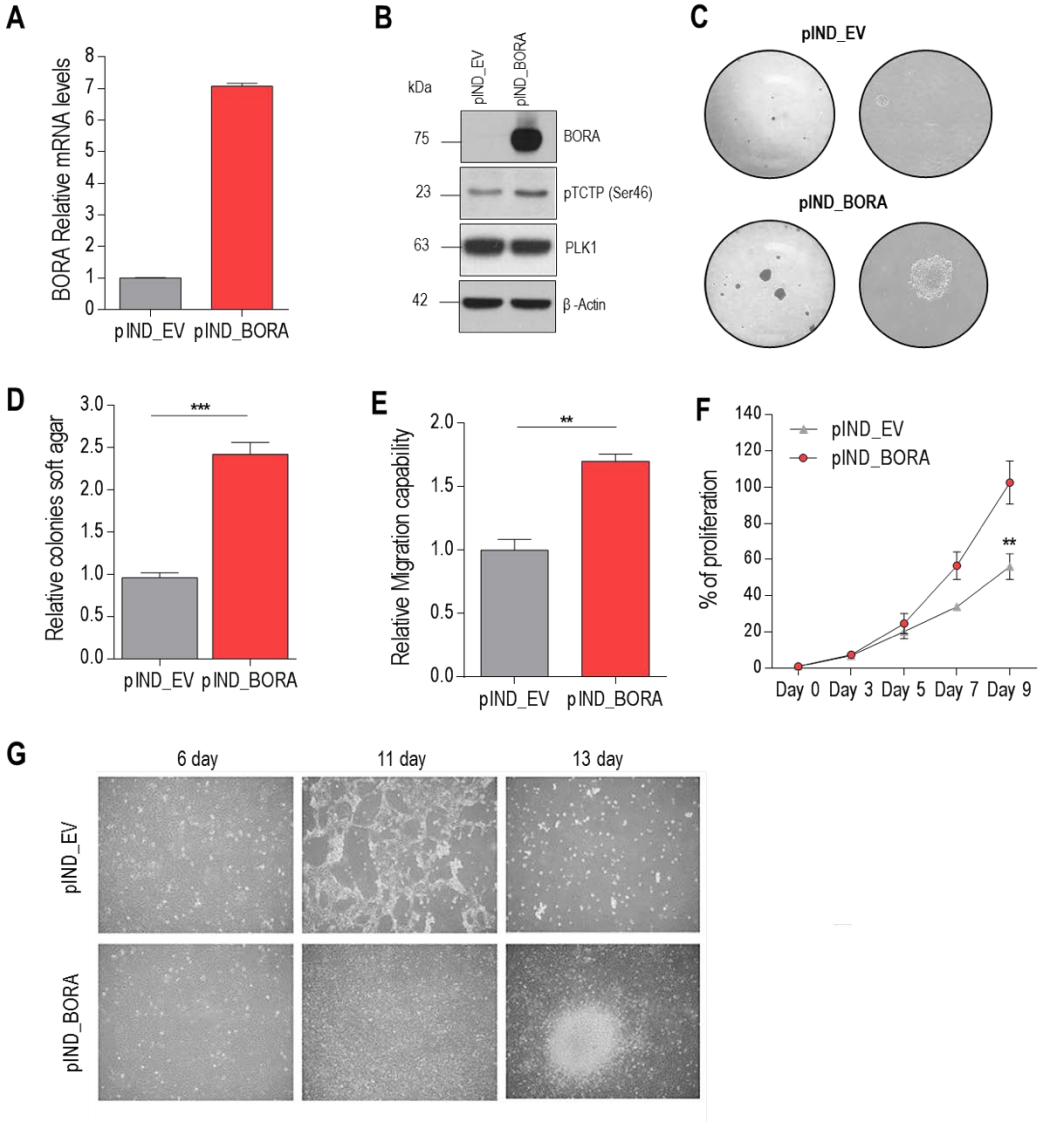

Figure 21. BORA contributes to the transformation of immortalized epithelial ovarian cells and favors malignant features *in vitro*. (A-B) Ovarian immortalized epithelial cells were transduced with lentiviral particles

expressing empty vector (EV) or the CDS of *BORA*. Overexpression was analyzed by RT-qPCR and immunoblot upon doxycycline addition (0,25 µg/mL) in both groups. *GAPDH* as endogenous control and β-Actin was used as a loading control, respectively. **(C)** Soft-agar colony formation assay of IOSE cells transduced as in (A). **(D)** Quantification of (C). **(E)** Migration capacities of transduced IOSE cells in transwell assays. **(f)** Cell proliferation of IOSE cells transduced as in (A). Cellular growth is shown for each cell line with three experimental replicates; error bars represent SEM. **(G)** Representative images taken in a time course period of IOSE cells (EV and BORA expression) after reaching confluence state. Images represents three independent experiment (n=3/condition). *P*-values were calculated using a two-tailed Student's *t*-test. ***P*<0,01; ****P*<0,001.

To add reproducibility to these results, we also ectopically increased BORA expression in the tumoral SK-OV-3 cell line, which harbors low-medium endogenous levels of BORA (Figure 22A). We could reproduce the increase in the proliferation capacity of BORA-overexpressing cells and the higher capacity to form colonies in soft-agar (Figure 22B-D), thereby suggesting that high levels of BORA can contribute to tumor progression in already transformed cells.

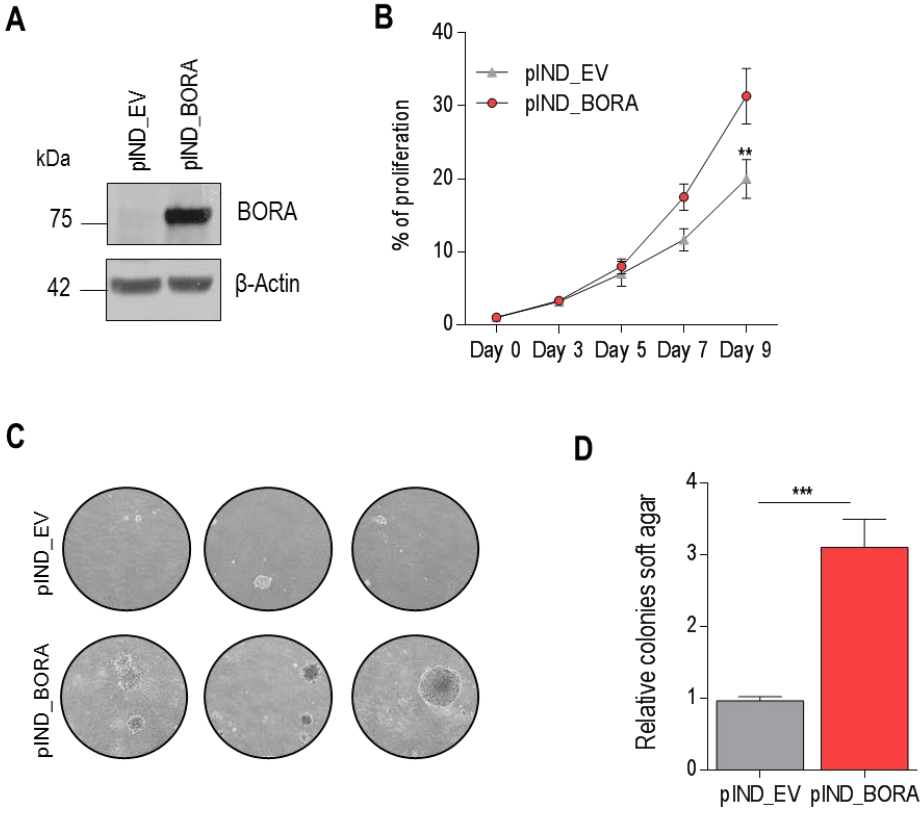

Figure 22. BORA enhances ovarian tumorigenesis features *in vitro*. (A) Immunoblot for the overexpression of BORA in the SK-OV-3 cell line upon doxycycline addition (0,25 µg/mL). **(B)** Growth proliferation curves of SK-OV-3 cell line transduced as in (A). **(C-D)** SK-OV-3 pIND_EV or pIND_BORA transduced cells were grown in soft agar culture for three weeks and colonies were photographed and counted. Data are mean ± SEM (n≥3 experiments). *P*-value was calculated using a two-tailed Student's *t*-test. ***P*<0,01; ****P*<0,001.

4.6 BORA enhances ovarian tumorigenesis *in vivo*

To go a step further, we moved to an *in vivo* xenograft model. We firstly proceeded to assess whether BORA overexpressing IOSE cells were able to form tumors when were injected subcutaneously into the flank of NMRI nude female mice. Following the mouse model design illustrated in Figure 23A, we injected IOSE-pIND_EV and IOSE-pIND_BORA cells in mice previously treated for a week with 1 mg/mL of doxycycline-supplemented water. Three weeks post-injection, in the IOSE-pIND_BORA group we observed tissue engraftment into the flank of the mice (near 40% of the flanks) and we considered it as potential tumors (red line; Figure 23B-C) while in the pIND_EV group (grey line) we did not observed any kind of engraftment in the flanks (Figure 23B-C). To our surprise, at the consecution of the experiment any of the flanks from the pIND_BORA group eventually developed a tumor. Histopathological examination by a specialized pathologist revealed neither malignant cells nor pre-neoplasia tissue in any of the flanks (Figure 23D-E). Flanks exhibited single tiny scars, presumably remnants of an initial intention of tumor engraftment. These scars appeared as small fibrotic lesions together with signs of chronic inflammation and fat tissue (Figure 23F). Interestingly, in the group of IOSE-pIND_EV with $5 \cdot 10^6$ cells one tumor spontaneously grown and a derived cell line was established. These results indicate BORA alone is not able to promote tumorigenesis *in vivo* in the IOSE cell line when injected subcutaneously into NMRI nude mice (see discussion).

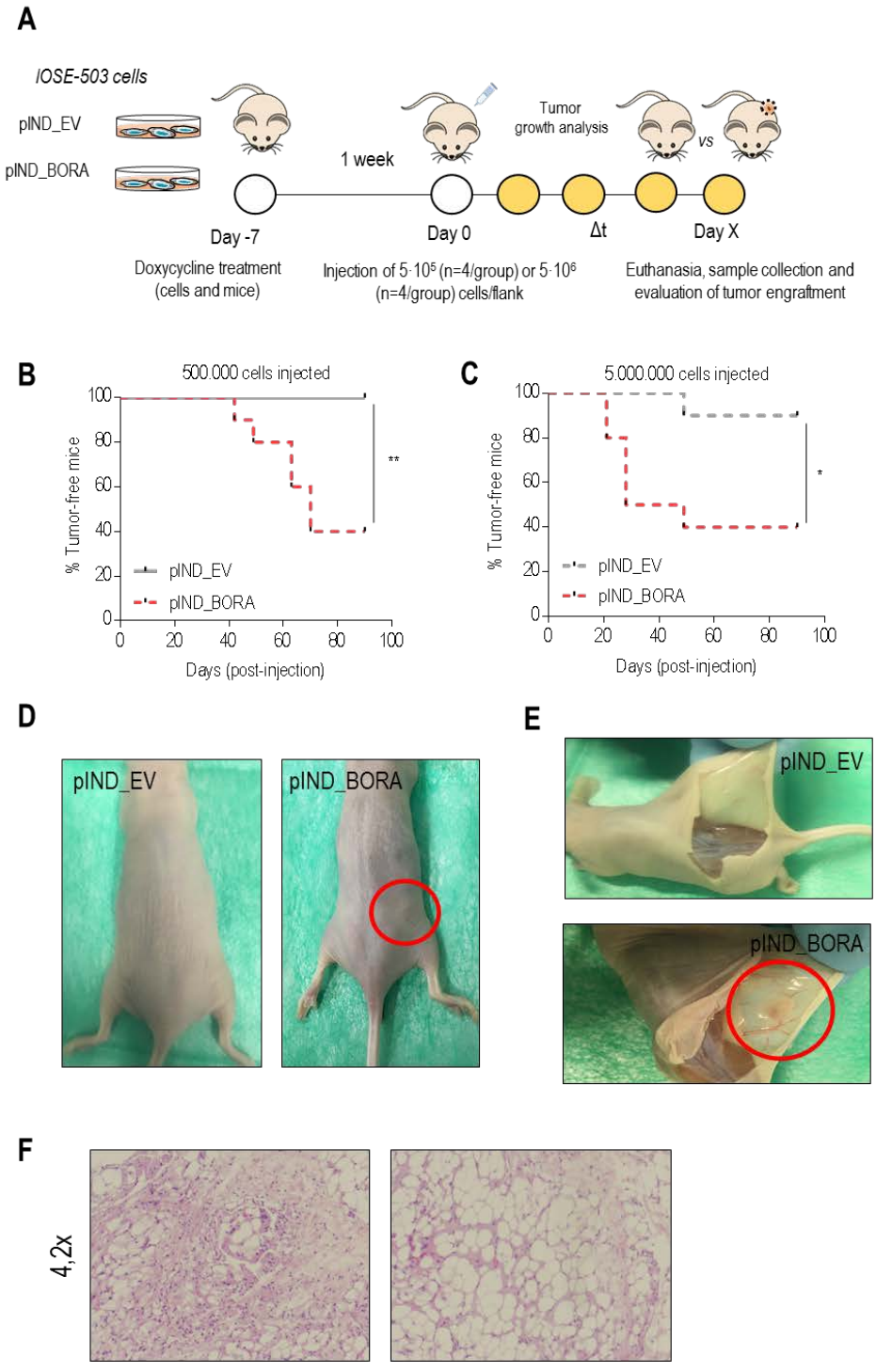

Figure 23. Overexpression of BORA does not induce IOSE cells to form subcutaneous tumors. (A) Schematic representation of the *in vivo* approach. The tumorigenic potential of IOSE overexpressing BORA cells was assessed *in vivo* by subcutaneous injection into NMRI nude mice using $5{\cdot}10^5$ and $5{\cdot}10^6$ cells per flank. Mice and cells were treated with 1 mg/mL of doxycycline *ad libitum*. **(B-C)** Diffuse tissue engraftment appearance in the flank of the mice depicted in a graph. *P*-values were estimated using a log-rank test to determine the difference in appearance between pIND_EV tumors (grey line) *vs* pIND_BORA tumors (red line). **P*<0,05; ***P*<0,01. **(D-E)** Representative macroscopic images of the mice flanks with the potential tumors in the IOSE pIND_BORA group. **(F)** Representative pictures taken at 4,2x magnification of H&E staining of sections of the tissue engraftment appeared in the pIND_BORA mice.

We also analyzed the effects of overexpressing BORA in the tumoral SK-OV-3 cell line when xenografted into NMRI nude mice. We used the SK-OV-3, a cell line that form tumors itself (tumoral background, i.e. with p53 mutated), with the goal of studying the contribution of BORA in tumor engraftment and development. Notably, one week post-injection, all mice bearing BORA overexpressing cells engrafted and developed into tumors (red line; Figure 24A), whereas in the control group (SK-OV-3 pIND_EV) none did so until week 8 (grey line; Figure 24A), indicating BORA has somehow an impact on tumor-initiation capacities. Moreover, SK-OV-3 BORA-overexpressing tumors grew more and faster compared to the slope curve of the control tumors, with an average size of 2.089 ± 444 mm^3 in contrast to SK-OV-3-pIND_EV tumors that measured 1.209 ± 316 mm^3 26 days post-engraftment (Figure 24B), suggesting that BORA provides a proliferative tumor advantage. At the consecution of the experiment, tumors were resected and photographed as illustrated in Figure 24C. Average tumor weight was heavier (albeit non significantly) in the BORA group compared to the control (*p*-value=0,077; Figure 24D). Immunoblot analysis of the excised tumors verified the overexpression of BORA, thereby indicating the system worked successfully *in vivo* (Figure 24E). Moreover, BORA overexpressing displayed higher number of proliferating cells, determined by increased Ki67-staining (84% compared to 68% in the control group). Taken all results together, BORA clearly contributes to OC tumorigenesis *in vivo*.

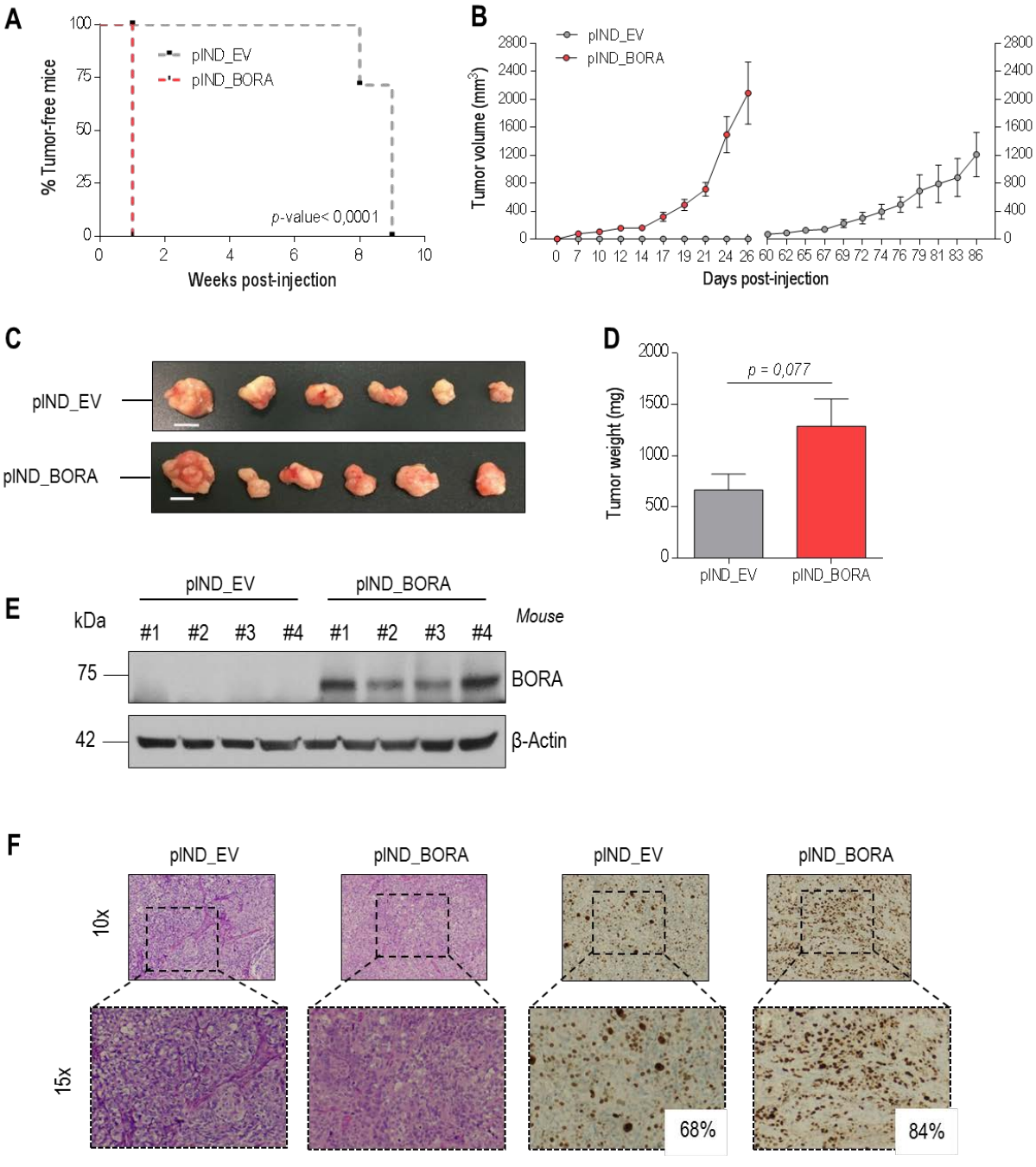

Figure 24. Overexpression of BORA favors tumor growth *in vivo*. (A) SK-OV-3 pIND_EV and pIND_BORA xenografts were grown in nude mice (n=7/condition). The percentage of tumors developed (incidence) in each group and the required days from cell injection until the tumors were measurable (latency) is shown on the middle. *P*-values were estimated using a log-rank test to determine the difference in appearance between pIND_EV tumors (grey line) *vs* pIND_BORA tumors (red line). **(B)** Tumor volume measured every 2-3 days. Error bars represent SEM. **(C)** Macroscopic images of the excised tumors at end-point. Scale bar: 1 cm. **(D)** Average tumor weight of the resected tumors. *P*-value was calculated using a two-tailed Student's *t*-test. **(E)** Immunoblot analysis of BORA in representative xenograft tumors from both experimental groups. β-Actin was used as loading control. **(F)** Representative microscopic H&E and Ki67 – stained images of OC xenografts.

4.7 BORA is essential for OC growth

The functions of PLK1 in sustaining the proliferative capacities of cancer cells has previously reported[310]. Thus, having established BORA as a determinant factor for ovarian tumorigenesis we hypothesize that BORA might also regulate the viability of OC cells. We engineered two different lentiviral-based short hairpin RNA (shRNA) particles by cloning two validated siRNA sequences already published[338] into the pLKO.1 lentiviral vector. The two independent shRNA efficiently reduced BORA protein levels (Figure 25A) and consistently impaired the cellular growth of all ovarian cell lines tested with distinct histological subtype, molecular features or p53 functionality (Figure 25B).

It is worth noting that these effects were not observed in the non tumoral IOSE cell line, where the depletion barely altered the proliferation rate of the cells; making BORA a potential selective target for malignant cells. Importantly, the shBORA#2 lentiviral particle worked better reducing the protein levels compared to shBORA#1, so that next experiments were performed using shBORA#2 (hereinafter shBORA). Furthermore, loss of BORA expression also reflected a reduced number of colonies in a colony formation assay; to different extend depending on the OC cell line. (Figure 25C-D).

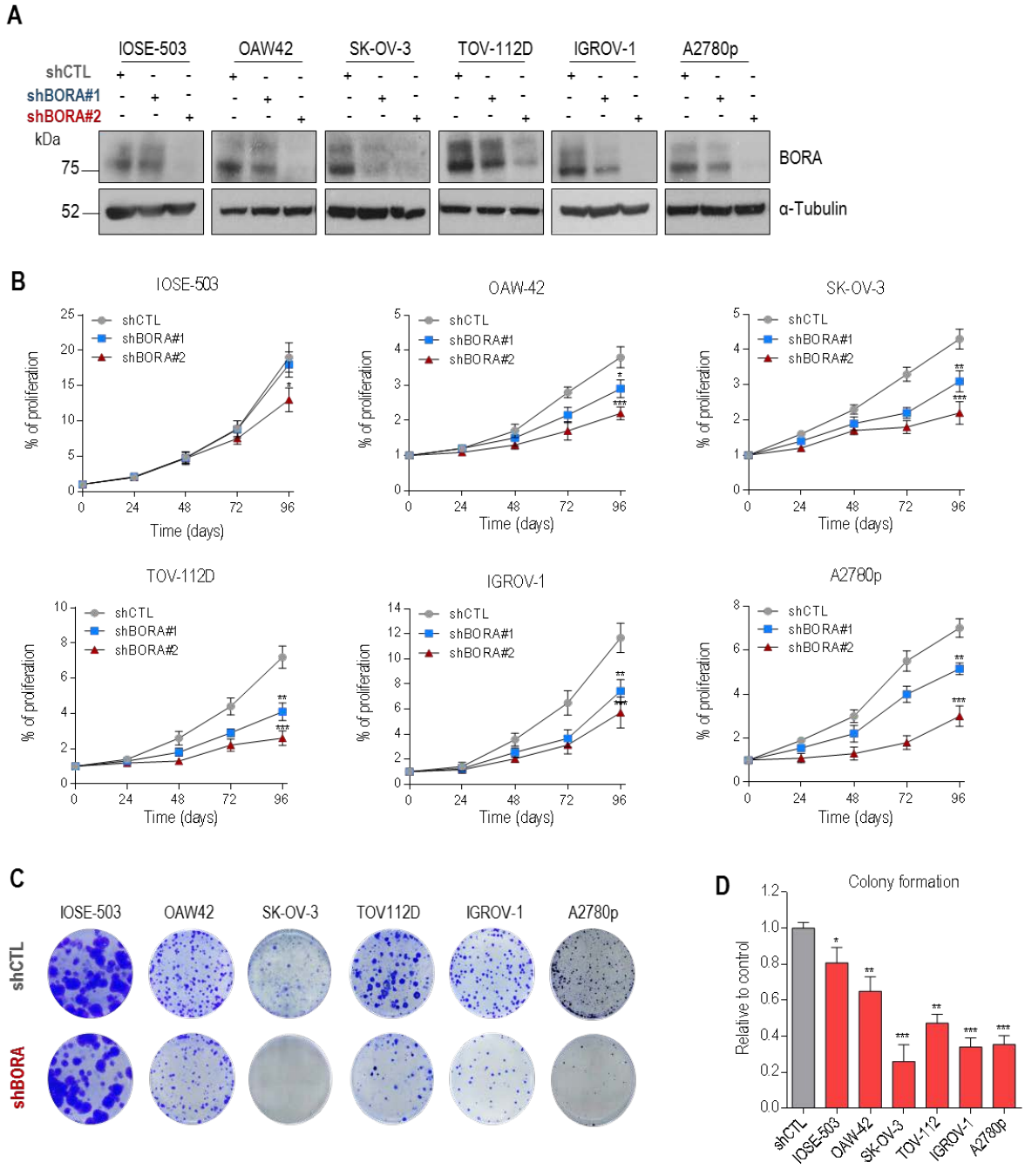

Figure 25. Knockdown of BORA abrogates tumorigenicity *in vitro*. (A) Efficiency of two different lentiviral-based BORA shRNA particles (shBORA#1 and shBORA#2) in the indicated cell lines visualized by immunoblotting with respect to a non-silencing control shRNA (shCTL). α-Tubulin was used as loading control. **(B)** Impaired growth of the indicated cell lines upon BORA depletion. Normalized proliferation curves of the indicated ovarian cell lines infected with shCTL (grey line), shBORA#1 (blue line) and shBORA#2 (red line) measured by crystal violet staining (n=6/condition). Growth is expressed as fold increase in the number of cells determined at each of the indicated days compared to day 0. **(C)** Representative macroscopic images of colony formation assay in shCTL and shBORA#2 (herein shBORA) infected ovarian cells after 10-11 days in culture. For each cell line, all dishes were fixed at the same time, stained and photographed. **(D)** Average quantification of three independent experiments ± SEM. *P*-values were calculated using a two-tailed Student's *t*-test. **P*<0,05; ***P*<0,01; ****P*<0,001.

Since our *in silico* data pointed out that BORA was also overexpressed in other tumor types and with the goal to extend our findings to other tumors, we wanted to know if BORA depletion in these tumors rendered similar phenotype that in OC. Immunoblot analysis revealed reduced protein expression upon transduction with the shBORA lentiviral particle in a panel of different cell lines including endometrial (HEC1A), breast (MDA-MB-231), neuroblastoma (SKNB2), prostate (LNCAP) and colon (SW480) adenocarcinomas (Figure 26A). The depletion consequently resulted in markedly reduced cell proliferation in all cell lines (Figure 26B). Thus, these results suggest an important role of BORA in cellular survival not only in OC, also in other tumor types.

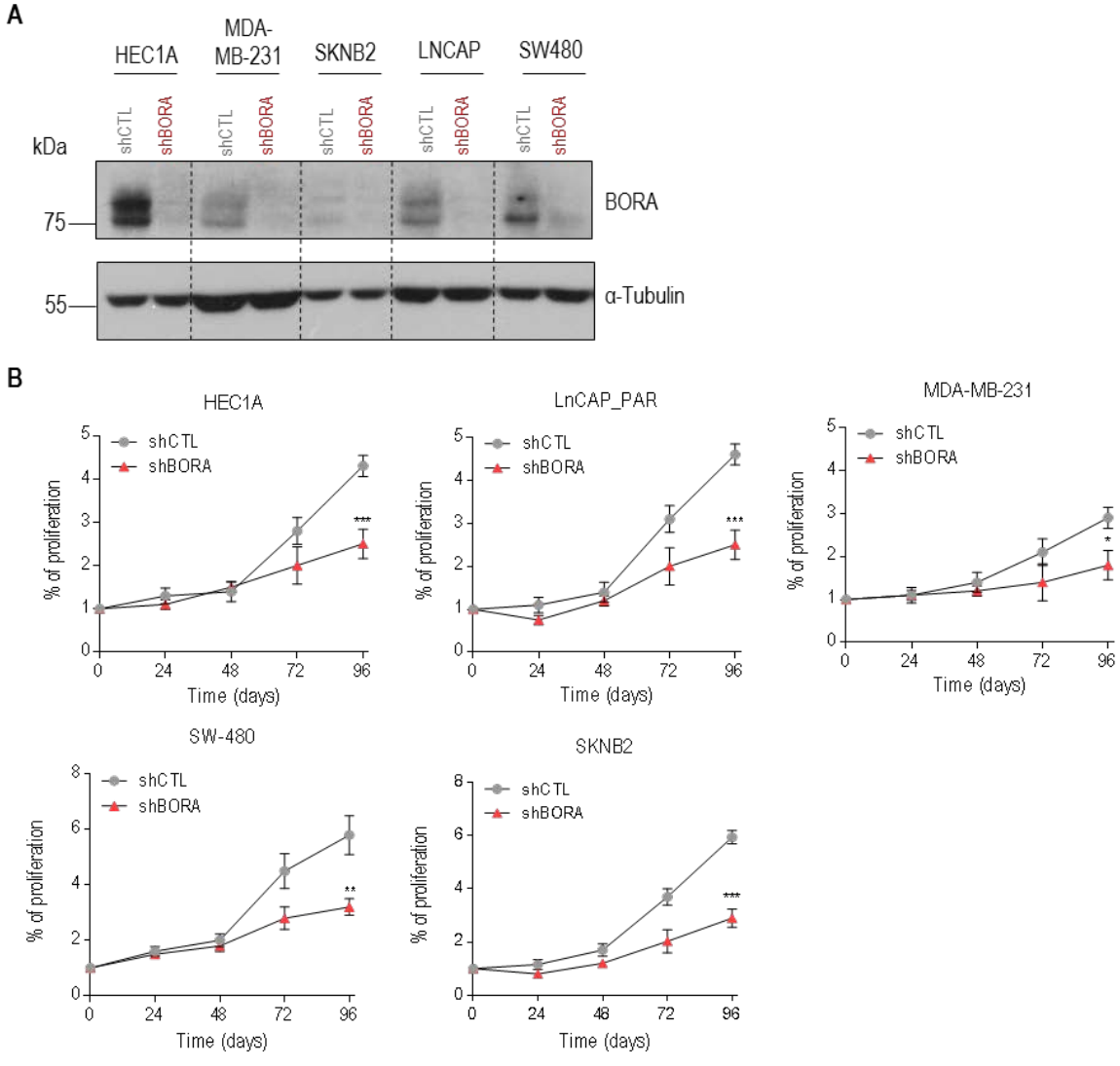

Figure 26. BORA inhibition results in suppression of proliferative capacities in cell lines from different tumors. (A) Representative immunoblot of BORA knockdown in endometrial, breast, neuroblastoma, prostate and colon carcinoma cell lines. α-Tubulin was used as loading control. **(B)** Normalized proliferation curves of shCTL (grey line) and shBORA (red line) -infected cells in the different tumor cell lines. Growth is expressed as fold increase in the number of cells determined at each of the indicated days. Graphs represent mean ± SEM of three independent experiments. *P*-value was calculated using a two-tailed Student's *t*-test. **P*<0,05; ***P*<0,01; ****P*<0,001.

4.8 BORA is essential for OC viability

We also sought to ascertain if OC cells were able to survive with complete BORA depletion. Inactivation of BORA has only been performed so far using siRNA and shRNA, which might not result in full depletion. We designed a gRNA to target the exon 2 of *BORA* and we cloned it into the CRISPR/Cas9 vector; pSpCas9 (BB)-2A-GFP[371], with the idea to generate a population with total lack of *BORA*. We then transfected SK-OV-3 cells and did single-cell cloning. Immunoblot analysis of the different clones revealed no clone population with full BORA levels depleted, only remaining clones with reduced levels compared to the control ones (Figure 27A). Importantly, these BORA knockdown clones (heterozygous) mirrored the decreased proliferation observed before (Figure 27B), confirming BORA silencing reduces cellular proliferation. These results made us to hypothesize that homozygous CRISPR-mediated *BORA* knock-out SK-OV-3 cells were not able to grown due to the fact that BORA is essential for cell division. In this line, we wondered what was happening with those shBORA#2 transduced cells that survived and were able to form colonies in the long-term colony formation assay.

Three different scenarios were hypothesized: (i) these cells escaped the depletion with same BORA levels as control cells; (ii) cells efficiently depleted but have developed alternative BORA-independent mechanisms for survival; or (iii) they had partially bypassed the downregulation and they kept very low BORA levels to survive. Immunoblot from the stable cell lines derived from single A2780p cells transduced with shBORA#2 or shCTL revealed that all shBORA#2 colonies maintained residual levels of BORA, which were in all cases lower than those detected in control colonies, with a wide range of expression (Figure 27C). We evaluated pTCTP (Ser46), as a read-out for efficient BORA function on PLK1 activation, and observed no consistent differences at protein level between control and BORA-depleted colonies. The fact that despite BORA levels were in some colonies almost no detectable by immunoblot and that PLK1 activity seems barely affected, let us hypothesized that total lack of BORA is lethal to OC, but much reduced levels of BORA were sufficient to maintain PLK1 activation and therefore cell survival.

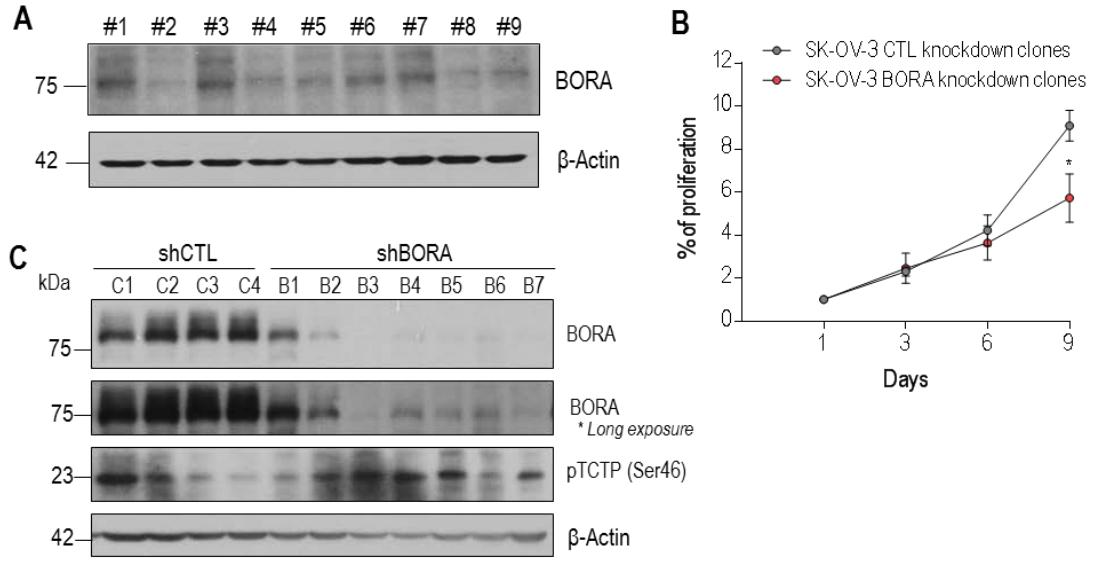

Figure 27. Immunoblot analysis of BORA levels in single clones. (A) Immunoblot of BORA in different CRISPR/Cas9 clones. β-Actin was used as loading control. **(B)** Proliferation curve of some of these CRISPR clones. *P*-value was calculated using a two-tailed Student's *t*-test. **P*<0,05. **(C)** Immunoblot of representative A2780-derived clones. Long exposure was done to indicate BORA is not full depleted in any clone. "C" means shCTL and "B" means shBORA-transduced A2780p clones.

4.9 Loss of BORA expression induces G2/M arrest and cell death

We then proceed to deepen into the mechanisms that cause the reduction in the proliferation capacities. Cell cycle profile was analyzed by flow-cytometry 72 hours post-depletion using the lentiviral particles. BORA knockdown caused a significant increase in G2/M phase in SK-OV-3 and A2780p cells with a concomitant decrease in the percentage of cells in S and G1 phase (Figure 28A). Conversely, IOSE shBORA-transduced cells were barely arrested in G2/M phase (Figure 28A). Cell death was analyzed by hoechst staining at 96h post-depletion. The number of cells with condensed or fragmented chromatin was found to be significantly increased upon BORA depletion in the OC cell lines, while shCTL-transduced cells displayed uniformly chromatin staining (Figure 28B, white arrowheads). In IOSE cell line, BORA depletion slightly increased the number of cells with fragmented chromatin compared to IOSE shCTL cells, but to much less extend compared to the tumoral cells (p<0,05; Figure 28C). BORA knockdown was accompanied by a reduction in the pTCTP (Ser46) but not in the protein basal levels of PLK1 and AURORA A kinases, as previously reported[338], indicating that at least part of the consequences of BORA depletion are due to lower PLK1 activity. Cyclin B1 immunoblot in SK-OV-3 transduced shBORA cells confirmed the pronounced G2/M arrest, and higher PARP cleaved levels pointed towards a caspase dependent apoptosis after BORA depletion (Figure 28D). Taken together, these results suggest BORA depletion causes a cell cycle arrest in G2/M phase and an induction of apoptotic cell death resulting in a decreased viability of OC cells.

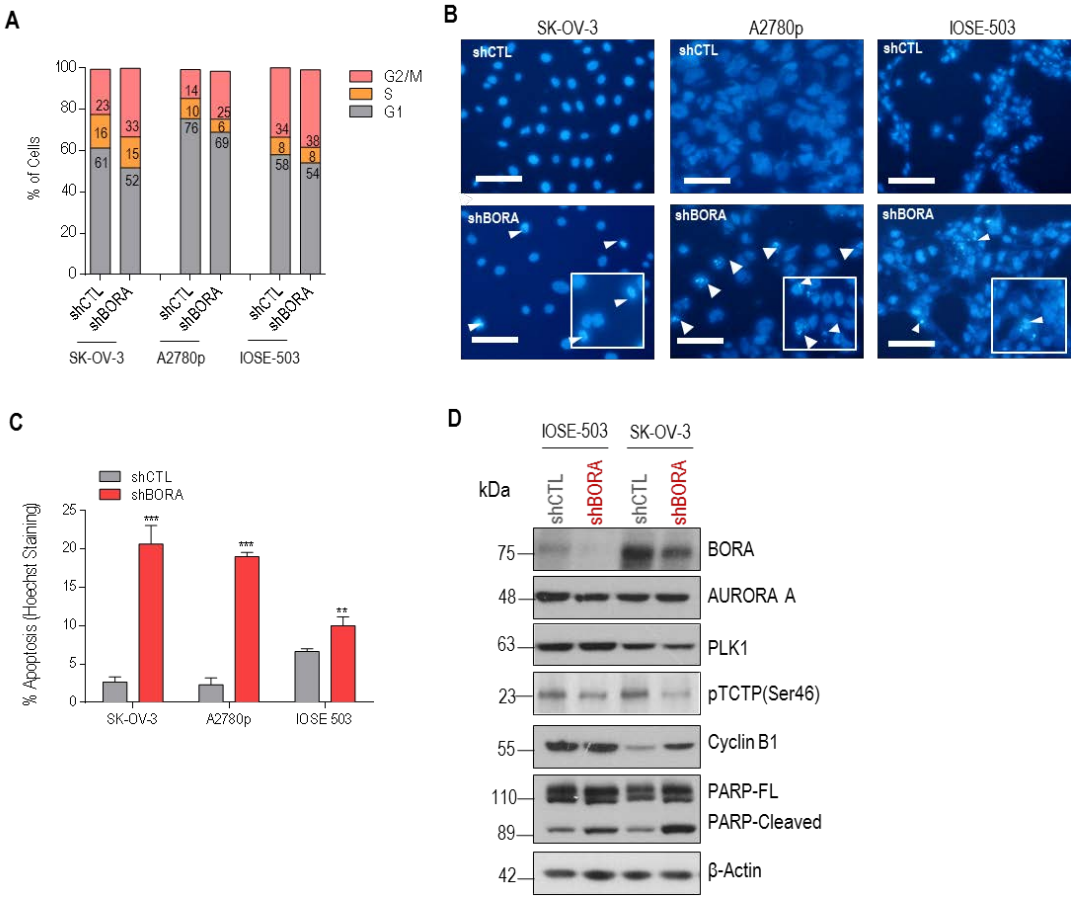

Figure 28. G2/M Phase arrest and apoptosis dependent cell death after BORA depletion in OC lines. (A) Cell cycle profile of shCTL and shBORA transduced IOSE-503, SK-OV-3 and A2780p cells. **(B)** Hoechst staining images of shCTL or shBORA-infected cells. Arrowheads point at nuclei with condensed or fragmented chromatin. Scale bar: 100 µm. **(C)** Quantification of cell death. Graph represent mean ± SEM of three independent experiments. *P*-value was calculated using a two-tailed Student's *t*-test. ***P*<0,01; ****P*<0,001. **(D)** Immunoblot analysis of BORA-silenced or control IOSE-503 and SK-OV-3 cells. β-Actin was used as loading control.

4.10 BORA depletion impairs tumor engraftment *in vivo*

We next proceeded to analyze the effects of silencing BORA in an OC subcutaneous xenograft model. Following the scheme illustrated in Figure 29A, the aggressive SK-OV-3 line was transduced with shCTL or shBORA lentiviral particles for 48 hours and injected in mice (n=7/group). BORA depletion was monitored with a fraction of these cells by immunoblotting (Figure 29B) and functionally in a proliferation assay (Figure 29C). Six weeks' post-injection, 85% of mice bearing shCTL cells developed tumors whereas only 42% of mice bearing shBORA-transduced cells did so. The last BORA depleted tumor eventually engrafted at 23 weeks post-injection (p<0,05; Figure 29D), showing BORA affects tumor-initiation development. Moreover, tumors detected in the shBORA group progressed at a very low pace thorough the experiment (Figure 29E). At end-point, excised tumors from the shCTL were larger and heavier compared to BORA depleted tumors (Figure 29F-G).

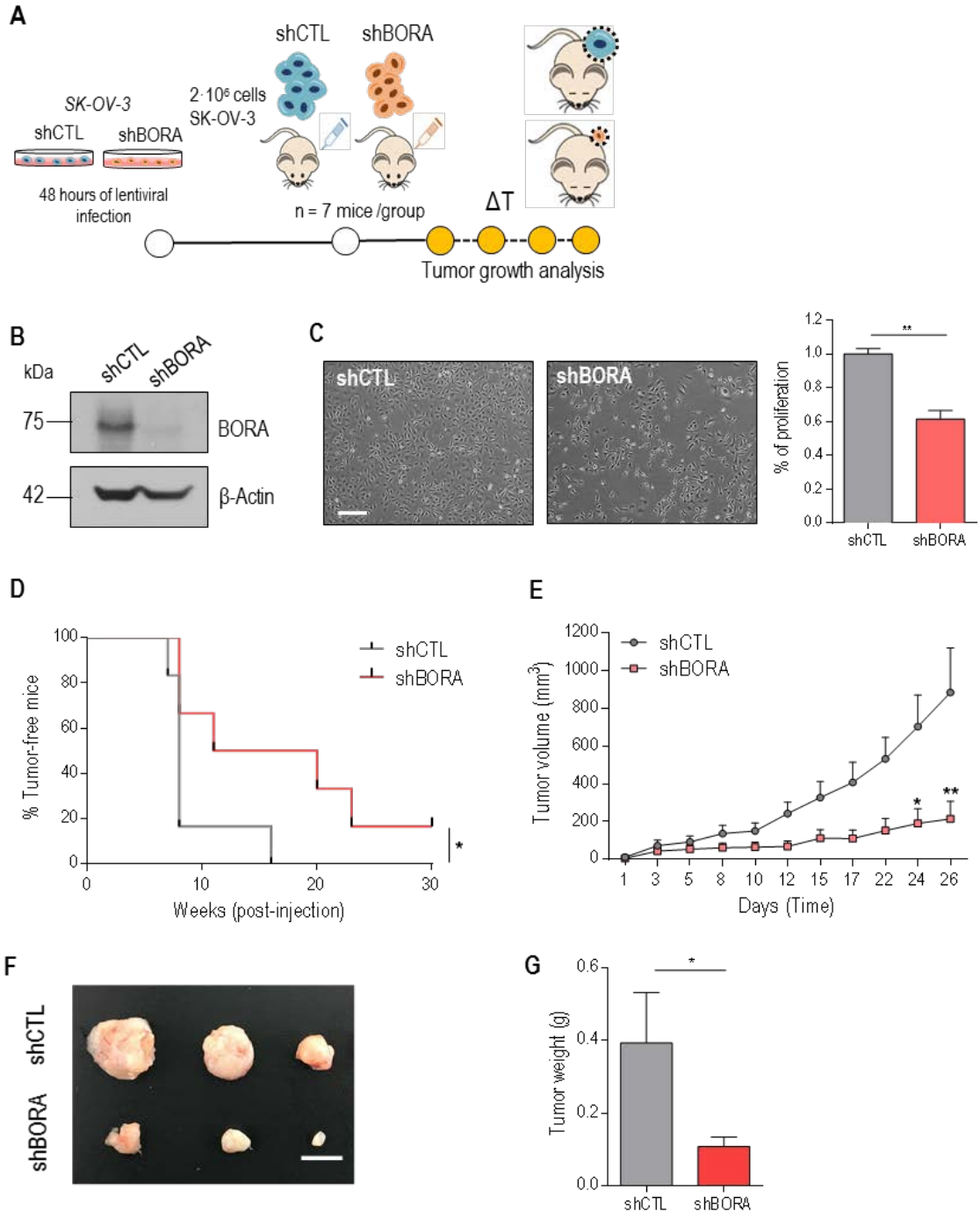

Figure 29. BORA impacts on tumor engraftment. (A) Schematic representation of the *in vivo* model. **(B)** A portion of shCTL and shBORA-transduced xenotransplant SK-OV-3 cells used for the *in vivo* model were analyzed by immunoblot showing BORA downregulation. β-Actin was used as loading control. **(C)** *In vitro* effect of a portion of transduced cells injected into the mice. Representative microscopic images of the cells (left) showing almost a 50% of reduction in proliferation (right) Scale bar represents 10 μm. **(D)** Tumor appearance incidence. *P*-value was estimated using a log-rank test to determine the difference in appearance between shCTL tumors (grey line) *vs* shBora tumors (red line) **P*<0,05. **(E)** Tumor volume was monitored over time using calipers. Two-way ANOVA analysis was used to calculate the significance (*p*-value) of the difference between shCTL and shBORA tumors; **P*<0,05. **(F)** Macroscopic images of representative resected tumors at end-point. Scale bar: 1 cm. **(G)** Average weight of the tumors taken at the time of the dissection. *P*-value was calculated using a two-tailed Student's *t*-test. **P*<0,05.

Immunoblot using protein lysates from representative tumors confirmed the downregulation of BORA in shBORA bearing tumors accompanied with an increase in the apoptotic markers (Figure 30A); in agreement with the *in vitro* results. Histopathological analyses revealed a significant reduction in the percentage of Ki67 positive cells in BORA depleted tumors (Figure 30B-C). In summary, constitutive BORA depletion in SK-OV-3-implanted mice, impacts on tumor engraftment, modulating tumor fate, and thereby reducing tumor growth.

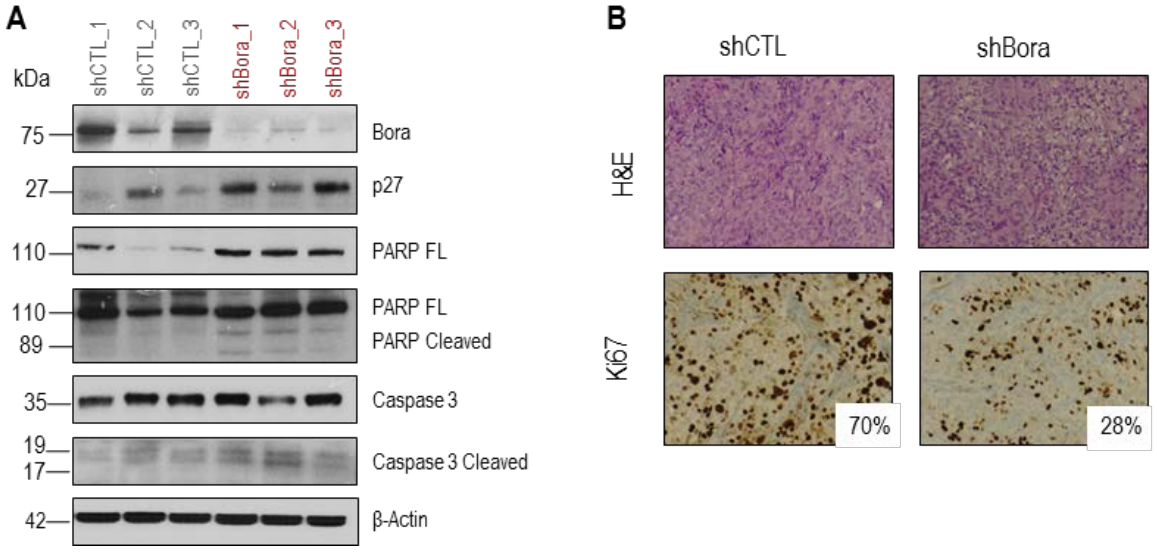

Figure 30. **BORA is necessary for the growth of OC cells *in vivo*.** Immunoblot analysis of BORA, p27, PARP and Caspase 3 protein markers using protein lysates from representative xenografts from both experimental groups. β-Actin was used as loading control. **(B)** Representative microscopic H&E and Ki67-stained images of OC xenografts. Images were taken at 15X.

4.11 BORA depletion reduces tumor growth *in vivo*

We then proceeded to engineer an inducible vector to modulate BORA expression *in vivo* once the tumor is formed. This situation reflects a closer therapeutic intervention into the clinics than the target depletion at the time of the tumor initiation. To do that, we used the Tet-On lentiviral inducible vector pTRIPZ (Dharmacon) which provides inducible depletion of BORA in presence of doxycycline. SK-OV-3 cells were infected with pTRIPZ-EV (empty vector) and two vectors that target BORA (harboring different shRNA sequences than those shown earlier); pTRIPZ-BORA-V1 and pTRIPZ-BORA-V2. Stable cells were selected with puromycin for seven days. The doxycycline addition to the culture media successfully depleted BORA in the cells transduced with the two vectors compared to empty vector (Figure 31A-B). Functionally, the inducible-mediated BORA silencing resulted in a reduction of the proliferation rate and impairment in the colony-formation capacities, while the effect of doxycycline alone did not have any affect (Figure 31C-E), mirroring our previous observations. Cells expressing the pTRIPZ-BORA-V1

vector reduced more efficiently BORA levels with functional consequences more pronounced, so that next experiments were carried out with these cells.

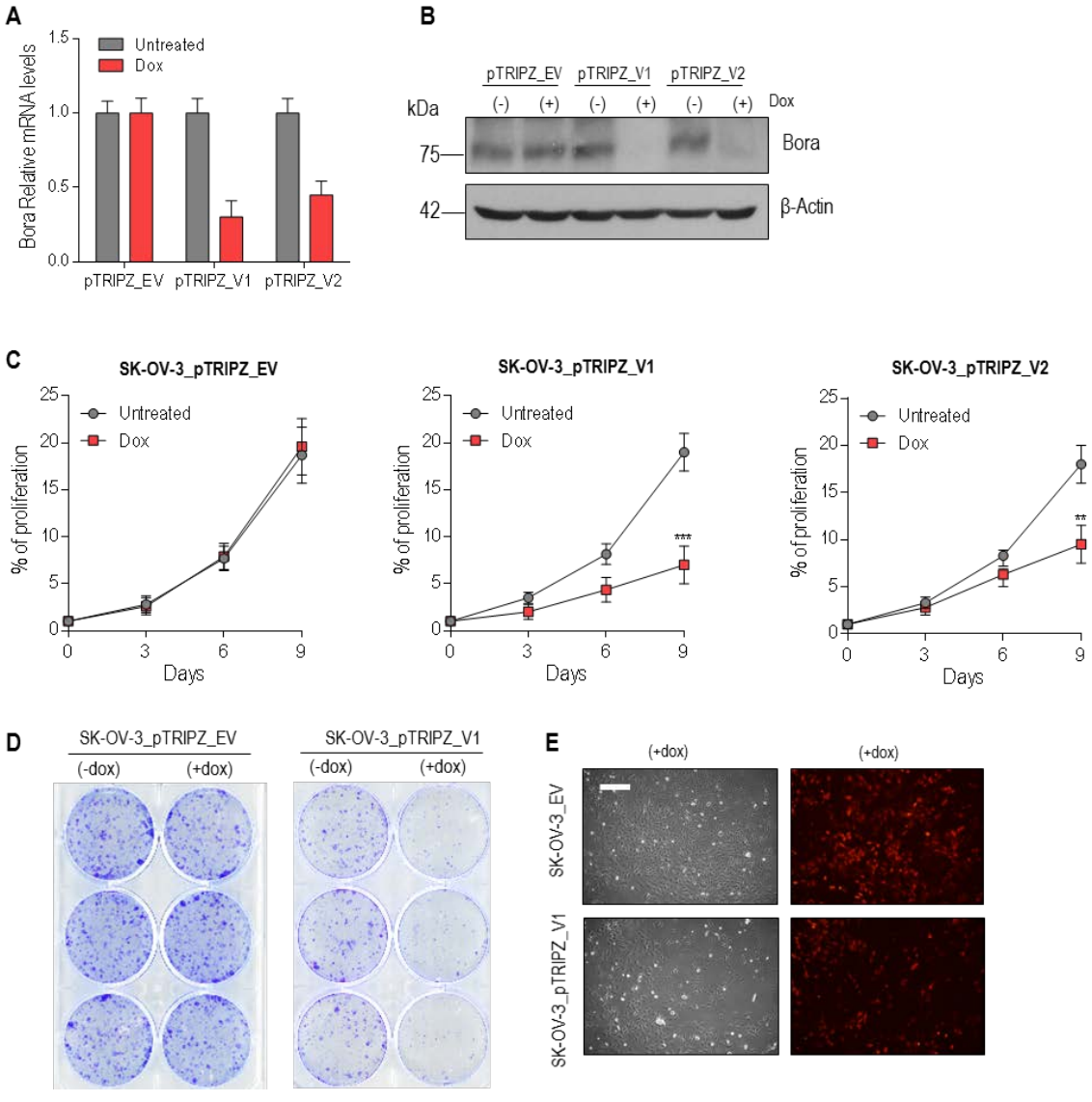

Figure 31. Inducible depletion of BORA impairs proliferation and colony formation capacities in SK-OV-3 cell line. **(A)** Relative *BORA* expression analyzed by RT-qPCR in the different stable pTRIPZ transduced SK-OV-3 cells treated or untreated with doxycycline (1 µg/mL) for 72h. *GAPDH* was used as endogenous control. The relative fold-change in expression was determined by the comparative $2^{(-\Delta\Delta Ct)}$ method and normalized against control (untreated) expression value. **(B)** Immunoblot showing effective BORA inducible depletion in doxycycline-treated cell lines (1 µg/mL). **(C)** Proliferation time-course for 9 days comparing pTRIPZ_EV or pTRIPZ_BORA-V1 or pTRIPZ_BORA-V2 treated or untreated with 1 µg/mL of doxycycline. Cells were counted each two days and relativized to day 0. **(D)** Representative images of a colony formation assay in pTRIPZ_EV and pTRIPZ_BORA-V1 infected cells treated with (+dox) or without (-dox) doxycycline and allowed to grow for 11-13 days. **(E)** Representative images of pTRIPZ-EV and pTRIPZ_BORA-V1– SK-OV-3 infected cells treated with 1 µg/mL of doxycycline. Expression of the pTRIPZ vector is followed by the expression of TurboRFP protein. Scale bar: 1 µm. Graphs represent mean ± SEM of three independent experiments. *P*-value was calculated using a two-tailed Student's *t*-test. ***P*<0,01; ****P*<0,001.

Next, we established xenograft tumors by the subcutaneous injection of SK-OV-3 pTRIPZ-BORA-V1 cells into the flank of 7-week-old female NMRI-nude mice. When tumors reached a volume of ~150 mm^3 in average, mice were randomly divided in two experimental groups: the BORA depletion group which received doxycycline (1 mg/mL) together with 2% of sucrose in drinking water *ad libitum* and the control group kept treated with the vehicle only (2% sucrose) (protocol depicted in Figure 32A). Differences in tumor growth between control (untreated group; grey line) and BORA inducible depletion (doxycycline treated group; red line) started to be significantly visible one week after doxycycline administration and sustained until the end of the experiment (Figure 32B; p<0,001). At the end-point of the experiment, mice treated with sustained doxycycline showed a significant reduction in tumor size and weight (Figure 32C-D) and a positive significant correlation was observed between volume and weight in BORA-depleted tumors (Figure 32E), indicative of the accuracy of the measures. Between the two groups, animal weight was not different thorough the experiment (Figure 32F), demonstrating good doxycycline tolerability in mice.

BORA and TurboRFP (tRFP) protein expression were verified by immunoblotting using representative tumors of both groups (Figure 32G), confirming BORA was consistently depleted and the system was successfully working during the period of the experiment. Histopathological analyses of the tumors revealed that BORA depleted tumors displayed reduced cellularity with extracellular matrix fueling empty spaces left by death cells (black arrows; Figure 32H), and a reduction in the percentage of Ki67 positive cells compared to untreated tumors (72% compared to 13% in control tumors; Figure 32H).

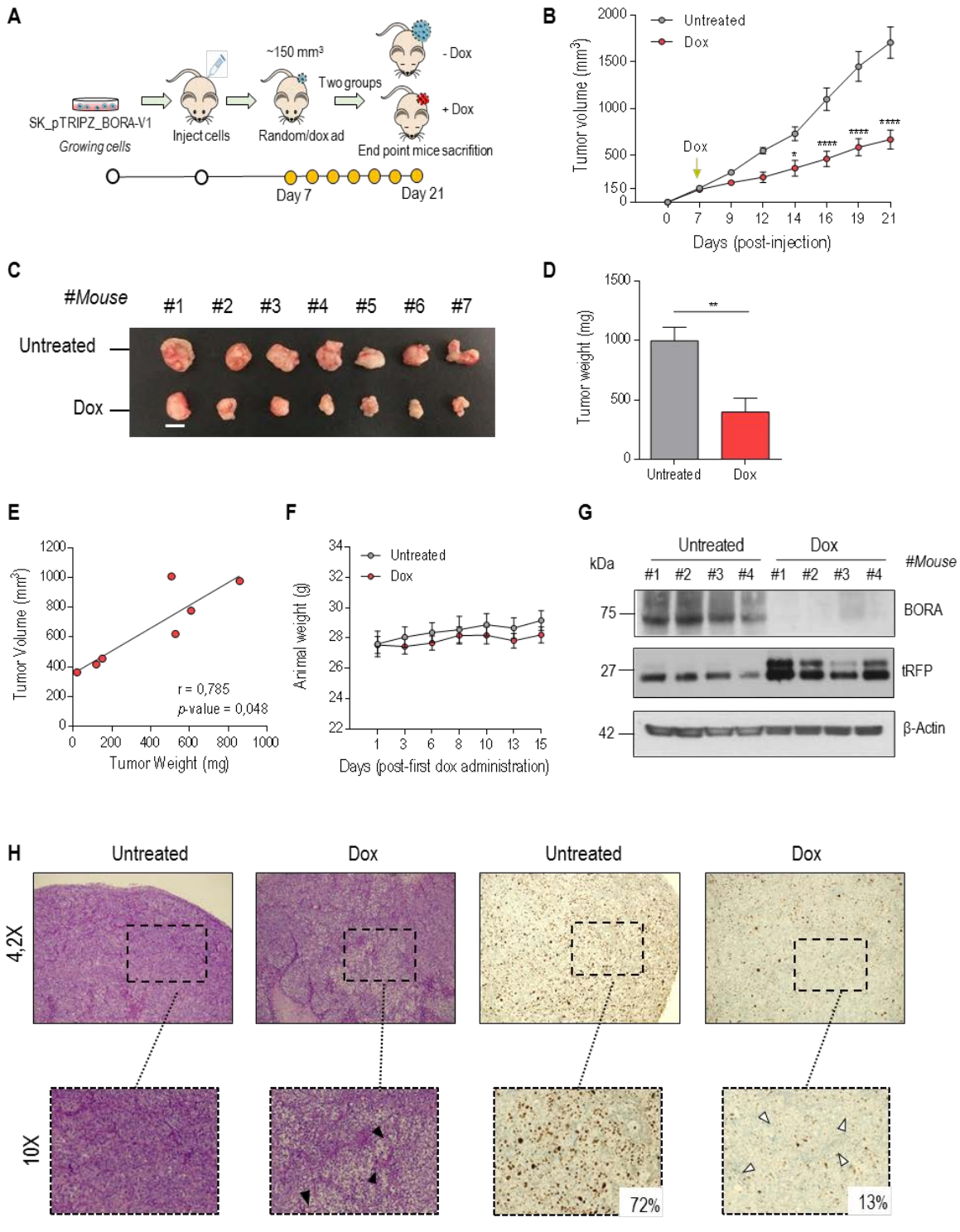

Figure 32. Knockdown of BORA *in vivo* attenuates tumor growth. (A) Schematic representation of the inducible mouse model design. **(B)** Tumor growth of SK-OV-3 pTRIPZ_BORA-V1 xenotransplant cells untreated (grey line) or after a sustained treatment with doxycycline (1 mg/mL) in drinking water (red line). Two-way ANOVA was used to calculate the significance (*p*-value) of the difference between the untreated and doxycycline treated group. **P*<0,05; *****P*<0,0001. **(C)** Representative tumors collected at the time of euthanasia. Scale bar: 1 cm. **(D)** Average weight of the tumors. *P*-value was calculated using a two-tailed Student's *t*-test. ***P*<0,01. **(E)** Body weight was monitored as an indicator of doxycycline tolerability during the experiment. **(F)** Spearman positive correlation between tumor volume and tumor weight in BORA depleted tumors. **(G)** Immunoblot analysis of BORA and tRFP protein levels in four representative xenograft tumors from both groups. β-Actin was used as loading

control. **(H)** Immunohistochemical analysis of H&E and Ki67 staining. Black arrows point extracellular matrix and withe arrows are showing remaining areas of non-proliferating tumor cells.

4.12 BORA silencing reduces the number and viability of patient-derived ascites cells

Tumor ascites cells, which survive aggregated into multicellular spheroids in the peritoneal cavity, represent a hallmark of OC[372]. These cells are chemoresistance and responsible for driving OC progression at later stages eventually causing disease recurrence[373]. Thus, to further evaluate the potential clinical therapeutic implications of our findings in advanced OC, we established a pre-clinical *ex vivo* model using the ascitic fluid from three metastatic OC patients collected at the time of the surgery.

Tumoral patient-derived ovarian ascitic cells were obtained and expanded as previously described[355]. Then, these cells were reversely transduced with shCTL and shBORA lentiviral particles and cultured as spheroids in anchorage-independent conditions (schematic representation illustrated in Figure 33A) to evaluate the therapeutic role of BORA inhibition (Figure 33B). At 36h post-transduction, spheroids were scored observing a significant reduction in the size and number in two out of three patients (Figure 33C). Immunoblot analysis confirmed the reduction in BORA levels in the three patients (First line; Figure 33E). Furthermore, MTS assay was performed at 96h to check the viability of the remaining spheroids. BORA depletion displayed a reduction in cell viability, remarkably in VH-3 patient, where the viability decreased up to 50% (Figure 33D). Immunoblot analysis confirmed increased in caspase-dependent apoptosis in the three patients after BORA silencing (Figure 33E), in agreement with the previous results in the representative OC lines growing in monolayer and in the shBORA bearing xenografts. The fact that the effects of BORA depletion are reproducible in patient-derived models grown in 3D, highlights BORA as a potential valid future therapeutic target for advanced and aggressive OC.

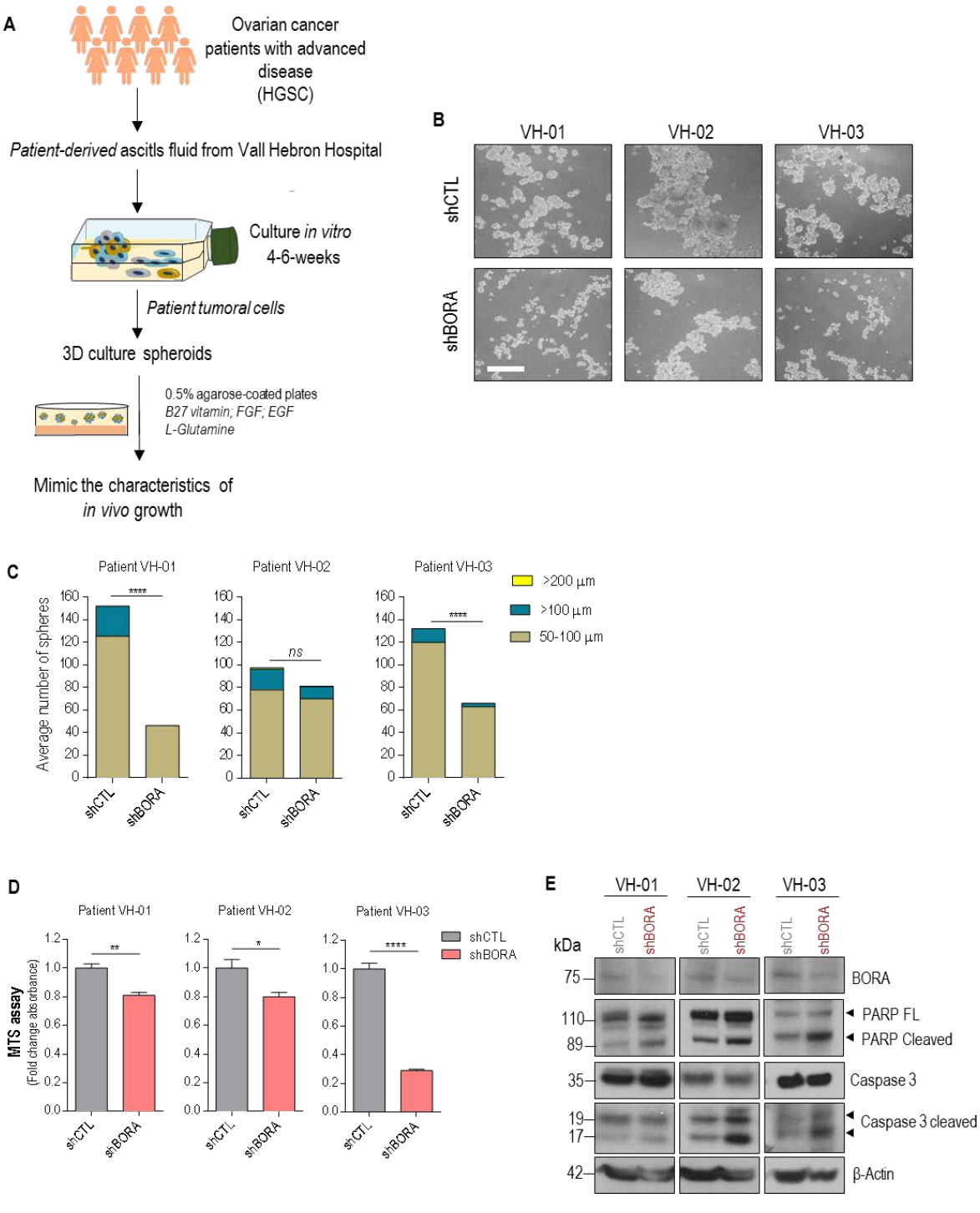

Figure 33. BORA knockdown reduces the number and viability of OC tumor spheroids from patient-derived ascitic cells. (A) Schematic representation of ascitic tumor cells isolation from advanced OC patients. **(B)** Representative images of the three OC patient-derived ascitic cells grown under anchorage independent conditions with shCTL and shBORA lentiviral transduction. Scale bar: 100 µm. (C) The number of spheres was scored after 36 h post-transduction with shCTL and shBORA in the indicated ascitic primary cells classified as being between 50-100 µm, ≥100 µm and ≥200 µm in diameter. **(D)** Viability assay (MTS) was performed at 96 h post-transduction with shCTL or shBORA in the indicated OC patient-derived ascitic cells cultured under anchorage independent conditions. **(E)** Spheres were used for protein extraction and immunoblot analysis with the indicated apoptosis antibodies 96h post-transduction. β-Actin was used as loading control. *P*-values were calculated using a two-tailed Student's *t*-test. **P*<0,05; ***P*<0,01; *****P*<0,0001.

4.13 Reduction in BORA levels impact in multiple cancer-related genes

Having established that BORA could represent a promising therapeutic target, we wanted to discern the landscape of genes and related-pathways modulated upon BORA silencing that caused this phenotype and thus identify potential BORA targets hitherto unknown. To this end, a whole-genome expression analysis comparing SK-OV-3 shCTL and shBORA -transduced cells was performed. Firstly, a time course immunoblot (24h, 36h and 48h) of BORA, pTCTP (Ser46) and Cyclin B1 proteins was conducted to decide the time when BORA was efficiently depleted but without increasing the levels of Cyclin B1 with the idea to detect the first molecular causes of BORA depletion rather than consequences (i.e. mitotic arrest) (Figure 34A). BORA knockdown was more efficiently in SK-OV-3 cell line at 48h with Cyclin B1 levels still equal compared to shCTL group at that time. Additionally, BORA mRNA levels carried out in a time-course confirmed the downregulation of BORA transcriptome levels at 48h (Figure 34B). Figure 34C illustrates BORA mRNA levels analyzed by RT-qPCR in the samples used for the microarray analysis.

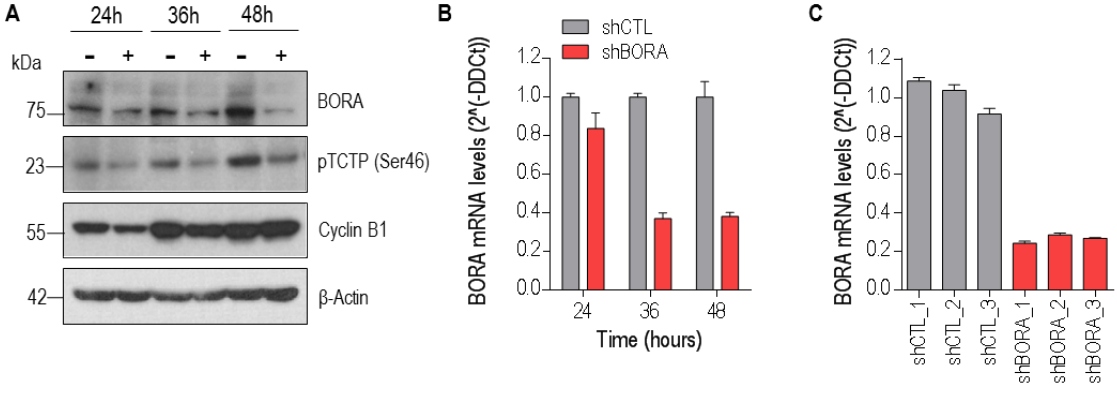

Figure 34. BORA depletion analysis for the microarray analysis. (A) Time-course immunoblot for BORA, Cyclin B1 and pTCTP (Ser46) upon shCTL (-) and shBORA (+) transduction. β-Actin was used as loading control. **(B)** Expression of *BORA* at different time-points analyzed by RT-qPCR. **(C)** *BORA* mRNA quantity in the samples used for the microarray analysis. *GAPDH* was used as endogenous control. The relative fold-change expression was determined by the comparative $2^{(-\Delta\Delta Ct)}$ method and normalized against shCTL expression values.

Principal component analysis (PCA) segregated samples on the basis of shCTL *vs* shBORA (n=3/group), indicating a robust and consistent transcriptional impact of BORA silencing (Figure 35A). After BORA knockdown, 192 genes were found to be up-regulated whereas 215 were downregulated (Fold change >± 1,5; p<0,05; Figure 35B; Annex 1). The top differentially expressed genes with higher fold change variation are listed in Figure 35C. The graph in Figure 35D summarizes the results from a gene set enrichment analysis (GSEA) of the transcriptome from BORA depleted cells. We observed enrichment in functions related to tumor biology, including cell commitment, disseminative process and inflammatory response.

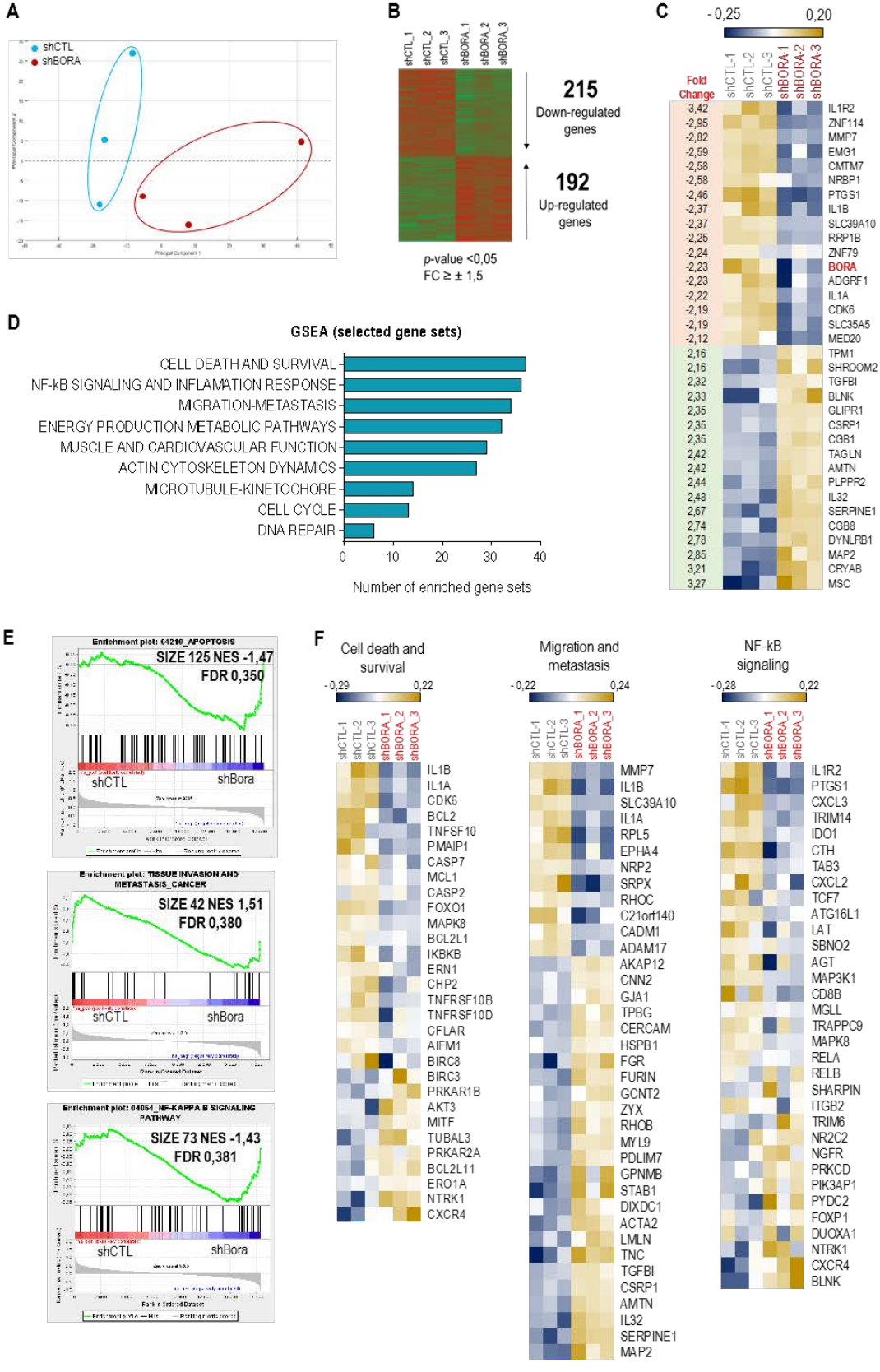

Figure 35. BORA knockdown alters multiple pathways related to cancer. (A) Principal component analysis (PCA) comparing expression profiles of shCTL and shBORA samples (n=3/group). Note that Principal Component 1, capturing around 38% of gene expression variance, effectively distinguishes BORA depleted and non-depleted samples. **(B)** Heatmap comparing the transcriptional profiles of shCTL and shBORA cells. **(C)** Heatmap

representation of the top differentially expressed genes with more fold change variation. **(D)** Gene set enrichment analysis using the GSEA software using the transcriptome data grouped in different term categories. Major collections from hallmarks, KEGG pathways and GO gene sets were downloaded from MSigDB.v6 and used for the GSEA. Graph represent total number of enriched genes sets with FDR<0,5 or *p*-value<0,05 plotted regarding each category. **(E)** Heat map representations of selected differentially expressed genes grouped in categories of functionally relevant pathways from the GSEA analysis. The color key shows relative expression levels of the differentially expressed genes (yellow corresponds to over-expressed genes while blue corresponds to under-expressed genes). **(F)** Representative GSEA curves for significant enriched gene sets related to the different pathways differentially regulated. In the enrichment plot, vertical bars in the red area indicate over-expressed query genes and vertical bars in the blue area indicate under-expressed query genes. *P*-values were calculated using 1000 gene permutations.

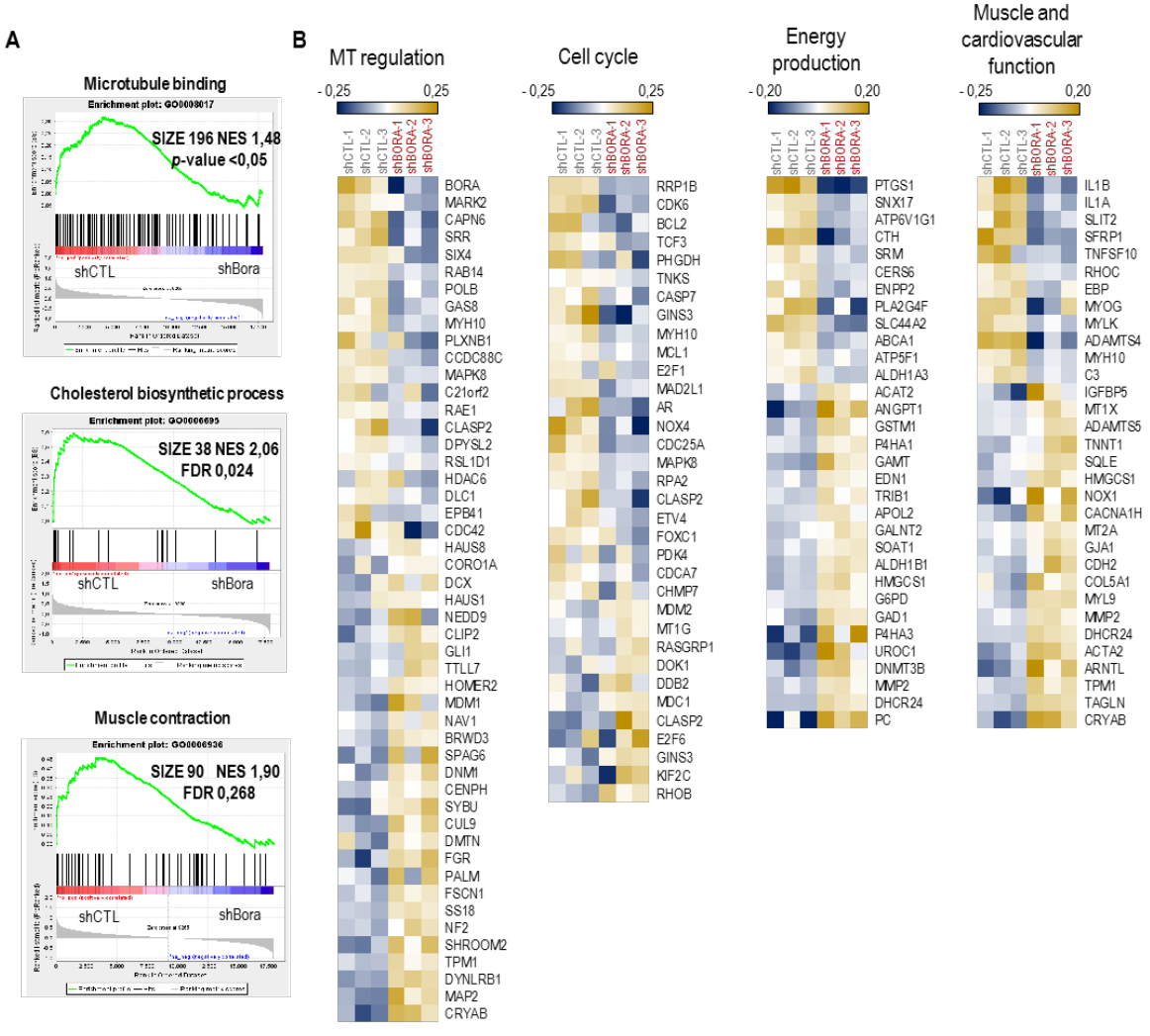

Figure 36. BORA downregulates different pathways including cell cycle, energy production or cardiovascular function. (A) Representative GSEA curves for significant enriched gene sets related to the different pathways differentially expressed. In the enrichment plot, vertical bars in the red area indicate overexpressed query genes and vertical bars in the blue area indicate underexpressed query genes. *P*-values were calculated using 1000 gene permutations. **(B)** Heat map representations of selected differentially expressed genes grouped in categories of functionally relevant pathways from the GSEA analysis. The color key shows relative expression levels of the differentially expressed genes (yellow corresponds to over-expressed genes while blue corresponds to under-expressed genes).

Furthermore, gene-sets composed of genes involved in energy production and cardiovascular system were found to be negatively enriched in shBORA cells, indicating impairment in these processes at the transcriptional level (Figure 35D and heat map representations in Figure 36C-B). Heat maps depicting the most relevant differentially expressed pathways illustrate how BORA knockdown impacts on the expression of several key oncogenic genes such *BCL*-2, *CDK6*, *MMP7* or *NF-kB* signaling factors (Figure 35F), suggesting that reduction of the expression of these genes might be contributing to the effects of BORA depletion on cell survival. Representative enrichment plots related to these differentially expressed pathways are plotted in Figure 35E.

Additionally, we selected cancer-related candidates from the list of genes differentially expressed and validated their expression levels by RT-qPCR in the SK-OV-3 line with the two shRNAs particles (Figure 37A). Interestingly, BORA depletion resulted in a significant down-regulation of genes involved in cell growth and survival (*BCL2*, *CDK6*, *RERG*), migration (*MMP7*), cell cycle (*MARK2*, *CLASP2*), the putative tumor-suppressor *SFRP1* and other genes involved in metabolic pathways (*SLC25A10*) as well as up-regulation of the cytokine *IL1B* and other genes with uncertain roles in cancer (*TPM1*, *SHROOM2* and *RHOB*); confirming the results from the array (Figure 37A). To add biological and clinical therapeutic relevance to these findings, we explored whether these genes were modulated also in two patient-derived tumor ascitic cells, to exclude a cell-line-specific phenomenon. BORA was successfully depleted in these patients grown in 2D and consequently the mRNA levels of these genes were altered in both patients' cells; VH-03 and VH-04 (Figure 37B), concurring with results seen in the cell line.

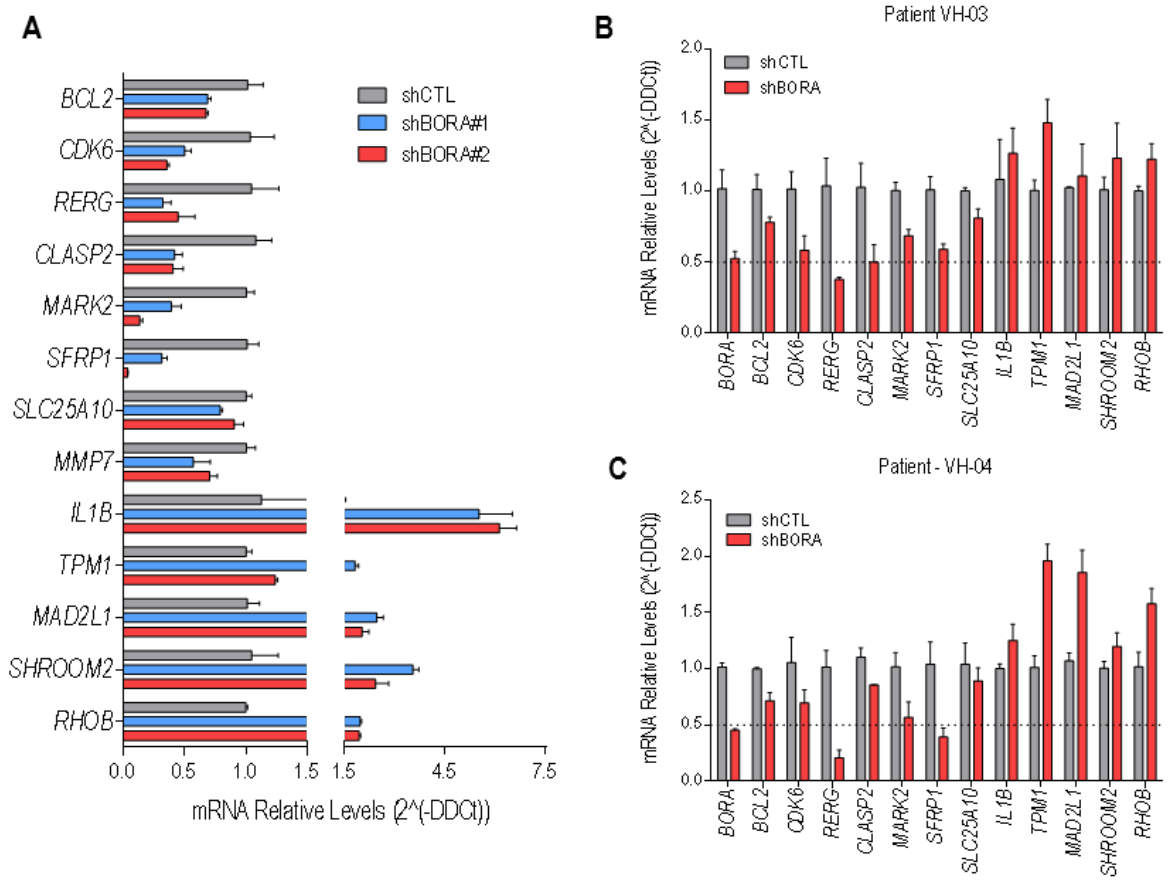

Figure 37. BORA depletion impacts on genes with different cancer related roles. **(A)** Array validation using the SK-OV-3 cell line with the two independent shRNA lentiviral particles. RT-qPCR using primers for eight downregulated genes (*BCL2*, *CDK6*, *RERG*, *CLASP2*, *MARK2*, *SFRP1*, *SLC25A10*, *MMP7*) and five upregulated genes (*IL1B*, *TPM1*, *MAD2L1*, *SHROOM2*, *RHOB*). Values are represented as fold change *vs* shCTL and are the mean ± SEM of one experiment. *GAPDH* was used as endogenous control. **(B)** Biological validation of the indicated differentially expressed targets in two patient-derived ascites cells grown in 2D (Patient VH-3 and VH-4) transduced with shCTL and shBORA lentiviral particles. The relative fold-change in expression was determined by the comparative $2^{(-\Delta\Delta Ct)}$ method and normalized against shCTL expression value.

Additionally, to confirm the involvement of several key oncogenic genes (*BCL2*, *CDK6*, *JNK1* or *RELA)* upon BORA depletion, we analyzed the protein expression in the representative tumor-xenografts protein extracts from the constitutive *in vivo* experiment. BORA depleted tumors exhibited a reduction in the antiapoptotic BCL-2 expression, CDK6 and JNK1 (*MAPK8*) kinases and in the subunit of the NF-κB complex; p65 (*RELA* gene), in a BORA-dependent manner compared to shCTL bearing tumors; confirming the results from the array and suggesting that reduction of the expression of these proteins contribute to the effects of BORA depletion on cell survival.

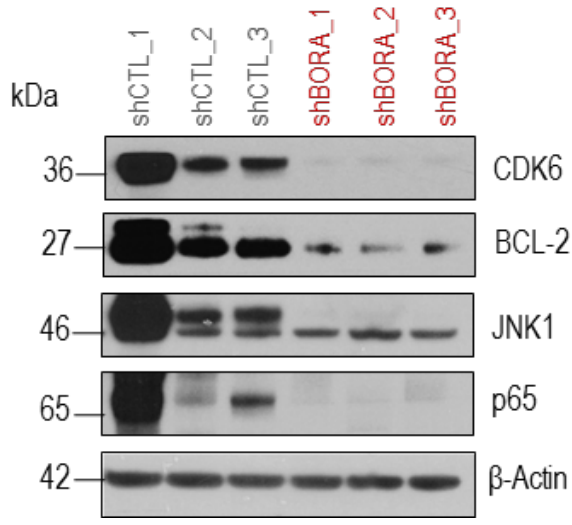

Figure 38. BORA inhibition alters oncogenic pathways at protein level. Immunoblot analysis showing representative cases from the shCTL (lanes 1, 2, 3) and shBORA (lanes 4, 5, 6) xenografts tumors verify the alteration in BCL-2, CDK6, p65 and JNK1 proteins. β-Actin was used as a loading control.

4.14 BORA mediates migration and metastasis pathways

The modulation of BORA in migration and adhesion related-pathways uncovered by the transcriptomic analysis encouraged us to further describe the role of BORA in OC progression. We evaluated the expression of BORA in 26 FFPE paired tissue samples (primary tumor matched with its metastasis tissue within the same patient; 13 patients in total) by RT-qPCR. BORA mRNA expression levels were significantly higher in the metastatic samples compared to its primary ovarian tumoral tissue (p<0,05), hence indicating a positive correlation between BORA expression and aggressive tissues (Figure 39A). *In vitro*, we observed that upon BORA depletion in SK-OV-3 cell line there was a reduction in the migration capacities compared to the shCTL -transduced cells (p<0,01; Figure 39B). These results are in agreement with the abovementioned described BORA capacities to promote malignant cell transformation *in vitro* and enhance the tumoral status *in vivo* (described in section 4.5-4.7 and Figure 21; Figure 22 and Figure 24). In sum, these findings, together with the pathways differentially expressed described in the microarray, suggest that BORA protein expression is not only related to the cellular survival, but also with the aggressiveness and metastatic capability of the malignant cells.

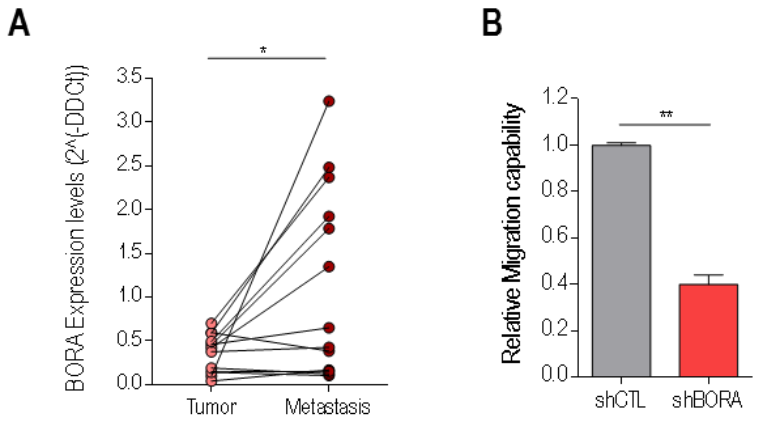

Figure 39. BORA mediates OC migration. (A) Graph represents *BORA* relative expression of the primary ovarian tumoral tissue to its paired metastatic sample. MRNA expression levels of each sample were normalized to its respective levels of *GAPDH* expression. The relative fold-change in expression was determined by the comparative $2^{(-\Delta\Delta Ct)}$ method and normalized against *BORA* expression value from the primary tumor. **(B)** Relative migration capacities of shCTL and shBORA -transduced SK-OV-3 cells. Data represents mean ± SEM of three independent experiments. *P*-values were calculated using a two-tailed Student's *t*-test. **P*<0,05; ***P*<0,01.

4.15 CDK6 and BCL-2 inhibitors exerts synergistic effect on OC viability

The results presented above convincingly demonstrate that BORA regulates the survival of OC cells. It was therefore hypothesized the depletion of BORA could have therapeutic translation in the clinical practice inhibiting ovarian tumor growth and metastasis. However pharmacological inhibition of BORA is currently not possible since no BORA inhibitors have been developed thus far due to the unstructured nature of the protein. Nonetheless, since the levels of CDK6, and the pro-survival protein BCL-2 were modulated upon BORA silencing and inhibitors of these pathways are FDA-approved drugs for breast cancer and leukemia[374,375], we sought to ascertain whether these inhibitors could phenocopy BORA depletion and thus could result in beneficial therapeutic effects for OC patients. To test this, we used *Palbociclib* and *Amebaciclib* (CDK6 inhibitors) and *Navitoclax* and *Venetoclax* (BCL-2 inhibitors); alone or in combination for five days in OC lines (SK-OV-3 and A2780p). As expected, the inhibition of both pathways resulted in a loss of proliferation in the OC cells tested as illustrated in Figure 40. The four inhibitors reduced cellular proliferation, but *Palbociclib* and *Navitoclax* were more efficient than *Amebaciclib* and *Venetoclax* in OC cells; thereby we decided to use *Palbociclib* in combination with *Navitoclax* to recapitulate BORA inhibition in our OC models.

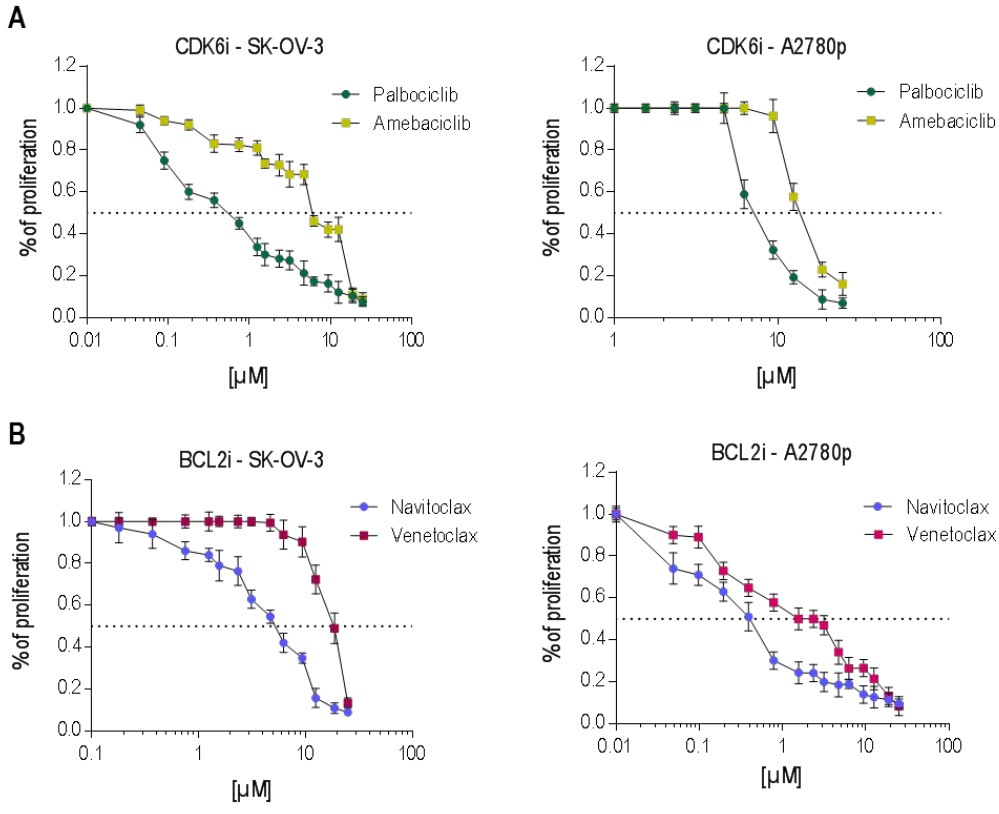

Figure 40. CDK6 and BCL-2 inhibitors reduce the cellular growth of OC cells. Normalized proliferation curves of the indicated OC cell lines treated with the **(A)** CDK6 inhibitors: *Palbociclib* and *Amebaciclib* and **(B)** BCL-2 inhibitors: *Venetoclax* and *Navitoclax* for 5 days measured by crystal violet staining (n=6/condition). Drug doses ranges from 0,01 µM to 25 µM. Data represent an average quantification of three independent experiments ± SEM (n=6/condition).

To identify potential synergies between *Palbociclib* and *Navitoclax*, we used a 4x4 checker-board matrix format to assess the compounds at four clinically representative concentrations with multiple drug ratios. Fraction affected (FA) were obtained for the multiple panel-comparisons measured by crystal violet for five days, and the combination index (CI) values for all combinations were calculated using Compusyn 2.0 software based on the Chou-Talalay method[361]. Our combination screening identified several promising drug combinations for the treatment of OC, which were sorted by cluster analysis for FA and for CI (Figure 41A-B). The greatest CI values of all combinations that yielded high FA were depicted in this figure. Of these, we narrowed the results from the combinations that produced different anti-tumor activity (fraction affected) with different CI (Figure 41C) demonstrating strong synergy between *Palbociclib*:*Navitoclax* in the two cell lines with different concentrations.

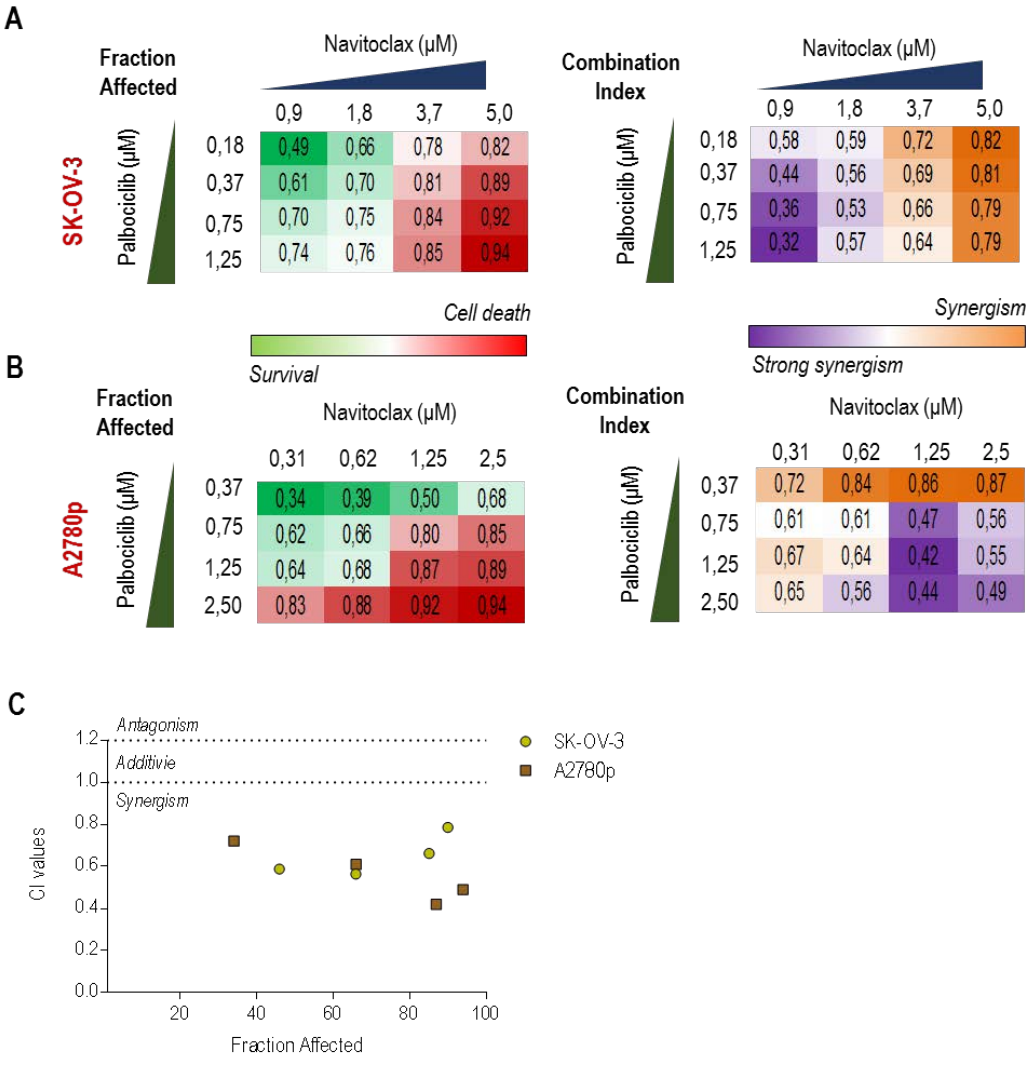

Figure 41. *Palbociclib* and *Navitoclax* compounds cooperate synergistically to impair OC growth. (A-B) Clustering results showing FA and CI of the top combinations evaluated in SK-OV-3 and A2780p cell line using non-constant ratio with different compounds. **(C)** Graphical representation of the combination index of *Navitoclax* and *Palbociclib* at different constant ratios. Data plotted are CI values at different fractions affected.

Of these, we narrowed the results from the top combination that produced the highest CI value with great anti-tumor activity demonstrating strong synergy with the two compounds in the two ovarian cell lines (Figure 42).

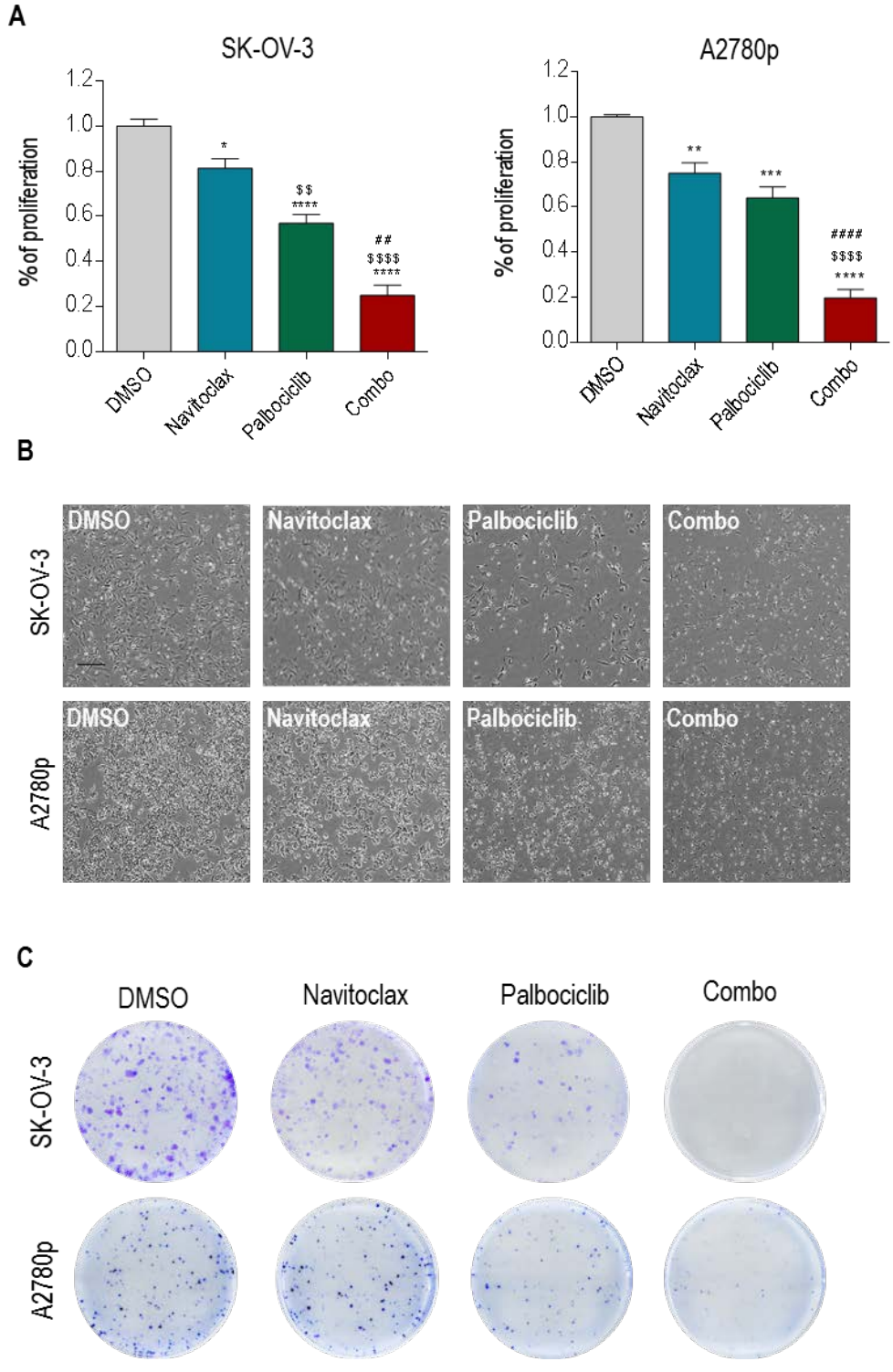

Figure 42. Impairment of the proliferative and colony formation capacities upon simultaneous administration of *Navitoclax* and *Palbociclib*. (A) Proliferation assay of the indicated cell lines treated with the two agents at the best CI for five days, (*Navitoclax* 0,9 and 1,25 μM; *Palbociclib* 1,25 and 1,25 μM; for SK-OV-3 and A2780 respectively) measured by crystal violet staining (n=6/condition). Graphs are the average of three independent experiment ± SEM. *P*-value was calculated using one-way ANOVA. * compares DMSO *vs* the rest of the conditions; # *Navitoclax vs* rest of conditions; $ *Palbociclib vs* Combo. $^{*,\#,\$}P<0,05$; $^{**,\#\#,\$\$}P<0,01$; $^{***,\#\#\#,\$\$\$}P<0,01$; $^{****,\#\#\#\#,\$\$\$\$}P<0,001$ **(B)** Representative macroscopic images of SK-OV-3 and A2780p cells lines treated with the inhibitors. Scale bar: 100 μm. **(C)** Colony formation capacity of the indicated cells lines treated with the two compounds alone and in combination.

To establish this potential treatment strategy in the clinics, we repeated the analysis of the pharmacologic compounds using multicellular tumor spheroid cultures derived from two advanced serous OC patients (VH-05 and VH-06) in our *ex vivo* patient-derived model setting. Once spheroids were formed, treatment with suboptimal concentrations of the two inhibitors impaired tumor spheroid growth exerting a more dramatic effect when combined (Figure 43A). Combinatorial treatment attenuated both sphere size and viability capacities of these spheroids (Figure 43B). Immunoblot confirmed an increased in hallmarks of apoptosis such as the presence of cleaved caspase-3 active fragments and the processing of the caspase-3 substrate, PARP, when both drugs were combined in the two patients (Figure 43C), hence showing a clear synergism effect. These results suggest that the combined inhibition of CDK6 and BCL-2, downstream effectors of BORA, might be a suitable therapy for advanced OC.

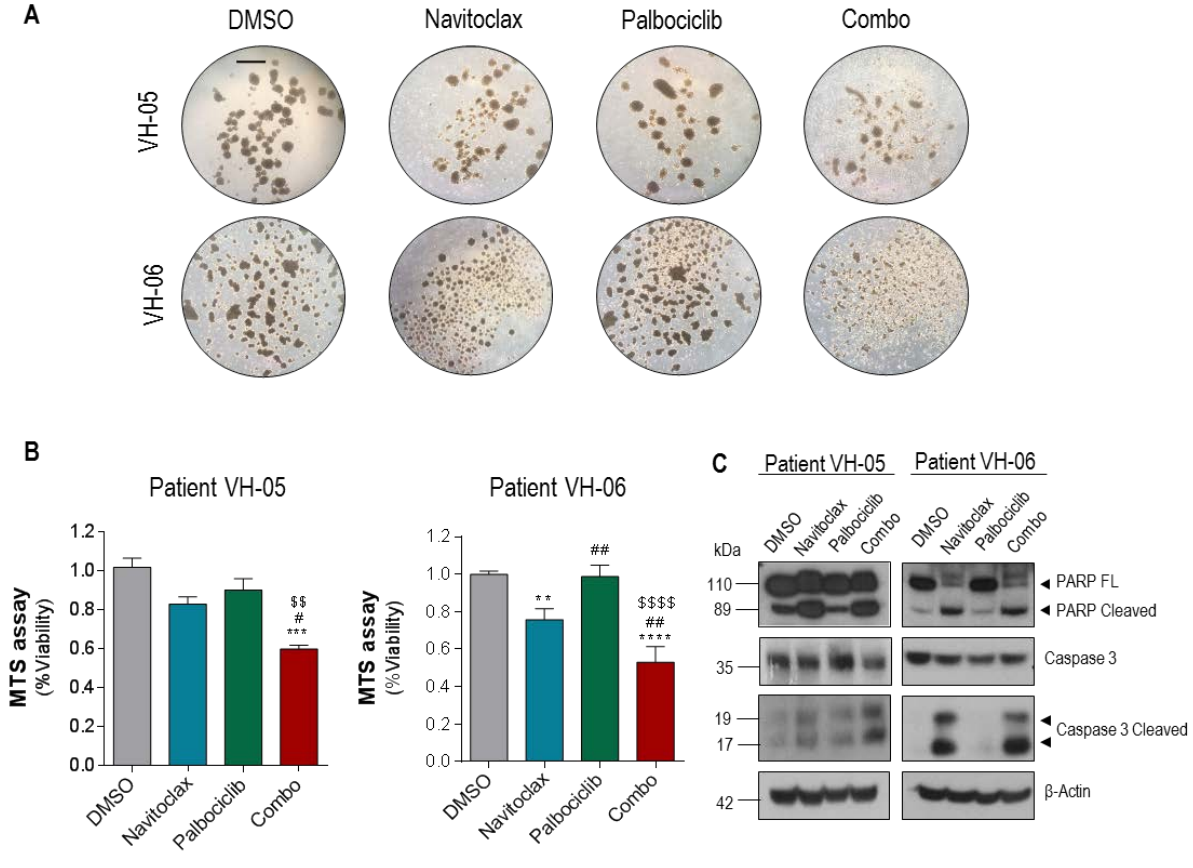

Figure 43. *Palbociclib* and *Navitoclax* agents cooperate to reduce the viability of patient-derived primary ascitic cells grown in anchorage-independent conditions. (A) Representative images of two patient-derived ascites cells (patients VH-04 and VH-05) grown under anchorage independent conditions (tumor spheroids) and treated with *Palbociclib* (12 μM) and *Navitoclax* (4 μM) during 96h. Scale bar: 100 μm **(B)** Viability assay (MTS) was performed on the spheres treated during 96h of the indicated drugs and the combo. Values are represented as fold change *vs* the control (DMSO). *P*-values were calculated using a one-way ANOVA analysis. * compares DMSO *vs* the rest of the conditions; # *Navitoclax vs* rest of conditions; $ *Palbociclib vs* Combo. *,#,$*P*<0,05; **,##,$$*P*<0,01; ***,###,$$$*P*<0,001; ****,####,$$$$*P*<0,001. **(C)** Immunoblot of the indicated apoptotic protein markers to confirm the efficacy of the inhibitors in primary ovarian spheres. β-Actin was used as a loading control.

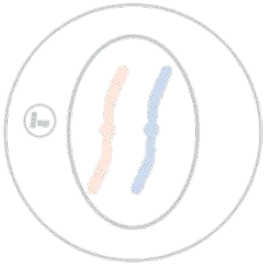
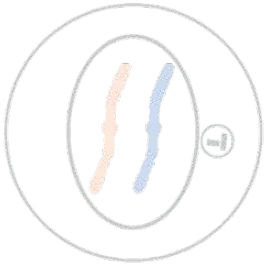
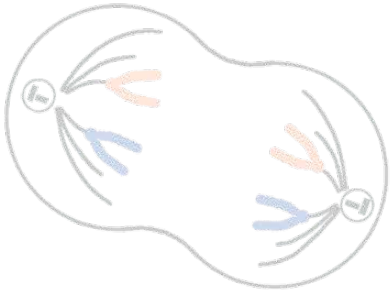

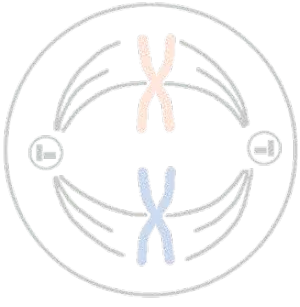
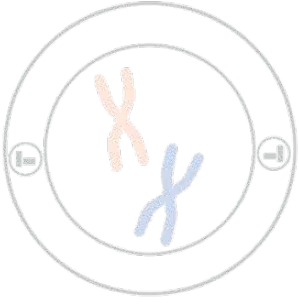
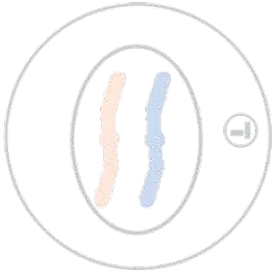

5. DISCUSSION

5.1 OC: A challenge for clinicians and researchers

OC is the most lethal gynecological malignancy. The lack of early warning symptoms together with no effective screening strategies make OC a disseminative and complex disease with limited therapeutic options. Standard treatment, which has not varied from the last two decades, consists in surgical debulking followed by a taxane/platinum-based chemotherapy. Approximately two-thirds of OC patients will respond to this, but tumor recurrence will occur in most patients (85%) at a median of 15 months from initial diagnosis[376]. Thus, clinical management of OC remains a challenge; for the clinicians because there are no definitive therapies available and for researchers due to the complexity of the tumor at that stage to design successful and novel therapeutic avenues. Recent advances in cancer genomics have revealed OC to be a vastly molecular heterogeneous disease with massive genetic instability, extensive copy-number variations and defects in the homologous recombination repair pathway[377]. These genomic aberrations contribute to the development of tumor resistance, hampering effective treatment and ultimately causing recurrence of the disease, but also offer novel potential actionable vulnerabilities that can enhance the effectiveness of existing therapies.

Targeted therapies, including anti-angiogenic agents and PARPi, are currently used in OC providing clinical long-lasting benefit but only in a determined subsets of patients[89]. Therefore, it is clinically necessary to seek for potential therapeutic tools that can work in a broader number of OC patients. In this line, the mitotic spindle is a validated target in cancer chemotherapy and currently used as standard of care in some types of cancer. Unlike the first generation of anti-mitotic drugs aimed to block cell division, the next generation is now emerging exploiting the concept of CIN[176,378]. CIN inducing-based therapies aim to target cancer-specific alterations such as centrosome amplification, SAC proteins or G2/M checkpoint altered regulators to cause cell death by triggering extensive chromosome missegregation, exceeding the cellular damage threshold and therefore yielding superior clinical results[206,379].

In the present work, we have carried out an integrative-bioinformatic screening of clinically relevant data sets that contains well-annotated transcriptomics data and survival information from OC patients to explore novel functional mitotic candidates to target. Among the identified molecules, we considered BORA as an attractive target owing to its essential role in the mitotic spindle assembly[346], the little knowledge of its function in OC and its relation with the master mitotic kinase, PLK1; considered a *bona fide* cancer target. Even though BORA depletion has been reported to greatly reduce the activity of PLK1 kinase, no data supporting a role of BORA as targeted therapy has been described yet in a cancer context. We found that BORA was consistently upregulated in OC and especially in advanced stages of

the disease, with high BORA levels being indicative of poor prognosis and tumoral aggressiveness. Gain and loss of functions experiments *in vitro*, *in vivo* and *ex vivo* showed oncogenic roles of BORA in OC, making it a potential selective target for therapeutic intervention. Furthermore, whole-genome transcriptome analysis revealed for the first time that BORA controls the expression of key elements of oncogenic pathways such as CDK6 and BCL-2. Inhibition of these downstream effectors also offers a promising new combinatory therapy for advanced OC.

5.2 Integrative analysis of transcriptomic and clinical data uncovers druggable candidates

In the last decade, cutting-edge sequencing technology has released massive data derived from cancer specimens. This data has become an important resource for identification and classification of key molecular drivers, planning appropriate therapeutic treatments and design targeted therapies. Indeed, the TCGA project has provided the most comprehensive genomic data resource from over 33 types of cancers with the identification of several so-called cancer driver genomic aberrations and generation of extremely valuable and profitable transcriptomic data[380]. Despite public availability of these relevant data, it is still underexploited by the scientific community due to the complexity of handling such quantities of information. In this regard, public transcriptome datasets, with biocomputational platforms for genomic analysis and visualization, are emerging as powerful strategies to carry out studies to understand the cancer genome biology[381,382]. It is important, especially in OC, where the deregulation of gene expression is a key for cancer pathogenesis and development[383,384]. Deleterious mutations in *BRCA1/2* genes and also aberrant expression in others genes involved in the HR DNA break repair process are well-associated with HGSC susceptibility. Deciphering the transcriptomic landscape of OC will identify novel drivers relevant to the OC tumorigenesis that can be used as actionable vulnerabilities. Thus, in this study we performed an integrative bioinformatic screening with the aim to identify aberrant up-regulated novel mitotic candidates involved in ovarian tumorigenesis. Our analysis concurred in eight unexplored mitotic genes differentially expressed with high expression correlated with worse survival in OC; including *KIF20B*, *CCDA*, *CDC25*, *FAM64A*, *SPC25*, *SPC24*, *OPI5* and *BORA*. These genes have been described to be altered in other tumor types and thus encourage us to explore their role in OC. The kinesin family member 20B protein (KIF20B) has been previously reported as biomarker of poor prognosis with pro-oncogenic functions in colorectal and lung cancers[385,386], as well as a role in sensitize prostate cancer cells to MTAs[387]. Of note, the study of the role of kinesins in tumorigenesis and their potential as therapeutic targets is a new focus in our laboratory and a new kinesin-targeted therapy is being developed by our group and collaborators. The spindle protein SPC25 has been associated with

cancer stem features both in lung and prostate cancer and knockdown of the protein inhibits tumor cell proliferation[388,389]. On the other hand, *FAM64A* gene, also referred to as PICALM Interacting Mitotic Regulator, has potential roles in the diagnostic and prognostic evaluation of patients with pancreatic cancer and leukemia[390,391]. Interestingly, *FAM64A* has been included in a gene panel signature to predict the efficacy of paclitaxel-based neoadjuvant therapy in HER2-negative breast cancer patients[392]. *CCNA* (Cyclin A) has been identified within a gene cluster related to different cellular processes such as proliferation and inflammatory response in lymphomas[393], but targeting CCNA protein is not a good option since is largely dispensable for non-tumoral cells[394]. CDCA5, also known as Sororin, is required for stable binding of cohesin to chromatid in the S and G2/M phases[395]. In cancer, high protein expression confers poor prognosis in bladder, hepatocellular and breast carcinomas[396,397] and it is linked to colorectal cancer progression by activating the ERK pathway[398]. More exploited is the protein codified by the *SPC24* gene, an important spindle protein in the mitotic checkpoint machinery. Its expression has been reported to be a good prognostic biomarker in a collection of tumor types[399,400] and it is responsible for driving breast and lung cancer progression through the modulation of EGFR/MAPK signaling and PI3K/AKT pathways[401,402]. Similarly, the overexpression of OPI5 (Opa interacting protein 5) increases the carcinogenesis of various tumors and also the acquisition of cisplatin resistance[403–406]. In contrast, much less information is reported about the role of BORA.

5.3 PLK1 activation in mitotic entry

Firstly, mechanistically our group and collaborators have demonstrated that CDK1 dependent BORA phosphorylation in three evolutionary conserved residues located in the N-terminal part of the protein supports the activation of PLK1 by AURORA A kinase phosphorylation on the threonine residue (Thr210)[333] priming mitotic entry in G2 recovery conditions. Using FRET technology, we obtained a direct read out for PLK1 activity monitored at single cell level testing different constructs of BORA. Though we have not tested the exact contribution of each one of the three phospho-sites separately, it is tempting to speculate that these phosphorylated sites have independent functions in modulating the interaction of BORA with PLK1 and/or with AURORA A. Importantly, the amino-acid sequence surrounding the 3 residues is different, supporting a model in which all these residues engage a unique set of interactions. Single mutants in these sites have resulted in a different delay cell cycle timing in the *C. elegans* embryo, indicating that each site contributes to the phenotype observed in triple mutants[334]. Knowledge of the precise mechanism by which BORA (and its phosphorylation by CDK1/Cyclin A) helps to activate PLK1 is still lacking and will likely require structural biology approaches. This PLK1 activation has always been

shown to be crucial to trigger mitotic entry after a DNA-damage-induced G2 arrest[331,335], but whether its activity is necessary to entry into mitosis in unperturbed cell cycle remains debatable.

Polo kinase has long been known to promote mitotic entry in various systems, as reported in *Xenopus* extracts[407] or in *Drosophila*[262]. But PLK1 activity might not be universally required for this transition. For example, in yeast, inactivation of Cdc5 (Polo) kinase results in a late anaphase arrest[408] and in human cells it has been questioned. Previous inactivation of PLK1 by RNAi or with ATP-competitive chemical inhibitors induced a prometaphase arrest after a delay in G2 or prophase, suggesting that PLK1 was not required for mitotic entry in cells progressing through normal cell cycle[308,409]. However, two recent studies have now firmly established that PLK1 activity is required for mitotic entry in some of the most commonly used human cell lines to study mitosis[410,411]. They demonstrated that complete inhibition of PLK1 can prevent mitotic entry for hours in a vast majority of hTERT-RPE1, HeLa or RKO cells, even without prior activation of the DNA damage checkpoint[410,411]. Interestingly, mitotic entry was blocked more efficiently in untransformed RPE-1 cells than in the tumoral HeLa cell line, probably because PLK1 is expressed in higher levels in tumoral cell lines. This can be explained by the fact that distinct activity thresholds are required for known functions of PLK1 and much less PLK1 activity is sufficient to ensure mitotic entry than the level of activity required for the cell to build a mitotic spindle or to ensure chromosome segregation[412] (reviewed in Lera and Bukard[412]). Additionally, Bruinsma *et al.,*[336] monitored activation of PLK1 during mitosis showing an extremely robust and sustained activation with even reduced levels of the BORA-AURORA A complex, suggestive indeed that minimal BORA levels already switch on the kinase. Once the threshold is reached, the activation of PLK1 functions as a bistable switch, a feature described for the mitotic kinase CDK1/Cyclin B1 and an integral mode of cell cycle control at the onset of mitosis[413]. In this thesis we have also used the phosphorylation on TCTP-Ser46, to monitor the activity of PLK1. It was demonstrated that phosphorylation at this site correlates with PLK1 level and kinase activity in G2 and mitotic cells[366]. Here we observed no correlation between the levels of BORA with the pTCTP (i.e. PLK1 activity) neither in the tumor samples nor in the cell lines. The likely explanation for this is that small amounts of BORA are already sufficient to switch on PLK1 kinase; and the limiting factor is instead the amount of the kinase (PLK1), whose levels do correlate with pTCTP levels.

Thus, besides some studies about the function of BORA in cell division performed with tumoral lines (e.g. Hela), it has not deepened yet into the role of the protein within the tumoral context. A wide-genome analysis revealed *BORA* gene expression as biomarker of radiation response in lymphoblastic cell lines[414] and recently it has been described as biomarker of poor prognosis in various tumors[351]. Taking into account (1) that we and others have demonstrated that BORA controls the activity of PLK1[330,331,338]; (2) that several clinical trials are currently ongoing testing PLK1 inhibitors as cancer therapy (as reviewed

in section 1.4.3) and; (3) that our laboratory has a focus on the development of cell cycle blockade therapeutics, we decided to further explore the role of BORA.

5.4 BORA expression as potential biomarker of poor prognosis

The functional implication of BORA in cancer has been hitherto described as independent prognostic parameter for OS and disease-free survival in three types of adenocarcinomas (namely, breast, lung and gastric). Notably, high expression of BORA was positively correlated with *Ki67* index and linked to poor survival outcome in the three tumor types, but especially in breast cancer patients with distinct clinical stages II/III and subtypes (HR+ and HER2+)[351]. Accordingly, here we showed that *BORA* is significantly up-regulated in OC patients when compared to normal specimens and high levels of *BORA* are correlated with poorly-differentiated tumors and with late clinical stage (advances stages of the disease). In addition, high expression of *BORA* was positively correlated with the cell proliferation index *Ki67* and with the *CIN25* score expression, a measure of chromosome instability linked to tumor progression and resistance[204,364]. These findings hold significant clinical application of BORA as biomarker to predict poor prognosis and to identify high risk OC patients to stratify them in the clinical practice. The action of BORA as potential prognostic marker concurred with the reported also in other tumor types, which potentiates BORA as validated biomarker across several types of adenocarcinomas, something that nowadays is not achieved with all currently-used protein biomarkers. Of note, an important issue will be to determine if the aberrant expression of BORA also discriminates between OC patients that are resistant to the treatment and eventually relapse and those patients that are sensible to the platinum-based chemotherapy (to search a potential correlation with treatment response and the platinum free interval). Remarkably, in the panel of ovarian cells lines, we observed low BORA expression in the cisplatin- resistance A2780p line compared to the parental one, suggesting low BORA levels might serve as indicator of cisplatin resistance. Interestingly, we mined through the Kaplan Meier Plotter platform and we correlated BORA expression with measures of patient outcome but splitting the patients regarding the chemotherapy treatment they had received (Annex 2). We strikingly noticed that OS and PFS are slightly higher in patients treated with cisplatin but harboring high levels of BORA, albeit not significant statistically, while no differences in patient outcome are observed when patients are treated with taxol (Annex 2), suggestive indeed of a role of BORA in cisplatin resistance. In this sense, BORA was recently found to be a biomarker of radiation response in human lymphobastoid cell lines in a genome-wide study[414], and subsequently, Cairns *et al.,*[415] reported that BORA-depleted tumor cells activate the DNA damage checkpoint in response to radiation, and they repair damaged DNA more effectively than BORA-sufficient tumor cells. Mechanistically, they found that this sensitization is due to

the inhibition of MDC1 and 53BP1 accumulation at the damage-repair site through direct binding of BORA to MDC1, leading to inhibition of the recruitment of other factors to the damage sites and, as a result, deficiency in DNA repair. To check whether BORA might be a prognostic biomarker of platinum resistance and also to validate in a higher cohort of patients our previous results, we are setting up the conditions to carry out immunohistochemistry staining to check BORA protein expression in a collection of tissue microarrays (TMAs) that we have prepared with a larger cohort of OC specimens, with different clinical outcome, histology and treatment response.

We also wondered whether other tumor types also harbor higher *BORA* levels and examined the transcriptional levels of 23 different tumor types characterized by the TCGA cohorts. We compared *BORA* expression into a data set that contains the expression of 353 different normal body tissues samples and we showed that *BORA* expression was higher in all tumors types, hence concurring with the results in OC. Of note, we observed that *BORA* is barely mutated in tumors without hot spot mutations areas. A possibility that could explain the low mutational rate in the *BORA* gene is probably the fact that *BORA* is an essential cell division gene and therefore cells cannot handle it loss of function.

5.5 BORA overexpression: cause or consequence?

Our data defines BORA as prognostic biomarker and as a novel intervention target in OC. But a question remains to be determined: Why BORA is up-regulated in OC? The answer to this critical question is underneath of a classical paradigm; if the consistent overexpression of BORA in cancer is due to its causal role in the neoplasic transformation of OC cells or whether it is a mere reflection of the higher proliferation rate due to the tumor development.

Our data clearly evidence that forced overexpression of BORA results in a malignant transformation of normal ovarian epithelial cells *in vitro*. Remarkably, ectopic expression of BORA promoted the loss of contact inhibition forming extreme multiple layers on the plates together with the ability to grow in soft agar, two classical hallmarks of malignant transformation. In addition, BORA enhances the aggressiveness of the tumoral status as we observed in the SK-OV-3 cell line upon overexpression in the proliferation rate and in the capacity to grow in soft agar. These results are in accordance with Zhang *et al.*, where the overexpression of BORA in MCF-7 cells (a breast cancer cell line) enhanced cell proliferation rate, resulting in a significant decrease of G0/G1 phase and an increased in S phase[351].

In vivo, IOSE cells overexpressing BORA failed to sustain tumorigenesis in nude NMRI mice, although an apparent engraftment was indeed observed. Mice with IOSE pIND_BORA cells exhibited single tiny scars, presumably remnants of an intention of tumor while pIND_EV cells did not show. These scars appeared as very small fibrotic lesions, composed of a dense network of collagen fibers: signs of chronic

inflammation. We have come up with two possible explanations to these results. The first one is related to the possible potent action of *TP53* in this line. Immunoblot for p53 protein comparing all ovarian cell lines revealed high expression in the IOSE cell lines compared to the cancer cell lines where p53 levels were abruptly lower. According to the TCGA ovarian cohort, 96% of HGSC patients harbor mutations in *TP53*, making the protein not functional. *TP53* wild type form can suppress tumor development by regulation of multiple pathways, however the mutations (either missense-mutant or nonsense-mutant) and the resultant inactivation of the gene might cause tumor progression. Thus, p53 protein could be counteracting, or ablating the tumoral capacities of BORA *in vivo* in this non-transformed line. In this sense, we tried to block p53 activity using the small chemical inhibitor, Nutlin-3, an antagonist of MDM2. However, after treatment with Nutlin-3, we observed that IOSE cells displayed increased senescence rate, as also described in other studies[416]. We will follow in the future other strategies to block p53 function. On the other site, as we observed after three weeks post-injection a diffuse tissue engraftment into the flanks of animals carrying BORA overexpressing cells that finally was confirmed as fibrosis, we hypothesized that maybe the mouse strain used was not the most appropriate and we should have used another one with a higher degree of immunosuppression. In a similar experiment but with a normal epithelial prostate cell line, the overexpression of PLK1 promoted formation of tumors in one of the most immunosuppressed strain, the NOD/SCID[417]. Thus, the same experimental approach planned before, is scheduled to do using NOD/SCID mice. In parallel, we observed that BORA overexpression in the SK-OV-3 line, a p53 mutated cell line with low-medium endogenous levels of BORA, drastically increased not only tumor engraftment but growth when xenografted into nude mice, suggesting BORA is capable to contribute to the OC progression. These data indicate BORA can potentiate the carcinogenesis once the tumoral status is already established, but strictly speaking it does not necessarily demonstrate that BORA is an oncogene *in vivo* (driving transformation itself). In this regard, we are planning to perform a whole transcriptome analysis using the tumor xenografts from the *in vivo* experiment to describe to pathways and genes modulated that enhanced the tumoral status with the BORA overexpression.

Another alternative that we consider in the near future is to directly introduce the IOSE cells (both the control and the ones with elevated BORA levels) into the ovarian bursa of the mice (orthotopic injection) to see if cells with a proper stromal environment that maximally mimics human OC, stimulates tumor formation.

Given that BORA is barely detectable in normal ovarian epithelial cells and how its aberrant expression displayed this causal role in aggressiveness, it is of interest to exanimate (1) if BORA endogenous levels are also low in other collection of epithelial cells and (2) if BORA displays a similar pro-oncogenic role in

tissue origins of other cancer types that also show abnormally high levels of BORA. Addressing these questions will help to clarify the potential causal role of BORA in tumor developing.

PLK1 overexpression in a normal epithelial prostate cell line has shown to promote independent soft-agar growth and *in vivo* tumorigenesis in NOD/SCID mouse by the induction of the EMT process activating the CRAF/ERK signaling[417]. Similarly, in gastric carcinoma PLK1 triggers the EMT process through regulation of the AKT pathway increasing the tumorigenesis[418] and mediates invasion through vimentin and β1 integrin in breast cancer cells[419]. As BORA increases PLK1 activity, these results might indicate that BORA carries out its oncogenic role through activation of PLK1. Nevertheless, other BORA-dependent but PLK1-independent mechanisms could be responsible to drive OC progression. For example, BORA might interact with other oncogenic effectors that so far remain largely uninvestigated leading this malignant transformation. Experiments in this regard are in progress in our group.

On the other site, other mitotic genes up-regulated in tumors have been artificially tested in equivalent conditions. For example, HEC1, MAD2, BUB1, CENP-E or AURORA B are reported to also act as a causal event for tumor initiation in different types of tumors[420–422]. Thus, these studies have shown that abnormalities during mitosis are not only correlated with tumorigenesis, but might in fact act as initiators of the process, with the underlying physiological mechanisms still unclear. Whole chromosome instability has long been thought to play a role in the tumorigenic process[423,424]. For example, the overexpression of the kinetochore protein HEC1, involved in the dynamic interface between centromeres and spindle microtubules, initiate tumorigenesis by activation of the mitotic checkpoint and acquisition of chromosome instability, as occurs with CENP-E or MAD2 proteins, that lead to an increase in anchorage-independent growth in human prostate epithelial cells[425].

These reports made us to theorize that BORA overexpression might also cause acquisition of chromosomal instability resulting in more aggressive cells, ultimately transforming IOSE cells and increasing the tumoral status. An experiment that could address this issue is the generation of a *BORA* inducible *knock-in* mouse model and report if the overexpression of BORA is linked to an increased incidence of spontaneous tumor formation. Mechanistically, any "*omics*" technologies, including genomics, transcriptomics or proteomics, could discern the underlying pathways.

5.6 Why is BORA overexpressed in OC?

It is still not clear how and when BORA overexpression arises during the tumor formation. *BORA* gene is located in a region of chromosome 13 (13q21-q22). This area has been implicated as a common site for somatic deletions in aggressive prostate cancer[348] which will explain the low levels of *BORA* mRNA expression in this cancer in the panel of the TCGA tumors. In contrast, there is no report of amplification

of this chromosome 13 region described in the literature in any cancer, hence indicating that BORA may have other mechanisms of regulation that explain its overexpression rather than genomic amplification. In OC, amplification of chromosome 20 is a non-random and common event that harbors *AURKA* gene (20q13.2-q13.3) yielding AURORA A protein overexpression. This amplification is reported to represent an important premalignant change in ovarian carcinogenesis and it is also is linked to the development of aggressive teratomas by centrosome amplification and CIN[426,427]. It will be interesting to know if this overexpression could somehow also boost BORA protein expression (as both proteins participate in the axis to promote mitotic entry) and be responsible partly of the chronic uncontrolled proliferation observed in cancer.

On the other site, epigenetics might play a role in deregulating *BORA*. Hypo or hypermethylation of CpG islands within the promoter and/or in 5'-regions of many genes is a common feature of cancer, associated with the activation or the repression of gene transcription and therefore the gain or and loss of the relevant protein in cancer cells[428,429]. For example, the hypermethylation of the tumor suppressor *FOXD3* promotes ovarian tumorigenesis[430], whereas the aberrant hypomethylation of *SLC6A12* induces ovarian metastasis [431]. Thus, it is not unreasonable to think that *BORA* expression could be regulated through this type of mechanism. Unfortunately, no studies have determined yet that a hypomethylation can rule the expression of *BORA*. This question could be addressed by the study of the methylation status of *BORA* in patient samples from different types of cancers. In this context, the hypomethylation of the *PLK1* promoter has been observed in hepatocellular carcinoma and hematological malignancies[432,433]. In this study, the loss of methylation in the promoter region correlated in 75,7% of hematological malignancies with elevated PLK1 expression in tumor cells[434]. Thus, epigenetic changes may contribute to the deregulation of PLK1.

Another option will be to study the upstream proteins, transcription factors (TFs), that interact with the promoter of *BORA* and that could also deregulate its functions. TFs are involved in driving gene expression and their misregulation can result in the acquisition of tumor-related properties[435]. To unravel TFs that modulate *BORA*, a ChIP-Seq (Chromatin Immunoprecipitation Sequencing) experiment could elucidate direct interactors of *BORA* promoter that could regulate its expression/transcription. Regarding to PLK1, it is published that some known interactors deregulate its function, however, a number of these upstream proteins are general broad effectors for cancer-related pathways, such as p53, MYC or RB (as described in section 1.4.1). Indeed, PLK1 harbors the canonical CDE/CHR cell cycle regulation binding sites that can be directly modulated by p53 or effectors (such as p21), indicating PLK1 expression can be modulated by the binding of p53[436]. Interestingly, we have identified the distribution of CHR-like elements in the promoter region of *BORA* sequence, strongly suggesting that BORA could

also be regulated by *E2F*, the *RB* family and/or *TP53* (though it is still necessary to functionally validate the interaction). Therefore, as *TP53* is mutated in almost all tumoral malignancies (i.e. 96% of the HGSC cases) with its function impaired, maybe it is not rare to find *PLK1* or *BORA* elevated, and maybe this is a possible mechanism by which p53 loss can contribute or initiate the tumoral status[437].

In this line, another possibility is that PLK1 overexpression itself contributes to BORA upregulation. As both proteins form a complex to promote mitotic entry, the individual increased expression of PLK1 could cause subunit imbalances and create dominant-negative effects that promotes the up-regulation of the complex and impacts in the regulation of cell division leading to chronic uncontrolled proliferation and ultimately cancer. Therefore, it will be interesting to test if PLK1 hyper activation enhances BORA expression.

So far, no published study has determined the regulation of BORA by any TF. However, we can take advantage of the large amounts of data sets generated with valuable information about the gene regulation in cancer patients. We carried out an *in silico* analysis using the ovarian TCGA data set to correlate BORA expression with 942 possible TFs through the R2 visualization platform. Remarkably, FoxM1 and different E2Fs are the major predicted TFs to interact with BORA; both closely related to oncogenic processes (Annex 3). FoxM1 plays an important role in promoting cell proliferation and cell cycle progression through transcriptional activation of many G2/M-specific genes[438]. Increased FoxM1 gene expression was detected in numerous cancer types and FoxM1 is a promising therapeutic target for cancer treatment[439]. A report from Thiru *et al.,* showed that a core of cell division genes in cancer are coordinately expressed under the induction of a specific cell division program driven by the behavior of FoxM1. These findings means that most of kinetochore genes up-regulated in tumors are coordinately expressed as part of a general activation of the cell division program that appears to function downstream of FoxM1[440]. Overall, that suggests that BORA it is overexpressed as being part of a larger cluster containing the core kinetochore and cell Cycle/DNA replication genes. In this line, FoxM1 binds to the promoter regions of the majority of kinetochore genes and cell division components based on recent chromatin immunoprecipitation followed by high-throughput DNA sequencing (ChIP-seq) analyses[441,442]. Coordinated expression of FoxM1-dependent genes suggests that regulation of FoxM1 itself could be a fundamental step in activating the cell division expression program in normal and malignant tissues, in part and among other targets, by binding to BORA. Supporting these results, a study showed a signature of cell cycle genes up-regulated predicting poor clinical outcome in multiple human cancers[204], thereby indicating that mitotic genes are frequently overexpressed together with other cell division genes in highly proliferating and chromosomally unstable tumors as consequences of the tumor development.

Something that should be highlighted is that is widely accepted that transformation process often involves alterations of more than one oncogene as well as silencing of tumor suppressor genes. It is completely uninvestigated whether BORA regulates tumor suppressor genes or vice versa in OC or in other tumor types which could further complicate the role of BORA and mechanisms regulated by BORA in cancer. Nevertheless, these outstanding questions can be better answered using genetically engineered mouse models for *BORA* and/or with other oncogene or tumor suppressor genes in the background of the mice.

5.7 The pro-oncogenic activities of BORA: exploring its use as therapeutic target

Besides the relevance of BORA as potential predictive prognostic factor, the novelty of our study also relies on the definition of oncogenic roles of BORA and thus its possible use as therapeutic target in OC. Contrary to what occurs with the non-tumoral IOSE cell line, BORA silencing impaired proliferation and colony formation capacities of OC lines, through a G2/M phase arrest and the induction on cell death by caspase dependent apoptosis. Therefore, targeting BORA represents an advantage when aiming at specifically targeting malignant dividing cells. The increase in mitotic index concurred with the previous assays carried out by Seki *et al.,*[346] and Chan *et al.,*[338]. Although prometaphase stage is normal upon BORA knockdown cells, the authors described how metaphase cells tended to have unaligned chromosomes that persisted for an extended time, impacting on the mitotic spindle and ultimately in the chromosome segregation rate. These observations support the use of BORA inhibition as potential CIN-based therapy and likely explains the induction of a caspase dependent cell death we observed in our results. It is reported that after a prolonged mitotic arrest, cell fate depends on two competing networks of caspase dependent apoptosis and Cyclin B1 degradation (as discussed in the introduction section 1.3.5). In the case of BORA-depleted cells, it will be interesting to identify the exact mechanism of death, as well as the metabolic and signaling pathways in which BORA is involved during the evolution of the disease, that will allow us to reach a favorable therapeutic index and therefore maximize the clinical response.

Our results are, to some extent, consistent with previous findings where BORA siRNA -depletion in MDA-MB-231, a metastatic breast cancer cell line, reduced cell proliferation[351]. We concurrently depleted BORA with the lentiviral particles in cells from of other tumor types: prostate, endometrial, colon, neuroblastoma and breast; exhibiting a consistent reduction in the proliferation rate in the panel of different cell lines tested. These results strengthen and broaden the essential role of BORA in cellular survival and pave the way to explored BORA as potential general cancer target.

It should be noted that BORA inactivation has been performed with RNAi, which might not result in full protein depletion and residual levels of BORA could be enough to sustain some of its functions as mentioned before. In fact, our first *in vitro* attempt to study the effects of BORA depletion was to use a mammalian CRISPR/Cas9 plasmid to generate a stable cell population with *BORA* gene knockout. Despite the devoted efforts, we did not obtain any OC cell line with homozygous CRISPR/Cas9-mediated *BORA* knockout. We were only able to obtain knockdown cells with much reduced levels of BORA (clones with *BORA* heterozygous allele). We did some experiments using these cell lines and functionality a slow-down in the proliferation was observed in these clones, in agreement with the previous results using lentiviral particles. However, possible off-targets of the system together with the fact that a cell line with prolonged depletion of BORA could compensate the protein reduction boosting alternative pathways to survive, led us to reconsidered working with these stable *BORA* knockdown clones. For that reason, we are now engineering a conditional lentiviral CRISPR/Cas9 system in which *BORA* genetic knockout will be achieved in an inducible manner. Interestingly, failing in getting clones with full BORA depletion made us consider that BORA is an essential regulator for cell viability of OC cells (and likely tumoral cells in general) and much reduced levels of BORA are sufficient to sustain the proliferation of OC cells. This hypothesis is in line with the results we obtained in the immunoblot for BORA using the A2780p surviving clones derived from the colony formation assays. All clones that did not die upon BORA depletion had residual levels of BORA, confirming that full lack of BORA impacts negatively on survival. These results highlight for the first time the dependence on BORA for cell survival.

It is worth highlighting the recent work reported by McKinley and Cheeseman where the authors generated inducible CRISPR/Cas9 knockout human cell lines targeting 209 genes involved in diverse cell-cycle processes and elegantly characterize the consequences of the elimination[443]. Despite the fact that a wide number of mitotic genes were tested describing the resultant cell fate, unfortunately *BORA* was not one of them.

Based on these findings, it will be interesting to study the phenotype of a mouse model with targeted inactivation of *BORA*, a whole *BORA*-knockout mice. While mice with homozygous *PLK1* inactivation result in not viable embryos at morula stage, heterozygous old mice develop tumors with a higher incidence of lymphomas, also accompanied by lung carcinomas, squamous cell carcinomas and sarcomas due to the aneuploidy generated by the lack of *PLK1*[270]. In this regard, there is no report yet about the phenotype consequences of a whole-body ablation of *BORA* gene and if it could be embryonic lethal (what we suspect) or compatible with life.

In vivo, this is the first time the therapeutic effect of BORA protein depletion in established xenograft tumors is tested. Our first xenograft model using BORA -depleted SK-OV-3 cells with constitutive

lentiviral particles affected tumor engraftment and thus compromised the fate of these tumors, reducing tumor growth. Interestingly, BORA depleted tumors were in the majority of the cases absent or dramatically smaller with a very slow growth at the consecution of the experiment. We speculate that this is due to irreversible molecular events originated by BORA silencing during the first days after the injection. Substantial reduced BORA protein levels in these tumors compared to the control ones were confirmed by immunoblot, supporting the notion that BORA exhibits oncogenic functions in OC and a minority of tumors were able to engraft and develop further with reduced levels of BORA. It is worth mentioning that these tumors displayed less tumor cellularity and a reduction in the proliferation rate seen by the Ki67 staining. Importantly, immunoblot carried out in these tumors also revealed an increase in the caspase dependent cell death, hence confirming the *in vitro* results. Although these results evidence a role of BORA regarding tumor growth, target depletion at the time of tumor initiation does not strictly mimic a potential therapeutic intervention in the clinics. For that reason, we proceeded to engineer an inducible system to control BORA depletion *in vivo* once the tumor was already formed; an approach that better reflects what will occur *in vivo* if BORA inhibition could arrive into the clinics. *In vitro,* the pTRIPZ system successfully depleted BORA by the addition of doxycycline in the transduced cells and consequently phenocopied the previous results related to proliferation and colony formation capacities. In mice, after tumor engraftment, the addition of doxycycline to mice ablated BORA protein expression and attenuated the growth of these tumors during the whole experiment resulting in smaller tumors compared to the untreated group. Collectively, the use of these *in vivo* xenografts models convincingly showed that (1) BORA controls the engraftment of the tumors, thereby controlling the fate of them and (2) BORA depletion results in tumor growth attenuation, rendering a good therapeutic strategy in OC. Importantly, these *in vivo* models constitute a proof of principle about BORA inhibition in OC as therapeutic instrument. However, these strategies fail to provide information regarding the toxic effects that might occur in the clinic when the targets are inhibited via systemic administration of the corresponding inhibitors. This is important to highlight as we envision a future BORA-targeted therapy in OC patients.

Additionally, as most of OC-related deaths are associated with peritoneal tumor spread, we took advantage of ascites fluid from three advanced stage OC patients to further validate the potential implications of BORA inhibition in the dissemination process. We were able to successfully isolate *ex vivo* tumoral ascitic cells and cultured them in a 3D model, which mimics *in vivo* growth of these cells. Of note, cells from the primary ovarian tumor sheds to the abdominal cavity with attachment and invasion into the mesothelial lining of the peritoneum, followed by formation of metastatic outgrowth[444,445]. During this process, the disseminative cells aggregate into spheroids. These multicellular spheroids are characterized by (1) living much longer than the floating single cells that normally undergo anoikis and

(2) generating a metabolite density gradient that inhibit the access of chemotherapy agents generating resistant to standard therapies[446,447]. These features underlie the clinical relevance of this *ex vivo* model to pre-clinically test the depletion of BORA. Remarkably, the protein depletion reduced the spheroid scoring in two out of three patients and the viability in the three patients by inducing the caspase dependent apoptosis, indicating that the effects of BORA depletion has potential therapeutic implications in primary cancer cells from advanced OC patients and confirming previous results. Importantly, we are currently setting up an *in vivo* patient-derived tumor model from tumor cells isolated from ascites fluid and injected intraperitoneally in mice with the goal to mimic a peritoneal metastasis disease that models the advanced OC carcinomatosis in the mouse. OC models based either in orthotopic or intraperitoneal injection or patient-derived xenograft (PDX) models are validated systems to evaluate novel therapies against OC[448,449] and a first step to characterize pre-clinically the potential of the inhibitors before enter in clinical trials. Therefore, once the model works in ours hands the idea is to modulate BORA expression (either the depletion or the overexpression) to quantify the ascites released and the number and place of metastasis generated.

Related to the treatment, another intriguing issue that remains to be determined is whether the depletion of BORA could sensitize OC cells to the treatment with first-line chemotherapeutic compounds (e.g. with paclitaxel, to exert a more dramatic effect on cellular viability) or in recurrence disease with the PARP inhibitor, *Olaparib*. Concomitant depletion of BORA combined with these drugs could potentially have a synergistic effect in OC cells, since inhibiting one pathway may not be enough to kill tumor cells and the combination could impact on different pathways simultaneously, being and effective strategy in the future. Furthermore, a potential combination with an already approved agent could introduce BORA inhibition in a combinatory treatment more easily than BORA inhibition alone. Thus, further studies in this direction are needed. Interestingly, the fact that in OC predominate mutations in *TP53*, *BRCA1* and *BRCA2* genes, among others, it provides opportunities to test if BORA inhibition could cause synthetic lethality with some recurrent OC mutated genes. For example, PLK1 inhibition is lethal in *K-RAS* mutant cells as described in lung cancer[311], and in OC, synthetic lethality is produced with PLK1 inhibition and paclitaxel in *CCNE1* amplified (Cyclin E) HGSC cells[450].

If BORA finally arrives to the clinics, a major hurdle is to identify those patients that can benefit maximally to the given therapy. For instance, currently there are no biomarkers available to identify the subset of patients who could most benefit of PLK1-targeted therapy. In the clinical trial performed in OC with *Volasertib vs* standard chemotherapy (NCT01121406) they found that 6 patients (11% of total) receiving *Volasertib* achieved a PFS for more than 1 year, whereas no patient receiving platinum-based chemotherapy did so, thus highlighting that there are patients who could indeed benefit from this anti

cell-cycle therapeutic approach[319]. But, how we can predict those patients that can respond to a BORA inhibition therapy? A recent study showed that activation of the spindle checkpoint is a critical component of response to PLK1 inhibition and they propose spindle checkpoint pathway components, like Securin, could be employed as novel biomarker to monitor the response to *Volasertib* therapy in OC[451], as Securin is an established prognostic biomarker in various cancers and is also known to be highly expressed in OC[452]. In a future, it will be interesting to look for components that also could predict response to BORA inhibition/silencing, related or not to the SAC pathway and if any of them is shared with PLK1 inhibition.

As we consider BORA as potential therapeutic target, we are aware about the possible acquisition of resistance that its inhibition can generate in long term in patients. In the literature there are some reports about altered molecules and pathways, consequence of a prolonged antimitotic-therapy. For example, continued activation of the spindle assembly checkpoint leading to multinucleation[453], or target modifications in the spindle kinesins and centromere-associated proteins[454,455]. Thus, for the future, we are planning to delve into the differential mechanisms that can promote the resistance to BORA inhibition. We would take advantage of the preclinical models and perform high-throughput proteomics and interactome analysis comparing a cell line that is able to grow ordinarily with reduced levels of BORA matched to a control line with the idea to identify proteins and partners associated with BORA involved in its location and functionality. Knowing this information will allow us to propose combined treatments with other drugs directed against the pathways or interactors that we find differentially expressed potentially associated with the resistance.

5.8 Reduction in BORA levels impact in multiple cancer-related genes

Our results from the transcriptomic data unraveled multiple pathways by which BORA depletion renders this phenotype in OC. We wanted to discern those genes and pathways that were differentially expressed just after the depletion of BORA. We observed that the most enriched genes sets are related to cellular survival, migration, energy production, cardiovascular function and NF-κB signaling related pathways, indicating an impairment of these processes upon BORA knockdown at transcriptional level. These data are of high importance as evidence for the first time the participation of BORA in multiple pathways non-related to mitosis by strict definition. Several canonical genes altered in the array from these pathways were confirmed in BORA depleted patient-derived ascites cells at transcriptional level and in control and BORA depleted tumor tissues from the *in vivo* experiment at protein level. Importantly, it is worth mentioning the modulation of two oncogenic proteins related to survival and proliferation as BCL-2 and CDK6. In fact, we have tried to mechanistically link BORA to BCL-2 and CDK6 regulation. Although BORA-depleted cells resulted in reduced BCL-2 and CDK6 protein levels, conversely BORA

overexpression did not change the protein levels of both proteins (Annex 4). Additionally, we did not observe a correlation between *BORA* with *BCL-2* and *CDK6* expression using the transcriptome date from the ovarian TCGA cohort (Annex 4), suggesting that there is no direct relation between the three proteins. We therefore hypothesize that BORA controls both proteins indirectly, perhaps via transcription factors, which does not preclude them as good potential candidates to be explored.

While this study focused primarily on BORA, our transcriptomic data uncovered multiple pathways previously linked to activated-PLK1 functions. Remarkably, Zhang *et al.,* carried out a whole-gene expression microarray analysis of PLK1 knockdown in bladder cancer cells. GO biological process analysis showed cell cycle, focal adhesions, VEGF and NF-κB signaling pathways differentially expressed, similarly what we found in our transcriptomic analysis, hence underlying most of the pathways modulated by BORA are PLK1-dependent[456]. Increasing evidence also support that PLK1 has multiple non-mitotic functions, and not only in cancer cells. Intriguingly, we found that BORA silencing modulates pathways related to cardiovascular homeostasis mainly due to the recent described function of PLK1 activity in regulating vascular smooth muscle cells[292]. In this study, performed by Guillermo de Carcer and collaborators, published in *Nature Medicine* in 2017, they carried out a microarray analysis using aortas from *PLK1*$^{+/-}$ and *PLK1*$^{+/+}$ mice. They showed downregulation of genes involved in similar pathways that we obtained: muscle and cardiovascular function, energy production and actin cytoskeleton dynamics. Although in their article, they did not discern how PLK1 is active to carry out these functions, our transcriptomic results propose that BORA in these pathways is controlling the activity of PLK1. As increasing evidence supports that PLK1 has roles beyond mitosis, we hypothesize BORA is the responsible factor that controls the PLK1 activity to carry out these non-mitotic functions as well, at least some of them. On the other hand, we also highlight that these results define BORA as promising molecular target for the development of drugs that might reshape or improve the action of PLK1 inhibitors.

Although in this thesis we did not differentiate whether BORA can modulate pathways via PLK1 independent activity, we recognize that this point deserves further attention. Gene expression profiling of control and BORA -depleted cells together with a condition of cells with PLK1 inhibited (either pharmacologically or by mutating the kinase domain of PLK1) will be a first straight forward approach to discover PLK1-independent functions of BORA, if they were.

5.9 BORA: a two-faced protein?

As BORA is the major PLK1 activator and recently some studies have postulated a dual role of PLK1 both as oncogene and as tumor suppressor regarding the tumor type[437,457], an interesting question to

address is whether BORA might act also as tumor suppressor in other tumor type contexts. Since nowadays there are no enough reports that correlate BORA protein expression with the clinical outcome, we retrieved transcriptomic expression data and patient clinical outcome information from a large collection of different cancer types using the Kaplan Meier plotter platform. We observed that in breast, liver and lung adenocarcinomas BORA expression is clearly associated with worse OS. On the contrary, we discovered that there is a group of tumors including bladder, rectum, stomach, thymoma and thyroid adenocarcinomas where high expression of BORA confers a better OS when compared to patients with low BORA expression (Annex 5) confirming the fact that BORA might fulfill as a tumor suppressor protein in other tumor types. These data describe for the first time a dichotomy role of BORA either promoting the tumor aggressiveness or being a tumor stopper indicating that BORA may have tumor type-dependent activities. Further experiments modulating BORA in cell lines derived from these types of cancer are needed to unveil the play of BORA and the underlying biological pathways. Importantly it is necessary to clarify the mechanisms by which BORA behaves such oncogene or tumor suppressor. Is it depending on the levels, a threshold that determinate one or the other role? Or it varies the function depending on the tissue subtype? In OC, we found that BORA promotes the tumoral activity, but it will be also interesting to deeply understand if even in the same tumor type, BORA can act promoting or repressing the tumor development, depending on the histological subtype or the genetic background. In this sense more, efforts are needed to identify those tumors that might benefit of BORA inhibition-based therapies and why.

5.10 Targeting BORA function: why and how? Different strategies for one purpose

PLK1 inhibitors are reported to successfully work in a collection of tumor types but the adverse side effects observed with current compounds limit its clinical used and evidence the urgent clinical need to improve PLK1 activity inhibition. Basically, two target sites of PLK1 have been considered for the development of small-molecule inhibitors: the ATP-binding site within the kinase domain and the substrate-recognition and binding site, or PBD. The classical target has been the kinase inhibition by multiple ATP-competitive inhibitors that have been clinically tested to different extend, but their application has been restricted due to dose-limiting and off-target side effects. Most of these PLK1 kinase inhibitors cause hematological toxicity, mainly neutropenia and leukopenia in cancer patients[458]. In addition, potential problems in kinase inhibitor development is that the ATP binding pocket is highly conserved across the protein kinases. Therefore, it is difficult to identify specific kinase inhibitors that can discriminate among the more than 500 protein kinases that have been identified in the human

genome[459]. For example, *BI-2536* also targets death-associated kinase 2 (DAPK-2) and calcium/calmodulin-dependent protein kinase 2 (CAMKK2)[460]. *Volasertib* is reported to also inhibit PLK2 and PLK3, two others members of the polo-like kinase family, which are considered as tumor suppressors. Thus, when using ATP-competitive PLK1 inhibitors, the roles of PLK1-related family members need to be considered carefully to improve treatment strategies against cancer. Because the PBD is unique to the five-member family of polo-like kinases, the development of inhibitors against the PBD represents an alternative approach to solve problems of selectivity for other kinases. Some inhibitors of PLK1 PBD, such as *poloxin*, *purpurogallin* and *thymoquinone* are currently undergoing preclinical trials but with no promising results so far[310]. Most of the peptides are not cell membrane permeable and better studies on the geometrical and shape arrangement of this part of the structure are still needed to design better compounds. Since BORA binds the PDB domain of PLK1 to activate the kinase, targeting directly BORA could represent an improved strategy to block PLK1 function, rendering perhaps a novel and better therapeutic avenue in cancer. Moreover, BORA inhibition could also enhance the efficacy of existing AURORA A or PLK1 inhibitors given in combination. In this sense, different strategies can be considered to efficaciously block BORA function as discussed in the next section.

Small molecule inhibitors

The use of small molecule inhibitors is broadly used in the clinics. The fact that they can accept structural modifications to be given in different administration routines and that they are able to easily interact with either cell-surface receptors or intracellular signaling molecules, has revolutionized targeted cancer therapy[461]. The development of these inhibitors usually requires a minimal knowledge on the crystallographic structure of the protein. To date, the crystallographic structure of the protein has not been resolved and it appears to be challenging due to the unstructured nature of the protein, and this has precluded the development of BORA inhibitors thus far. Using known automated protein structure homology-modelling servers (SWISS-MODEL), we could model a fragment of about 60 aa (BORA is 559 aa in total) with only 25% identity (which is very low as ideally, it should be between 40-50% to give some validity to the results) (Annex 6). Our efforts in collaboration with the company iProteos using their own algorithms has also failed up to now in trying to model BORA 3D structure. A crystal structure of the complex of the *Danio rerio* Kinase Domain and PBD together with a PBD-binding motif of *Drosophila* microtubule-associated protein 205 (Map205(PBM)) shed light onto the activation mechanisms of PLK1[462] and might offer a good framework in the future to understand the BORA-PLK1 complex structurally. Nevertheless, as we envision that this option will still take time, other alternatives should be considered.

Protein-protein interaction disruption

A reasonable alternative to block BORA regulation is the disruption of the protein-protein interaction (PPI). PPIs are broadly considered potential drug targets for cancer therapy[463,464]. Remarkably, one of the most successful PPi example in oncology is the *Omomyc*. This peptide described by Soucek *et al.,* sequesters *MYC* in complexes with low DNA binding efficiency preventing binding to MAX and inhibiting MYC transcriptional activator function resulting in a tumor growth decrease in MYC dependent tumors such lung and breast carcinomas[465,466]. It is well reported that BORA precisely binds to the PBD of PLK1 to promote its activation, so the design of peptides to disrupt the interaction between the N-terminal part of BORA and C-terminal part of PLK1 is a worthy strategy. Interestingly, novel compounds targeting the PLK1-BORA interaction using a Proteochip platform was screened[467]. In this study, a monoclonal antibody against GST was immobilized on the Proteochip for PLK1-GST binding. After immobilization of PLK1, fluorescence-labeled BORA peptide was applied to the Proteochip and the fluorescence intensities were detected to determine the PLK1-BORA interaction *in vitro*. With this system the authors obtained a chemical compound that inhibited the proliferation *in vitro* in a dose-dependent manner in the lung cancer cell line NCI-H460. Unfortunately, the authors do not describe the chemical structure of the compound nor the origin and did not further explore functionally its use neither *in vitro* nor *in vivo*.

Importantly, since BORA has been reported to be the unique activator of PLK1 in mitosis, identifying inhibitors of the BORA/PLK1 interaction might overcome the potential cross reactivity of anti-PLK1 drugs with other members of the polo like kinase family. However, whether BORA is or is not required for PLK2 and PLK3 activation, is something that remains to be tested. As our group has described how the CDK1-phosphorylation on three conserved residues located in the N-terminal part of BORA are essential to activate PLK1 and thus promote cell division, other strategy to block part of the BORA function will be to specifically block this interaction region, between BORA and CDK1. However, BORA might bind other proteins in the context of OC to carry out the pro-oncogenic functions here described (a part from binding the axis AURORA A/PLK1 or with CDK1). Next experiments carrying out high-throughput interactome analysis in ovarian cells lines and also in primary tumors from OC patients are focused on searching for BORA novel interactors that functionally might contribute to its oncogenic activity in OC.

RNA strategies: The use ncRNAs

Noncoding RNAs (ncRNAs) are useful targets for therapeutic interventions of human cancer[468]. In particular, siRNAs are widely used to target proteins that are difficult to design small molecule inhibitors. In parallel, a lot of efforts are being invested in the development of nanoparticles that can be conjugated with these therapeutic molecules to direct deliver to the tumors *in situ*. For example, *TKM-080301* is a lipid nanoparticle formulation comprising a synthetic siRNA directed against human *PLK1* mRNA. Phase

I clinical trial of *TKM-080301* revealed that is a well-tolerated drug in solid tumors patients[469]. In our hands two specific shRNA sequences are potent blockers of the mRNA sequence of BORA. Further preclinical experiments are needed to conjugate these shRNAs into a lipid formulation (if it is feasible) and check if efficiently are able to knockdown BORA function. On the other site, the use of ncRNAs (miRNA and lncRNA) are emerging as promising therapeutic agents. One successful example studied in our laboratory is the hsa-miR-654-5p, tumor suppressor miRNA that impairs the proliferative capacities of OC *in vitro*, *in vivo* and also *ex vivo* targeting the *CDCP1* and *PLAGL2* oncogenes[470]. To date there are no study of any miRNA or lncRNA regulating BORA. Multiple algorithms are available online to predict miRNA interaction sites with the 3' UTR of BORA: TargetScan, miRWalk or miRANDA. We found the conserved human hsa-miR-23 family (a,b,c), predicted in all three algorithms, as possible regulators of BORA (Annex 7). Hsa-miR-23a has been described as tumor suppressor in pancreatic cancer and surprisingly hsa-miR-23b inhibits OC tumorigenesis[471,472]. As our laboratory has previous expertise in working with miRNA *in vitro* and *in vivo*, the functional consequences of regulating BORA through the abovementioned miRNA family will be tested. Interestingly, a considerable number of pre-clinical studies involving miRNA therapeutics are being translated into clinical trials. For example, the lipid encapsulation of miR-34a downregulates the expression of >30 oncogenes across multiple oncogenic pathways. A phase I trial with this compound revealed acceptable safety and showed evidence of antitumor activity in a subset of patients with refractory advanced solid tumors[473].

Mimicking BORA inhibition through its downstream effectors

An alternative is to seek for currently druggable proteins or pathways among its immediate downstream effectors that mimic BORA depletion phenotype. The transcriptional profiling performed after BORA silencing shed light about the modulation of pathways involved in cell survival and proliferation among which the central players, *BCL-2* and *CDK6* genes, were found downregulated.

The master regulator of apoptosis, BCL-2 has shown inconsistent correlation with clinical variables in OC. Immunohistochemistry studies determined higher BCL-2 expression was associated with worse survival and resistance to chemotherapy in OC[474,475]. However, in a recent larger study, positive BCL-2 expression had no prognostic value with no differences neither in OS nor in PFS[476]. In spite of its inconclusiveness as a possible biomarker, BCL-2 inhibition has effectively suppressed tumor growth and sensitized OC cells to DNA damage agents such cisplatin and carboplatin[477,478], thereby establishing BCL-2 as a promising drug target in OC. In fact, the BH3 mimetics seem destined to become powerful avenues against several types of cancer as reviewed in Cory *et al.,*[479]. Currently there are several BCL-2 inhibitors running in clinical trials. In fact, *Venetoclax* is an FDA-approved inhibitor in chronic

lymphocytic leukemia and the next generation of the inhibitor, *Navitoclax*, is currently under clinical scrutiny in 13 phase II clinical trials alone or combined with other chemotherapeutic drugs.

CDK6, along with its partner CDK4, are key players in cell cycle progression. In OC, high CDK6 expression predicts poor patient survival and confers protection from platinum-induced cell death via FOXO3 regulation[480,481], suggesting its inhibition could improve platinum efficacy in OC patients. Importantly, CDK6 has been described to bear kinase-independent functions stimulating tumor angiogenesis[482], what encourage its therapeutic use to simultaneously inhibits two relevant pathways in cancer. Unlike normal cells, tumor cells rely on interphase CDKs such as CDKs 2, 4, and 6 to proliferate. Therefore, selective CDK4/6 inhibition may cause fewer side effects in normal cells[483]. In the clinics, CDK4/6 inhibitors are becoming a standard treatment in advanced breast cancer with three FDA-approved inhibitors and their effect in other tumor types is currently under preclinical and clinical examination[484].

In our OC models, both BCL-2 and CDK6 inhibitors reduced cellular proliferation, but *Navitoclax* was more efficient than *Venetoclax* and similarly to *Palbociclib* compared to *Amebaciclib*. Thereby, we decided to use *Navitoclax* in combination with *Palbociclib* to recapitulate BORA inhibition in OC models. *Navitoclax* and *Palbociclib* combination resulted in a strong synergism not only recapitulating BORA inhibition in 2D cellular growth, but also in our *ex vivo* 3D model using patient-derived cells. Although it makes a rational initial proof of principle for the use of these inhibitors in OC patients, the underlying mechanisms related to the synergistic effect observed awaits examination.

Accordingly, Dominicie *et al.,* reported that pharmacologic inhibition of CDK6 and BCL-2 markedly suppressed *in vitro* and *in vivo* viability of leukemic cancer cells[485], supporting the notion that inhibiting both pathways could be of clinical relevance in other tumor types. Taken together, our data provides a rationale for further clinical evaluation and encourages researchers and physicians to immediately transfer the combination approach into clinical trials. The approval of the usage of this inhibitors' combination in OC patients will be faster than developing a BORA targeted therapy and patients could benefit of these discoveries before a specific drug against BORA is tested and commercialized.

In summary, the findings included in this thesis constitute an important contribution to the field of targeted therapy in OC, specially related to cell cycle blockade therapeutics with direct consequences on OC patients' prognosis and therapy. On the one side, BORA protein emerges as potential biomarker with prognostic value in OC and would perfectly complement the current prognostic procedure. On the other hand, the oncogenic functions of BORA revealed a potent inducer of tumoral aggressiveness and a stimulator of tumor cell survival specifically in malignant cells, making it a potential selective target for therapeutic intervention. Although further studies are needed in the future, a first step has been achieved

defining the downstream biological consequences and signaling pathways regulated by BORA in OC. Remarkably, our findings paves the way to reshape future strategies to develop PLK1 inhibitors since current compounds cause adverse effects and encourage to use inhibitors of BORA and BORA-downstream effectors as potential therapies. In the long term, the implementation of BORA inhibition-based therapy is expected to improve the therapeutic management of OC patients and substantially increase their survival.

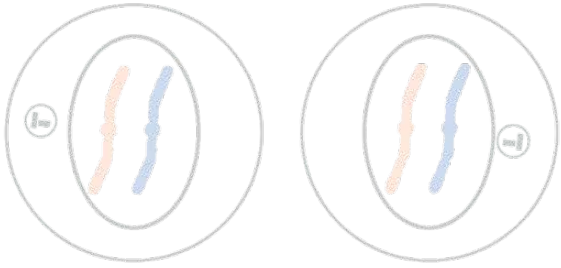

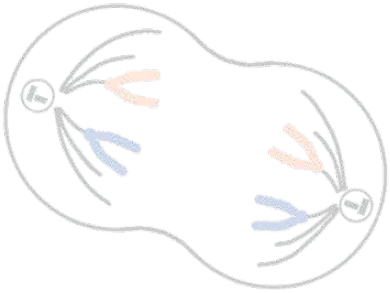

6. CONCLUSIONS

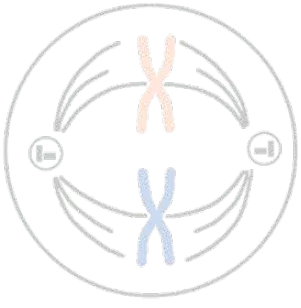

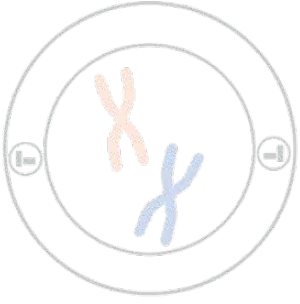

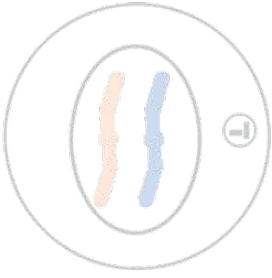

First: An integrative bioinformatic screening of transcriptomic data combined with survival outcome enables the identification of multiples up-regulated mitotic genes as potential therapeutic targets to explore in OC.

Second: BORA is overexpressed in human OC specimens compared to benign samples. High levels of BORA correlate with advanced stages and with the most aggressive histological neoplasm grade; indicating that BORA could be a good prognostic biomarker in OC.

Third: BORA displays oncogenic activities in ovarian surface epithelium cells *in vitro* and enhances the tumoral status of OC cells *in vivo*, leading to an aggressive tumoral phenotype.

Fourth: BORA is indispensable for the growth and viability of OC cells *in vitro*, *in vivo* and *ex vivo*, highlighting BORA as a putative novel therapeutic target for OC patients.

Fifth: BORA regulates essential cell survival signaling pathways in OC such as growth, migration, and inflammatory related pathways. BORA activates PLK1 kinase to carry out non-mitotic functions, such as energy production, vascular homeostasis and actin cytoskeleton dynamics.

Sixth: The combination of the CDK6 inhibitor *Palbociclib* and the BCL-2 inhibitor *Navitoclax*, mimics BORA knockdown on cell lines and patient-derived tumor spheres; hence proposing this combination therapy as novel potential avenue for OC treatment.

7. ANNEXES

ANNEX 1

Annex 1. Differentially expressed genes after *BORA* knockdown (192 genes up-regulated and 215 down-regulated filtered at fold change >± 1,5 and *p*-value<0,05).

Gene Symbol	Fold Change (linear) (shBORA *vs* shCONTROL)	ANOVA *p*-value (shBORA *vs* shCONTROL)
IL1R2	-3,42	0,01046
ZNF114	-2,95	0,00022
MMP7	-2,82	0,00013
EMG1	-2,59	0,02104
CMTM7	-2,58	0,00067
NRBP1	-2,58	0,02351
PTGS1	-2,46	0,00049
IL1B	-2,37	0,01102
SLC39A10	-2,37	0,03399
RRP1B	-2,25	0,00008
ZNF79	-2,24	0,03997
BORA	-2,23	0,02288
ADGRF1	-2,23	0,04480
SLC39A10	-2,22	0,00018
IL1A	-2,22	0,00698
CDK6	-2,19	0,00449
SLC35A5	-2,19	0,00680
SLC25A36	-2,17	0,00578
MED20	-2,12	0,00418
GLCCI1	-2,11	0,00484
PIGM	-2,11	0,00766
ARL5B	-2,11	0,01646
RPL5	-2,10	0,02199
TMEM41A	-2,08	0,02376
USP46	-2,07	0,02095
CAPN6	-2,04	0,01032
SRR	-2,03	0,03196
CTBP2	-2,01	0,01357
MICU3	-2,01	0,02682
AP2S1	-1,99	0,00986
HIF1AN	-1,98	0,02587
SLC7A8	-1,97	0,02999
CXCL3	-1,97	0,04085
RUFY2	-1,95	0,01976
ZDHHC12	-1,93	0,00539
ST3GAL6	-1,93	0,01706
TMEM241	-1,92	0,00623
DUSP5	-1,92	0,00747
NOP16	-1,91	0,00400
ZNF547	-1,91	0,02907
UMAD1	-1,90	0,00480
MOAP1	-1,90	0,02571
ZNF792	-1,90	0,04228
MTHFD2	-1,89	0,02071
FAM217B	-1,89	0,02173
SLIT2	-1,89	0,03633
RARRES3	-1,88	0,00183
EPHA4	-1,88	0,04474
ANXA2R	-1,87	0,00962
LRRC8A	-1,87	0,04876
TRIM14	-1,85	0,00311
MALL	-1,85	0,00460
SLC22A23	-1,85	0,00830
TMEM5	-1,84	0,01068
SBNO1; MIR8072	-1,83	0,00014
PARD6G	-1,83	0,00241
TRPC6	-1,83	0,00325
BICD2	-1,83	0,03053

SFRP1	-1,82	0,00405
SNX17	-1,82	0,00504
USP12	-1,82	0,03657
IDO1	-1,81	0,00816
PLEKHA1	-1,80	0,00081
FAM185A	-1,80	0,01196
ATP6V1G1	-1,80	0,01297
SCIN	-1,80	0,03198
POLE2	-1,80	0,04191
BUD31	-1,80	0,04227
ATPAF2	-1,79	0,01386
SPRY1	-1,78	0,00026
NMUR2	-1,78	0,00511
PURB; MIR4657	-1,77	0,00210
PCIF1	-1,77	0,04543
NRP2	-1,76	0,00137
PMAIP1	-1,75	0,03448
SRPX	-1,74	0,00174
TMC5	-1,74	0,00577
CTH	-1,74	0,02128
TAB3	-1,73	0,00411
DKK4	-1,73	0,00522
TOMM20	-1,72	0,00069
RAB14	-1,72	0,00357
HMG20A	-1,72	0,00840
PEX11B	-1,72	0,03618
PADI1	-1,71	0,02142
GCN1; MIR4498	-1,71	0,04903
MPZL2	-1,70	0,00045
KDSR	-1,70	0,01064
POLB	-1,70	0,02780
RHOF	-1,70	0,02933
QRSL1	-1,69	0,01454
MRS2	-1,69	0,04387
ARFGEF2	-1,68	0,00076
RHOC	-1,68	0,00600
DENND6A	-1,68	0,00616
ARL6IP6	-1,68	0,00969
ETFDH	-1,68	0,03198
COMMD9	-1,67	0,00598
SLC7A2	-1,67	0,01733
C21orf140	-1,67	0,04592
C21orf140	-1,67	0,04592
TMEM199	-1,67	0,04706
PPP2R1B	-1,66	0,00419
TRHDE	-1,66	0,00441
SLC4A11	-1,66	0,01665
TLE3	-1,66	0,02956
LIMD2	-1,65	0,02806
RPL39L	-1,65	0,03426
MED21	-1,64	0,01071
SRM	-1,64	0,01132
CADM1	-1,64	0,01760
GINS3	-1,64	0,04252
ID3	-1,63	0,00220
SERPINB8	-1,63	0,00345
ADAM17	-1,63	0,00510
C16orf52	-1,63	0,01222
DIO2	-1,63	0,01691
GBP4	-1,63	0,04443
OR2T8	-1,62	0,00184
PAPSS2	-1,62	0,04062
ENPP4	-1,62	0,04463
SLC35D1	-1,61	0,00532
TMEM64	-1,61	0,01220
GAS8	-1,61	0,02145
TMTC2	-1,61	0,03944
ZNF749	-1,61	0,04036

WDR12	-1,60	0,00629
IAH1	-1,60	0,00953
FAM206A	-1,60	0,01205
CERS6	-1,60	0,01897
MFSD1	-1,60	0,02008
ADAMTS4	-1,59	0,00605
NFIA	-1,59	0,00957
ISOC2	-1,59	0,00964
MYH10	-1,59	0,01692
MYLK	-1,59	0,01939
PLCZ1	-1,59	0,02229
SYT14	-1,59	0,02464
SLC2A12	-1,59	0,03773
OR2B3	-1,59	0,04344
FOXO1	-1,58	0,00170
CLDN10	-1,58	0,00626
HACE1	-1,58	0,01801
UBIAD1	-1,58	0,02671
ELOVL4	-1,58	0,03240
SRSF11	-1,57	0,01141
C3	-1,57	0,01159
UBE2E3	-1,57	0,02574
MCL1	-1,57	0,03044
REV3L	-1,57	0,04138
ATG16L1	-1,57	0,04831
GLUD1	-1,56	0,00773
MS4A10	-1,56	0,01196
SMUG1	-1,56	0,02013
PSMB6	-1,56	0,02273
SLC25A10	-1,56	0,02802
ALG5	-1,56	0,04050
ZNF814	-1,56	0,04699
LCLAT1	-1,55	0,00818
MEX3C	-1,55	0,00960
PAPOLG	-1,55	0,01269
EHF	-1,55	0,01602
BUD31	-1,55	0,01788
TMEM107	-1,55	0,03974
EIF4E	-1,54	0,00661
BMP1	-1,54	0,00764
MGST2	-1,54	0,00889
CRIPAK	-1,54	0,00955
ID1	-1,54	0,01124
EMC6	-1,54	0,01475
OR6J1	-1,54	0,01706
NDUFA12	-1,54	0,01848
AVPI1	-1,54	0,02152
ENPP2	-1,54	0,03492
FAM25A	-1,53	0,00470
KIAA1109	-1,53	0,00548
PLEKHA2	-1,53	0,00647
DPM1	-1,53	0,01241
SNX5	-1,53	0,01362
TTLL4	-1,53	0,01450
MAD2L1	-1,53	0,01862
FUBP3	-1,53	0,02434
AP1M1	-1,53	0,04015
PLA2G4F	-1,53	0,04240
KRTAP20-1	-1,52	0,00059
KLHDC2	-1,52	0,00358
ERLIN1	-1,52	0,01436
ATG16L1	-1,52	0,01555
FAM234B	-1,52	0,02268
KLHL8	-1,52	0,02428
TTPAL	-1,52	0,02928
MFSD6	-1,52	0,04393
TMEM206	-1,52	0,04633
SLC44A2	-1,51	0,00257

LRRC45	-1,51	0,00536
RPS29; RPL32P29	-1,51	0,01250
AR	-1,51	0,04162
RAB21	-1,50	0,00347
BTBD7	-1,50	0,00524
BMP2K	-1,50	0,00826
PIGF	-1,50	0,01037
FAM107B	-1,50	0,01259
PPP2R3B	-1,50	0,01271
PPP2R3B	-1,50	0,01271
SLC29A3	-1,50	0,01821
TOMM7	-1,50	0,02234
BTBD9	-1,50	0,02558
ISY1	-1,50	0,02901
ARPC4-TTLL3	-1,50	0,03281
ATP2B2	-1,50	0,03431
MMP28	-1,50	0,03811
HBP1	-1,50	0,04007
VTA1	-1,50	0,04011
SLC34A2	-1,50	0,04957
C14orf119	-1,50	0,04973
ALDH1B1	1,50	0,00164
DLX1	1,50	0,01137
NCOA7	1,50	0,01392
ZDHHC3	1,50	0,01735
BCDIN3D	1,50	0,02248
AASDH	1,50	0,02595
PDE7A	1,50	0,03564
GRK4	1,50	0,03704
MDC1	1,50	0,04108
PGAP1	1,51	0,01062
MPP4	1,51	0,01107
TMEM87B	1,51	0,02585
MLXIP	1,51	0,02750
RAET1L	1,51	0,02927
PSG1	1,52	0,00055
NEUROG3	1,52	0,00338
GCC2	1,52	0,01789
TLK1	1,52	0,01884
MT1X	1,52	0,02499
ZSCAN26	1,52	0,04188
CCRL2	1,52	0,04360
RIMBP3C	1,52	0,04371
CDH6	1,53	0,00193
HOMER2	1,53	0,00589
ERO1A	1,53	0,00615
IFI27	1,53	0,02161
AIFM3	1,53	0,02266
KLRF2	1,53	0,02278
PRKCD	1,53	0,02478
ITPRIPL2	1,53	0,04086
KRT33B	1,54	0,00027
GBP1	1,54	0,01660
CXorf51A	1,54	0,02084
CCDC102B	1,54	0,02598
ZNF474	1,54	0,03045
OLFML2A	1,54	0,03107
CDH10	1,54	0,03260
ADAMTS5	1,54	0,03326
NTNG1	1,55	0,01627
LINC01296; DUXAP10	1,55	0,02479
ZNF473	1,55	0,03283
ZNF18	1,55	0,03642
FAM195B	1,55	0,04247
SFN	1,56	0,00042
C6orf52	1,56	0,01910
TBX15	1,56	0,02912

MATN2	1,56	0,02964
BBS10	1,57	0,00220
TENM1	1,57	0,00533
PRELID3B; ATP5E	1,57	0,00579
MLLT11	1,57	0,02025
PSG4	1,58	0,00161
MYO3B	1,58	0,00394
HIST1H2AK	1,58	0,02531
LRRC8E	1,58	0,03142
MED19	1,59	0,00089
RAB3C	1,59	0,00223
GNGT2	1,59	0,00224
SLC6A9	1,59	0,00541
ARID5B	1,59	0,01087
CUL7	1,59	0,01185
SMIM1	1,59	0,01917
CREB3L2	1,60	0,00556
KANK4	1,60	0,00685
HMGCS1	1,60	0,01291
BRWD3	1,60	0,01424
LACTBL1	1,60	0,02707
GADL1	1,60	0,03783
BEAN1-AS1	1,61	0,00373
FAM101A	1,61	0,02071
SFXN3	1,61	0,03866
SLC7A9	1,61	0,04647
FAM133A	1,62	0,02372
DNM1	1,62	0,04057
ZNF570	1,62	0,04099
CASC10	1,63	0,00420
LIX1L	1,63	0,00608
CUL9	1,63	0,01357
ZNF84	1,63	0,03553
LARP1	1,63	0,03911
GMNC	1,63	0,04158
BHLHE40	1,63	0,04607
SYBU	1,63	0,04845
STC1	1,64	0,00473
G6PD	1,64	0,00822
SLC16A3	1,65	0,00047
AKAP12	1,65	0,00165
SERPINB10	1,65	0,00809
ULBP3	1,65	0,00838
CNN2	1,65	0,00963
CACNA1H	1,65	0,01508
PGK2	1,65	0,01539
SIK1	1,66	0,00516
GAD1	1,66	0,02147
MT2A	1,66	0,03389
ZSCAN21	1,66	0,04799
GJA1	1,67	0,03034
GNAI2	1,67	0,04161
SYNPO	1,68	0,00330
CREB5	1,68	0,00363
VGLL3	1,68	0,02922
SAMD11	1,68	0,04483
KRTAP3-1	1,69	0,00134
GLIPR2	1,69	0,02440
SOX4	1,70	0,00257
TPBG	1,70	0,01538
CERCAM	1,72	0,00355
ANPEP	1,72	0,00541
NPFFR2	1,72	0,02004
P4HA3	1,72	0,04085
PIK3C2B	1,73	0,01554
THBS3	1,73	0,01627
BEND6	1,73	0,01980
SNAI3	1,74	0,01104

REXO1; MIR1909	1,74	0,01191
SYT1	1,74	0,01347
ZNF645	1,74	0,02064
HSPB1	1,74	0,02672
OLFML3	1,74	0,03928
UROC1	1,74	0,04635
NKX2-3	1,75	0,00576
FGR	1,75	0,01990
PITPNM3	1,75	0,02446
SNX15	1,76	0,00467
FURIN	1,76	0,00770
HIPK2	1,76	0,00970
TMEM262	1,76	0,04379
IPCEF1	1,77	0,02868
LDLRAD4	1,77	0,03877
GCNT2	1,77	0,04120
ASIC2	1,78	0,00532
ZYX	1,78	0,02023
RHOB	1,78	0,02291
BAIAP3	1,78	0,03028
ZNF777	1,79	0,03779
MYL9	1,80	0,00521
F2RL2	1,82	0,01627
EIF4EBP2	1,84	0,00652
UBE2U	1,84	0,01381
PVRL1	1,84	0,01473
DNMT3B	1,84	0,01823
RCAN2	1,85	0,00010
TSPAN18	1,85	0,00993
ICK	1,85	0,03240
PDLIM7	1,86	0,01154
MMP2	1,86	0,01202
C16orf45	1,86	0,04773
BEND7	1,87	0,03496
DHCR24	1,88	0,00093
GNG3	1,89	0,02096
FOXS1	1,92	0,02758
CLCA1	1,93	0,03043
GPNMB	1,93	0,04992
KRT33A	1,94	0,01196
NKAIN4	1,95	0,00015
STAB1	1,95	0,02887
DIXDC1	1,95	0,03995
ACTA2	1,97	0,00718
FSCN1	1,97	0,01142
NREP	2,00	0,00177
SS18	2,01	0,00091
LMLN	2,01	0,02220
PC	2,02	0,02757
TLL1	2,03	0,01066
RFX3	2,03	0,02509
ARNTL	2,03	0,03020
KCNN1	2,04	0,03050
KIAA2012	2,05	0,02604
TNC	2,07	0,02113
NF2	2,11	0,02584
CGB7	2,12	0,01749
TPM1	2,16	0,01107
SHROOM2	2,16	0,01845
TGFBI	2,32	0,00333
BLNK	2,33	0,03296
GLIPR1	2,35	0,00002
CSRP1	2,35	0,00069
CGB1	2,35	0,00162
TAGLN	2,42	0,00053
AMTN	2,42	0,00160
PLPPR2	2,44	0,00347
CGB; CGB5	2,45	0,02237

CGB2	2,47	0,00509
IL32	2,48	0,00514
MIR99AHG	2,50	0,00701
CGB8	2,59	0,01074
SERPINE1	2,67	0,00192
CGB5; CGB8	2,74	0,00070
DYNLRB1	2,78	0,00016
MAP2	2,85	0,01342
CRYAB	3,21	0,00484
MSC	3,27	0,01606

ANNEX 2

OS with patients containing cisplatin

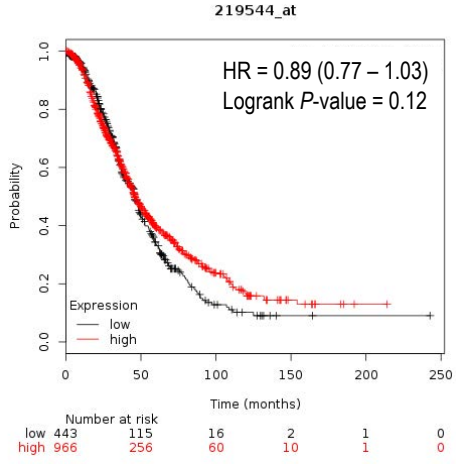

OS with patients containing taxol

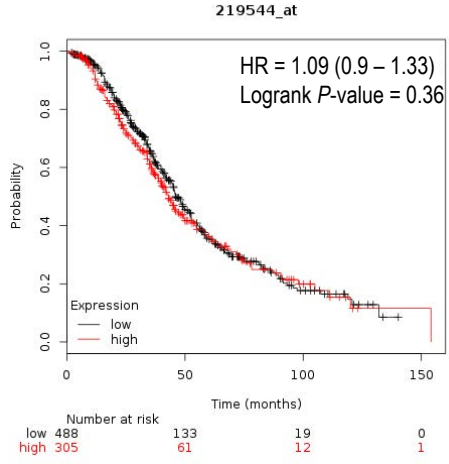

PFS with patients containing ciplatin

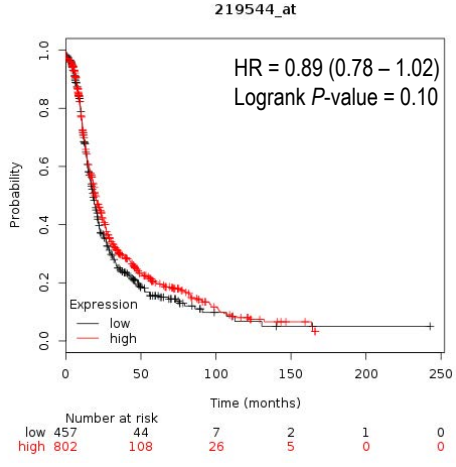

PFS with patients containing taxol

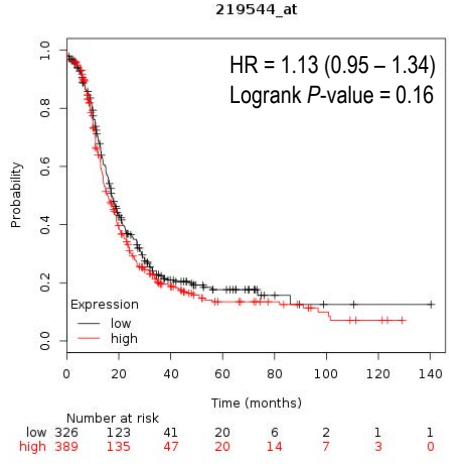

Annex 2. Prognostic value of *BORA* expression in OC patients categorized by chemotherapy regimen. Plots illustrate the OS and PFS regarding the treatment (platinum or taxanes agents). Data is retrieved from the Kaplan Meier Plotter Initiative (*www.kmplot.com*), showing that *BORA* overexpressing tumors (red line) compared to negative or low *BORA* tumors (black line). Affymetrix ID: 219544_at corresponds to *BORA* transcript.

ANNEX 3

TCGA (341 patients)		
HUGO	r	*p* -value
KLF12	0.443	2.3e-27
FOXM1	0.383	2.4e-20
E2F7	0.378	7.4e-20
E2F8	0.374	2.3e-19
ZNF92	0.342	3.0e-16
PBX4	0.338	6.9e-16
TFDP1	0.333	1.7e-15
MYBL2	0.326	7.2e-15
E2F2	0.320	2.3e-14
HMGB2	0.311	1.4e-13
CBFA2T2	0.308	2.4e-13
RFXAP	0.296	1.9e-12
UHRF1	0.296	2.2e-12
PTTG1	0.290	5.9e-12
FOXA3	0.283	2.0e-11
TARDBP	0.277	5.1e-11
E2F1	0.271	1.5e-10
CEBPG	0.253	2.4e-09
KLF5	0.250	3.9e-09

Tumor Ovarian Serous Cystoadenocarcinoma (TCGA)
Source: TCGA

OVARIAN-EXPO (296 patients)		
HUGO	r	*p* -value
PTTG1	0.619	1.9e-28
FOXM1	0.613	8.7e-28
HMGB2	0.511	2.1e-18
E2F8	0.506	4.4e-18
TARDBP	0.503	8.1e-18
MYBL2	0.497	2.4e-17
UHRF1	0.482	2.6e-16
TFDP1	0.434	3.4e-13
ZNF367	0.405	1.6e-11
TCF19	0.404	1.9e-11
E2F1	0.386	1.7e-10
HMGA1	0.379	3.4e-10
E2F3	0.356	4.8e-09
E2F2	0.354	5.4e-09
GTF2IRD1	0.347	1.2e-08
TAF5	0.342	2.1e-08
MYNN	0.342	1.9e-08
PLAGL2	0.336	3.6e-08
HDAC2	0.327	8.8e-08
YBX1	0.315	2.7e-07
E2F7	0.314	3.0e-07
GTF2H4	0.311	3.8e-07
CEBPG	0.303	8.1e-07
PA2G4	0.301	9.2e-07
SMC3	0.301	9.1e-07
NR2F6	0.300	1.0e-06
TEAD2	0.294	1.6e-06
TEAD4	0.292	2.0e-06
ENO1	0.291	2.2e-06
TGIF2	0.278	6.1e-06
BUD31	0.271	1.1e-05
ADNP	0.270	1.2e-05
PBX4	0.266	1.6e-05
RFXANK	0.262	2.2e-05
STAT1	0.261	2.4e-05
HDAC1	0.260	2.5e-05

Expression Project for Oncology (expO)
Source: GEO ID: GSE2109

OVARIAN-BOWTELL (285 patients)		
HUGO	r	*p* -value
FOXM1	0.626	1.8e-32
PTTG1	0.604	1.0e-29
MYBL2	0.602	1.5e-29
E2F8	0.590	4.4e-28
E2F1	0.509	3.3e-20
E2F2	0.475	1.8e-17
TCF19	0.460	2.6e-16
HMGB2	0.442	4.8e-15
UHRF1	0.424	7.2e-14
MYNN	0.419	1.5e-13
ZNF93	0.390	8.8e-12
TAF5	0.387	1.3e-11
TFDP1	0.383	2.2e-11
CEBPG	0.368	1.4e-10
STAT1	0.365	2.1e-10
E2F7	0.365	2.1e-10
ZNF367	0.345	2.1e-09
PLAGL2	0.333	8.4e-09
VPS72	0.316	4.8e-08
ZNF207	0.303	1.9e-07
TARDBP	0.296	3.5e-07
SOX18	0.287	8.2e-07
TEAD2	0.287	8.4e-07
SLC2A4RG	0.287	8.2e-07
HEY2	0.287	8.2e-07
ZBTB17	0.279	1.8e-06
ZIC1	0.273	3.0e-06
DMRT3	0.273	2.9e-06
DMRT1	0.273	2.9e-06
MTA3	0.271	3.6e-06
YBX1	0.265	5.9e-06
MEOX1	0.256	1.2e-05
BATF2	0.252	1.7e-05

Australian Ovarian Cancer Study
Source: GEO ID: GSE9891

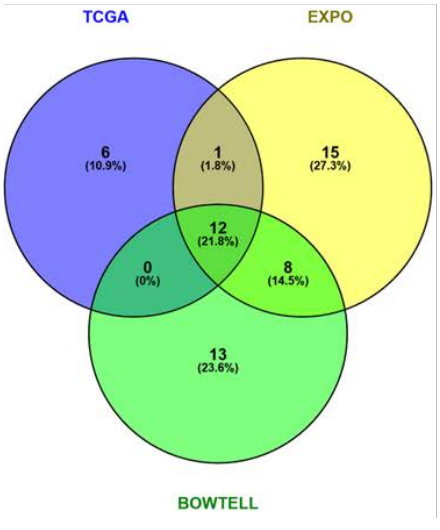

#	Transcription Factor
FOXM1	Forkhead box protein M1
E2F1	E2F Transcription Factor 1
E2F2	E2F Transcription Factor 2
E2F7	E2F Transcription Factor 7
E2F8	E2F Transcription Factor 8
HMGB2	High-mobility group protein 2
UHRF1	Ubiquitin Like With PHD And Ring Finger Domains 1
PTTG1	Regulator Of Sister Chromatid Separation, Securin
TARDBP	TAR DNA Binding Protein
TFDP1	Transcription Factor Dp-1
MYBL2	(MYB Proto-Oncogene Like 2
CEBPG	CCAAT Enhancer Binding Protein Gamma

Annex 3. Correlation analysis between the expression of *BORA* and 945 TFs in primary ovarian specimens from different OC datasets (TCGA, EXPO, and BOWTELL). Patient sample sizes: TCGA n=341; EXPO n=296 and BOWTELL n=285. Only positive correlations were selected. R means Pearson Correlation. Venn diagram representing the overlap of predicted TFs between the three OC data sets. Table showing the TFs that overlaps in the three datasets.

ANNEX 4

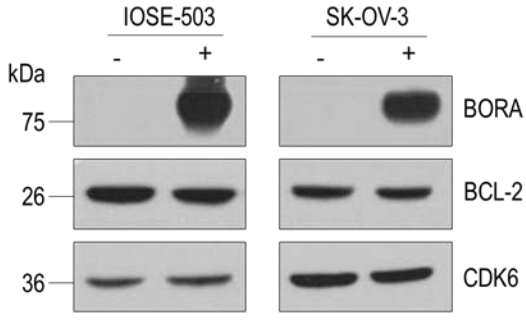

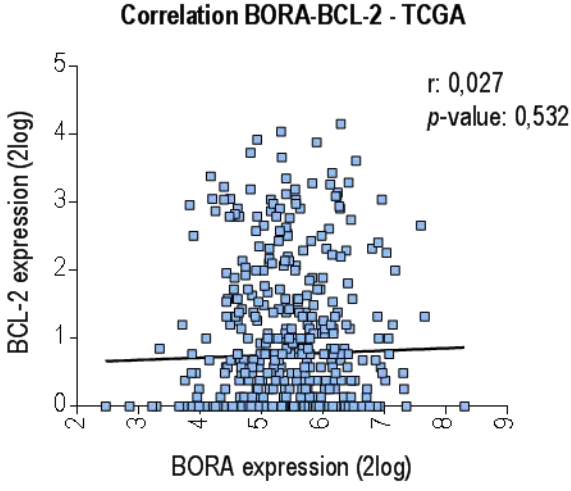

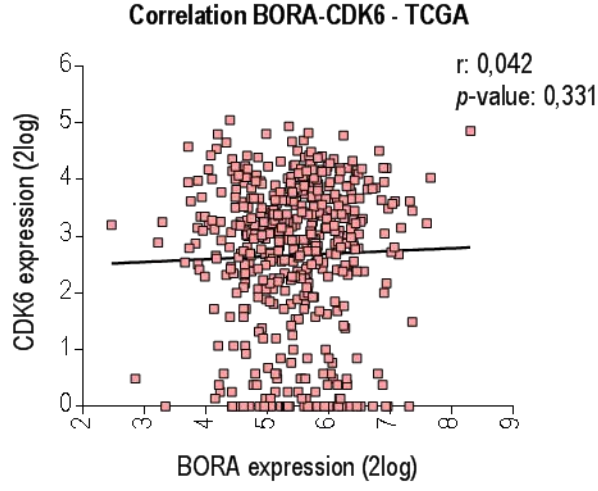

Annex 4. Immunoblot of BORA, BCL-2 and CDK6 upon BORA overexpression in SK-OV-3 cell line. "+" means pIND_BORA and "-" means pIND_EV. Correlation analysis of *BORA* with *BCL-2* and *CDK6* expression in patients from the ovarian TCGA cohort. Sample size: 341 patients. r means Spearman correlation. Data was retrieved using the R2 genomics website and plotted in Graphpad Prism Software.

ANNEX 5

Better OVERALL SURVIVAL

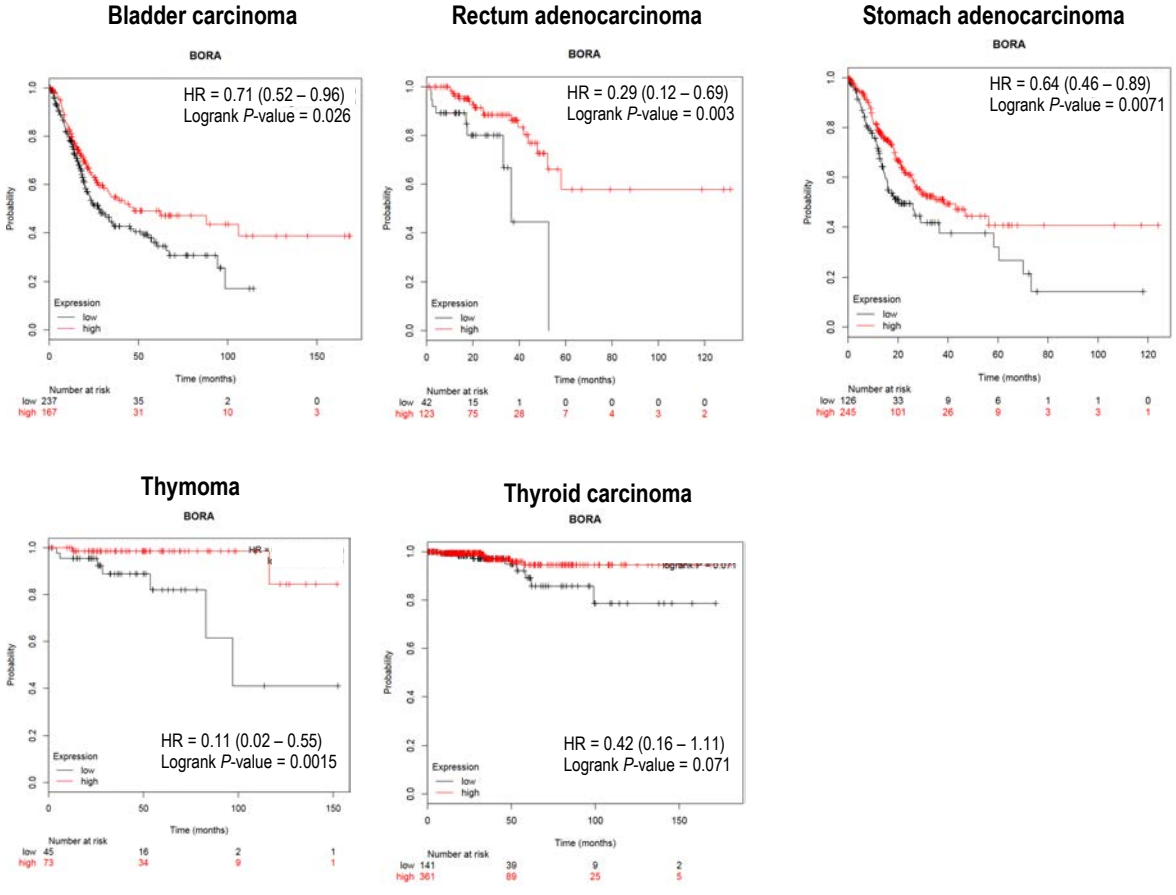

Annex 5. Prognostic value of *BORA* expression in bladder, rectum, stomach, thymoma and thyroid carcinomas. Plots depict the overall survival in the different tumors. Data is retrieved from the Kaplan Meier Plotter initiative (*www.kmplot.com*), showing that *BORA* overexpressing tumors (red line) have a better outcome when compared to negative or low *BORA* tumors (black line).

ANNEX 6

Template 1

Template 2

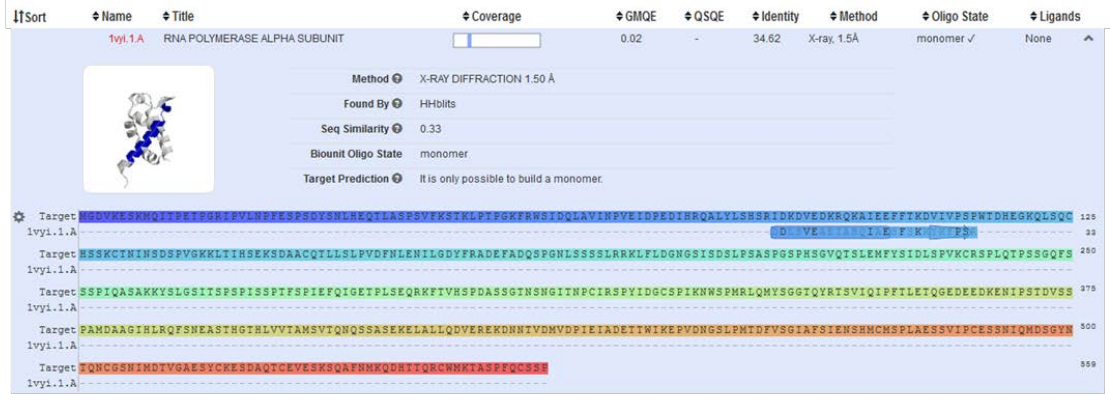

Annex 6. BORA aa sequence was introduced in the SWISS-MODEL server, an automated protein structure homology-modelling pipeline. Accessed through: *https://swissmodel.expasy.org*. Only 25% and 34,62% of identity was observed for the two templates. Template 1 corresponds to a phosphoprotein accession 3t4r.1.A; and template 2 corresponds to a RNA polymerase alpha subunit accession 1vji1.a.

ANNEX 7

miRNA	ID Accesion	Family	Sequence	Locus
hsa-miR-23b-3p	MIMAT0000418	miR-23	aucacauugccagggauuaccac	chr9: 95085208-95085304 [+]
hsa-miR-23a-3p	MIMAT0000078	miR-23	aucacauugccagggauuucc	chr19: 13836587-13836659 [-]
hsa-miR-23c	MIMAT0018000	miR-23	aucacauugccagugauuaccc	chrX: 20017088-20017187 [-]
hsa-miR-130a-5p	MIMAT0004593	miR-130	gcucuuuucacauugugcuacu	chr11: 57641198-57641286 [+]
hsa-miR-129-1-3p	MIMAT0004548	miR-129	aagcccuuaccccaaaaaguau	chr7: 128207872-128207943 [+]
hsa-miR-129-2-3p	MIMAT0004605	miR-129	aagcccuuaccccaaaaagcau	chr11: 43581394-43581483 [+]
hsa-miR-665	MIMAT0004952	miR-665	accaggaggcugaggccccu	chr14: 100875033-100875104 [+]

Annex 7. Table containing the miRNA that are predicted to target *BORA* in the three algorithms (TargetScan, microRNA.org and miRDB).

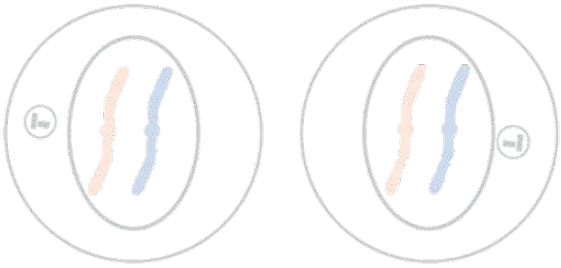

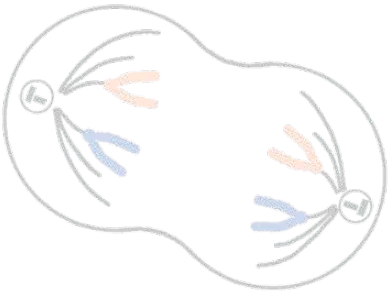

8. BIBLIOGRAPHY

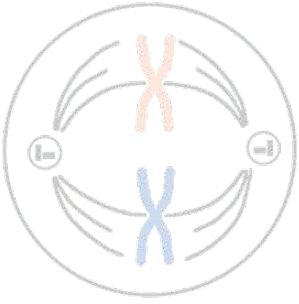

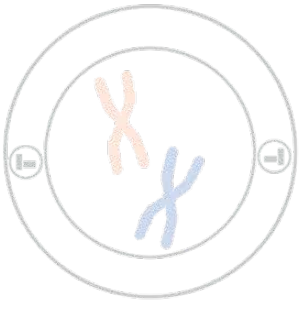

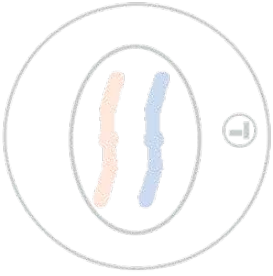

1. Society, A. C. Learn about cancer. Available at: https://www.cancer.org/cancer/cancer-basics/history-of-cancer.html. (Accessed: 9th March 2019)
2. Bray, F. *et al.* Global cancer statistics 2018: GLOBOCAN estimates of incidence and mortality worldwide for 36 cancers in 185 countries. *CA. Cancer J. Clin.* **68,** 394–424 (2018).
3. Bray, F., Jemal, A., Grey, N., Ferlay, J. & Forman, D. Global cancer transitions according to the Human Development Index (2008-2030): A population-based study. *Lancet Oncol.* **13,** 790–801 (2012).
4. Ferlay, J. *et al.* Cancer incidence and mortality worldwide: Sources, methods and major patterns in GLOBOCAN 2012. *Int. J. Cancer* **136,** 359–86 (2015).
5. DeVita, V. T. & Chu, E. A history of cancer chemotherapy. *Cancer Res.* **68,** 8643–53 (2008).
6. Driscoll CE. Cancer care in the 1980s. *Prim Care* **14,** 243–54 (1987).
7. Hanahan, D. & Weinberg, R. A. The hallmarks of cancer. *Cell* **100,** 57–70 (2000).
8. Chabner, B. A. & Roberts, T. G. Chemotherapy and the war on cancer. *Nat. Rev. Cancer* **5,** 65–72 (2005).
9. Hanahan, D. & Weinberg, R. A. Hallmarks of cancer: The next generation. *Cell* **144,** 646–74 (2011).
10. Lord, C. J. & Ashworth, A. PARP inhibitors: Synthetic lethality in the clinic. *Science (80-.).* **355,** 1152–1158 (2017).
11. Drake, C. G., Lipson, E. J. & Brahmer, J. R. Breathing new life into immunotherapy: Review of melanoma, lung and kidney cancer. *Nat. Rev. Clin. Oncol.* **11,** 24–37 (2014).
12. Zacharakis, N. *et al.* Immune recognition of somatic mutations leading to complete durable regression in metastatic breast cancer. *Nat. Med.* **24,** 724–730 (2018).
13. Prat, J. Ovarian, fallopian tube and peritoneal cancer staging: Rationale and explanation of new FIGO staging 2013. *Best Pract. Res. Clin. Obstet. Gynaecol.* **29,** 858–69 (2015).
14. Cannistra SA, Gershenson DM, R. A. Ovarian Cancer, Fallopian Tube Carcinoma, and Peritoneal Carcinoma. *Rosenberg's Cancer Princ. Pract. Oncol.* **4,** 1368–91 (2011).
15. Siegel, R. L., Miller, K. D. & Jemal, A. Cancer statistics, 2018. *CA. Cancer J. Clin.* **68,** 7–30 (2018).
16. Sociedad Española de Oncología Médica. Las cifras del cáncer en España. (2018).
17. Delgado-Ortega, L. *et al.* The economic burden of disease of epithelial ovarian cancer in Spain: the OvarCost study. *Eur. J. Heal. Econ.* **20,** 135–147 (2018).
18. Reid, B. M., Permuth, J. B. & Sellers, T. A. Epidemiology of ovarian cancer: a review. *Cancer Biol. Med.* **14,** 9–32 (2017).
19. National Cancer Institute. SEER stat fact sheets: ovarian cancer. SEER. (2018).
20. Webb, P. M. & Jordan, S. J. Epidemiology of epithelial ovarian cancer. *Best Practice and Research: Clinical Obstetrics and Gynaecology* **41,** 3–14 (2017).
21. Stratton, J. F., Pharoah, P., Smith, S. K., Easton, D. & Ponder, B. A. J. A systematic review and meta-analysis of family history and risk of ovarian cancer. *BJOG An Int. J. Obstet. Gynaecol.* **105,** 493–499 (1998).
22. Boyd, J. Specific Keynote: Hereditary Ovarian Cancer: What We Know. *Gynecol. Oncol.* **88,** 8–13 (2003).
23. Lynch, H. T. *et al.* Hereditary ovarian carcinoma: Heterogeneity, molecular genetics, pathology, and management. *Mol. Oncol.* **3,** 97–137 (2009).
24. Risch, H. A. *et al.* Population BRCA1 and BRCA2 mutation frequencies and cancer penetrances: A kin-cohort study in Ontario, Canada. *J. Natl. Cancer Inst.* **98,** 1694–706 (2006).
25. Pennington, K. P. & Swisher, E. M. Hereditary ovarian cancer: Beyond the usual suspects. *Gynecol. Oncol.* **124,** 347–53 (2012).
26. Rebbeck, T. R. *et al.* Association of type and location of BRCA1 and BRCA2 mutations with risk of breast and ovarian cancer. *Jama* **313,** 1347–61 (2015).
27. Antoniou, A. *et al.* Average Risks of Breast and Ovarian Cancer Associated with BRCA1 or BRCA2 Mutations Detected in Case Series Unselected for Family History: A Combined Analysis of 22 Studies. *Am. J. Hum. Genet.* **72,** 1117–30 (2003).
28. Lord, C. J. & Ashworth, A. BRCAness revisited. *Nat. Rev. Cancer* **16,** 110–20 (2016).
29. King, M.-C. *et al.* Mutations in 12 genes for inherited ovarian, fallopian tube, and peritoneal carcinoma identified by massively parallel sequencing. *Proc. Natl. Acad. Sci.* **108,** 18032–7 (2011).

30. Norquist, B. M. *et al.* Inherited mutations in women with ovarian carcinoma. *JAMA Oncol.* **2,** 482–90 (2016).
31. Suwaki, N., Klare, K. & Tarsounas, M. RAD51 paralogs: Roles in DNA damage signalling, recombinational repair and tumorigenesis. *Semin. Cell Dev. Biol.* **22,** 898–905 (2011).
32. Prakash, R., Zhang, Y., Feng, W. & Jasin, M. Homologous recombination and human health: The roles of BRCA1, BRCA2, and associated proteins. *Cold Spring Harb. Perspect. Biol.* **7,** a016600 (2015).
33. Ketabi, Z. *et al.* Ovarian cancer linked to lynch syndrome typically presents as early-onset, non-serous epithelial tumors. *Gynecol. Oncol.* **121,** 462–5 (2011).
34. Engel, C. *et al.* Risks of less common cancers in proven mutation carriers with lynch syndrome. *J. Clin. Oncol.* **30,** 4409–15 (2012).
35. Helder-Woolderink, J. M. *et al.* Ovarian cancer in Lynch syndrome; a systematic review. *Eur. J. Cancer* **55,** 65–73 (2016).
36. Plagens-Rotman K, Chmak-Wierzchowska K, Pieta B, B. I. Modifiable lifestyle factors and ovarian cancer incidence in women. *Ann Agric Env. Med* **14,** 36–40 (2018).
37. Wentzensen, N. *et al.* Ovarian cancer risk factors by histologic subtype: An analysis from the Ovarian Cancer Cohort Consortium. *J. Clin. Oncol.* **34,** 2888–98 (2016).
38. Matulonis, U. A. *et al.* Ovarian cancer. *Nat. Rev. Dis. Prim.* **2,** 16061 (2016).
39. Kaku, T. *et al.* Histological classification of ovarian cancer. *Med Electron Microsc* **36,** 9–17 (2003).
40. Blagden, S. P. Harnessing Pandemonium: The Clinical Implications of Tumor Heterogeneity in Ovarian Cancer. *Front. Oncol.* **5,** 149 (2015).
41. Kurman, R. J. & Shih, I. M. Molecular pathogenesis and extraovarian origin of epithelial ovarian cancer - Shifting the paradigm. *Hum. Pathol.* **42,** 918–31 (2011).
42. Mackenzie, R. *et al.* Targeted deep sequencing of mucinous ovarian tumors reveals multiple overlapping RAS-pathway activating mutations in borderline and cancerous neoplasms. *BMC Cancer* **15,** 415 (2015).
43. Catasús, L. *et al.* Molecular genetic alterations in endometrioid carcinomas of the ovary: Similar frequency of beta-catenin abnormalities but lower rate of microsatellite instability and PTEN alterations than in uterine endometrioid carcinomas. *Hum. Pathol.* **35,** 1360–8 (2004).
44. Cuatrecasas, M., Villanueva, A., Matias-Guiu, X. & Prat, J. K-ras mutations in mucinous ovarian tumors: A clinicopathologic and molecular study of 95 cases. *Cancer* **79,** 1581–6 (1997).
45. Vereczkey I, Serester O, Dobos J, Gallai M, Szakacs O, Szentirmay Z, T. E. Molecular characterization of 103 ovarian serous and mucinous tumors. *Pathol Oncol Res* **17,** 551–9 (2011).
46. Zhao, Y. *et al.* ARID1A Mutations in Endometriosis-Associated Ovarian Carcinomas. *N. Engl. J. Med.* **363,** 1532–43 (2010).
47. Anglesio, M. S. *et al.* Molecular characterization of mucinous ovarian tumours supports a stratified treatment approach with HER2 targeting in 19% of carcinomas. *J. Pathol.* **229,** 111–20 (2013).
48. Bell, D. *et al.* Integrated genomic analyses of ovarian carcinoma. *Nature* **474,** 609–615 (2011).
49. Ahmed, A. A. *et al.* Driver mutations in TP53 are ubiquitous in high grade serous carcinoma of the ovary. *J. Pathol.* **221,** 49–56 (2010).
50. Karnezis, A. N., Cho, K. R., Gilks, C. B., Pearce, C. L. & Huntsman, D. G. The disparate origins of ovarian cancers: Pathogenesis and prevention strategies. *Nat. Rev. Cancer* **17,** 65–74 (2017).
51. Cools, M., Wolffenbuttel, K. P., Drop, S. L. S., Oosterhuis, J. W. & Looijenga, L. H. J. Gonadal development and tumor formation at the crossroads of male and female sex determination. *Sex. Dev.* **5,** 167–80 (2011).
52. Zhao, C. *et al.* Identification of the most sensitive and robust immunohistochemical markers in different categories of ovarian sex cord-stromal tumors. *Am. J. Surg. Pathol.* **33,** 354–66 (2009).
53. Lee, I. H. *et al.* Clinicopathologic characteristics of granulosa cell tumors of the ovary: A multicenter retrospective study. *J. Gynecol. Oncol.* **22,** 118–195 (2011).
54. Kim, J. H. *et al.* Differential apoptotic activities of wild-type FOXL2 and the adult-type granulosa cell tumor-associated mutant FOXL2 (C134W). *Oncogene* **30,** 1653–63 (2011).

55. Kalfa, N. *et al.* Aberrant Expression of Ovary Determining Gene FOXL2 in the Testis and Juvenile Granulosa Cell Tumor in Children. *J. Urol.* **180,** 1810–3 (2008).
56. Lee, Y. *et al.* A candidate precursor to serous carcinoma that originates in the distal fallopian tube. *J. Pathol.* **211,** 23–65 (2007).
57. Labidi-Galy, S. I. *et al.* High grade serous ovarian carcinomas originate in the fallopian tube. *Nat. Commun.* **8,** 1093 (2017).
58. Kessler, M., Fotopoulou, C. & Meyer, T. The molecular fingerprint of high grade serous ovarian cancer reflects its fallopian tube origin. *Int. J. Mol. Sci.* **14,** 6571–6596 (2013).
59. Klinkebiel, D., Zhang, W., Akers, S. N., Odunsi, K. & Karpf, A. R. DNA Methylome Analyses Implicate Fallopian Tube Epithelia as the Origin for High-Grade Serous Ovarian Cancer. *Mol. Cancer Res.* **14,** 787–794 (2016).
60. Powell, C. B. *et al.* Long term follow up of BRCA1 and BRCA2 mutation carriers with unsuspected neoplasia identified at risk reducing salpingo-oophorectomy. *Gynecol. Oncol.* **129,** 364–371 (2013).
61. Coscia, F. *et al.* Integrative proteomic profiling of ovarian cancer cell lines reveals precursor cell associated proteins and functional status. *Nat. Commun.* **7,** 12645 (2016).
62. Kelemen, L. E. & Köbel, M. Mucinous carcinomas of the ovary and colorectum: Different organ, same dilemma. *Lancet Oncol.* **12,** 1071–80 (2011).
63. Seidman, J. D., Kurman, R. J. & Ronnett, B. M. Primary and metastatic mucinous adenocarcinomas in the ovaries: Incidence in routine practice with a new approach to improve intraoperative diagnosis. *Am. J. Surg. Pathol.* **27,** 985–993 (2003).
64. Versteege, I. *et al.* Truncating mutations of hSNF5/INI1 in aggressive paediatric cancer. *Nature* **394,** 203–206 (1998).
65. Goff, B. A., Mandel, L. S., Melancon, C. H. & Muntz, H. G. Frequency of symptoms of ovarian cancer in women presenting to primary care clinics. *J. Am. Med. Assoc.* **291,** 2705–2712 (2004).
66. Goff, B. A., Mandel, L., Muntz, H. G. & Melancon, C. H. Ovarian carcinoma diagnosis. *Cancer* **89,** 2068–2075 (2002).
67. Ebell, M. H., Culp, M., Lastinger, K. & Dasigi, T. A systematic review of the bimanual examination as a test for ovarian cancer. *Am. J. Prev. Med.* **48,** 350–356 (2015).
68. Kang, S. K. *et al.* ACR Appropriateness Criteria®Staging and Follow-Up of Ovarian Cancer. *J. Am. Coll. Radiol.* **15,** 198–207 (2018).
69. Tolman, C. J., Vaid, T. & Schreuder, H. W. R. Extremely elevated CA-125 in benign ovarian disease due to stretch of the peritoneum. *BMJ Case Rep.* **27,** 201 (2012).
70. Demir, R. H. & Marchand, G. J. Adnexal Masses Suspected to Be Benign Treated with Laparoscopy. *JSLS J. Soc. Laparoendosc. Surg.* **16,** 71–84 (2012).
71. Mutch, D. G. & Prat, J. 2014 FIGO staging for ovarian, fallopian tube and peritoneal cancer. *Gynecol. Oncol.* **133,** 401–404 (2014).
72. Buchen, L. Cancer: Missing the mark. *Nature* **471,** 428–432 (2011).
73. Jacobs, I. J. *et al.* Ovarian cancer screening and mortality in the UK Collaborative Trial of Ovarian Cancer Screening (UKCTOCS): A randomised controlled trial. *Lancet* **26,** 66–71 (2016).
74. Majem, B., Rigau, M., Reventós, J. & Wong, D. T. Non-coding RNAs in saliva: Emerging biomarkers for molecular diagnostics. *Int. J. Mol. Sci.* **16,** 8676–8698 (2015).
75. Chang, S. J., Hodeib, M., Chang, J. & Bristow, R. E. Survival impact of complete cytoreduction to no gross residual disease for advanced-stage ovarian cancer: A meta-analysis. *Gynecol. Oncol.* **130,** 493–8 (2013).
76. Horowitz, N. S. *et al.* Does aggressive surgery improve outcomes? Interaction between preoperative disease burden and complex surgery in patients with advanced-stage ovarian cancer: An analysis of GOG 182. *J. Clin. Oncol.* **33,** 937–943 (2015).
77. Bois, A. Du *et al.* Role of surgical outcome as prognostic factor in advanced epithelial ovarian cancer: A combined exploratory analysis of 3 prospectively randomized phase 3 multicenter trials: by the arbeitsgemeinschaft gynaekologische onkologie studiengruppe ovarialkarzin. *Cancer* **115,** 1234–44 (2009).
78. SEGO. *Guías de práctica clínica en cáncer ginecológico y mamario. ONCOGUÍAS SEGO.* (2014).
79. Kehoe, S. *et al.* Primary chemotherapy versus primary surgery for newly diagnosed advanced ovarian cancer (CHORUS): An open-label, randomised, controlled, non-inferiority trial. *Lancet* **386,** 249–57 (2015).

80. Kristensen, G. B. *et al.* Neoadjuvant Chemotherapy or Primary Surgery in Stage IIIC or IV Ovarian Cancer. *N. Engl. J. Med.* **363,** 943–953 (2010).

81. Gadducci, A. *et al.* Patterns of Recurrence and Clinical Outcome of Patients with Stage IIIC to Stage IV Epithelial Ovarian Cancer in Complete Response after Primary Debulking Surgery Plus Chemotherapy or Neoadjuvant Chemotherapy Followed by Interval Debulking Surgery: An Ita. *Int. J. Gynecol. Cancer* **27,** 28–36 (2017).

82. Onda, T. *et al.* Comparison of treatment invasiveness between upfront debulking surgery versus interval debulking surgery following neoadjuvant chemotherapy for stage III/IV ovarian, tubal, and peritoneal cancers in a phase III randomised trial: Japan Clinical Oncology Gr. *Eur. J. Cancer* **64,** 22–31 (2016).

83. *National Comprehensive Cancer Netwwork. Clinical practice guidelines in oncology (NCCN guidelines). Ovarian cancer including fallopian tube cancer and primary peritoneal cancer.* (2016).

84. Berek, J. S., Crum, C. & Friedlander, M. Cancer of the ovary, fallopian tube, and peritoneum. *Int. J. Gynecol. Obstet.* **131,** 111–122 (2015).

85. Alberts, D. S. *et al.* Intraperitoneal cisplatin plus intravenous cyclophosphamide versus intravenous cisplatin plus intravenous cyclophosphamide for stage III ovarian cancer. *N. Engl. J. Med.* **335,** 1950–5 (1996).

86. Walker, J. L. *et al.* Intraperitoneal catheter outcomes in a phase III trial of intravenous versus intraperitoneal chemotherapy in optimal stage III ovarian and primary peritoneal cancer: A Gynecologic Oncology Group study. *Gynecol. Oncol.* **100,** 27–32 (2006).

87. Agarwal, R. & Kaye, S. B. Ovarian cancer: Strategies for overcoming resistance to chemotherapy. *Nat. Rev. Cancer* **3,** 502–16 (2003).

88. Markman, M. *et al.* Phase III randomized trial of 12 versus 3 months of maintenance paclitaxel in patients with advanced ovarian cancer after complete response to platinum and paclitaxel-based chemotherapy: A Southwest Oncology Group and Gynecologic Oncology Group Trial. *J. Clin. Oncol.* **21,** 2460–5 (2003).

89. Kathleen Moore, Nicoletta Colombo, Giovanni Scambia, Byoung-Gie Kim, Ana Oaknin, Michael Friedlander, Alla Lisyanskaya, Anne Floquet, Alexandra Leary, Gabe S. Sonke, Charlie Gourley, Susana Banerjee, Amit Oza, Antonio González-Martín, Carol Aghajanian, Wi, P. D. Maintenance Olaparib in Patients with Newly Diagnosed Advanced Ovarian Cancer. *N. Engl. J. Med.* **379,** 2495–2505 (2018).

90. Siegel RL, Miller KD, Jemal A. Cancer statistics, 2019. *CA. Cancer J. Clin.* **69,** 7–34 (2019).

91. Alvarez, R. D. *et al.* Moving beyond the platinum sensitive/resistant paradigm for patients with recurrent ovarian cancer. *Gynecol. Oncol.* **141,** 405–409 (2016).

92. Luvero, D., Milani, A. & Ledermann, J. A. Treatment options in recurrent ovarian cancer: Latest evidence and clinical potential. *Ther. Adv. Med. Oncol.* **6,** 229–39 (2014).

93. Jelovac, D. & Armstrong, D. K. Recent progress in the diagnosis and treatment of ovarian cancer. *CA. Cancer J. Clin.* **61,** 183–203 (2011).

94. Vencken, P. M. L. H. *et al.* Chemosensitivity and outcome of BRCA1- and BRCA2-associated ovarian cancer patients after first-line chemotherapy compared with sporadic ovarian cancer patients. *Ann. Oncol.* **22,** 1346–52 (2011).

95. Gallagher, D. J. *et al.* Survival in epithelial ovarian cancer: A multivariate analysis incorporating BRCA mutation status and platinum sensitivity. *Ann. Oncol.* **22,** 1127–32 (2011).

96. Rudaitis, V. *et al.* BRCA1/2 mutation status is an independent factor of improved survival for advanced (stage III-IV) ovarian cancer. *Int. J. Gynecol. Cancer* **24,** 1395–400 (2014).

97. Gudmundsdottir, K. & Ashworth, A. The roles of BRCA1 and BRCA2 and associated proteins in the maintenance of genomic stability. *Oncogene* **25,** 5864–74 (2006).

98. Yang, H. *et al.* BRCA2 function in DNA binding and recombination from a BRCA2-DSS1-ssDNA structure. *Science (80-.).* **13,** 1837–48 (2002).

99. Huertas, P. DNA resection in eukaryotes: Deciding how to fix the break. *Nat. Struct. Mol. Biol.* **17,** 11–6 (2010).

100. Sakai, W. *et al.* Secondary mutations as a mechanism of cisplatin resistance in BRCA2-mutated cancers. *Nature* **28,** 1116–20

(2008).

101. Patch, A. M. *et al.* Whole-genome characterization of chemoresistant ovarian cancer. *Nature* **521,** 489–494 (2015).
102. Etemadmoghadam, D. *et al.* Integrated genome-wide DMA copy number and expression analysis identifies distinct mechanisms of primary chemoresistance in ovarian carcinomas. *Clin. Cancer Res.* **15,** 1417–27 (2009).
103. Banerjee, S. & Kaye, S. B. New strategies in the treatment of ovarian cancer: Current clinical perspectives and future potential. *Clin. Cancer Res.* **19,** 961–8 (2013).
104. Rojas, V., Hirshfield, K. M., Ganesan, S. & Rodriguez-Rodriguez, L. Molecular characterization of epithelial ovarian cancer: Implications for diagnosis and treatment. *Int. J. Mol. Sci.* **17,** 2113 (2016).
105. Schmitt, J. & Matei, D. Targeting angiogenesis in ovarian cancer. *Cancer Treat. Rev.* **38,** 272–83 (2012).
106. Burger, R. A. *et al.* Incorporation of bevacizumab in the primary treatment of ovarian cancer. *N. Engl. J. Med.* **365,** 2473–2483 (2011).
107. Essapen, S. *et al.* A Phase 3 Trial of Bevacizumab in Ovarian Cancer. *N. Engl. J. Med.* **365,** 2484–96 (2011).
108. Liu, J. F. *et al.* Combination cediranib and olaparib versus olaparib alone for women with recurrent platinum-sensitive ovarian cancer: A randomised phase 2 study. *Lancet Oncol.* **15,** 1207–14 (2014).
109. Mullard, A. PARP inhibitors plough on. *Nat. Rev. Drug Discov.* **16,** 229 (2017).
110. Ashworth, A. A synthetic lethal therapeutic approach: Poly(ADP) ribose polymerase inhibitors for the treatment of cancers deficient in DNA double-strand break repair. *J. Clin. Oncol.* **26,** 3785–90 (2008).
111. Leung, A. W. Y., de Silva, T., Bally, M. B. & Lockwood, W. W. Synthetic lethality in lung cancer and translation to clinical therapies. *Mol. Cancer* **15,** 61 (2016).
112. Yap, T. A. *et al.* Inhibition of Poly(ADP-Ribose) Polymerase in Tumors from BRCA Mutation Carriers. *N. Engl. J. Med.* **361,** 123–34 (2009).
113. Audeh, M. W. *et al.* Oral poly(ADP-ribose) polymerase inhibitor olaparib in patients with BRCA1 or BRCA2 mutations and recurrent ovarian cancer: A proof-of-concept trial. *Lancet* **376,** 245–51 (2010).
114. Ledermann, J. *et al.* Olaparib maintenance therapy in patients with platinum-sensitive relapsed serous ovarian cancer: A preplanned retrospective analysis of outcomes by BRCA status in a randomised phase 2 trial. *Lancet Oncol.* **15,** 852–61 (2014).
115. Konstantinopoulos, P. A. *et al.* Gene expression profile of BRCAness that correlates with responsiveness to chemotherapy and with outcome in patients with epithelial ovarian cancer. *J. Clin. Oncol.* **28,** 3555–61 (2010).
116. Mullen, M. M., Kuroki, L. M. & Thaker, P. H. Novel treatment options in platinum-sensitive recurrent ovarian cancer: A review. *Gynecol. Oncol.* **152,** 416–425 (2019).
117. Fong, P. C. *et al.* Inhibition of Poly(ADP-Ribose) Polymerase in Tumors from BRCA Mutation Carriers. *N. Engl. J. Med.* **361,** 123–34 (2009).
118. ClinicalTrials.gov NCT01874353. Olaparib Treatment in BRCA Mutated Ovarian Cancer Patients After Complete or Partial Response to Platinum Chemotherapy. [(accessed on 11 March 2019)];
119. Swisher, E. M. *et al.* Rucaparib in relapsed, platinum-sensitive high-grade ovarian carcinoma (ARIEL2 Part 1): an international, multicentre, open-label, phase 2 trial. *Lancet Oncol.* **18,** 75–87 (2017).
120. Niraparib in Recurrent Ovarian Cancer. *N. Engl. J. Med.* **376,** 801–802 (2017).
121. George, A., Kaye, S. & Banerjee, S. Delivering widespread BRCA testing and PARP inhibition to patients with ovarian cancer. *Nat. Rev. Clin. Oncol.* **14,** 284–296 (2017).
122. Cheaib, B., Auguste, A. & Leary, A. The PI3K/Akt/mTOR pathway in ovarian cancer: Therapeutic opportunities and challenges. *Chin. J. Cancer* **34,** 4–16 (2015).
123. Husseinzadeh, N. & Husseinzadeh, H. D. MTOR inhibitors and their clinical application in cervical, endometrial and ovarian cancers: A critical review. *Gynecol. Oncol.* **133,** 375–81 (2014).
124. Emons, G. *et al.* Temsirolimus in women with platinum-refractory/resistant ovarian cancer or advanced/recurrent endometrial carcinoma. A phase II study of the AGO-study group (AGO-GYN8). *Gynecol. Oncol.* **140,** 450–6 (2016).
125. ClinicalTrials.gov NCT01623349. Phase I study of the oral PI3kinase Inhibitor BKM120 or BYL719 and the oral PARP Inhibitor

Olaparib in Patients with Recurrent Triple Negative Breast Cancer or High Grade Serous Ovarian Cancer. [(accessed on 10 March 2019)].

126. Lokadasan, R., James, F. V., Narayanan, G. & Prabhakaran, P. K. Targeted agents in epithelial ovarian cancer: Review on emerging therapies and future developments. *Ecancermedicalscience* **10,** 626 (2016).
127. ClinicalTrials.gov NCT02208375. A Phase Ib Study of the Oral PARP Inhibitor Olaparib With the Oral mTORC1/2 Inhibitor AZD2014 or the Oral AKT Inhibitor AZD5363 for Recurrent Endometrial, Triple Negative Breast, and Ovarian, Primary Peritoneal, or Fallopia.
128. Michalarea V., Lorente D., L. J. Accelerated phase I trial of 2 schedules of the combination of the PARP inhibitor olaparib and AKT inhibitor AZD5363 using a novel intrapatient dose escalation design in advanced cancer patients. *Proc. Am. Assoc. Cancer Res. Annu. Meet. Philadelphia, PA, USA.* (2015).
129. Farley, J. *et al.* Selumetinib in women with recurrent low-grade serous carcinoma of the ovary or peritoneum: An open-label, Single-arm, Phase 2 study. *Lancet Oncol.* **14,** 134–40 (2013).
130. ClinicalTrials.gov NCT02101788. Trametinib in Treating Patients with Recurrent or Progressive Low-Grade Ovarian Cancer or Peritoneal Cavity Cancer. [(accessed on 07 March 2019)]; (2019). Available at: https://clinicaltrials.gov/ct2/show/NCT02101788.
131. ClinicalTrials.gov NCT02022982. Palbociclib + PD-0325901 for NSCLC & Solid Tumors. [(accessed on 10 March 2019)].
132. Bookman, M. A., Darcy, K. M., Clarke-Pearson, D., Boothby, R. A. & Horowitz, I. R. Evaluation of monoclonal humanized anti-HER2 antibody, trastuzumab, in patients with recurrent or refractory ovarian or primary peritoneal carcinoma with overexpression of HER2: A phase II trial of the Gynecologic Oncology Group. *J. Clin. Oncol.* **21,** 283–90 (2003).
133. Garcia, A. A. *et al.* A phase II evaluation of lapatinib in the treatment of persistent or recurrent epithelial ovarian or primary peritoneal carcinoma: A gynecologic oncology group study. *Gynecol. Oncol.* **124,** 569–574 (2012).
134. Makhija, S. *et al.* Clinical activity of gemcitabine plus pertuzumab in platinum-resistant ovarian cancer, fallopian tube cancer, or primary peritoneal cancer. *J. Clin. Oncol.* **28,** 1215–23 (2010).
135. Robert, C. *et al.* Nivolumab in Previously Untreated Melanoma without BRAF Mutation. *N. Engl. J. Med.* **372,** 320–330 (2015).
136. Antonia, S. *et al.* Nivolumab versus Docetaxel in Advanced Squamous-Cell Non–Small-Cell Lung Cancer. *N. Engl. J. Med.* **373,** 123–135 (2015).
137. Varga, A. et al. Pembrolizumab in patients with programmed death ligand 1–positive advanced ovarian cancer: Analysis of KEYNOTE-028. *Gynecol. Oncol.* **152,** 243–250 (2019).
138. Hamanishi, J. *et al.* Safety and antitumor activity of Anti-PD-1 antibody, nivolumab, in patients with platinum-resistant ovarian cancer. *J. Clin. Oncol.* **33,** 4015–22 (2015).
139. Avelumab fails to extend PFS in ovarian cancer. Available at: https://www.healio.com/hematology-oncology/gynecologic-cancer/news/online/%7B8c362a46-e38f-4c1c-b943-706c5382097b%7D/avelumab-fails-to-extend-pfs-in-ovarian-cancer. (Accessed: 10th March 2019)
140. ClinicalTrials.gov NCT02718417. A Randomized, Open-LABEL., Multicenter, Phase 3 Study to Evaluate the Efficacy and Safety of Avelumab (msb0010718c) in Combination with and/or Following Chemotherapy in Patients with Previously Untreated Epithelial Ovarian .
141. Konstantinopoulos PA, Waggoner SE, Vidal GA, et al. TOPACIO/KEYNOTE-162 (NCT02657889): a phase 1/2 study of niraparib + pembrolizumab in patients (pts) with advanced triple-negative breast cancer or recurrent ovarian cancer (ROC)—results from ROC cohort. *J Clin Oncol* **36,** Abstract 106 (2018).
142. OncLive. PARP/Immunotherapy Combo Shows Promise in Recurrent Ovarian Cancer. Available at: https://www.onclive.com/web-exclusives/parpimmunotherapy-combo-shows-promise-in-recurrent-ovarian-cancer. (Accessed: 10th March 2019)
143. Hortobagyi, G. N. *et al.* Ribociclib as First-Line Therapy for HR-Positive, Advanced Breast Cancer. *N. Engl. J. Med.* **375,** 1738–1748 (2016).
144. Konecny, G. E. *et al.* Expression of p16 and retinoblastoma determines response to CDK4/6 inhibition in ovarian cancer. *Clin. Cancer Res.* **17,** 1591–602 (2011).

145. Patnaik, A. *et al.* Efficacy and safety of Abemaciclib, an inhibitor of CDK4 and CDK6, for patients with breast cancer, non–small cell lung cancer, and other solid tumors. *Cancer Discov.* **6,** 740–53 (2016).

146. ClinicalTrials.gov NCT02897375. Palbociclib With Cisplatin or Carboplatin in Advanced Solid Tumors. [(accessed on 07 March 2019)]; Available at: https://clinicaltrials.gov/ct2/show/NCT02897375.

147. Colon-Otero, G. *et al.* Phase 2 trial of everolimus and letrozole in relapsed estrogen receptor-positive high-grade ovarian cancers. *Gynecol. Oncol.* **146,** 64–68 (2017).

148. Xue, Y. *et al.* CDK4/6 inhibitors target SMARCA4-determined cyclin D1 deficiency in hypercalcemic small cell carcinoma of the ovary. *Nat. Commun.* **10,** 558 (2019).

149. Hartwell, L. H. Cell division from a genetic perspective. *J. Cell Biol.* **77,** 627–37 (1978).

150. Hunt, T. Cyclins and their partners: from a simple idea to complicated reality. *Semin. Cell Biol.* **2,** 213–22 (1991).

151. Minshull, J. *et al.* The role of cyclin synthesis, modification and destruction in the control of cell division. *J. Cell Sci. Suppl.* **12,** 77–97 (1989).

152. Malumbres, M. & Barbacid, M. Mammalian cyclin-dependent kinases. *Trends Biochem. Sci.* **30,** 630–41 (2005).

153. Nigg, E. A. Cyclin-dependent protein kinases: Key regulators of the eukaryotic cell cycle. *BioEssays* **17,** 471–80 (1995).

154. El-Aouar Filho, R. A. *et al.* Heterogeneous family of cyclomodulins: Smart weapons that allow bacteria to hijack the eukaryotic cell cycle and promote infections. *Front. Cell. Infect. Microbiol.* **23,** 208 (2017).

155. Takizawa, C. G. & Morgan, D. O. Control of mitosis by changes in the subcellular location of cyclin-B1-Cdk1 and Cdc25C. *Curr. Opin. Cell Biol.* **12,** 658–65 (2000).

156. Heim, A., Rymarczyk, B., Malhotra, S. & Mayer, T. U. in *Advances in Experimental Medicine and Biology* **953,** 83–116 (2017).

157. Combes, G., Alharbi, I., Braga, L. G. & Elowe, S. Playing polo during mitosis: PLK1 takes the lead. *Oncogene* **36,** 4819–4827 (2017).

158. Fry, A. M., O'Regan, L., Sabir, S. R. & Bayliss, R. Cell cycle regulation by the NEK family of protein kinases. *J. Cell Sci.* **125,** 4423–33 (2012).

159. Crane, R., Gadea, B., Littlepage, L., Wu, H. & Ruderman, J. V. Aurora A, meiosis and mitosis. *Biol. Cell* **96,** 215–29 (2004).

160. Welburn, J. P. I. The molecular basis for kinesin functional specificity during mitosis. *Cytoskeleton* **70,** 476–93 (2013).

161. Kinoshita, K. & Hirano, T. Dynamic organization of mitotic chromosomes. *Curr. Opin. Cell Biol.* **46,** 46–53 (2017).

162. Burgess, A., Vuong, J., Rogers, S., Malumbres, M. & O'Donoghue, S. I. SnapShot: Phosphoregulation of Mitosis. *Cell* **169,** 1358–1358 (2017).

163. Kim, H.-S., Fernandes, G. & Lee, C.-W. Protein Phosphatases Involved in Regulating Mitosis: Facts and Hypotheses. *Mol. Cells* **39,** 654–62 (2016).

164. Gilberto, S. & Peter, M. Dynamic ubiquitin signaling in cell cycle regulation. *J. Cell Biol.* **216,** 2259 (2017).

165. Hershko, A. Mechanisms and regulation of the degradation of cyclin B. *Philos. Trans. R. Soc. B Biol. Sci.* **354,** 1571–1576 (1999).

166. Shaltiel, I. A., Krenning, L., Bruinsma, W. & Medema, R. H. The same, only different - DNA damage checkpoints and their reversal throughout the cell cycle. *J. Cell Sci.* **128,** 607–20 (2015).

167. Harashima, H., Dissmeyer, N. & Schnittger, A. Cell cycle control across the eukaryotic kingdom. *Trends Cell Biol.* **23,** 345–56 (2013).

168. Negrini, S., Gorgoulis, V. G. & Halazonetis, T. D. Genomic instability an evolving hallmark of cancer. *Nat. Rev. Mol. Cell Biol.* **11,** 220–8 (2010).

169. Jordan, M. A. & Wilson, L. Microtubules as a target for anticancer drugs. *Nat. Rev. Cancer* **4,** 253–65 (2004).

170. Orr, G. A., Verdier-Pinard, P., McDaid, H. & Horwitz, S. B. Mechanisms of Taxol resistance related to microtubules. *Oncogene* **4,** 253–65 (2003).

171. Wang, T. H., Wang, H. S. & Soong, Y. K. Paclitaxel-induced cell death: Where the cell cycle and apoptosis come together. *Cancer* **88,** 2619–28 (2000).

172. Weaver, B. A. How Taxol/paclitaxel kills cancer cells. *Mol. Biol. Cell* **25,** 2677–2681 (2014).

173. Marty, M. *et al.* Advances in vinca-alkaloids: Navelbine. *Nouv Rev Fr Hematol* **31,** 77–84 (1989).

174. Hortobagyi, G. N. & Kris, M. G. Expanding horizons: An update on the use of docetaxel in non[ndash]small cell lung, ovarian, and breast cancers. *Semin. Oncol.* **29,** 1–3 (2002).
175. Kavallaris, M. Microtubules and resistance to tubulin-binding agents. *Nat. Rev. Cancer* **10,** 194–204 (2010).
176. Dominguez-Brauer, C. *et al.* Targeting Mitosis in Cancer: Emerging Strategies. *Molecular Cell* **60,** 524–536 (2015).
177. Musacchio, A. & Salmon, E. D. The spindle-assembly checkpoint in space and time. *Nat. Rev. Mol. Cell Biol.* **8,** 379–93 (2007).
178. Gascoigne, K. E. & Taylor, S. S. Cancer Cells Display Profound Intra- and Interline Variation following Prolonged Exposure to Antimitotic Drugs. *Cancer Cell* **14,** 111–22 (2008).
179. Brito, D. A. & Rieder, C. L. The ability to survive mitosis in the presence of microtubule poisons differs significantly between human nontransformed (RPE-1) and cancer (U2OS, HeLa) cells. *Cell Motil. Cytoskeleton* **66,** 437–47 (2009).
180. Shi, J., Orth, J. D. & Mitchison, T. Cell type variation in responses to antimitotic drugs that target microtubules and kinesin-5. *Cancer Res.* **68,** 3269–76 (2008).
181. Cheng, B. & Crasta, K. Consequences of mitotic slippage for antimicrotubule drug therapy. *Endocr. Relat. Cancer* **24,** 97–106 (2017).
182. Gascoigne, K. E. & Taylor, S. S. How do anti-mitotic drugs kill cancer cells? *J. Cell Sci.* **122,** 2579–85 (2009).
183. Topham, C. H. & Taylor, S. S. Mitosis and apoptosis: How is the balance set? *Curr. Opin. Cell Biol.* **25,** 780–5 (2013).
184. Haschka, M., Karbon, G., Fava, L. L. & Villunger, A. Perturbing mitosis for anti-cancer therapy: is cell death the only answer? *EMBO Rep.* **19,** e45440 (2018).
185. Bah, N. *et al.* Bcl-xL controls a switch between cell death modes during mitotic arrest. *Cell Death Dis.* **12,** e1291 (2014).
186. Deng, X., Gao, F., Flagg, T. & May, W. S. Mono- and multisite phosphorylation enhances Bcl2's antiapoptotic function and inhibition of cell cycle entry functions. *Proc. Natl. Acad. Sci.* **101,** 153–8 (2004).
187. Fhearraigh, S. Mac & Mc Gee, M. M. Cyclin B1 interacts with the BH3-only protein Bim and mediates its phosphorylation by Cdk1 during mitosis. *Cell Cycle* **10,** 3886–96 (2011).
188. Terrano, D. T., Upreti, M. & Chambers, T. C. Cyclin-Dependent Kinase 1-Mediated Bcl-xL/Bcl-2 Phosphorylation Acts as a Functional Link Coupling Mitotic Arrest and Apoptosis. *Mol. Cell. Biol.* **30,** 640–56 (2009).
189. Huang, H. C., Shi, J., Orth, J. D. & Mitchison, T. J. Evidence that Mitotic Exit Is a Better Cancer Therapeutic Target Than Spindle Assembly. *Cancer Cell* **16,** 347–58 (2009).
190. Haschka, M. D. *et al.* The NOXA-MCL1-BIM axis defines lifespan on extended mitotic arrest. *Nat. Commun.* **6,** 6891 (2015).
191. Harley, M. E., Allan, L. A., Sanderson, H. S. & Clarke, P. R. Phosphorylation of Mcl-1 by CDK1-cyclin B1 initiates its Cdc20-dependent destruction during mitotic arrest. *EMBO J.* **29,** 2407–20 (2010).
192. Wertz, I. E. *et al.* Sensitivity to antitubulin chemotherapeutics is regulated by MCL1 and FBW7. *Nature* **471,** 110–4 (2011).
193. Shi, J., Zhou, Y., Huang, H. C. & Mitchison, T. J. Navitoclax (ABT-263) accelerates apoptosis during drug-induced mitotic arrest by antagonizing Bcl-xL. *Cancer Res.* **71,** 4518–26 (2011).
194. Tan, N. *et al.* Navitoclax enhances the efficacy of taxanes in non-small cell lung cancer models. *Clin. Cancer Res.* **17,** 1394–404 (2011).
195. Allan, L. A. & Clarke, P. R. Phosphorylation of Caspase-9 by CDK1/Cyclin B1 Protects Mitotic Cells against Apoptosis. *Mol. Cell* **26,** 301–10 (2007).
196. Topham, C. *et al.* MYC Is a Major Determinant of Mitotic Cell Fate. *Cancer Cell* **28,** 129–40 (2015).
197. McMahon, S. B. MYC and the control of apoptosis. *Cold Spring Harb. Perspect. Med.* **4,** a014407 (2014).
198. Hoffman, B. & Liebermann, D. A. Apoptotic signaling by c-MYC. *Oncogene* **27,** 6462–72 (2008).
199. Cisyk, A. L. *et al.* Characterizing the Prevalence of Chromosome Instability in Interval Colorectal Cancer. *Neoplasia* **17,** 306–316 (2015).
200. Burrell, R. A. *et al.* Replication stress links structural and numerical cancer chromosomal instability. *Nature* **494,** 492–496 (2013).
201. Bakhoum, S. F. & Compton, D. A. Chromosomal instability and cancer: A complex relationship with therapeutic potential. *J. Clin. Invest.* **122,** 1138–43 (2012).
202. Thompson, S. L., Bakhoum, S. F. & Compton, D. A. Mechanisms of Chromosomal Instability. *Curr. Biol.* **20,** 285–95 (2010).

203. Ganem, N. J., Godinho, S. A. & Pellman, D. A mechanism linking extra centrosomes to chromosomal instability. *Nature* **460,** 278–282 (2009).

204. Carter, S. L., Eklund, A. C., Kohane, I. S., Harris, L. N. & Szallasi, Z. A signature of chromosomal instability inferred from gene expression profiles predicts clinical outcome in multiple human cancers. *Nat. Genet.* **38,** 1043–8 (2006).

205. Lengauer, C., Kinzler, K. W. & Vogelstein, B. Genetic instability in colorectal cancers. *Nature* **386,** 623–7 (1997).

206. Thompson, L. L., Jeusset, L. M. P., Lepage, C. C. & McManus, K. J. Evolving therapeutic strategies to exploit chromosome instability in cancer. *Cancers (Basel).* **9,** E151 (2017).

207. Ertych, N. *et al.* Increased microtubule assembly rates influence chromosomal instability in colorectal cancer cells. *Nat. Cell Biol.* **16,** 779–91 (2014).

208. Manning, A. L. *et al.* Suppression of genome instability in prb-deficient cells by enhancement of chromosome cohesion. *Mol. Cell* **53,** 993–1004 (2014).

209. Burrell, R. A., McGranahan, N., Bartek, J. & Swanton, C. The causes and consequences of genetic heterogeneity in cancer evolution. *Nature* **501,** 338–345 (2013).

210. Birkbak, N. J. *et al.* Paradoxical relationship between chromosomal instability and survival outcome in cancer. *Cancer Res.* **71,** 3447–52 (2011).

211. Jamal-Hanjani, M. *et al.* Extreme chromosomal instability forecasts improved outcome in ER-negative breast cancer: A prospective validation cohort study from the TACT trial. *Ann. Oncol.* **26,** 1340–6 (2015).

212. Zasadil, L. M. *et al.* Cytotoxicity of paclitaxel in breast cancer is due to chromosome missegregation on multipolar spindles. *Sci. Transl. Med.* **6,** 229ra43 (2014).

213. Bae, T. *et al.* Restoration of paclitaxel resistance by CDK1 intervention in drug-resistant ovarian cancer. *Carcinogenesis* **36,** 1561–71 (2015).

214. Zhang, R. *et al.* The aberrant upstream pathway regulations of CDK1 protein were implicated in the proliferation and apoptosis of ovarian cancer cells. *J. Ovarian Res.* **10,** 60 (2017).

215. Knezevic, D. *et al.* Selective small-molecule inhibitor reveals critical mitotic functions of human CDK1. *Proc. Natl. Acad. Sci.* **103,** 10660–5 (2006).

216. Zhang, P. *et al.* Targeting CDK1 and MEK/ERK Overcomes Apoptotic Resistance in BRAF-Mutant Human Colorectal Cancer. *Mol. Cancer Res.* **16,** 378–389 (2017).

217. Abate, A. A., Pentimalli, F., Esposito, L. & Giordano, A. ATP-noncompetitive CDK inhibitors for cancer therapy: an overview. *Expert Opin. Investig. Drugs* **22,** 895–906 (2013).

218. Gelbert, L. M. *et al.* Preclinical characterization of the CDK4/6 inhibitor LY2835219: In-vivo cell cycle-dependent/independent anti-tumor activities alone/in combination with gemcitabine. *Invest. New Drugs* **32,** 825–37 (2014).

219. Murphy, C. G. & Dickler, M. N. The Role of CDK4/6 Inhibition in Breast Cancer. *Oncologist* **20,** 52 (2015).

220. Kurasawa, Y. & Yu-Lee, L. y. PICH and Cotargeted Plk1 Coordinately Maintain Prometaphase Chromosome Arm Architecture. *Mol. Biol. Cell* **21,** 1188–1199 (2010).

221. Rath, O. & Kozielski, F. Kinesins and cancer. *Nat. Rev. Cancer* **12,** 527–539 (2012).

222. Slangy, A. *et al.* Phosphorylation by p34cdc2regulates spindle association of human Eg5, a kinesin-related motor essential for bipolar spindle formation in vivo. *Cell* **83,** 1159–69 (1995).

223. Purcell, J. W. *et al.* Activity of the kinesin spindle protein inhibitor ispinesib (SB-715992) in models of breast cancer. *Clin. Cancer Res.* **16,** 566–76 (2010).

224. Yen, T. J. *et al.* CENP-E, a novel human centromere-associated protein required for progression from metaphase to anaphase. *EMBO J.* **10,** 1245–54 (1991).

225. Mao, Y., Desai, A. & Cleveland, D. W. Microtubule capture by CENP-E silences BubR1-dependent mitotic checkpoint signaling. *J. Cell Biol.* **170,** 873–80 (2005).

226. Putkey, F. R. *et al.* Unstable kinetochore-microtubule capture and chromosomal instability following deletion of CENP-E. *Dev. Cell* **3,** 351–65 (2002).

227. Schauer, S. P. *et al.* Antitumor activity of an allosteric inhibitor of centromere-associated protein-E. *Proc. Natl. Acad. Sci.* **107,** 5839–5844 (2010).

228. Chung, V. *et al.* First-time-in-human study of GSK923295, a novel antimitotic inhibitor of centromere-associated protein e (CENP-E), in patients with refractory cancer. *Cancer Chemother. Pharmacol.* **69,** 733–41 (2012).

229. Block, S. M., Milic, B., Han, K., Bassik, M. C. & Chakraborty, A. KIF15 nanomechanics and kinesin inhibitors, with implications for cancer chemotherapeutics. *Proc. Natl. Acad. Sci.* **115,** 4613–4622 (2018).

230. Tcherniuk, S. *et al.* Relocation of aurora B and survivin from centromeres to the central spindle impaired by a kinesin-specific MKLP-2 inhibitor. *Angew. Chemie - Int. Ed.* **49,** 8228–31 (2010).

231. Varetti, G. & Musacchio, A. The spindle assembly checkpoint. *Curr. Biol.* **22,** 966–80 (2008).

232. Keen, N. & Taylor, S. Mitotic drivers-inhibitors of the Aurora B Kinase. *Cancer Metastasis Rev.* **28,** 185–95 (2009).

233. Salmela, A. L. & Kallio, M. J. Mitosis as an anti-cancer drug target. *Chromosoma* **122,** 431–49 (2013).

234. Abrieu, A. *et al.* Mps1 is a kinetochore-associated kinase essential for the vertebrate mitotic checkpoint. *Cell* **106,** 83–93 (2001).

235. Tighe, A., Staples, O. & Taylor, S. Mps1 kinase activity restrains anaphase during an unperturbed mitosis and targets Mad2 to kinetochores. *J. Cell Biol.* **181,** 893–901 (2008).

236. Wengner, A. M. *et al.* Novel Mps1 Kinase Inhibitors with Potent Antitumor Activity. *Mol. Cancer Ther.* **15,** 583–92 (2016).

237. Colombo, R. *et al.* Targeting the mitotic checkpoint for cancer therapy with NMS-P715, an inhibitor of MPS1 kinase. *Cancer Res.* **70,** 10255–64 (2010).

238. Siemeister, G. *et al.* Inhibition of BUB1 Kinase by BAY 1816032 Sensitizes Tumor Cells towards Taxanes, ATR and PARP Inhibitors in vitro and in vivo. *Clin. Cancer Res.* **25,** 1404–1414 (2018).

239. Kaitna, S., Mendoza, M., Jantsch-Plunger, V. & Glotzer, M. Incenp and an Aurora-like kinase form a complex essential for chromosome segregation and efficient completion of cytokinesis. *Curr. Biol.* **10,** 1172–81 (2000).

240. Xie, F. *et al.* In vitro and in vivo characterization of a benzofuran derivative, a potential anticancer agent, as a novel Aurora B kinase inhibitor. *Eur. J. Med. Chem.* **89,** 310–9 (2015).

241. Ditchfield, C. *et al.* Aurora B couples chromosome alignment with anaphase by targeting BubR1, Mad2, and Cenp-E to kinetochores. *J. Cell Biol.* **161,** 267 (2003).

242. Janssen, A. & Medema, R. H. Mitosis as an anti-cancer target. *Oncogene* **30,** 2799–809 (2011).

243. Lee, M.-H. *et al.* Aurora B kinase phosphorylates and instigates degradation of p53. *Proc. Natl. Acad. Sci.* **109,** 1513–22 (2012).

244. Tao, Y. *et al.* Enhancement of radiation response in p53-deficient cancer cells by the Aurora-B kinase inhibitor AZD1152. *Oncogene* **27,** 3244–55 (2008).

245. Mross, K. *et al.* A phase I study of BI 811283, an Aurora B kinase inhibitor, in patients with advanced solid tumors. *Cancer Chemother. Pharmacol.* **78,** 405–17 (2016).

246. Döhner, H. *et al.* A phase I trial investigating the Aurora B kinase inhibitor BI 811283 in combination with cytarabine in patients with acute myeloid leukaemia. *Br. J. Haematol.* **185,** 583–587 (2018).

247. Voets, E. & Wolthuis, R. M. F. MASTL is the human orthologue of Greatwall kinase that facilitates mitotic entry, anaphase and cytokinesis. *Cell Cycle* **9,** 3591–601 (2010).

248. Álvarez-Fernández, M. *et al.* Therapeutic relevance of the PP2A-B55 inhibitory kinase MASTL/Greatwall in breast cancer. *Cell Death Differ.* **25,** 828–840 (2018).

249. Wang, L., Luong, V. Q., Giannini, P. J. & Peng, A. Mastl kinase, a promising therapeutic target, promotes cancer recurrence. *Oncotarget* **5,** 11479–89 (2015).

250. Rogers, S. *et al.* MASTL overexpression promotes chromosome instability and metastasis in breast cancer. *Oncogene* **37,** 4518–4533 (2018).

251. Ocasio, C. A. *et al.* A first generation inhibitor of human Greatwall kinase, enabled by structural and functional characterisation of a minimal kinase domain construct. *Oncotarget* **7,** 71182–71197 (2015).

252. Ammarah, U., Kumar, A., Pal, R., Bal, N. C. & Misra, G. Identification of new inhibitors against human Great wall kinase using in silico approaches. *Sci. Rep.* **8,** 4894 (2018).

253. O'Connell, M. J., Walworth, N. C. & Carr, A. M. The G2-phase DNA-damage checkpoint. *Trends Cell Biol.* **10,** 296–303 (2000).

254. Ciccia, A. & Elledge, S. J. The DNA Damage Response: Making It Safe to Play with Knives. *Mol. Cell* **40,** 179–204 (2010).

255. Maréchal, A. & Zou, L. DNA damage sensing by the ATM and ATR kinases. *Cold Spring Harb. Perspect. Biol.* **5,** a012716 (2013).

256. Matsuoka, S. *et al.* ATM and ATR substrate analysis reveals extensive protein networks responsive to DNA damage. *Science (80-.).* **316,** 1160–6 (2007).

257. Clinicaltrials.gov Study to Assess the Safety and Preliminary Efficacy of AZD0156 at Increasing Doses Alone or in Combination With Other Anti-cancer Treatment in Patients With Advanced Cancer. (AToM) [Accesed 12 March 2019]. Available at: https://clinicaltrials.gov/ct2/show/results/NCT02588105.

258. Dillon Mt, Boylan Z, Smith D, Guevara J, Mohammed K, Peckitt C. PATRIOT: A phase I study to assess the tolerability, safety and biological effects of a specific ataxia telangiectasia and Rad3-related (ATR) inhibitor (AZD6738) as a single agent and in combination with palliative radiation therapy in patients with solid. *Clin transl Radiat Oncol* **8,** 16–20 (2018).

259. Mendez, E. *et al.* A phase I clinical trial of AZD1775 in combination with neoadjuvant weekly docetaxel and cisplatin before definitive therapy in head and neck squamous cell carcinoma. *Clin. Cancer Res.* **24,** 2740–2748 (2018).

260. Leijen, S. *et al.* Phase II study of WEE1 inhibitor AZD1775 plus carboplatin in patientswith tp53-mutated ovarian cancer refractory or resistant to first-line therapy within 3 months. *J. Clin. Oncol.* **34,** 4354–4361 (2016).

261. Döhner, H. *et al.* Randomized, phase 2 trial of low-dose cytarabine with or without volasertib in AML patients not suitable for induction therapy. *Blood* **124,** 1426–1433 (2014).

262. Sunkel, C. E. & Glover, D. M. polo, a mitotic mutant of Drosophila displaying abnormal spindle poles. *J. Cell Sci.* **89,** 25–38 (1988).

263. Lane, H. A. & Nigg, E. A. Cell-cycle control: POLO-like kinases join the outer circle. *Trends Cell Biol.* **7,** 63–8 (1997).

264. Van De Weerdt, B. C. M. & Medema, R. H. Polo-like kinases: A team in control of the division. *Cell Cycle* **5,** 853–64 (2006).

265. Winkles, J. A. & Alberts, G. F. Differential regulation of polo-like kinase 1, 2, 3, and 4 gene expression in mammalian cells and tissues. *Oncogene* **24,** 260–6 (2005).

266. de Carcer, G. *et al.* Plk5, a Polo Box Domain-Only Protein with Specific Roles in Neuron Differentiation and Glioblastoma Suppression. *Mol. Cell. Biol.* **31,** 1225–39 (2011).

267. Zitouni, S., Nabais, C., Jana, S. C., Guerrero, A. & Bettencourt-Dias, M. Polo-like kinases: Structural variations lead to multiple functions. *Nature Reviews Molecular Cell Biology* **15,** 433–452 (2014).

268. Petronczki, M., Lénárt, P. & Peters, J. M. Polo on the Rise-from Mitotic Entry to Cytokinesis with Plk1. *Dev. Cell* **14,** 646–59 (2008).

269. Liu, X. Targeting polo-like kinases: A promising therapeutic approac for cancer treatment. *Transl. Oncol.* **8,** 185–95 (2015).

270. Lu, L.-Y. *et al.* Polo-Like Kinase 1 Is Essential for Early Embryonic Development and Tumor Suppression. *Mol. Cell. Biol.* **28,** 6870–6 (2008).

271. Roshak, A. K. *et al.* The human polo-like kinase, PLK, regulates cdc2/cyclin B through phosphorylation and activation of the cdc25C phosphatase. *Cell. Signal.* **12,** 405–11 (2000).

272. Kumagai, A. & Dunphy, W. G. Purification and molecular cloning of Plx1, a Cdc25-regulatory kinase from Xenopus egg extracts. *Science (80-.).* **273,** 1377–80 (1996).

273. Inoue, D. & Sagata, N. The Polo-like kinase Plx1 interacts with and inhibits Myt1 after fertilization of Xenopus eggs. *EMBO J.* **24,** 1057–1067 (2005).

274. Watanabe, N. *et al.* M-phase kinases induce phospho-dependent ubiquitination of somatic Wee1 by SCF -TrCP. *Proc. Natl. Acad. Sci.* **101,** 4419–4424 (2004).

275. Lane, H. A. & Nigg, E. A. Antibody microinjection reveals an essential role for human polo-like kinase 1 (Plk1) in the functional maturation of mitotic centrosomes. *J. Cell Biol.* **135,** 1701–13 (1996).

276. Casenghi, M. *et al.* Polo-like kinase 1 regulates Nlp, a centrosome protein involved in microtubule nucleation. *Dev. Cell* **5,** 113–25 (2003).

277. De Luca, M., Lavia, P. & Guarguaglini, G. A functional interplay between Aurora-A, Plk1 and TPX2 at spindle poles: Plk1 controls

centrosomal localization of Aurora-A and TPX2 spindle association. *Cell Cycle* **5,** 296–303 (2006).

278. Strebhardt, K. Multifaceted polo-like kinases: Drug targets and antitargets for cancer therapy. *Nat. Rev. Drug Discov.* **9,** 643–60 (2010).
279. Sumara, I. *et al.* The dissociation of cohesin from chromosomes in prophase is regulated by polo-like kinase. *Mol. Cell* **9,** 515–25 (2002).
280. Golan, A., Yudkovsky, Y. & Hershko, A. The cyclin-ubiquitin ligase activity of cyclosome/APC is jointly activated by protein kinases Cdk1-cyclin B and Plk. *J. Biol. Chem.* **277,** 15552–7 (2002).
281. Neef, R. *et al.* Choice of Plk1 docking partners during mitosis and cytokinesis is controlled by the activation state of Cdk1. *Nat. Cell Biol.* **9,** 436–444 (2007).
282. Neef, R. *et al.* Phosphorylation of mitotic kinesin-like protein 2 by polo-like kinase 1 is required for cytokinesis. *J. Cell Biol.* **162,** 863–75 (2003).
283. Wolfe, B. A., Takaki, T., Petronczki, M. & Glotzer, M. Polo-like kinase 1 directs assembly of the HsCyk-4 RhoGAP/Ect2 RhoGEF complex to initiate cleavage furrow formation. *PLoS Biol.* **7,** e1000110 (2009).
284. Barr, F. A., Silljé, H. H. W. & Nigg, E. A. Polo-like kinases and the orchestration of cell division. *Nat. Rev. Mol. Cell Biol.* **5,** 429–40 (2004).
285. Takaki, T., Trenz, K., Costanzo, V. & Petronczki, M. Polo-like kinase 1 reaches beyond mitosis-cytokinesis, DNA damage response, and development. *Curr. Opin. Cell Biol.* **20,** 650–60 (2008).
286. Tsvetkov, L. & Stern, D. F. Interaction of chromatin-associated Plk1 and Mcm7. *J. Biol. Chem.* **280,** 11943–7 (2005).
287. Yim, H. & Erikson, R. L. Polo-Like Kinase 1 Depletion Induces DNA Damage in Early S Prior to Caspase Activation. *Mol. Cell. Biol.* **29,** 2609–21 (2009).
288. Wu, Z. Q., Yang, X., Weber, G. & Liu, X. Plk1 phosphorylation of TRF1 is essential for its binding to telomeres. *J. Biol. Chem.* **283,** 25503–13 (2008).
289. Ando, K. *et al.* Polo-like kinase 1 (Plk1) inhibits p53 function by physical interaction and phosphorylation. *J. Biol. Chem.* **279,** 25549–61 (2004).
290. Momand, J., Wu, H. H. & Dasgupta, G. MDM2 - Master regulator of the p53 tumor suppressor protein. *Gene* **242,** (2000).
291. Kreis, N. N. *et al.* Long-term downregulation of Polo-like kinase 1 increases the cyclin-dependent kinase inhibitor p21WAF1/CIP1. *Cell Cycle* **8,** 460–72 (2009).
292. De Cárcer, G. *et al.* Plk1 regulates contraction of postmitotic smooth muscle cells and is required for vascular homeostasis. *Nat. Med.* **23,** 964–974 (2017).
293. Lee, M. Y., Daniels, M. J. & Venkitaraman, A. R. Phosphorylation of BRCA2 by the Polo-like kinase Plk1 is regulated by DNA damage and mitotic progression. *Oncogene* **23,** 865–72 (2004).
294. Tsvetkov, L., Xu, X., Li, J. & Stern, D. F. Polo-like kinase 1 and Chk2 interact and co-localize to centrosomes and the midbody. *J. Biol. Chem.* **278,** 8468–75 (2003).
295. Van Vugt, M. A. T. M., Smits, V. A. J., Klompmaker, R. & Medema, R. H. Inhibition of Polo-like Kinase-1 by DNA Damage Occurs in an ATM- or ATR-dependent Fashion. *J. Biol. Chem.* **276,** 41656–60 (2001).
296. Ree, A. H., Bratland, Å., Nome, R. V., Stokke, T. & Fodstad, Ø. Repression of mRNA for the PLK cell cycle gene after DNA damage requires BRCA1. *Oncogene* **22,** 8952–5 (2003).
297. Zhang, Y. *et al.* Reciprocal activation between PLK1 and Stat3 contributes to survival and proliferation of esophageal cancer cells. *Gastroenterology* **142,** 521–530 (2012).
298. Fu, Z. *et al.* Plk1-dependent phosphorylation of FoxM1 regulates a transcriptional programme required for mitotic progression. *Nat. Cell Biol.* **10,** 1076–82 (2008).
299. Arai, T. *et al.* Identification of β-catenin as a novel substrate of Polo-like kinase 1. *Cell Cycle* **7,** 3556–63 (2008).
300. Gunawardena, R. W. *et al.* Hierarchical requirement of SWI/SNF in retinoblastoma tumor suppressor-mediated repression of Plk1. *J. Biol. Chem.* **279,** 29278–85 (2004).
301. Liu, X. S. *et al.* Polo-like kinase 1 facilitates loss of Pten tumor suppressorinduced prostate cancer formation. *J. Biol. Chem.* **286,**

35795–800 (2011).

302. Kasahara, K. *et al.* PI 3-kinase-dependent phosphorylation of Plk1-Ser99 promotes association with 14-3-3γ and is required for metaphase-anaphase transition. *Nat. Commun.* **4,** 1882 (2013).

303. Vogelstein, B. *et al.* Cancer genome landscapes. *Science (80-.).* **339,** 1546–58 (2013).

304. Cholewa, B. D., Liu, X. & Ahmad, N. The role of polo-like kinase 1 in carcinogenesis: Cause or consequence? *Cancer Res.* **73,** 6848–55 (2013).

305. Strebhardt, K., Kneisel, L., Linhart, C., Bernd, A. & Kaufmann, R. Prognostic value of pololike kinase expression in melanomas. *J. Am. Med. Assoc.* **283,** 479–80 (2000).

306. Knecht, R. *et al.* Prognostic significance of polo-like kinase (PLK) expression in squamous cell carcinomas of the head and neck. *Cancer Res.* **59,** 2794–7 (1999).

307. Liu, X. & Erikson, R. L. Polo-like kinase (Plk) 1 depletion induces apoptosis in cancer cells. *Proc. Natl. Acad. Sci. U. S. A.* **100,** 5789–94 (2003).

308. Lénárt, P. *et al.* The Small-Molecule Inhibitor BI 2536 Reveals Novel Insights into Mitotic Roles of Polo-like Kinase 1. *Curr. Biol.* **17,** 304–15 (2007).

309. Steegmaier, M. *et al.* BI 2536, a Potent and Selective Inhibitor of Polo-like Kinase 1, Inhibits Tumor Growth In Vivo. *Curr. Biol.* **17,** 316–22 (2007).

310. Gutteridge, R. E. A., Ndiaye, M. A., Liu, X. & Ahmad, N. Plk1 Inhibitors in Cancer Therapy: From Laboratory to Clinics. *Mol. Cancer Ther.* **15,** 1427–35 (2016).

311. Wang, J. *et al.* Suppression of KRas-mutant cancer through the combined inhibition of KRAS with PLK1 and ROCK. *Nat. Commun.* **7,** 11363 (2016).

312. Luo, J. *et al.* A Genome-wide RNAi Screen Identifies Multiple Synthetic Lethal Interactions with the Ras Oncogene. *Cell* **137,** 835–48 (2009).

313. Ren, Y. *et al.* PLK1 stabilizes a MYC-dependent kinase network in aggressive B cell lymphomas. *J. Clin. Invest.* **128,** 5517–5530 (2018).

314. Kiyokawa, J. *et al.* PLK1 Inhibition Targets Myc-Activated Malignant Glioma Cells Irrespective of Mismatch Repair Deficiency–Mediated Acquired Resistance to Temozolomide. *Mol. Cancer Ther.* **17,** 2551–2563 (2018).

315. Bhola, N. E. *et al.* Kinome-wide functional screen identifies role of PLK1 in hormone-independent, ER-positive breast cancer. *Cancer Res.* **75,** 405–14 (2015).

316. Yao, Y. D. *et al.* Targeted delivery of PLK1-siRNA by ScFv suppresses Her2+breast cancer growth and metastasis. *Sci. Transl. Med.* **4,** 130ra48 (2012).

317. Jeong, S. B. *et al.* Essential role of Polo-like kinase 1 (Plk1) oncogene in tumor growth and metastasis of tamoxifen-resistant breast cancer. *Mol. Cancer Ther.* **17,** 825–837 (2018).

318. Liu, X. S. *et al.* Plk1 Phosphorylation of Orc2 and Hbo1 Contributes to Gemcitabine Resistance in Pancreatic Cancer. *Mol. Cancer Ther.* **12,** 58–68 (2012).

319. Pujade-Lauraine, E. *et al.* Volasertib versus chemotherapy in platinum-resistant or-refractory ovarian cancer: A randomized phase II groupe des investigateurs nationaux pour l'etude des cancers de l'ovaire study. *J. Clin. Oncol.* **34,** 706–713 (2016).

320. Fu, F., Nowak, M. A. & Bonhoeffer, S. Spatial Heterogeneity in Drug Concentrations Can Facilitate the Emergence of Resistance to Cancer Therapy. *PLoS Comput. Biol.* **11,** e1004142 (2015).

321. Van den Bossche, J. *et al.* Spotlight on Volasertib: Preclinical and Clinical Evaluation of a Promising Plk1 Inhibitor. *Medicinal Research Reviews* **36,** 749–786 (2016).

322. Goroshchuk, O., Kolosenko, I., Vidarsdottir, L., Azimi, A. & Palm-Apergi, C. Polo-like kinases and acute leukemia. *Oncogene* **38,** 1–16 (2019).

323. Gumireddy, K. *et al.* ON01910, a non-ATP-competitive small molecule inhibitor of Plk1, is a potent anticancer agent. *Cancer Cell* **7,** 275–86 (2005).

324. Chapman, C. M. *et al.* ON 01910.Na is selectively cytotoxic for chronic lymphocytic leukemia cells through a dual mechanism of

action involving PI3K/AKT inhibition and induction of oxidative stress. *Clin. Cancer Res.* **18,** 1979–91 (2012).

325. Christoph, D. C. & Schuler, M. Polo-like kinase 1 inhibitors in mono- and combination therapies: A new strategy for treating malignancies. *Expert Rev. Anticancer Ther.* **11,** 1115–30 (2011).
326. Awada, A. *et al.* Phase I trial of volasertib, a Polo-like kinase inhibitor, plus platinum agents in solid tumors: Safety, pharmacokinetics and activity. *Invest. New Drugs* **33,** 611–20 (2015).
327. Hutterer, A. *et al.* Mitotic Activation of the Kinase Aurora-A Requires Its Binding Partner Bora. *Dev. Cell* **11,** 147–157 (2006).
328. Noatynska, A., Panbianco, C. & Gotta, M. SPAT-1/Bora acts with Polo-like kinase 1 to regulate PAR polarity and cell cycle progression. *Development* **137,** 3315–25 (2010).
329. Tavernier, N., Panbianco, C., Gotta, M. & Pintard, L. Cdk1 plays matchmaker for the Polo-like kinase and its activator SPAT-1/Bora. *Cell Cycle* **14,** 2394–2398 (2015).
330. Seki, A., Coppinger, J. A., Jang, C. Y., Yates, J. R. & Fang, G. Bora and the kinase Aurora A cooperatively activate the kinase Plk1 and control mitotic entry. *Science (80-.).* **320,** 1655–1658 (2008).
331. Macůrek, L. *et al.* Polo-like kinase-1 is activated by aurora A to promote checkpoint recovery. *Nature* **455,** 119–23 (2008).
332. Vigneron, S. *et al.* Cyclin A-cdk1-Dependent Phosphorylation of Bora Is the Triggering Factor Promoting Mitotic Entry. *Dev. Cell* **45,** 637–650 (2018).
333. Thomas, Y. *et al.* Cdk1 Phosphorylates SPAT-1/Bora to Promote Plk1 Activation in C. elegans and Human Cells. *Cell Rep.* **15,** 510–518 (2016).
334. Tavernier, N. *et al.* Cdk1 phosphorylates SPAT-1/Bora to trigger PLK-1 activation and drive mitotic entry in C. elegans embryos. *J. Cell Biol.* **208,** 661 (2015).
335. Parrilla, A. *et al.* Mitotic entry: The interplay between Cdk1, Plk1 and Bora. *Cell Cycle* **4101,** 1–6 (2016).
336. Bruinsma, W., Macůrek, L., Freire, R., Lindqvist, A. & Medema, R. H. Bora and Aurora-A continue to activate Plk1 in mitosis. *J. Cell Sci.* **127,** 801–811 (2014).
337. Zheng, G. & Yu, H. Cyclin A Turns on Bora to Light the Path to Mitosis. *Dev. Cell* **45,** 542–543 (2018).
338. Chan, E. H. Y., Santamaria, A., Silljé, H. H. W. & Nigg, E. A. Plk1 regulates mitotic Aurora A function through βTrCP-dependent degradation of hBora. *Chromosoma* **117,** 457–469 (2008).
339. Feine O, Hukasova E, Bruinsma W, Freire R, Fainsod A, Gannon J, Mahbubani HM, Lindqvist A, B. M. Phosphorylation-mediated stabilization of Bora in mitosis coordinates Plx1/Plk1 and Cdk1 oscillations. *Cell Cycle* **13,** 1727–36 (2014).
340. Lee, Y. C. *et al.* Glycogen synthase kinase 3 β activity is required for hBora/Aurora A-mediated mitotic entry. *Cell Cycle* **12,** 953–60 (2013).
341. Bo Qin, Bowen Gao, Jia Yu, Jian Yuan, Z. Lou. Ataxia Telangiectasia-mutated- and Rad3-related Protein Regulates the DNA Damage-induced G2/M Checkpoint through the Aurora A Cofactor Bora Protein. *J. Biol. Chem.* **288,** 16139–16144 (2013).
342. Lössl, P. *et al.* Deciphering the interplay among multisite phosphorylation, interaction dynamics, and conformational transitions in a tripartite protein system. *ACS Cent. Sci.* **2,** 445–455 (2016).
343. Bruinsma, W. *et al.* Spatial Separation of Plk1 Phosphorylation and Activity. *Front. Oncol.* **5,** 1–8 (2015).
344. Jang, Y. J., Ma, S., Terada, Y. & Erikson, R. L. Phosphorylation of threonine 210 and the role of serine 137 in the regulation of mammalian polo-like kinase. *J. Biol. Chem.* **277,** 4415–20 (2002).
345. Lindqvist, A., Rodríguez-Bravo, V. & Medema, R. H. The decision to enter mitosis: feedback and redundancy in the mitotic entry network. *J. Cell Biol.* **185,** 193–202 (2009).
346. Seki, A. *et al.* Plk1- and β-TrCP-dependent degradation of Bora controls mitotic progression. *J. Cell Biol.* **181,** 65–78 (2008).
347. Chen, C. *et al.* Defining a common region of deletion at 13q21 in human cancers. *Genes Chromosom. Cancer* **31,** 333–44 (2001).
348. Dong, J. T., Chen, C., Stultz, B. G., Isaacs, J. T. & Frierson H.F., J. Deletion at 13q21 is associated with aggressive prostate cancers. *Cancer Res.* **60,** 3880–3883 (2000).
349. Dong, J. T., Boyd, J. C. & Frierson, H. F. Loss of heterozygosity at 13q14 and 13q21 in high grade, high stage prostate cancer. *Prostate* **49,** 166–71 (2001).
350. Wright, P. E. & Dyson, H. J. Intrinsically disordered proteins in cellular signalling and regulation. *Nat. Rev. Mol. Cell Biol.* **16,** 18–

29 (2015).

351. Zhang, Q.-X. *et al.* Cell cycle protein bora serves as a novel poor prognostic factor in multiple adenocarcinomas. *Oncotarget* **8,** 43838–43852 (2017).
352. Huang, D. W., Sherman, B. T. & Lempicki, R. A. Systematic and integrative analysis of large gene lists using DAVID bioinformatics resources. *Nat. Protoc.* **4,** 44–57 (2009).
353. Gyorffy, B., Lánczky, A. & Szállási, Z. Implementing an online tool for genomewide validation of survival-associated biomarkers in ovarian-cancer using microarray data from 1287 patients. *Endocr. Relat. Cancer* **19,** 197–208 (2012).
354. Livak, K. J. & Schmittgen, T. D. Analysis of relative gene expression data using real-time quantitative PCR and the 2-ΔΔCT method. *Methods* **25,** 402–408 (2001).
355. Shepherd, T. G., Thériault, B. L., Campbell, E. J. & Nachtigal, M. W. Primary culture of ovarian surface epithelial cells and ascites-derived ovarian cancer cells from patients. *Nat. Protoc.* **1,** 2643–2649 (2007).
356. Addgene. pLKO.1 - TRC Cloning Vector - ADDGENE. (2006). Available at: https://www.addgene.org/tools/protocols/plko/.
357. Ann Ran, F. *et al.* Genome engineering using the CRIPR-Cas9 system. *Nat. Protoc.* **8,** 2281–2308 (2013).
358. Liu, D., Davydenko, O. & Lampson, M. A. Polo-like kinase-1 regulates kinetochore-microtubule dynamics and spindle checkpoint silencing. *J. Cell Biol.* **198,** 491–9 (2012).
359. Naldini, L., Blomer, U., Gage, F. H., Trono, D. & Verma, I. M. Efficient transfer, integration, and sustained long-term expression of the transgene in adult rat brains injected with a lentiviral vector. *Proc. Natl. Acad. Sci.* **93,** 11382–11388 (1996).
360. Jubierre, L. *et al.* BRG1/SMARCA4 is essential for neuroblastoma cell viability through modulation of cell death and survival pathways. *Oncogene* **35,** 5179–5190 (2016).
361. Chou, T. C. Drug combination studies and their synergy quantification using the chou-talalay method. *Cancer Research* **70,** 440–446 (2010).
362. Tramier, M., Zahid, M., Mevel, J. C., Masse, M. J. & Coppey-Moisan, M. Sensitivity of CFP/YFP and GFP/mCherry pairs to donor photobleaching on FRET determination by fluorescence lifetime imaging microscopy in living cells. *Microsc. Res. Tech.* **69,** 933–9 (2006).
363. Institute, N. C. The Cancer Genoma Atlas Program https://www.cancer.gov/about-nci/organization/ccg/research/structural-genomics/tcga.
364. Ogden, A., Rida, P. C. G. & Aneja, R. Prognostic value of CA20, a score based on centrosome amplificationassociated genes, in breast tumors. *Sci. Rep.* **7,** 262 (2017).
365. Bottoni, P. & Scatena, R. The role of CA 125 as tumor marker: Biochemical and clinical aspects. *Adv. Exp. Med. Biol.* **867,** 229–44 (2015).
366. Cucchi, U. *et al.* Phosphorylation of TCTP as a marker for polo-like kinase-1 activity in vivo. *Anticancer Res.* **30,** 4973–4986 (2010).
367. Hu, G. *et al.* The pINDUCER lentiviral toolkit for inducible RNA interference in vitro and in vivo. *Proc. Natl. Acad. Sci.* **108,** 3665–3670 (2011).
368. Cifone, M. A. & Fidler, I. J. Correlation of patterns of anchorage-independent growth with in vivo behavior of cells from a murine fibrosarcoma. *Proc. Natl. Acad. Sci.* **77,** 1039–1043 (1980).
369. Mori, S. *et al.* Anchorage-independent cell growth signature identifies tumors with metastatic potential. *Oncogene* **28,** 2796–805 (2009).
370. Sasaki, R. *et al.* Oncogenic transformation of human ovarian surface epithelial cells with defined cellular oncogenes. *Carcinogenesis* **30,** 423–431 (2009).
371. Ran, F. A. *et al.* Genome engineering using the CRISPR-Cas9 system. *Nat. Protoc.* **8,** 2281–2308 (2013).
372. Szender, J. B. *et al.* Impact of ascites volume on clinical outcomes in ovarian cancer: A cohort study. *Gynecol. Oncol.* **146,** 491–497 (2017).
373. Kipps, E., Tan, D. S. P. & Kaye, S. B. Meeting the challenge of ascites in ovarian cancer: New avenues for therapy and research. *Nature Reviews Cancer* **13,** 273–282 (2013).

374. Beaver, J. A. *et al.* FDA approval: Palbociclib for the treatment of postmenopausal patients with estrogen receptor-positive, HER2-negative metastatic breast cancer. *Clin. Cancer Res.* **21,** 4760–4766 (2015).

375. Roberts, A. W. *et al.* Targeting BCL2 with venetoclax in relapsed chronic lymphocytic leukemia. *N. Engl. J. Med.* **374,** 311–322 (2016).

376. Harter, P. *et al.* Prospective validation study of a predictive score for operability of recurrent ovarian cancer: The multicenter intergroup study DESKTOP II. A project of the AGO kommission OVAR, AGO study group, NOGGO, AGO-Austria, and MITO. *Int. J. Gynecol. Cancer* **21,** 289–95 (2011).

377. Kossaï, M., Leary, A., Scoazec, J. Y. & Genestie, C. Ovarian Cancer: A Heterogeneous Disease. *Pathobiology* **85,** 41–49 (2018).

378. Penna, L. S., Henriques, J. A. P. & Bonatto, D. Anti-mitotic agents: Are they emerging molecules for cancer treatment? *Pharmacol. Ther.* **173,** 67–82 (2017).

379. Tanaka, K. & Hirota, T. Chromosomal instability: A common feature and a therapeutic target of cancer. *Biochim. Biophys. Acta - Rev. Cancer* **1866,** 64–75 (2016).

380. Lee, J.-S. Exploring cancer genomic data from the cancer genome atlas project. *BMC CancererB reports* **49,** 607–611 (2016).

381. Gao, J. *et al.* Integrative Analysis of Complex Cancer Genomics and Clinical Profiles Using the cBioPortal Complementary Data Sources and Analysis Options. *Sci Signal* **6,** 1 (2013).

382. Klonowska, K. *et al.* Oncogenomic portals for the visualization and analysis of genome-wide cancer data. *Oncotarget* **7,** 176–192 (2016).

383. Bacolod, M. D. *et al.* Examination of Epigenetic and other Molecular Factors Associated with mda-9/Syntenin Dysregulation in Cancer Through Integrated Analyses of Public Genomic Datasets. *Adv. Cancer Res.* **127,** 49–121 (2015).

384. Olvedy, M. *et al.* Comparative oncogenomics identifies tyrosine kinase FES as a tumor suppressor in melanoma. *J. Clin. Invest.* **127,** 2310–2315 (2017).

385. Li, Z. Y., Wang, Z. X. & Li, C. C. Kinesin family member 20B regulates tongue cancer progression by promoting cell proliferation. *Mol. Med. Rep.* **19,** 2202–2210 (2019).

386. W.-F., L. *et al.* Pseudopod-associated protein KIF20B promotes Gli1-induced epithelial-mesenchymal transition modulated by pseudopodial actin dynamic in human colorectal cancer. *Mol. Carcinog.* **57,** 911–925 (2018).

387. Liu, X. *et al.* Inhibition of kinesin family member 20B sensitizes hepatocellular carcinoma cell to microtubule-targeting agents by blocking cytokinesis. *Cancer Sci.* **109,** 3450–3460 (2018).

388. Chen, J., Chen, H., Yang, H. & Dai, H. SPC25 upregulation increases cancer stem cell properties in non-small cell lung adenocarcinoma cells and independently predicts poor survival. *Biomed. Pharmacother.* **100,** 233–239 (2018).

389. Cui, F., Tang, H., Tan, J. & Hu, J. Spindle pole body component 25 regulates stemness of prostate cancer cells. *Aging (Albany. NY).* **10,** 3273–3282 (2018).

390. Archangelo, L. F. *et al.* The CALM and CALM/AF10 interactor CATS is a marker for proliferation. *Mol. Oncol.* **2,** 356–67 (2008).

391. Saad, S. T. O. *et al.* CATS (FAM64A) abnormal expression reduces clonogenicity of hematopoietic cells. *Oncotarget* **7,** 68385–68396 (2016).

392. Li, Z., Zhang, Y., Zhang, Z., Zhao, Z. & Lv, Q. A four-gene signature predicts the efficacy of paclitaxel-based neoadjuvant therapy in human epidermal growth factor receptor 2–negative breast cancer. *J. Cell. Biochem.* **120,** 6046–6056 (2019).

393. Cuadros, M. *et al.* Identification of a proliferation signature related to survival in nodal peripheral T-cell lymphomas. *J. Clin. Oncol.* **25,** 3321–9 (2007).

394. Lee, Y. M. & Sicinski, P. Targeting cyclins and cyclin-dependent kinases in cancer: Lessons from mice, hopes for therapeutic applications in human. *Cell Cycle* **5,** 2110–4 (2006).

395. Schmitz, J., Watrin, E., Lénárt, P., Mechtler, K. & Peters, J. M. Sororin Is Required for Stable Binding of Cohesin to Chromatin and for Sister Chromatid Cohesion in Interphase. *Curr. Biol.* **17,** 630–6 (2007).

396. Tian, Y. *et al.* CDCA5 overexpression is an Indicator of poor prognosis in patients with hepatocellular carcinoma (HCC). *BMC Cancer* **18,** 1187 (2018).

397. Phan, N. N. *et al.* Distinct expression of CDCA3, CDCA5, and CDCA8 leads to shorter relapse free survival in breast cancer

patient. *Oncotarget* **9,** 6977–6992 (2018).

398. Shen, A. *et al.* Cell division cycle associated 5 promotes colorectal cancer progression by activating the ERK signaling pathway. *Oncogenesis* **8,** 19 (2019).
399. Zhu, P. *et al.* A novel prognostic biomarker SPC24 up-regulated in hepatocellular carcinoma. *Oncotarget* **6,** 41383–97 (2015).
400. Zhou, J. *et al.* A potential prognostic biomarker SPC24 promotes tumorigenesis and metastasis in lung cancer. *Oncotarget* **8,** 65469–65480 (2017).
401. Zhou J, Pei Y, Chen G, Cao C, Liu J, Ding C, Wang D, Sun L, Xu P, N. G. SPC24 Regulates breast cancer progression by PI3K/AKT signaling. *Gene* **30,** 272–277 (2018).
402. Sheng, J. *et al.* SPC24 promotes osteosarcoma progression by increasing EGFR/MAPK signaling. *Oncotarget* **8,** 105276–105283 (2017).
403. Wang, D. *et al.* OIP5 Promotes growth, metastasis and chemoresistance to cisplatin in bladder cancer cells. *J. Cancer* **9,** 4684–4695 (2018).
404. Li, H. *et al.* OIP5, a target of miR-15b-5p, regulates hepatocellular carcinoma growth and metastasis through the AKT/mTORC1 and B-catenin signaling pathways. *Oncotarget* **8,** 18129–18144 (2017).
405. Kim, T. W. *et al.* Opa-interacting protein 5 modulates docetaxel-induced cell death via regulation of mitophagy in gastric cancer. *Tumor Biol.* **39,** 10104283 (2017).
406. Gong, M. *et al.* Expression of Opa interacting protein 5 (OIP5) is associated with tumor stage and prognosis of clear cell renal cell carcinoma. *Acta Histochem.* **115,** 810–5 (2013).
407. Qian, Y. W., Erikson, E., Taieb, F. E. & Maller, J. L. The polo-like kinase Plx1 is required for activation of the phosphatase Cdc25C and cyclin B-Cdc2 in Xenopus oocytes. *Mol. Biol. Cell* **12,** 1791–9 (2001).
408. Ratsima, H. *et al.* Independent modulation of the kinase and polo-box activities of Cdc5 protein unravels unique roles in the maintenance of genome stability. *Proc. Natl. Acad. Sci. U. S. A.* **108,** E914-23 (2011).
409. Sumara, I. *et al.* Roles of Polo-like Kinase 1 in the Assembly of Functional Mitotic Spindles. *Curr. Biol.* **14,** 1712–22 (2004).
410. Gheghiani, L., Loew, D., Lombard, B., Mansfeld, J. & Gavet, O. PLK1 Activation in Late G2 Sets Up Commitment to Mitosis. *Cell Rep.* **19,** 2060–2073 (2017).
411. Aspinall, C. F., Zheleva, D., Tighe, A. & Taylor, S. S. Mitotic entry: Non-genetic heterogeneity exposes the requirement for Plk1. *Oncotarget* **36,** 472–36 (2015).
412. Lera, R. F. & Burkard, M. E. High mitotic activity of polo-like kinase 1 is required for chromosome segregation and genomic integrity in human epithelial cells. *J. Biol. Chem.* **287,** 42812–25 (2012).
413. Medema, R. H. & Lindqvist, A. Boosting and suppressing mitotic phosphorylation. *Trends Biochem. Sci.* **36,** 578–584 (2011).
414. Niu, N. *et al.* Radiation pharmacogenomics: A genome-wide association approach to identify radiation response biomarkers using human lymphoblastoid cell lines. *Genome Res.* **20,** 1482–1492 (2010).
415. Cairns, J., Peng, Y., Yee, V. C., Lou, Z. & Wang, L. Bora downregulation results in radioresistance by promoting repair of double strand breaks. *PLoS One* **10,** 1–18 (2015).
416. Arya, A. K. *et al.* Nutlin-3, the small-molecule inhibitor of MDM2, promotes senescence and radiosensitises laryngeal carcinoma cells harbouring wild-type p53. *Br. J. Cancer* **103,** 186–95 (2010).
417. Wu, J., Ivanov, A. I., Fisher, P. B. & Fu, Z. Polo-like kinase 1 induces epithelial-to-mesenchymal transition and promotes epithelial cell motility by activating CRAF/ERK signaling. *Elife* **5,** e10734 (2016).
418. Cai XP, Chen LD, Song HB, Zhang CX, Yuan ZW, X. Z. PLK1 promotes epithelial-mesenchymal transition and metastasis of gastric carcinoma cells. *Am J Transl Res* **15,** 4172–5183 (2016).
419. Rizki, A., Mott, J. D. & Bissell, M. J. Polo-like kinase 1 is involved in invasion through extracellular matrix. *Cancer Res.* **67,** 11106–10 (2007).
420. Sotillo, R. *et al.* Mad2 Overexpression Promotes Aneuploidy and Tumorigenesis in Mice. *Cancer Cell* **11,** 9–23 (2007).
421. Diaz-Rodriguez, E., Sotillo, R., Schvartzman, J.-M. & Benezra, R. Hec1 overexpression hyperactivates the mitotic checkpoint and induces tumor formation in vivo. *Proc. Natl. Acad. Sci.* **105,** 16719–24 (2008).

422. Ricke, R. M., Jeganathan, K. B. & van Deursen, J. M. Bub1 overexpression induces aneuploidy and tumor formation through Aurora B kinase hyperactivation. *J. Cell Biol.* **193,** 1049–64 (2011).

423. Bharadwaj, R. & Yu, H. The spindle checkpoint, aneuploidy, and cancer. *Oncogene* **23,** 2016–2027 (2004).

424. Weaver, B. A. A., Silk, A. D., Montagna, C., Verdier-Pinard, P. & Cleveland, D. W. Aneuploidy Acts Both Oncogenically and as a Tumor Suppressor. *Cancer Cell* **11,** 25–36 (2007).

425. To-Ho, K. W., Cheung, H. W., Ling, M. T., Wong, Y. C. & Wang, X. MAD2ΔC induces aneuploidy and promotes anchorage-independent growth in human prostate epithelial cells. *Oncogene* **27,** 347–357 (2008).

426. Chung, C. M. *et al.* Amplification and overexpression of Aurora kinase A (AURKA) in immortalized human ovarian epithelial (HOSE) cells. *Mol. Carcinog.* **43,** 165–174 (2005).

427. Ohmine, S. *et al.* Aurora-A overexpression is linked to development of aggressive teratomas derived from human iPS cells. *Oncol. Rep.* **39,** 1725–1730 (2018).

428. Esteller, M., Corn, P. G., Baylin, S. B. & Herman, J. G. A gene hypermethylation profile of human cancer. *Cancer Res.* **61,** 3225–9 (2001).

429. Dong, S. M., Kim, H. S., Rha, S. H. & Sidransky, D. Promoter hypermethylation of multiple genes in carcinoma of the uterine cervix. *Clin. Cancer Res.* **7,** 1982–6 (2001).

430. Luo, G. F. *et al.* FOXD3 may be a new cellular target biomarker as a hypermethylation gene in human ovarian cancer. *Cancer Cell Int.* **19,** 44 (2019).

431. Sung, H. Y., Yang, S. D., Park, A. K., Ju, W. & Ahn, J. H. Aberrant hypomethylation of solute carrier family 6 member 12 promoter induces metastasis of ovarian cancer. *Yonsei Med. J.* **58,** 27–34 (2017).

432. Ward, A., Morettin, A., Shum, D. & Hudson, J. W. Aberrant methylation of Polo-like kinase CpG islands in Plk4 heterozygous mice. *BMC Cancer* **11,** 71 (2011).

433. Ward, A. & Hudson, J. W. p53-dependent and cell specific epigenetic regulation of the polo-like kinases under oxidative stress. *PLoS One* **9,** e87918 (2014).

434. Ward, A. *et al.* The deregulated promoter methylation of the Polo-like kinases as a potential biomarker in hematological malignancies. *Leuk. Lymphoma* **56,** 2123–33 (2015).

435. Jiang, P., Freedman, M. L., Liu, J. S. & Liu, X. S. Inference of transcriptional regulation in cancers. *Proc. Natl. Acad. Sci.* **112,** 7731–6 (2015).

436. Uchiumi, T., Longo, D. L. & Ferris, D. K. Cell Cycle Regulation of the Human Polo-like Kinase (*PLK*) Promoter. *J. Biol. Chem.* **272,** 9166–9174 (1997).

437. De Cárcer, G. The Mitotic Cancer Target Polo-Like Kinase 1: Oncogene or Tumor Suppressor? *Genes (Basel).* **10,** 208 (2019).

438. Laoukili, J. *et al.* FoxM1 is required for execution of the mitotic programme and chromosome stability. *Nat. Cell Biol.* **7,** 126–136 (2005).

439. Alvarez-Fernández, M. & Medema, R. H. Novel functions of FoxM1: From molecular mechanisms to cancer therapy. *Front. Oncol.* **5,** 30 (2013).

440. Thiru, P. *et al.* Kinetochore genes are coordinately up-regulated in human tumors as part of a FoxM1-related cell division program. *Mol. Biol. Cell* **25,** 1983–1994 (2014).

441. Chen, X. *et al.* The Forkhead Transcription Factor FOXM1 Controls Cell Cycle-Dependent Gene Expression through an Atypical Chromatin Binding Mechanism. *Mol. Cell. Biol.* **33,** 227–36 (2012).

442. Grant, G. D. *et al.* Identification of cell cycle-regulated genes periodically expressed in U2OS cells and their regulation by FOXM1 and E2F transcription factors. *Mol. Biol. Cell* **24,** 3634–50 (2013).

443. McKinley, K. L. & Cheeseman, I. M. Large-Scale Analysis of CRISPR/Cas9 Cell-Cycle Knockouts Reveals the Diversity of p53-Dependent Responses to Cell-Cycle Defects. *Dev. Cell* **40,** 405–420 (2017).

444. Weidle, U. H., Birzele, F., Kollmorgen, G. & Rueger, R. Mechanisms and targets involved in dissemination of ovarian cancer. *Cancer Genomics and Proteomics* **13,** 407–423 (2016).

445. Yeung, T.-L. *et al.* Cellular and molecular processes in ovarian cancer metastasis. A Review in the Theme: Cell and Molecular

Processes in Cancer Metastasis. *Am. J. Physiol. Cell Physiol.* **309,** 444–56 (2015).

446. Peart, T. *et al.* Intact LKB1 activity is required for survival of dormant ovarian cancer spheroids. *Oncotarget* **6,** 2242–38 (2015).
447. Dong, Y. *et al.* Paclitaxel Resistance and Multicellular Spheroid Formation Are Induced by Kallikrein-Related Peptidase 4 in Serous Ovarian Cancer Cells in an Ascites Mimicking Microenvironment. *PLoS One* **8,** e57056 (2013).
448. Liu, J. F. *et al.* Establishment of patient-derived tumor xenograft models of epithelial ovarian cancer for preclinical evaluation of novel therapeutics. *Clin. Cancer Res.* **23,** 1263–1273 (2017).
449. Scott, C. L., Becker, M. A., Haluska, P. & Samimi, G. Patient-Derived Xenograft Models to Improve Targeted Therapy in Epithelial Ovarian Cancer Treatment. *Front. Oncol.* **3,** 295 (2013).
450. Noack, S. *et al.* Synthetic lethality in CCNE1-amplified high grade serous ovarian cancer through combined inhibition of polo-like kinase 1 and microtubule dynamics. *Oncotarget* **9,** 25842–25859 (2018).
451. Nagaraj, A. B. *et al.* Mitotic exit dysfunction through the deregulation of APC/C characterizes cisplatin-resistant state in epithelial ovarian cancer. *Clin. Cancer Res.* **24,** (2018).
452. Panguluri, S., Yeakel, C. & Kakar, S. S. PTTG: an important target gene for ovarian cancer therapy. *J. Ovarian Res.* **1,** 6 (2008).
453. Anand, S., Penrhyn-Lowe, S. & Venkitaraman, A. R. AURORA-A amplification overrides the mitotic spindle assembly checkpoint, inducing resistance to Taxol. *Cancer Cell* **3,** 51–62 (2003).
454. Rebucci, M. & Michiels, C. Molecular aspects of cancer cell resistance to chemotherapy. *Biochemical Pharmacology* **85,** 1219–1226 (2013).
455. Ruan, W., Lim, H. H. & Surana, U. Mapping Mitotic Death: Functional Integration of Mitochondria, Spindle Assembly Checkpoint and Apoptosis. *Front. Cell Dev. Biol.* **6,** (2019).
456. Zhe Zhang, Guojun Zhang, Zhipeng Gao, Shiguang Li, Zeliang Li, Jianbin Bi, Xiankui Liu, Zhenhua Li, C. K. Comprehensive analysis of differentially expressed genes associated with PLK1 in bladder cancer. *BMC Cancer* **17,** 861 (2017).
457. de Cárcer, G. *et al.* Plk1 overexpression induces chromosomal instability and suppresses tumor development. *Nat. Commun.* **9,** 3012 (2018).
458. Gjertsen, B. T. & Schöffski, P. Discovery and development of the Polo-like kinase inhibitor volasertib in cancer therapy. *Leukemia* **29,** 11–9 (2015).
459. Kirkland, L. O. & McInnes, C. Non-ATP competitive protein kinase inhibitors as anti-tumor therapeutics. *Biochem. Pharmacol.* **77,** 1561–71 (2009).
460. Raab, M. *et al.* Quantitative chemical proteomics reveals a Plk1 inhibitor-compromised cell death pathway in human cells. *Cell Res.* **24,** 1141–1145 (2014).
461. Lavanya, V., Adil, M., Ahmed, N., Rishi, A. K. & Jamal, S. Small molecule inhibitors as emerging cancer therapeutics. *Integr. Cancer Sci. Ther. Integr Cancer Sci Ther.* **6,** 155–176 (2014).
462. Xu, J., Shen, C., Wang, T. & Quan, J. Structural basis for the inhibition of Polo-like kinase 1. *Nat. Struct. Mol. Biol.* **20,** 1047–53 (2013).
463. Arkin, M. R. & Whitty, A. The road less traveled: modulating signal transduction enzymes by inhibiting their protein-protein interactions. *Curr. Opin. Chem. Biol.* **13,** 284–90 (2009).
464. Arkin, M. R., Tang, Y. & Wells, J. A. Small-molecule inhibitors of protein-protein interactions: Progressing toward the reality. *Chem. Biol.* **21,** 1102–14 (2014).
465. Soucek, L. *et al.* Design and properties of a Myc derivative that efficiently homodimerizes. *Oncogene* **12,** 2463–72 (1998).
466. Beaulieu, M.-E. *et al.* Intrinsic cell-penetrating activity propels Omomyc from proof of concept to viable anti-MYC therapy. *Sci. Transl. Med.* **11,** 484 (2019).
467. Lee JK, K. I. Analysis of Plk1-Bora interaction using a Protein Chip system. *Bio Chip J* **7,** 151–55 (2013).
468. Anastasiadou, E., Jacob, L. S. & Slack, F. J. Non-coding RNA networks in cancer. *Nat. Rev. Cancer* **18,** 5–18 (2017).
469. Ahmad, H. *et al.* An open-label, multi-center, phase I/II, dose escalation study of IV TKM-080301 in subjects with advanced hepatocellular carcinoma. *Eur. J. Cancer* **24,** 747–758 (2016).
470. Majem, B. *et al.* MicroRNA-654-5p suppresses ovarian cancer development impacting on MYC, WNT and AKT pathways.

Oncogene **38,** 6035–6050 (2019).

471. Yan, J., Jiang, J. Y., Meng, X. N., Xiu, Y. L. & Zong, Z. H. MiR-23b targets cyclin G1 and suppresses ovarian cancer tumorigenesis and progression. *J. Exp. Clin. Cancer Res.* **13,** 31–45 (2016).
472. Chen, B. *et al.* miR-23a suppresses pancreatic cancer cell progression by inhibiting PLK-1 expression. *Mol. Med. Rep.* **18,** 105–112 (2018).
473. Beg, M. S. *et al.* Phase I study of MRX34, a liposomal miR-34a mimic, administered twice weekly in patients with advanced solid tumors. *Invest. New Drugs* **35,** 180–188 (2017).
474. Elstrand, M. B., Kleinberg, L., Kohn, E. C., Tropé, C. G. & Davidson, B. Expression and clinical role of antiapoptotic proteins of the bag, heat shock, and Bcl-2 families in effusions, primary tumors, and solid metastases in ovarian carcinoma. *Int. J. Gynecol. Pathol.* **28,** 211–21 (2009).
475. Kassim, S. K. *et al.* Increased bcl-2 expression is associated with primary resistance to chemotherapy in human epithelial ovarian cancer. *Clin. Biochem.* **32,** 333–8 (1999).
476. Høgdall, E. V. S. *et al.* Limited prognostic value of tissue protein expression levels of BCl-2 in Danish ovarian cancer patients: From the Danish 'MALOVA' ovarian cancer study. *APMIS* **118,** 557–64 (2010).
477. Xie, Q. *et al.* ABT737 reverses cisplatin resistance by regulating ER-mitochondria Ca2+ signal transduction in human ovarian cancer cells. *Int. J. Oncol.* **49,** 2507–2519 (2016).
478. Dai, Y., Jin, S., Li, X. & Wang, D. The involvement of Bcl-2 family proteins in AKT-regulated cell survival in cisplatin resistant epithelial ovarian cancer. *Oncotarget* **8,** 1354–1368 (2016).
479. Cory, S., Roberts, A. W., Colman, P. M. & Adams, J. M. Targeting BCL-2-like Proteins to Kill Cancer Cells. *Trends in Cancer* **2,** 443–460 (2016).
480. Ling C, Liu S, Wang Y, Zhang FC, D. Y. Expression of CDK6 in early ovarian cancer and its clinical significance. **20,** 1271–1275 (2016).
481. Dall'Acqua, A. *et al.* CDK6 protects epithelial ovarian cancer from platinum-induced death via FOXO3 regulation. *EMBO Mol. Med.* **9,** 1415–1433 (2017).
482. Kollmann, K. *et al.* A kinase-independent function of CDK6 links the cell cycle to tumor angiogenesis. *Cancer Cell* **24,** 167–181 (2013).
483. PJ, R. *et al.* Multiple roles of cyclin-dependent kinase 4/6 inhibitors in cancer therapy. *J. Natl. Cancer Inst.* **104,** 476–487 (2012).
484. Hamilton, E. & Infante, J. R. Targeting CDK4/6 in patients with cancer. *Cancer Treat. Rev.* **45,** 129–38 (2016).
485. De Dominici, M. *et al.* Targeting CDK6 and BCL2 exploits the 'MYB addiction' of Ph þ acute lymphoblastic leukemia. *Cancer Res.* **78,** 1097–1109 (2018).